THE
PHYSICAL REVIEW
A Journal of Experimental and Theoretical Physics Established by E. L. Nichols in 1893
VOL. 15, NO. 11 JUNE 1, 1937 SECOND SERIES

The Radioactivity Produced in Nickel by Deuteron Bombardment[1]

R. L. THORNTON
University of Michigan, Ann Arbor, Michigan[2]
(Received March 29, 1937)

Nickel bombarded with 5 MV deuterons exhibits an intense positron activity of half-life 3.4 ± 0.1 hours. Chemical analysis shows this activity to be isotopic with copper. The energy excitation curve for this reaction (proton capture) between 3 and 5 MV has been obtained, and is found to be very different from that found for copper (neutron capture). The variation with energy of the disintegration cross section agrees satisfactorily with theoretical formulae for the penetration of a deuteron into a nucleus of radius 4.5×10^{-13} cm. This result does not support the larger nuclear radii recently suggested by Bethe. The upper limit of the positron spectrum is approximately at $H\rho$ 4400 gauss-cm.

EARLY attempts to induce artificial radioactivity in nickel through neutron bombardment by Fermi and his collaborators[3] led to negative results. More recently Rotblat[4] has obtained evidence for two active isotopes by this method—a water-sensitive activity of several hours half-life which he attributes to an isotope of nickel, and a shorter period of twenty minutes which could be associated with cobalt. In view of the extreme weakness of the activity produced, however, these disintegrations cannot be regarded as being definitely established.

In the experiments to be described, nickel has been subjected to bombardment with several microamperes of deuterons accelerated to 5 MV by means of a magnetic resonance accelerator or cyclotron. The results obtained show the production of a single positron radioactive isotope of copper; no evidence being found for the nickel activity reported by Rotblat. The dependence of the induced activity upon the deuteron energy, and the energy distribution of the positrons have also been ascertained.

The nickel was bombarded in the form of a pure metal. For the determination of the period and of the excitation curve, thin foils (0.0001″ in thickness) were used; while for the later experiments on the β-ray spectrum a somewhat thicker target was employed. In each case the purity of the nickel was attested by the observation that only a single period that could be ascribed to an impurity was obtained—the ten-minute period of radionitrogen.

The energy excitation curve was determined through the simultaneous bombardment of a number of thin foils. The foils were mounted in suitable holders which were protected from bombardment, and the decay curve of each was established. A typical group of such curves is shown in Fig. 1. From these plots the relative activities of the several foils could be readily and accurately

[1] A preliminary report of these experiments has been made to the American Physical Society, Phys. Rev. **49**, 207 (1936).
[2] The greater part of the experiments described were carried out while the writer was at the Radiation Laboratory of the University of California. The cloud chamber experiments were performed at the University of Michigan.
[3] Amaldi *et al.*, Proc. Roy. Soc. **A149**, 522 (1935).
[4] Rotblat, Nature **136**, 515 (1935).

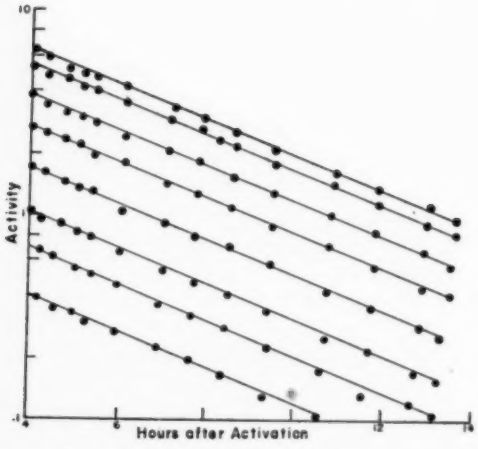

FIG. 1. Semi-logarithmic plot of the decay curves for activated nickel foils.

ascertained, and from the known stopping power of the foils the differential excitation curve of the reaction determined. But before this can be done a number of corrections must be applied to the observations.

The stopping power of the individual foils was measured relative to air by means of polonium α-particles. It was found that the metal was not completely uniform, and a correction to reduce all foils to a common thickness was necessary. This amounted to as much as 10 percent—the mean thickness being 8.6 mm air equivalent. In addition it is necessary to correct for the variation of stopping power with the velocity of the incident deuterons. This was done using the theory developed by Mano.[5] The activation of each foil except the first is enhanced through the recoil of activated atoms from the preceding foil; it is thus to be expected that the measured intensity of the first foil will be somewhat too low. Since the observed points lie along a smooth curve, it was assumed that this correction was small and no allowance was made for it.

The energy of the incident deuterons was determined from range measurements in aluminum. Errors arising from this determination may be as high as 6 percent; relative energy measurements between the several foils are certainly considerably more accurate than this.

The decay curves for the foils were followed with a Lauritsen type electroscope, and with a pressure ionization chamber vacuum tube electrometer combination constructed by Dr. S. N. Van Voorhis.

The complete decay curves for the activated nickel may be satisfactorily explained on the basis of two periods—an intense ten-minute activity which in all probability is due to carbon contamination, and a 3.4 ± 0.1 hour activity which chemical analysis established as being isotopic with copper. The chemical procedure followed that outlined by Bray.[6] Copper and cobalt salts were added to the dissolved nickel, and the three elements precipitated separately. It was found that the relative activities of the three precipitates were 10.0, 0.1 and 0.05 for the copper, nickel and cobalt, respectively.

Investigation of the active copper in a Wilson cloud chamber showed that positive electrons were emitted, and thus the resulting element must be an isotope of nickel. The isotopic constitution of nickel has been investigated by Dempster[7] who found isotopes of mass numbers 58, 60, 61, 62 and 64. The reaction may thus be most probably written

$$_{28}\mathrm{Ni}^{N}+{}_{1}\mathrm{H}^{2}\rightarrow{}_{29}\mathrm{Cu}^{N+1}+{}_{0}n^{1}$$

$$_{29}\mathrm{Cu}^{N+1}\rightarrow{}_{28}\mathrm{Ni}^{N+1}+e^{+}$$

where the possible values of N are 58, 60 and 61. Of these the first possibility results finally in an unknown isotope of nickel, and since no other activity than the single period was observed, it is more probable that the disintegration involves either Ni^{60} or Ni^{61}. The possibility of a radiative capture of the deuteron, although unlikely, is of course not excluded.

Since the formation of this active copper isotope results from the capture of a proton accompanied by neutron emission, considerable interest attaches to the shape of the energy excitation curve in comparison with those obtained for cases of neutron capture and proton emission. In order to account for the shape of the latter curves, and for the large disintegration cross sections observed for neutron capture reactions for elements of high

[5] Mano, J. de phys. et rad. **5**, 628 (1934).

[6] Noyes and Bray, *Qualitative Analysis for the Rare Elements* (Macmillan, 1927). I am indebted to Dr. H. W. Newson for his help with the chemical analysis.

[7] Dempster, Phys. Rev. **50**, 98 (1936).

atomic number, Oppenheimer and Phillips[8] have suggested that such disintegrations do not require the penetration of the deuteron as a whole into the nucleus. On this basis a formula giving the variation of yield with deuteron energy was obtained, which has been shown by Lawrence, McMillan and Thornton[9] and by Henderson[10] to be in excellent agreement with experiment for such reactions in the cases of sodium, aluminum, silicon, copper and magnesium.

More recently, however, Bethe[11] has suggested that such considerations are not necessary to explain the observations, and that they may be interpreted as evidence for a larger nuclear radius than has hitherto been accepted. In addition to the arguments advanced by Bethe, further support for this view is given by Pollard[12] through the observation of low energy protons emitted from certain light elements under α-particle bombardment, and from estimates of the yields obtained.

In a number of papers Sexl[13] has investigated the penetration of charged particles through nuclear potential barriers, and has developed a formula showing the dependence of the disintegration cross section σ upon the energy of the projectile and upon the nuclear radius. This formula may be written

$$\sigma(E) = (\text{const.}/E)e^{-\chi(2\alpha_0 - \sin 2\alpha_0)},$$

where E is the energy of the bombarding deuteron of velocity v, $\chi = 2e^2Z/\hbar v$, $\cos^2 \alpha_0 = Er_0/e^2Z$ and r_0 is the nuclear radius. In deriving this expression, only the probability of penetration of the deuteron has been taken into account. To completely describe the cross section, the probability of the reaction proceding after the penetration of the deuteron should also be considered. This, however, cannot be done as yet, but we may reasonably assume that the emission of a charged particle will correspond to a somewhat steeper excitation curve than that for the emission of a neutron.

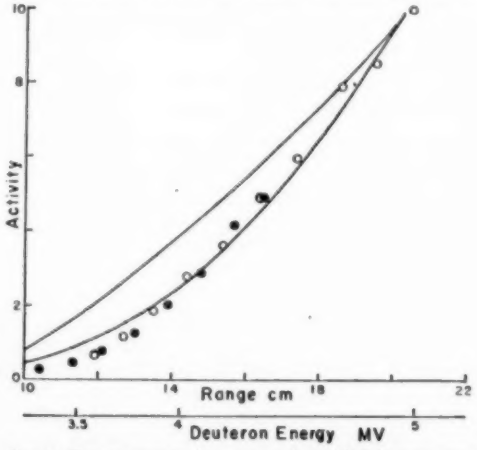

FIG. 2. Energy excitation curves for nickel (lower curve) and for copper (upper curve). The curve through the experimental points for nickel corresponds to a nuclear radius of 4.5×10^{-13} cm.

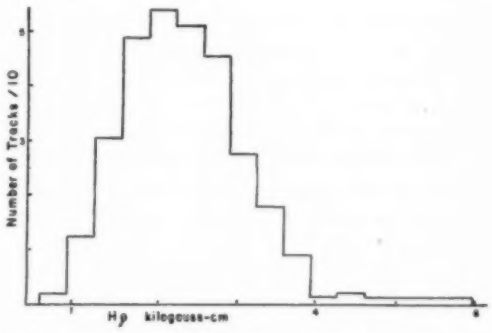

FIG. 3. Momentum distribution of 300 positrons from activated nickel target.

Thus the comparision of the excitation curves for proton capture in nickel ($Z=28$) with those for neutron capture in copper ($Z=29$) provides a convenient test for these points of view. Since the nuclear radius is approximately proportional to the cube root of the total number of nuclear particles, it should not be very different for the two cases. Hence if in each case the deuteron as a whole penetrates the nucleus, we may expect the copper curve to be slightly steeper than that for nickel (Z is larger and a charged particle must escape). On the other hand if the views of Oppenheimer and Phillips are correct, and also if we assume a radius for the natural radioactive atoms of 9×10^{-13} cm (about 5×10^{-13} for nickel), then the nickel curve should be the steeper.

The experimental data presented in Fig. 2, corrected as outlined previously, are the result of two independent runs taken at different initial

[8] Oppenheimer and Phillips, Phys. Rev. **48**, 500 (1935).
[9] Lawrence, McMillan and Thornton, Phys. Rev. **48**, 493 (1935).
[10] M. C. Henderson, Phys. Rev. **48**, 855 (1935).
[11] Bethe, Phys. Rev. **50**, 977 (1936).
[12] Pollard, Phys. Rev. **51**, 290 (1937).
[13] Sexl, Zeits. f. Physik **87**, 105 (1933).

deuteron energies. The two curves were adjusted to fit at 16.5 cm deuteron range. In comparison with the observations for nickel are shown the data obtained by Van Voorhis[14] for copper (the upper curve in Fig. 2). The different character of the two curves is immediately evident. The second curve in Fig. 2 through the experimental points is a plot of Sexl's formula for a nuclear radius $r_0=4.5\times10^{-13}$ cm, adjusted to fit the experimental points at 20 cm range. The agreement would appear to be satisfactory. It was found that an increase of the radius to 5.0×10^{-13} cm resulted in a curve lying completely above the experimental points, while a value of 8×10^{-13}, which Bethe's value of 13×10^{-13} for the natural radioactive elements would suppose, is very decidedly too large. Thus from the data presented here it would seem that it is not possible to account for the "flat" excitation curves observed for neutron capture reactions by solely supposing an increase in the nuclear radius.

Measurements of the radii of curvature of 300 positron tracks in a Wilson cloud chamber in a plane perpendicular to a magnetic field of 340 gauss resulted in the histogram presented in Fig. 3. Only tracks were measured which clearly originated in the target and had a length greater than 7 cm. The presence of the five tracks observed beyond the "inspection" upper limit at $H\rho$ 4400 gauss-cm (0.9 MV) may be explained either as being due to γ-rays which are known to be present but have not as yet been measured, or to the presence of a second and higher energy positron group as has been observed in other cases.[15] Decision between these alternatives must await further experiments.

It is a pleasure for the writer to acknowledge his very great indebtedness to Professor E. O. Lawrence, and to Professor J. R. Oppenheimer for his friendly advice upon the theoretical questions involved. The support of the Research Corporation, the Chemical Foundation and the Josiah Macy, Jr. Foundation at the University of California, and of the Horace H. and Mary A. Rackham Fund at the University of Michigan is also gratefully acknowledged.

[14] Van Voorhis, Phys. Rev. **50**, 895 (1936). I am much indebted to Dr. Van Voorhis for his kindness in sending me a copy of his experimental curve.

[15] E.g., Kurie, Richardson and Paxton, Phys. Rev. **49**, 368 (1936); M. V. Brown and Mitchell, Phys. Rev. **50**, 593 (1936).

JUNE 1, 1937 PHYSICAL REVIEW VOLUME 51

Neutron Yields from Artificial Sources

E. AMALDI,
Royal University of Rome

L. R. HAFSTAD AND M. A. TUVE
Department of Terrestrial Magnetism, Carnegie Institution of Washington, Washington, D. C.

(Received March 13, 1937)

Measurements of the total yields of neutrons from the reactions D+D, D+Li, D+Be and D+C have been carried out for the voltage range between 300 kv and 1000 kv using the observing technique developed by Amaldi and Fermi, in which the neutron source is surrounded by a large tank of water. Neutrons of all energies are thus reduced to thermal energies, and the total yield of neutrons is obtained by integration from measurements of the density of slow neutrons at various distances from the source. Similar measurements were made on the neutrons from Rn+Be, with the same geometrical conditions. The neutron yields per microampere of pure D^2 ions from the artificial sources are shown in the table below for various voltages; each entry gives the number of millicuries of Rn+Be required to give the same total yield of neutrons per second. A total yield of 25,000 neutrons per second from one millicurie of Rn+Be is calculated from the measurements of this source. Absolute yields for the various sources computed on the basis of this figure should not be considered as reliable within 20 percent, perhaps the chief error arising from the fact that the average ionization per beta-ray is assumed to be the same for the beta-rays from the rhodium detector and for those from

REACTION	300 kv	400 kv	600 kv	800 kv	1000 kv
D+$D_2O(P_2O_5)$	48	140	250	550	860
D+Li	(40)	(160)	(800)	(4200)	...
D+Be	9	100	700	2400	6800
D+C	..	...	10	140	680

the uranium standard which is used to convert the rhodium measurements into numbers of disintegrations per second. The relative yields for the artificial sources are obtained by direct comparison of the curves, and should be correspondingly more reliable. The yields for lithium are given in parenthesis because the (metallic) target was apparently not perfectly clean, the yields increasing somewhat under continued bombardment, so that a reliable distribution curve could not be obtained. The yields given were obtained on the assumption that the energies of the neutrons from Li were as high as, or higher than, the energies of the neutrons from Be. The $D_2O(P_2O_5)$ target contained 0.113 gram D_2O, 0.342 gram P_2O_5, and 0.005 gram H_2O. A check on the deuterium reaction by measurements on another target would be desirable but has not yet been carried out.

Introduction

ONE of the principal difficulties in measuring the total number of neutrons emitted by various sources arises from the fact that the neutrons are usually heterogeneous in energy. Available detectors respond differently to neutrons of different energies. The difficulty is avoided in the method of Amaldi and Fermi[1] in which all the neutrons are ultimately reduced to thermal energies by immersing the source in a large body of water, and the activity produced by these slow neutrons in a suitable detector (rhodium) is measured as a function of the distance from the source, the total activity then being obtained by integration.

Various corrections and approximations are involved in obtaining absolute values by this method, but it appears reasonable to believe that the results obtained, expressed as a total number of neutrons emitted per second, are reliable to within perhaps 20 percent on an absolute scale. This degree of accuracy is ample at present for a survey of the total neutron yields from various artificial sources at different voltages. Relative or equivalent yields, in terms of the total neutron yield of one millicurie of Rn+Be, are obtained by direct comparison of the integrated curves, with somewhat higher accuracy.

Using this technique we have carried out measurements on the neutrons emitted when deuterons were used to bombard separate targets of $D_2O+P_2O_5$, metallic lithium, metallic beryllium, and carbon in the form of Acheson graphite, the measurements extending over the voltage range from 300 to 1000 kilovolts.

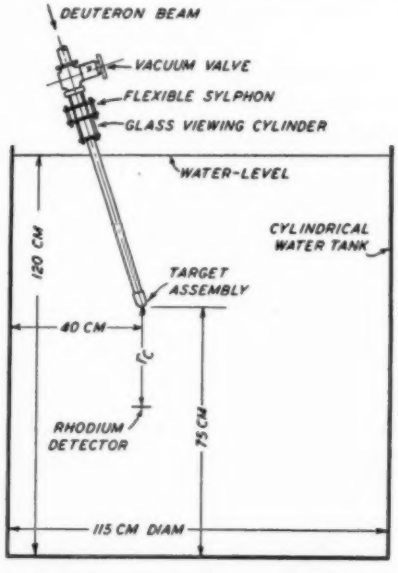

FIG. 1. Arrangement of target and water tank.

Technique

Experimental arrangement

The accelerating apparatus used in this work is that developed by the Department of Terrestrial Magnetism of the Carnegie Institution of Washington and has been described previously.[2] Magnetic analysis of the ion beam was used throughout the observations, and the measured deuteron currents were demonstrated to be always in excess of 97 percent full speed deuterium ions (upper limit of H^1H^1 contamination much less than 2.7 percent). The arrangement of the target and water tank are shown in Fig. 1 and the details of the target assembly in Fig. 2. To insure that all the ion current measured actually was impinging on the target, provision was made for accurate axial alignment by the flexible sylphon connection shown in Fig. 1. With the solid brass hemispherical cap and the opaque

[1] Amaldi and Fermi, Ricerca Scient. **7**, 454 (1936); Phys. Rev. **50**, 899–928 (1936).

[2] Tuve, Hafstad and Dahl, Phys. Rev. **48**, 316–337 (1935); Hafstad, Heydenberg and Tuve, Phys. Rev. **50**, 504–514 (1936).

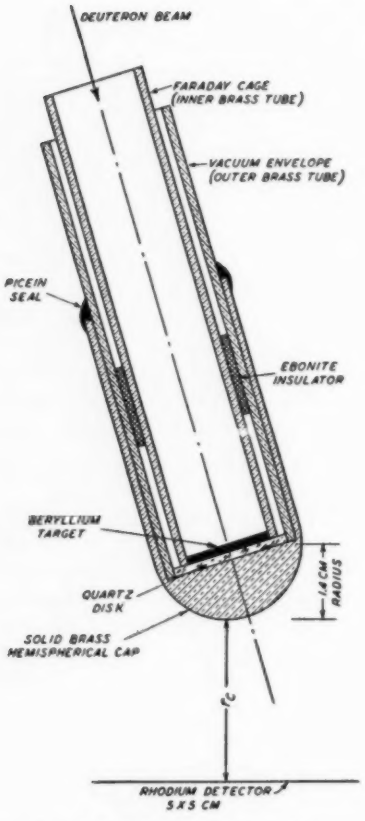

FIG. 2. Detail of target assembly.

target removed, the beam was focused through a 10-mm hole in a quartz disk within the viewing cylinder (above the water tank) and then, by means of the sylphon, the tube position was adjusted until the beam was impinging on the center of the quartz disk indicated in the target position at the end of the tube.

Since in this work magnetic analysis of the ion beam was used, the only error involved in specifying the number of incident deuterons is that due to the presence of molecular H_2^+ ions in the deuteron beam. This error may be evaluated as follows. For a typical run the currents in the analyzed beams were 0.15, 1.20, 0.09, 0.26, 0.16, and 0.35 microampere for the mass-one to mass-six beams, respectively. Assuming that the mass-four beam is composed solely of D_2^+ ions and that the ratio of H_2^+ ions to H^+ ions is the same as that of D_2^+ to D^+, we find that the mass-two beam is 97.3 percent deuterium ions. The beams of mass five and mass six show that the mass-four beam contains several molecular species; the mass-two beam is correspondingly more than 97.3 percent deuterons.

All measurements of activity were made using two pieces of rhodium, each 5 cm square and 0.23 g/cm² thick. Their activity was measured with an ionization chamber similar to that used by Amaldi and Fermi,[1] filled with oxygen at a pressure of three atmospheres and connected to the exceedingly convenient Edelmann electrometer.

Effect of dimensions of source

During the measurements we adopted the convention of calling the distance between the source and the target zero (that is, $r_C=0$) when its center was in contact with the brass hemispherical cap of Fig. 2. Since the entire cap must be considered as a source of fast neutrons, and since the dimensions of the cap cannot be considered negligible in comparison with the distance between the source and the detector, we have taken as the corrected distance (r_k) the root-mean-square distance between points on the detector and on the source, assumed to be a sphere of radius 1.4 cm (water boundary). For ease in reading the figures we have arbitrarily called this r_k. The result is $r_k^2=(r_C+1.4)^2+1.4^2+(\frac{1}{3})Y^2$, where $2Y=5$ cm, the linear dimension of the detector.

Since the finite size of the source disturbs the distribution of thermal neutrons, and the above defined r_k is to some extent a conventional distance, the results obtained with the above

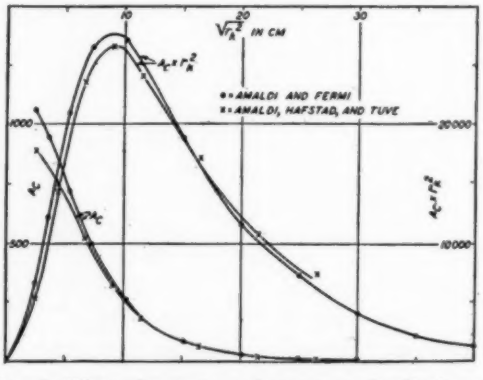

FIG. 3. Effect of geometry of source on distribution of (Rn+Be) neutrons in water.

apparatus for artificial sources are not directly comparable with the original measurements of Amaldi and Fermi[1] for (Rn+Be). To make the comparison as valid as possible, the (Rn+Be) experiments have been repeated by one of us (Amaldi), placing the (Rn+Be) source inside a brass tube of the same outside form as that for the artificial source above described. The effect of the difference in geometry is shown in Fig. 3, which shows the depression of the density of slow neutrons at small distances from the source due to the effectively larger volume of this source. The error due to this difference, however, appears to be negligible compared to other sources of error which will be discussed below.

Standardization of observations

In order to give our results in a form comparable with the results of Amaldi and Fermi, we have used the following definition of the "activability" of a detector in a given position with respect to a given artificial source at a given voltage

$$A = 1000\ (a/iU),$$

where a is the initial activity of the detector after infinite time irradiation, i is the current of deuterons in microamperes on the target, U is the activity of a standard uranium solution, as used by Amaldi and Fermi (840 disintegrations per second), measured under the same conditions as the artificial radioactivity (the same instrument, recalibrated with a uranium sub-standard immediately following each single observation, with the same sensitivity and over the same divisions of the scale, in order to avoid errors due to non-linearity). The difference between this definition and the definition used by Amaldi and Fermi is that in our case the activability is defined per microampere of current of deuterons on the target instead of per unit of (Rn+Be) neutron intensity [corresponding to about 6 mC of (Rn+Be)]. It is to be noted that one of these original units of neutron-intensity corresponds to a very small number of alpha particles impinging per second on Be, compared with the number of particles in a microampere of deuterons. Therefore, we must expect that the activabilities given in this work will be very large.

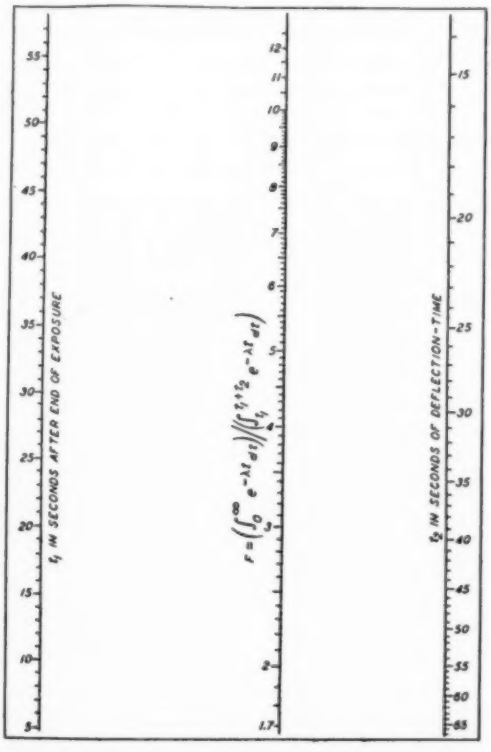

FIG. 4. Nomogram for rhodium (44 second period).

In practice, we have used a uranium preparation as our "working standard" [$UO_2(NO_3)_2$ in paraffin, spread over an area 5 by 5 cm and enclosed in 0.10 mm of aluminum foil] whose activity, compared in our laboratory with the standard solution[1] was found to be 2.5_5 times the activity of the similar preparation used in Rome as a working standard.

The initial activity a after an infinite time of irradiation is simply determined for elements with long periods. For elements with short periods, as, for instance, rhodium (44 seconds), it is convenient to follow a standard procedure in making the observations. We will explain in detail the procedure used for rhodium, with which all measurements in this work were made.

The nomogram devised and used by Amaldi and Fermi[1] is shown in Fig. 4, and is made as follows. The first two of the parallel straight lines are drawn at convenient distances one from the other, and the third is located by calculation and graphical construction. The first one is marked

off in seconds on a linear scale reading upward from a zero origin. This scale corresponds to the time t_1 between the end of the irradiation of the rhodium and the beginning of the reading of the activity. The third line is scaled in seconds (non-linear; calculated) to correspond to the time t_2 during which the ionization chamber is exposed to the rhodium for the collection of a suitable charge (time of deflection between two selected points on the electrometer-scale, calibrated by the uranium). If the reading could begin just at the moment when the irradiation is stopped ($t_1=0$), and if we could wait an infinite time ($t_2=\infty$), the number of divisions indicated by the electrometer would be proportional to the total activity of the rhodium. In practice, the reading begins some seconds after the irradiation and takes a finite time; hence the electrometer deflection is smaller than this value. The line of the nomogram between the two scales above described is accordingly scaled logarithmically to read the factor F, calculated by simple formulas, by which we must multiply the number of divisions D (corrected for the residual effect) deflected in t_2 seconds, the deflection beginning at a time t_1 seconds after the end of the irradiation, in order to obtain the number of divisions corresponding to the total activity ($t_1=0$, $t_2=\infty$). It is clear that the origin of this middle scale must be marked unity, the origins of the three scales (infinite time for scale 3) being on one straight line (which slants downward in our nomogram, for convenient location of scale values). For any given reading the factor F is then found by reading the intercept on the middle scale when the observed values of t_1 and t_2 are connected by a straight-edge.

By integrating we see that to obtain the initial activity we divide the total activity FD by the mean life $\tau=63.5$ seconds (half-life=44 seconds). If the rhodium has been irradiated t seconds, we must divide its activity (initial or total) by $(1-2^{-t/44})$ in order to obtain the activity corresponding to infinite time of irradiation. In general, we irradiated for only 60 seconds, in order to be able to neglect the activity of the second period of this element (4.2 minutes). Even with infinite time of irradiation the activity of this second period is only one-tenth of the 44-second activity.[3, 4] Readings were made at regular 10-minute intervals, so each piece of rhodium was used again only after 20 minutes had elapsed. The initial activity a corresponding to an infinite time of irradiation is accordingly given, from the observations after 60 seconds irradiation, by

$$a=F\cdot D/[63.5(1-2^{-60/44})]=F\cdot D\cdot 0.0257.$$

We will designate the standard uranium solution and its activity by U. If the activity of this uranium standard is read over the same divisions of the scale as was the rhodium (correcting for residual in each case) and we call t_U the corresponding time, the activity U of this preparation is given by D/t_U and the activability of rhodium, according to the definition above, by

$$A=25.7Ft_U/i.$$

In order to make a large number of measurements rapidly, it is convenient to determine experimentally the various factors for a second nomogram, characteristic of the ionization chamber and the electrometer. This second nomogram is used to obtain the value of the deflection time for the standard, t_U, when the electrometer is set for a given sensitivity (divisions per volt) and the deflection occurs between any two points on the scale. However, in this work we have actually measured D/t_U after each rhodium observation.

The activability above defined corresponds to the ionization of rhodium divided by the ionization of uranium. In order to express the activability in numbers of disintegrations per second, we must introduce the quantities η and η_U which represent the mean ionization per beta-particle respectively of rhodium and UX_2 in the ionization chamber used. The uranium preparation corresponds to 840 disintegrations per second; therefore, we must multiply the activability by 840 η_U/η in order to obtain the corresponding number of disintegrations per second. The factor η_U/η is unknown, although it might be measured by a suitable experiment. In the calculation of the results we have assumed $(\eta_U/\eta)=1$. The error due to this assumption can be evaluated from the

[3] E. Amaldi, O. D'Agostino, E. Fermi, B. Pontecorvo, F. Rasetti, and E. Segrè, Proc. Roy. Soc. **A149**, 522–558 (1935).

[4] E. Amaldi and E. Fermi, reference 1, Ricerca Scient. **7**, 443 (1935); E. Segrè, Ricerca Scient. **7**, 389 (1936).

results obtained by Amaldi and Fermi on the number of neutrons of group C (thermal neutrons) coming out from a block of paraffin containing the source of fast neutrons (the "numerosity"). This number was measured by observing the activities of different elements. The differences between the results obtained with different elements are certainly due in great part to the different ionizations of the beta particles of different elements. From a consideration of these data and the fact that the energies of the beta particles from the two elements are nearly equal (half-thickness in aluminum 0.10 g/cm² for UX_2; 0.15 for Rh, 44 sec.), we believe that the error due to the assumption $\eta_U = \eta$ will not be larger than 20 percent in the resulting absolute numerical yields.

Correction for absorption within the detector

The absorption coefficient of electrons of Rh in Rh is $\mu = 7.3$ cm²/g. If we indicate by $f(Kx)$ the absorption curve of neutrons in rhodium (K = absorption-coefficient of neutrons in rhodium and $f(Kx) = e^{-Kx}$ if the impinging neutrons form a parallel beam), it is clear that the effective thickness of a rhodium detector of thickness δ is

$$\delta_{eff} = \int_0^{\delta} f(Kx) e^{-\mu x} dx \qquad (1)$$

if the neutrons impinge on only one surface of the detector and we measure its activity on the same face. If the neutrons impinge on both faces of the detector, it is necessary to sum two expressions similar to (1).

If the detector is inside a hydrogenated substance under such conditions that the density of neutrons close to the detector is about constant, it is more correct to take for $f(Kx)$ the absorption curve $b(Kx)$ corresponding to the cosine law;[1] if the detector is outside the hydrogenated substance but close to its surface, or inside but with a total absorber of thermal neutrons on one side, it is more correct to take for $f(Kx)$ the curve $c(Kx)$ corresponding[1] to the angular law $\cos\theta + \sqrt{3}\cos^2\theta$. In the following paragraphs we will calculate this correction under these conditions.

For our rhodium detector $\delta = 0.23$ g/cm² and $K = 0.7$ cm²/g for thermal neutrons (group C, strongly absorbed by Cd). In order to calculate δ_{eff} we notice that $c(Kx)$ can be represented for $0 \leqq x \leqq \delta$ with an exponential $e^{-K_{eff}x}$ with a good approximation. We determine K_{eff} as follows:[1] $c(0.7 \times 0.23) = 0.69 = e^{-K_{eff}(0.23)}$; $K_{eff} = 0.37/0.23 = 1.6$; $\delta_{eff} = (1 - e^{-(\mu + K_{eff})\delta})/(\mu + K_{eff}) = 0.098$ g/cm².

Correction for presence of group D

With our detector the total activity (group C + group D) measured on the face towards the source is, within the experimental error, equal to the total activity measured on the other face. On the other hand, the activity due to group D alone (activity of rhodium with cadmium over both faces) measured on the face opposite to the source is equal to 93 percent of the activity measured on the face towards the source. This different behavior of our rhodium detector in groups C and D is due to the difference between its absorption coefficients for these two groups (group C, 0.7, and group D, 1.8 cm²/g). For the artificial sources we have always measured the activity of our rhodium detector on the face towards the source; in order to obtain the mean value of the activity due to group D which would be measured on both faces we have multiplied the observed activity due to group D, measured on the face towards the source, by 1.93/2.

We know also that the ratio of the activity due to group D to the total activity is not constant but is a function of the distance from the source. Such a function has been measured by one of us (Amaldi) in the case of the source (Rn+Be); we have found that this ratio is equal to 0.11_4 for $r_C = 0$ and decreases about linearly up to $r_C = 15$ cm, where it reaches a value of about 0.057; beyond this distance it remains constant. Such a constant value is reached at a distance where fast and slow neutrons are in equilibrium (see below).

In the case of the artificial sources we have measured the activity using cadmium with the rhodium only at $r_C = 0$, 2.5, and 5 cm. For larger distances we have calculated the activity of rhodium with cadmium by applying the criteria deduced from the data with the source (Rn+Be). It is to be noted that the distance from the source where fast and slow neutrons are in equilibrium is different for different sources.

Space distribution of neutrons in water

Let us consider a point source emitting neutrons of some million volts energy at the center of

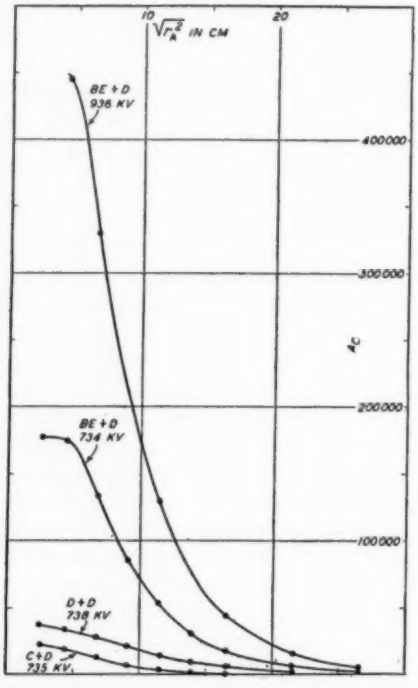

FIG. 5. Thermal neutrons in water at different linear distances from the source.

a very large water tank. The fast neutrons, through successive impacts with hydrogen atoms of water, lose energy until they reach the energy of thermal agitation. At the same time, the mean free path, which for neutrons of some million volts energy is of the order of 5 cm, decreases rapidly and reaches a value a little over one cm. This value of the mean free path remains constant for all lower energies down to the point where, in the impact of neutron and proton, the chemical bond of the hydrogen atom in the molecule can no longer be neglected with respect to the energy of the incident neutron. In practice the mean free path of neutrons in water is about one cm for neutron energies from say 10,000 volts down to energies of the order of one volt. For energies of the impinging neutron lower than one volt, the chemical bond of the hydrogen atom changes very strongly the law of scattering (of neutrons by protons) in such a way that the mean free path of thermal neutrons in water is about 0.35 cm. The neutrons which have reached thermal energy will diffuse through water and will traverse, on the average, 140 mean free paths before being captured by the protons with formation of deuterons. If we call r the distance from the source of fast neutrons, it is clear that the density of thermal neutrons is a function of r which decreases with increasing r. In order to determine the density of thermal neutrons in water as a function of the distance from the source, we can use the activity induced by thermal neutrons in a detector, for instance, rhodium. We know that this element is sensitive to thermal neutrons (group C) and also to neutrons of about 1 volt energy (group D). In order to determine the part of the activity of rhodium due to thermal neutrons only, it is necessary to observe the difference of the activities of rhodium with and without a cadmium screen on each side thick enough to absorb all impinging thermal neutrons (in practice we have used cadmium of 0.43 g/cm^2).

If the detector were very thin, its activity would be proportional to the density of thermal neutrons in water close to the detector; in our case the detector can be considered thin for group C and thick for group D; we must introduce, therefore, a small correction as explained in the paragraphs above. Fig. 5 shows the activability A_C due to group C of our detector as a function of the distance from the source, using different sources of fast neutrons as indicated.

These curves, multiplied by the square of the distance from the source, are shown in Fig. 6. The meaning of these last curves is evident; they are proportional to the function $n(r)dr$, which represents the number of thermal neutrons contained between two spheres of radius r and $r+dr$.

In order to determine the total number of fast neutrons emitted from the source, it will be necessary to calculate the integral of $n(r)dr$ from zero to infinity. This integral (properly normalized in terms of the detector constants and geometry—see B_C below) divided by the diffusion length resulting in capture (thermal neutrons) gives the total neutron emission from the source; see Section 12, Eq. (27), and Section 7, Eq. (12), of reference 1, above. The curves of Fig. 6 are equal to $n(r)$ multiplied by a factor which depends on the thickness of the detector, on its absorption coefficients for neutrons and electrons, and on the value of the albedo (reflection coefficient of water for thermal neutrons).

Correction for disturbance produced by the detector

The facts that thermal neutrons have a very high albedo in water ($\beta=0.83$), and that the detector absorbs more than an infinitesimal number of neutrons, give rise to a depression of the density of thermal neutrons in the region close to the detector. It is possible to take into account all of these effects in determining the proportionality factor between $n(r)$ and $A_C r^2$; the result is, however, very sensitive to small errors in the absorption-coefficients of the detector for neutrons and electrons.

Therefore, it is convenient to use an experimental arrangement in which thermal neutrons traverse the detector only once. For this purpose we have measured the activability B_C on one face of our detector due to thermal neutrons when it is screened on the other face by a cadmium sheet, thick enough to absorb all impinging thermal neutrons (0.43 g/cm²). Under these conditions thermal neutrons impinge on the detector only on the exposed face, and if they are not captured by the rhodium nuclei, they are absorbed by the cadmium.

In this case, however, it is evident that the activability B_C is a function of the orientation of the detector with respect to the source of fast neutrons; therefore, it is necessary to take a mean value of B_C on all orientations. In practice it is sufficient to take the average of the two values of B_C obtained when we have the exposed face of rhodium, or conversely the face protected by cadmium, oriented toward the source of fast neutrons. Remembering that the activity of rhodium is due in part to group D, B_C will be the difference between this mean value and the mean value of the activabilities of rhodium measured on both its faces when it is screened on both sides by cadmium.

Calculation of the total number of neutrons emitted

The activability B_C is given by[5]

$$B_C = K\delta S q \lambda N^{\frac{1}{4}}(1000/Ui), \qquad (2)$$

where $K=0.7$ cm²/g is the absorption coefficient of rhodium for thermal neutrons, $N=140$ is the average number of mean free paths traversed by a thermal neutron before being captured by a proton, $\lambda=0.35$ cm is their mean free path in water (in paraffin $\lambda=0.30$ cm—we have assumed λ inversely proportional to the density of hydrogen atoms), and S and δ are the area and the thickness of the detector. In order to take into account the absorption of electrons in the mass of the detector we must substitute for δ the magnitude δ_{eff} (see preceding section). Finally q is the number of thermal neutrons produced per second and per cm³ in water in the region close to the detector. It is evident that q is a function of the distance from the source of fast neutrons. If now

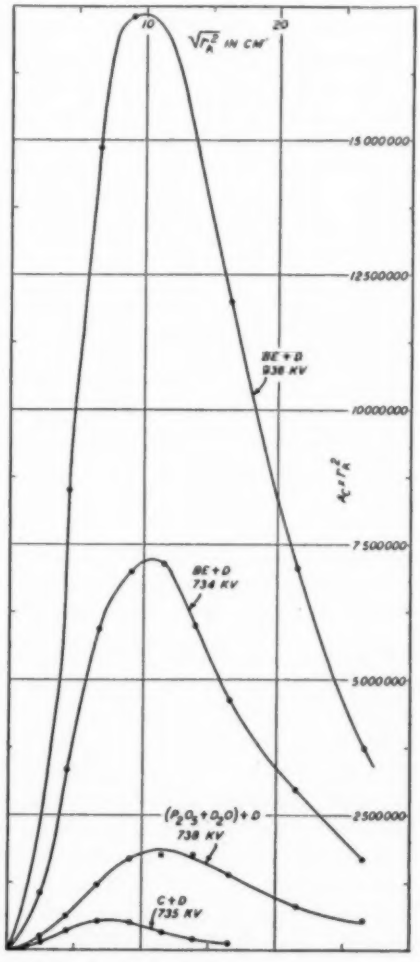

FIG. 6. Thermal neutrons in water between successive spherical shells.

[5] E. Fermi, Ricerca Scient. **7**, 13 (1936).

we want to know the number of disintegrations corresponding to the activability B_C, we must multiply the left side of (2) by $840(\eta_V/\eta)$.

If we integrate this expression over all the volume and we call $Q=\int q d\tau$ the total number of fast neutrons emitted per second from the source (the capture cross section of protons seems to be considerable only for neutrons of thermal energy), we have (see reference 1, Eq. (27)):

$$Q/i=0.84(\eta_V/\eta)\int B_C d\tau/K\lambda N^1 S\delta_{eff}$$
$$=0.118(\eta_V/\eta)\int B_C d\tau. \quad (3)$$

In order to calculate $\int B_C d\tau$ we make the reasonable assumption that B_C is proportional to A_C; therefore, by measuring B_C at a given distance from the source ($r_k^2=4.4$ cm), as was done separately for each of the sources (reactions) used below, we can write

$$\int B_C d\tau=4\pi[B_C(4.4)/A_C(4.4)]\int_0^\infty A_C r^2 dr. \quad (4)$$

In order to calculate the integral of the right side of Eq. (4), we need to extrapolate $A_C(r)r^2$ for large values of r. In practice this function for large values of r can be represented by an exponential $e^{-r/\Lambda}$. In our case the determination of such an exponential is not very accurate because it would be necessary to measure A_C with high accuracy up to distances from the source much larger than the greatest distance we have used ($r_C=25$ cm). However, the value of the integral is not very sensitive to errors on the value of Λ; we will see later how small this sensitivity is.

Approximation involved for large values of r

In reality, the curves of Fig. 6 will not be accurately exponential for large values of r. It is easy to understand qualitatively the general slope of these curves if we consider that the fast neutrons emitted from the source can be considered as a primary radiation which is absorbed in water with formation of a secondary radiation (thermal neutrons) softer than the primary one (mean free path of fast neutrons 4 or 5 cm, mean free path of thermal neutrons 0.35 cm). At large distances from the source the secondary radiation is in equilibrium with the primary one; both decrease with increasing r, corresponding to the absorption law of the primary radiation (fast neutrons). It is to be noted that in this consideration the expression "absorption of the primary radiation" does not mean a real absorption but a diffusion process in which neutrons lose energy in such a way that their mean free path decreases very rapidly.

From these rough considerations it is clear that the slope of $A_C r^2$, for large values of r, is connected with the mean free path λ_0 in water of fast neutrons emitted from the source. An exact calculation of $A_C r^2$ for large values of r presents some difficulties; it is, however, possible to make the following rough considerations suggested by G. C. Wick.

Let us consider a source emitting neutrons of energy E_0 and mean free path in water λ_0; we will call primary neutrons all neutrons of energy between E_0 and $(E_0-\Delta E)$, where ΔE is small. One neutron emitted from the source with energy E_0 after some collision in water will have lost, on the average, a large fraction of its energy; we can, however, consider the probability that after n impacts the energy of the neutron considered is contained between E_0 and $(E_0-\Delta E)$. It is evident that neutrons which satisfy this condition cannot have suffered any great deviation from the initial direction of motion; in all impacts they must have been deviated through a very small angle. Now it can be shown that the probability that a neutron after n impacts has energy between E_0 and $(E_0-\Delta E)$ is

$$(1/n!)(\Delta E/E_0)^n.$$

On the other hand, the probability that a neutron diffusing with mean free path λ_0, after n impacts is at distance between r and $(r+dr)$ from the starting point is

$$(1/n!)(r^n/\lambda_0^{(n+1)})e^{-r/\lambda_0}dr.$$

Therefore, the number of neutrons which arrive at distance r from the source with energy between E_0 and $(E_0-\Delta E)$ is represented roughly by

$$e^{-r/\lambda_0}\sum_0^\infty(1/\lambda_0^{(n+1)})(\Delta E/E_0)^n[r^n/(n!)^2]$$
$$\sim\text{const. } r^{-1/4}e^{-r/\lambda_0}\exp\{2[(\Delta E/E_0)(r/\lambda_0)]^{\frac{1}{2}}\}. \quad (5)$$

From this equation we see that from the meas-

urement of $A_C r^2$ it is possible to obtain λ_0 because

$$-1/\lambda_0 = \lim_{r\to\infty} (\log A_C r^2)/r. \qquad (6)$$

However, it is evident that this method is not convenient for an experimental determination because in practice A_C is measured only up to distances of the order of some decimeters. If the source emits neutrons of different energies, the method permits, in principle, the determination of the mean free path of the fastest component.

It is also evident that $A_C r^2$ is not much different from an exponential $e^{-r/\Lambda}$ where Λ is an empirical length not connected by any simple relation to λ_0. The experimental determination of Λ for different sources of neutrons permits, however, the establishment of the order of increasing mean free path, and therefore energy. With sources which emit neutrons of several different energies, the situation is much more complicated.

Another parameter, whose value is connected with Λ and which is very useful in characterizing different sources of fast neutrons, is

$$(r^2)_{Av} = \int_0^\infty n(r) r^2 dr \Big/ \int_0^\infty n(r) dr,$$

that is, the average of the square of the distance from the source of fast neutrons reached by the slow neutrons[1,5]. This $(r^2)_{Av}$ depends very strongly on the value of Λ. In the present work the determination of Λ is not accurate enough to calculate $(r^2)_{Av}$ for different sources. However, we are able to make some qualitative considerations regarding the energy of the fast neutrons emitted from the different sources, starting from a comparison of their space distributions of thermal neutrons in water.

TABLE I. *(D+D) at 738 kv (phosphorus pentoxide+heavy water target); distribution of thermal neutrons in water.*

r_C	$(r_k^2)^{\frac{1}{2}}$	A_C+A_D	A_D	A_D corr.	A_C	$A_C r_k^2$
0	2.45	42100±1500		(4800)	37300	224000
2.5	4.4	37500±1300	4120	3980	33520	640000
5	6.7	29500± 600	2500	2410	27090	1220000
7.5	9.1	22100± 400		(1500)	20600	1700000
10	11.5	14200± 200		(900)	13300	1770000
12.5	13.9	9550± 200		(540)	9010	1770000
15	16.5	5440± 300		(310)	5130	1400000
20	21.5	1860± 150		(106)	1750	810000
25	26.5	830± 40		(47)	780	547000

EXPERIMENTAL RESULTS

(Rn+Be)

The reaction which gives rise to neutrons is ${}_4Be^9+{}_2He^4\rightarrow{}_6C^{12}+{}_0n^1$. The space distribution in water of thermal neutrons obtained from a source (Rn+Be) was measured by Amaldi and Fermi.[1] However, the geometry in the experiments of these authors was very different from the geometry used in the present work for the artificial sources. Therefore, as previously stated, these measurements were repeated with the source (Rn+Be) inside a brass tube of the same form as that of the artificial source (Fig. 2). The details of the disposition used have been given above.

In Fig. 3 the activability of the rhodium detector is plotted against the corrected distance (curves A_C); the corresponding scale is given on the left-hand side. The upper curve represents the results of Amaldi and Fermi. We see that at small distances the relatively small volume of our source gives rise to a perturbation in the density of thermal neutrons of about 20 percent. In the same figure we see these two curves multiplied by r_k^2 (right-hand scale). For very large distances from the source the two curves must coincide. The curve of Amaldi and Fermi was measured up to distances of 40 cm; therefore, we have extrapolated our curve $A_C r^2$ using the same Λ. We find (Eq. (4))

$$\int_0^{24} A_C r^2 dr + 1.06\times10^5 \int_{24}^{\infty} e^{-r/9.45} dr$$
$$= 38.7\times10^4 + 7.9\times10^4 = 46.6\times10^4,$$
$$\int B_C d\tau = 4\pi(1.66/753)46.6\times10^4 = 1.29\times10^6.$$

From this value we find (Eq. (3)) $Q/I = 150{,}000$ neutrons per second per unit[1] of neutron intensity. If we remember that one unit of neutron intensity corresponds to about 6 mC of radon plus beryllium, we find 25,000 neutrons per second per millicurie of (Rn+Be).

The value given by Amaldi and Fermi is 27,000. The difference arises for two different reasons besides errors: In the calculation of Amaldi and Fermi $\lambda = 0.3$ cm was used, that is, the mean free path of thermal neutrons in paraffin instead of in water; also the value of N was a little different. Taking all this into account

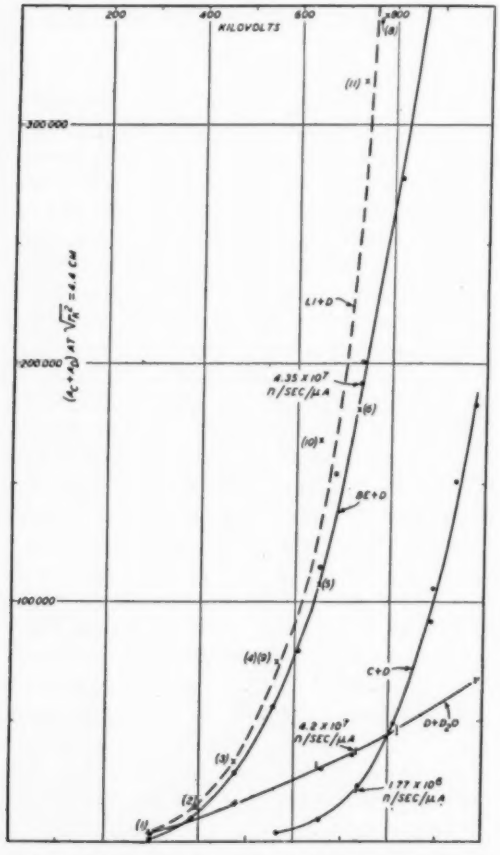

FIG. 7. Thermal neutrons at fixed distance, source at various voltages, for several deuteron reactions. (For absolute yield multiply curve for D+D_2O by 0.93.)

we find from the data of Amaldi and Fermi a value of 24,000 neutrons per second per millicurie. Thus in spite of the slightly higher value of $\int B_C d\tau$ we find a lower number of neutrons. This result is due in great part to the fact that the area of the detector of Amaldi and Fermi is larger than the area of our detector. It may be recalled that the rhodium used by Amaldi and Fermi[1] was 0.36 g/cm² thick ($\delta_{eff}=0.108$ g/cm²) and 28 cm² in area. The activity measured with the ionization chamber is not proportional to the area because beta particles emitted close to the edge of the detector "see" the ionization chamber through a smaller solid angle. It would be more correct to introduce an effective surface $S_{eff}<S$ whose value would depend on the geometrical disposition of the chamber. We will neglect this correction and conclude that the number of neutrons emitted from a source of (Rn+Be) is about 25,000 neutrons per second per millicurie.

If we remember that the alpha-particles of Ra C′ (7.68×10^6 volts) are at least three times more efficient[1] than the alpha-particles of Rn (5.49×10^6 volts) and Ra A (6.00×10^6 volts), which are also active in (Rn+Be) neutron sources, we can conclude that $(5\times3.7\times10^7/2.5\times10^4)$ $\leqq$7000 alpha-particles of 5.5 to 6 million volts energy impinging on Be are necessary for the emission of one neutron. The yield found by this method is much higher than the yield given for this reaction by other authors.[6] We must notice further, however, that in a source of the type used by Amaldi and Fermi a non-negligible fraction of the alpha-particles emitted from (Rn+Ra A+Ra C) impinges on the walls of the small glass tube and not on Be. The error due to this fact is in the sense that even the above yield of the beryllium reaction is too low.

(D+D)

The reaction which gives the neutrons in this case is

$$_1D^2+D^2\rightarrow{}_2He^3+{}_0n^1.$$

The target, the constancy of which was tested by the satisfactory consistency of our observed points on the neutron yield curve during two days of observations, was prepared by adding excess heavy water (99 percent) to dry P_2O_5 in a copper cup and inserting this target immediately into the tube. It is unfortunate that we had time

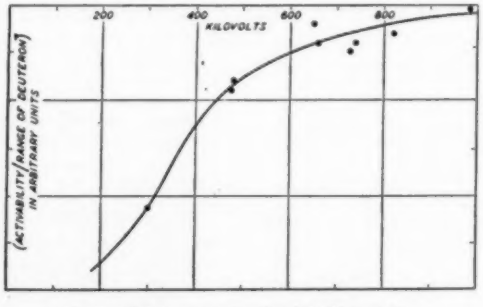

FIG. 8. Efficiency curve for D+D reaction.

[6] See, for example, R. Jaeckel, Zeits. f. Physik **91**, 493–510 (1934); F. A. Paneth and H. Loleit, Nature **136**, 950 (1935); F. A. Paneth and E. Glückaut, Proc. Roy. Soc., **A157**, 412 (1936); G. A. Fink, Phys. Rev., **50**, 738 (1936).

to make observations only on a single deuterium target. It obviously would be desirable to check the yields observed by measurements on other targets, with independent chemical analyses, but opportunity for this has not been presented. We have no reason to suspect our present results, but the possibility of an error of a few percent should be borne in mind (percentage of water in P_2O_5 mixtures depends on the equilibrium reached).

In order to determine the percentage of deuterium in the target, we adopted the following procedure: In removing the target a stopwatch was started at the instant when air was allowed to come in contact with the target, and then the increase in weight was observed as a function of time by frequent measurements on a sensitive balance over a period of about 15 minutes. It was found that the weight increased linearly due to the absorption of water from the air. Extrapolating to time zero, the weight of the target as bombarded was found to be 0.460 gram.

By chemical analysis, for which we are indebted to Dr. P. H. Emmett of the United States Department of Agriculture, it was found that the quantity of P_2O_5 contained in the target was 0.342 gram, and a sample of the original dry P_2O_5 showed that this material contained 1.4 percent of (ordinary) water. The quantity of heavy water in this target, which was used for all the work here reported, was therefore $[0.460-(0.342+0.005)]=0.113$ gram. Since we used 99 percent heavy water, the amount of pure heavy water in our target was 0.112 gram.

In order to obtain the neutron yields from deuterium targets of other composition, or to calculate the absolute yield of the deuterium reaction, it is necessary to divide the observed yield by the fraction of the total stopping power of our $D_2O(P_2O_5)$ target, which was actually deuterium. Unfortunately, the stopping powers for no elements have been measured for deuterons. The stopping power of phosphorus for alpha-particles is not listed in the table given by Rutherford, Chadwick, and Ellis (p. 100) but the values for Si (1.23) and Cl (1.76) indicate that it may be reasonable to take 1.5 as the value for this element. The stopping power for protons of moderate velocity in hydrogen relative to air is given by Blackett and Lees,[7] being 0.24, 0.22, and 0.217 for protons of range 0.5, 1.0, and 2.0 cm, respectively. We accordingly accept 0.22 as reasonable for the stopping power of deuterons in deuterium, relative to air, for the velocities we have used. For alpha-particles in oxygen the SP relative to air varies from 1.07 to 0.98 (Rutherford, Chadwick and Ellis, p. 97). For our case in which the velocity of the particles is low, we have arbitrarily taken the SP of deuterons in

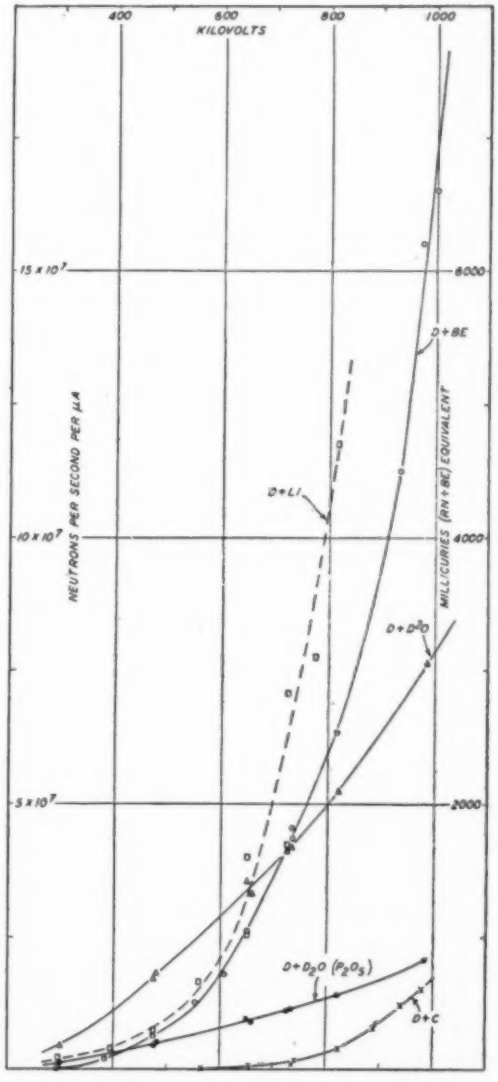

FIG. 9. Total neutron yields at various voltages for several deuteron reactions. (Multiply curve for D+D₂O by 0.93.)

[7] P. M. S. Blackett and D. S. Lees, Proc. Roy. Soc. **A134**, 658–671 (1932).

TABLE II. *(D+Be) distribution of thermal neutrons in water.*

	734 kv					936 kv		
$(r_k^2)^{\frac{1}{2}}$	A_C+A_D	A_D	A_D corr.	A_C	A_Cr^2	A_C+A_D	A_C	A_Cr^2
2.45	198500	22400	21600	176900	1060000			
4.4	192000±200	18000	17400	174600	3340000	494000±6500	446000	8520000
6.7	144000	12500	12100	131900	5930000	360000	330000	14850000
9.1	90800		(6170)	84630	6980000			
11.5	57400		(3620)	53780	7160000	139000	130000	17300000
13.9	32400		(1850)	30550	6010000			
16.5	18100		(1030)	17070	4640000	46800	44100	12000000
21.5	6840		(390)	6450	2980000	16200	15300	7070000
26.5	2570		(150)	2420	1690000	5690	5370	3750000

oxygen as unity relative to air. The total stopping power of our target was accordingly

$$\begin{aligned}SP&=(0.112/20)(2\times0.22+1)\\&\quad+(0.342/142)(2\times1.5+5\times1)\\&\quad+[(0.005+0.001)/18](2\times0.22+1)\\&\quad=0.00807+0.01927+0.00048=0.0278.\end{aligned}$$

Of this total stopping power 0.00807, or 29 percent, was then due to D_2O. The stopping power of the deuterium alone was $(0.44/1.44)=30.6$ percent of the stopping power of the heavy water, or 8.88 percent of the total target. [Note: The curves for $(D+D_2O)$ in Figs. 7 and 9 are drawn assuming 27 percent, instead of 29 percent, for the stopping power of the heavy water in our target, on the basis of preliminary calculations.]

In Table I are collected the experimental data for an energy of the impinging deuterons of 738 kv. The third column contains the total activability of our detector at different distances; we give the quadratic error calculated from two or three readings for each value. Column four contains the rhodium activability with a cadmium sheet on both sides of the detector, as measured on the rhodium face towards the source. Column five contains the preceding value multiplied by 1.93/2; the values in brackets are calculated as explained above. Columns six and seven represent respectively A_C (difference of the data of columns three and five) and $A_Cr_k^2$.

This last can be extrapolated for large values of r by means of the exponential $7.1\times10^6e^{-r/10}$; we find

$$\begin{aligned}\int_0^{24}A_Cr^2dr+7.1\times10^6\int_{21}^{\infty}e^{-r/10}dr\\=26.5\times10^6+6.4\times10^6=32.9\times10^6.\end{aligned}$$

Using the value $B_C(4.4)=(12400+11100)/2-3980=7770$ we have

$$\int B_Cd\tau=4\pi(7770/33500)32.9\times10^6=9.58\times10^7.$$

Therefore, $Q/i=1.13\times10^7$ neutrons per second per microampere of deuterons at 738 kv impinging on the heavy phosphoric acid target. In order to obtain the number of neutrons corresponding to a heavy water target, we must divide the preceding value by 0.29; we have, therefore, $Q/i=3.90\times10^7$ neutrons per second per microampere of deuterons at 738 kv impinging on a heavy water target. For a pure deuterium target we again divide this value by 0.31, and since one microampere corresponds to 6.25×10^{12} deuterons per second we have a yield corresponding roughly to 43,000 deuterons of energy 738 kv impinging on a pure deuterium target per neutron emitted. We must notice that the value of $\int B_Cd\tau$ changes only by six percent if we extrapolate A_Cr^2 with $e^{-r/13}$; from this example we see that the number of neutrons emitted from a source found by this method is not very sensitive to errors in the value of Λ.

In order to determine the yield of this reaction as a function of the voltage, we have measured

TABLE III. *(D+C) at 735 kv, distribution of thermal neutrons in water.*

$(r_k^2)^{\frac{1}{2}}$	A_C+A_D	A_D	A_D corr.	A_C	A_Cr^2
2.45	25400±500	3440	3320	22080	132500
4.4	21900±600	2860	2760	19140	366000
6.7	13500±600	1350	1300	12200	549000
9.1	6710±150		(537)	6170	509000
11.5	2760±200		(193)	2570	342000
13.9	1210± 40		(79)	1130	222000
16.5	526± 20		(34)	492	134000

the total activity of our rhodium detector at a given distance from the source $[(r_k^2)^{\frac{1}{2}}=4.4$ cm$]$ for different energies of the impinging deuterons. The results are plotted in Fig. 7; some points are given with the quadratic error, the others were measured only once; some were measured hours later, or the next day, in order to check the constancy of the target. With a current of about 2 microamperes we see that the target is very satisfactory on this point. The arrow corresponds to the energy of the impinging deuterons of 738 kv, for which we have determined the number of emitted neutrons from the above experiment.

In Fig. 8 is plotted the ratio of the activabilities of rhodium given in Fig. 7 to the range of deuterons, against the energy of these last; in order to calculate the range of the deuterons, we have used the data of Blackett and Lees[7] on the range of protons of low energy in hydrogen. We have made the reasonable assumption that a deuteron of a given velocity, having an energy twice that of a proton, also has a double range. There is some indication from Fig. 8 that for low energies of the impinging deuterons the yield increases more than the range; for energies higher than 500 kv the ratio yield to range seems to be constant.

(D+Li)

The reactions involved are probably ${}_3Li^7+{}_1D^2 \rightarrow {}_4Be^8+{}_0n^1$ and ${}_3Li^7+{}_1D^2 \rightarrow 2{}_2He^4+{}_0n^1$. Some undoubtedly also arise from Li^6 reactions. The target of lithium was cut under petroleum and was put in a tube in a current of helium; nevertheless, the readings did not check one another, the yield increasing with continued bombardment. Therefore, we did not measure the curve of the activity as a function of the distance from the source at a given voltage, but only some points of the yield curve at a given distance $[(r_k^2)^{\frac{1}{2}}=4.4$ cm$]$ as a function of the voltage. In Fig. 7 the points measured for this reaction are indicated by small crosses; the number written against each cross corresponds to the order of the successive readings. The points do not repeat; nevertheless, we can conclude that, on the average, they are a little higher than the points of Be for the same voltage. If we take into account the fact that the neutrons emitted from Li are faster than neutrons emitted from Be^8 we conclude that Li emits, for the same energy of the impinging deuterons, more neutrons than Be. This reaction must be further investigated. The excitation curve (total neutrons emitted) for Li given in Fig. 9 is calculated assuming that the $A_c r^2$ curve for Li is the same as that measured for Be.

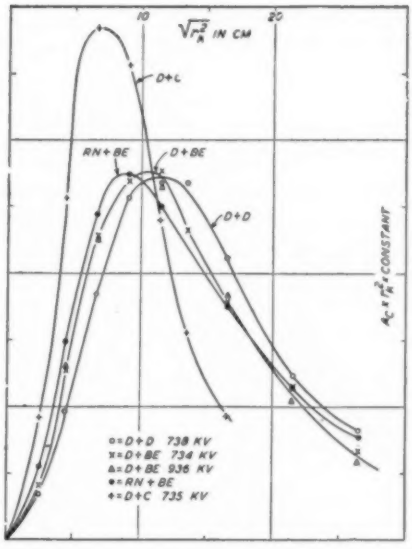

FIG. 10. Thermal neutrons in water between successive spherical shells (ordinates adjusted to give equal areas under curves).

(D+Be)

The reaction is ${}_4Be^9+{}_1D^2 \rightarrow {}_5B^{10}+{}_0n^1$. The Be target was a piece of solid metallic beryllium (impurity one percent of iron). Table II is similar to Table I; the activability as a function of the distance was measured for two different energies of the impinging neutrons, namely, 734 and 936 kv. The two curves are proportional. $A_c r^2$ can be represented fairly well for large values of r by $4.5\times10^7\times e^{-r/8}$ at 734 kv and by $10.3\times10^7\times e^{-r/8}$ at 936 kv.

At 734 kv we have

$$\int_0^{24} A_c r^2 dr + 4.5\times10^7 \int_{24}^{\infty} e^{-r/8} dr$$
$$= 10.37\times10^7 + 1.79\times10^7 = 12.16\times10^7.$$

[8] T. W. Bonner and W. M. Brubaker, Phys. Rev. **48**, 742–746 (1935).

From the value $B_C(4.4)=(64900+53800)/2-17400=41900$ we have

$$\int B_C d\tau = 4\pi(41900/175000)1.22\times10^8=3.68\times10^8.$$

We conclude $Q/i=4.35\times10^7$ neutrons per second per microampere of deuterons at 734 kv impinging on Be, or $(6.25\times10^{12})/(4.35\times10^7)=144000$ deuterons at 734 kv impinging on Be per neutron emitted. The curve of the total activability at a given distance $[(r_k^2)^{\frac{1}{2}}=4.4$ cm$]$ as a function of the voltage is given in Fig. 7; the arrow corresponds to 4.35×10^7 neutrons per second per microampere, as found above.

(D+C)

The reaction is ${}_6C^{12}+{}_1D^2\rightarrow{}_7N^{13}+{}_0n^1$. The target was a piece of Acheson graphite. Table III is similar to Tables I and II for an energy of the impinging deuterons of 735 kv. $A_C r^2$ is represented fairly well for large values of r, by $3.64\times10^6\times e^{-r/5}$. We have

$$\int_0^{16} A_C r^2 dr+3.64\times10^6\int_{16}^{\infty} e^{-r/5}dr = 51.2\times10^5+7.4\times10^5=58.6\times10^5.$$

$B_C(4.4)=(7450+5880/2)-2760=3900$; $\int B_C d\tau = 4\pi(3900/19100)5.86\times10^6=15\times10^6 Q/i=1.77\times10^6$ neutrons per second per microampere of deuterons at 735 kv impinging on C, or 3,500,000 deuterons of 735 kv energy impinging on C per neutron emitted. Fig. 7 contains also the neutron yield of carbon as a function of the voltage of the impinging deuterons.

Summary and Discussion

Neutron yields

Since, due to differences in initial neutron energies, the numbers of neutrons emitted in various reactions are not directly proportional to the activabilities, the data of Fig. 7 have been replotted in Fig. 9 with a uniform scale for neutron yields per microampere. In other words, the total yield of neutrons has been evaluated from $\int A_C r^2$ or by measuring the distribution of thermal neutrons throughout the water tank at a particular value of the bombarding voltage (indicated by an arrow for each curve of Fig. 9), and this total yield has been multiplied by the ratio of the activabilities of the rhodium detector at a fixed position in the water for the different voltages used, thus giving the total neutron yield as a function of the voltage for each reaction. The distribution curve in water is thus assumed not to vary appreciably with the energy of the incident neutrons. Adopting from above the value 1 mC (Rn+Be) $\leqq$25000 neutrons per second, an immediate comparison with radon-beryllium sources can be made. This comparison is given by the second scale of ordinates. For convenient reference curves for both (D+D_2O) and [D+$D_2O(P_2O_5)$] have been given.

These results may be compared with those of other investigators. The first measurements on the yield of the (D+D) neutron reactions are due to Oliphant, Harteck, and Rutherford.[9] In order to compare our value with their result, we may make use of the yield ratio of 8 for 300 kv to 100 kv deuterons given by Ladenburg and Roberts.[10] With our data this gives a yield of one neutron per 4×10^6 deuterons at 100 kv to be compared with that of one per 1×10^6 reported by the Cavendish investigators, and one per 6×10^6 reported by Ladenburg and Roberts. These results, as well as those of Alexopoulos[11] who gives a yield of one neutron per 0.7×10^6 deuterons at 140 kv, may therefore be considered to be in reasonably good agreement, since hitherto no method involving the integration of the total neutron intensity has been used. The results of Alexopoulos[11] appear to be open to question.

Agreement is also obtained with the observation of Ladenburg, Roberts, and Sampson[12] that at 100 kv a total ion current of 100 microamperes produces an activity in silver equal to that produced by 400 mC of (Rn+Be) if we assume that 10 percent of their beam was deuterons, which appears reasonable.

However, at 730 kv Bonner and Brubaker[13]

[9] Oliphant, Harteck, and Rutherford, Proc. Roy. Soc. **A144**, 692–703 (1934).
[10] Ladenburg and Roberts, Phys. Rev. **50**, 1190 (1936).
[11] K. D. Alexopoulos, *Promotionsarbeit von der Eidg. Tech. Hochschule* (Zürich, 1935); H. Kallman and E. Kuhn, Naturwiss. **15**, 231–232 (1937).
[12] Ladenburg, Roberts, and Sampson, Phys. Rev. **48**, 467 (1935).
[13] Bonner and Brubaker, Phys. Rev. **49**, 19–21 (1936).

give a yield for the (D+D) reaction of only one neutron per 10^7 deuterons, which is two hundred times smaller than our yield at that voltage. Similarly, for the (D+Be) reaction their yield at 730 kv is about one per 5.5×10^7 compared to our yield of one per 1.4×10^5, again smaller by a factor of several hundred. Crane, Lauritsen, and Soltan[14] have given yields which are also very low. These large differences between the Pasadena results and our own are probably to be ascribed to their use of an alternating current voltage on their tube and lack of analysis of the ion-beam striking their targets.

Extrapolating our data for the (D+Be) reaction to 1300 kv, we find that the yield reported by Livingston, Henderson, and Lawrence[15] is 30 times *smaller* than we would expect at this voltage, while at 5 million volts Lawrence and Cooksey[16] report a neutron yield more than 10^5 times that from one curie of (Rn+Be) when a beryllium target is bombarded by 7 microamperes of deuterons. This is a yield per microampere more than 2000 times *larger* than our yield, and much larger than can be accounted for by assuming a Gamow exponential and extrapolating from one million to five million volts, taking into account the increased deuteron range. The Berkeley value corresponds to an absolute yield of one neutron emitted per 17 incident deuterons.[17]

Neutron energies

The space distributions of thermal neutrons from the different sources are not determined accurately enough in our observations to permit a calculation of the mean value of the square of the distance from the source. We can, however, make some qualitative considerations by comparing the space distributions of thermal neutrons from different sources in order to interpret our curves in terms of known data on the energy of the emitted neutrons. In Fig. 10 the curves of Fig. 6, reduced to the equal areas from 0 up to $(r_k^2)^{\frac{1}{2}}=24$ cm, are drawn. We have used this normalization, instead of dividing by the area of the curves from zero up to infinity, in order to avoid introducing uncertainties due to the values of Λ.

From Fig. 10 we see that the maxima of the curves are at different distances from the source. The order of decreasing distance is (D+D), (D+Be), (Rn+Be), (D+C). The neutrons emitted from monochromatic artificial sources have somewhat different energies in different directions with respect to the incident beam, following the law of conservation of momentum. In the case of (D+D), with an energy of 1000 kv for the incident particles, the energy of the neutrons emitted at 90° to the beam will be about 2.5 million volts according to Bonner and Brubaker.[18]

The neutrons emitted from carbon reaction have a very low energy; the data of Tuve and Hafstad[19] indicate (at 735 kv for the impinging deuterons) an upper limit of 1000 kv. The data of Bonner and Brubaker[20] (reaction energy −0.37 million volts) give 240 kv for neutrons at 90° with the impinging beam. The neutrons emitted from this reaction are also homogeneous; therefore, the position of the maxima of the curves given in Figs. 5, 6, 8, and 10 is connected with the law by which the same curves decrease for large values of r.

In the case of (D+Be) and (Rn+Be) the spectrum of the emitted neutrons is complex.[20, 21] Therefore, it is possible to have curves with the maxima very close to the source and decreasing at the same time only slowly with the distance from the source. Such a behavior must be interpreted as due to the superposition of neutrons of very low and very high energy. This seems to be the case of (Rn+Be). The curve of this reaction has the maximum closer to the source than the curve of (D+Be), and at the same time there is some indication that

[14] Crane, Lauritsen, and Soltan, Phys. Rev. **45**, 507–512 (1934).
[15] Livingston, Henderson, and Lawrence, Phys. Rev. **44**, 782 (1933).
[16] Lawrence and Cooksey, Phys. Rev. **50**, 1131–1140 (1936).
[17] While working on another problem we have observed that the neutrons and gamma-rays from D+Be at 1000 kv give discharge rates per microampere for a Victoreen condenser dosimeter roughly 1/100 of the rates reported for a duplicate instrument at Berkeley when operating the cyclotron at 5 to 6 Mev. This would indicate any equivalent neutron yield of 10^4 curies from the cyclotron, in agreement with Aebersold's later estimate.
[18] Bonner and Brubaker, Phys. Rev. **49**, 19–21 (1936).
[19] Tuve and Hafstad, Phys. Rev. **48**, 106–107 (1935).
[20] Bonner and Brubaker, Phys. Rev. **50**, 308–314 (1936).
[21] J. R. Dunning, Phys. Rev. **45**, 586–600 (1934); G. Bernardini and D. Bocciarelli, Ricerca Scient. **7**, 129 (1936), and Rend. Acc. Lincei **24**, 132 (1936).

for high values of r it decreases more slowly. We know that from the (Rn+Be) reaction there are emitted, in considerable numbers, neutrons of 4.8 to 6.5 million volts energy. If we could measure the space distribution up to higher distances, we must expect the curve of (Rn+Be) to decrease more slowly than the curve of (D+D). The small distance from the source of the maximum of the curve of (Rn+Be) and also the high absolute number of neutrons found with our method for this reaction indicate that relatively high numbers of neutrons of low energy are emitted from (Rn+Be) sources.

The (D+Be) reaction gives rise also to a complex spectrum of neutrons as shown by Bonner and Brubaker;[20] from the spectrum given by these authors it seems reasonable to find that the curve of Fig. 10 relative to this reaction has the maximum closer to the source than does the (D+D) reaction.

Artificial production of radioactive isotopes

The problem of evaluating the quantity of artificial substances that can be prepared using slow neutrons is now reduced to the evaluation of the fraction of the neutrons emitted from a source which can be absorbed from the substance we wish to make radioactive. It is evident that the most convenient way is to irradiate substances in solution.

First, we must choose the dimensions of the tank containing the solution corresponding to the distribution of thermal neutrons in water of the source of fast neutrons used. By surrounding the solution tank with water we will avoid the border disturbance, and we will be able to evaluate the fraction of fast neutrons lost. For instance, with a source of (D+Be) and a solution tank of 50 cm diameter we lose 15 percent of the fast neutrons emitted from the source. The remaining 85 percent is slowed down by the water and is absorbed by the hydrogen atoms ($\sigma_H = 0.31 \times 10^{-24}$ cm^2) or by other nuclei present in solution ($\sigma_A = KM1.66 \times 10^{-24}$ cm^2, where K is absorption coefficient for thermal neutrons in cm^2/g, and M is atomic mass). In order to obtain a reasonable quantity of radioactive substance of a kind A, we need to prepare a solution with a concentration n_A large enough to have $\sigma_A n_A$ of the same order of magnitude or larger than $\sigma_H n_H$. This condition can be easily satisfied for many elements. The difficulty arises in many cases when we need to concentrate the active product by chemical separation, following the method of Szilard and Chambers.[22] In other cases, however (iodine, manganese, arsenic, etc.), very simple processes are known which may be used to separate the active material. For instance, by irradiating a concentrated solution of sodium permanganate of convenient dimensions it is possible to absorb about 50 percent of the emitted fast neutrons; the active material can be separated by a simple filtration.

Assuming the useful absorption of 20 percent of the neutrons emitted, the number of millicuries of an activated radio element produced by bombardment for a time equal to twice the half-life of the element produced is conveniently obtained by dividing the (Rn+Be) equivalent of the artificial neutron source, expressed in millicuries, by the approximate factor 10,000. This factor is obviously independent of the half-life of the radio element produced.

[22] L. Szilard and T. A. Chambers, Nature **134**, 462 (1934).

Radiation Probabilities, Auger Effect and Energy Level Widths for Au(79)

E. G. RAMBERG* AND F. K. RICHTMYER†
Cornell University, Ithaca, New York

(Received April 7, 1937)

The theory of energy level widths developed by Weisskopf and Wigner and by Wentzel is applied to the calculation of the energy level widths of Au(79). Radiation and Auger transition probabilities are determined separately with the aid of numerically integrated nonrelativistic eigenfunctions, the latter being calculated for electrons moving in the Fermi-Thomas field of $Tl(81)^{++}$. Sources of error are considered, the major one being the nonrelativistic treatment. The band width due to the interaction of electrons in different atoms in the crystal lattice does not add materially to the level width of the O_I and lower states. Except for the K state, the Auger contribution to the width exceeds that of the radiation transitions. Where the majority of the significant Auger effects have been calculated (L_I, M_I, N_I) the total calculated width is found to be appreciably in excess of the observed width, but of the same order. The results confirm the view that the contributions of radiation transitions and Auger effects to the level widths of the initial and final states of the atom suffice to explain the magnitude of the widths of the x-ray lines emitted by the heavy elements.

I. INTRODUCTION

WITHIN recent years improvements in experimental techniques and measurements made by use of the two-crystal spectrometer have made it possible to obtain dependable estimates of the true shape and widths of spectral lines in extended regions of the x-ray spectrum. It has been found (1) that the shape, or contour, of lines agrees well within experimental error[1] with that predicted by either the classical or the quantum theory of radiative processes; but (2) that x-ray lines are in general much wider than either theory predicts.

Classically,[2] an emitting atom is treated as a damped harmonic oscillator whose energy at time t is proportional to $e^{-2\pi\Gamma t}$. A Fourier analysis of the emitted wave train gives a spectral energy distribution, $J(\nu)d\nu$, as follows:

$$J(\nu)d\nu=\frac{\Gamma}{2\pi}\cdot\frac{d\nu}{(\nu_0-\nu)^2+(\Gamma/2)^2}. \qquad (1)$$

where ν_0 is the frequency of the undamped oscillator and Γ is the full width of the contour at half-maximum intensity.

In quantum theory, it is assumed that the probability that in unit time an atom in state A may pass, at time t, to any other state is equal to $2\pi\Gamma_A$. The mean life of state A is then given by $1/(2\pi\Gamma_A)$. Weisskopf and Wigner[3] have shown by a wave-mechanical treatment, that on these assumptions the spectral intensity distribution in a spectral line resulting from transitions from state A to state B is given by (1) provided we put

$$\Gamma\equiv\Gamma_A+\Gamma_B, \quad h\nu_0\equiv E_A-E_B=h\nu_{AB},$$

where $1/(2\pi\Gamma_A)$ and $1/(2\pi\Gamma_B)$ are the mean lives, and E_A and E_B the atomic energies of states A and B, respectively. True line width, therefore, is an atomic phenomenon and is determined by the mean lives of the initial and the final states of the emitting atoms.

The mean life of any atomic state is determined by two factors: (1) the probability that, in unit time, the atom may pass spontaneously from that state to a state of lower energy with the emission of radiation (radiation transition); and (2) that it may change to a new state without the emission of radiation, the energy freed by filling a vacancy in an inner electron shell being used to expel a less tightly bound electron (Auger effect). The present work was undertaken to determine the relative importance of the several radiation and Auger transitions for different states of

* At present with Electronic Research Laboratory, RCA Manufacturing Company, Camden, N. J.

† This research was made possible by a grant from the American Philosophical Society. F. K. R.

[1] The troublesome instrumental correction due to the finite resolving power of the spectrometer, is in general small compared to the total width of lines. See Parratt, Rev. Sci. Inst. 6, 387 (1935).

[2] For an outline of the classical and of the quantum theory of line widths, including references to original sources, see "The Widths of the L-Series Lines and of the Energy Levels of Au(79)," by F. K. Richtmyer, S. W. Barnes and E. Ramberg, Phys. Rev. 46, 843 (1934), hereinafter referred to as RBR.

[3] V. Weisskopf and E. Wigner, Zeits. f. Physik 63, 54 (1930).

excitation; and also to ascertain whether the observed width of x-ray spectral lines could be thus explained. Au(79) was chosen as the element to be studied, since the measurements of RBR on its L series lines furnish adequate experimental data for comparison with theory.

II. Definitions and General Formulas

According to the above mentioned theory of natural line widths proposed by Weisskopf and Wigner the energy distribution in a spectral line of frequency ν_{AB}, corresponding to a transition from atomic state A to atomic state B, is given by

$$J_{AB}(\nu)d\nu=\frac{(\Gamma_A+\Gamma_B)d\nu/(2\pi)}{(\nu_{AB}-\nu)^2+[(\Gamma_A+\Gamma_B)/2]^2}. \quad (1')$$

$(\Gamma_A+\Gamma_B)$ is the width at half-maximum (or simply "the width") of the line on a frequency scale. Γ_A and Γ_B individually represent, but for a factor $1/(2\pi)$, the sum of the probabilities of all spontaneous transitions from state A or B respectively to any other state and will be termed, for convenience, the frequency widths of the energy levels A and B:

$$\Gamma_A=\frac{1}{2\pi\tau_A}=\sum_{E_C\leq E_A}{}'(C)\gamma_{AC},$$
$$\Gamma_B=\frac{1}{2\pi\tau_B}=\sum_{E_D\leq E_B}{}'(D)\gamma_{BD}, \quad (2)$$

where τ_A is the mean life of state A; and $2\pi\gamma_{AC}$ is the probability in unit time of a transition from state A to any state C. E_C and E_A represent, respectively, the atomic energies for state C and state A. The sign "$<$" under the sum refers to the radiation transitions; the sign "$=$" to the Auger jumps. In order to calculate the magnitude of Γ_A for any particular level A we substitute for γ_{AC} the known expression for the transition probabilities in the form of matrix elements of the coordinates and of the electronic interaction energies:[4]

$$\Gamma_A/R=\sum_{E_C<E_A}(C)\frac{\alpha^3}{3}(\nu_{AC}/R)^3\{|(A|\sum_i x_i/a_0|C)|^2$$
$$+|(A|\sum_i y_i/a_0|C)|^2+|(A|\sum_i z_i/a_0|C)|^2$$
$$+\sum_{E_D<E_A}(D)\frac{\alpha^5}{240}(\nu_{AD}/R)^5\{|(A|\sum_i x_i^2/a_0^2|D)|^2$$
$$+|(A|\sum_i y_i^2/a_0^2|D)|^2+|(A|\sum_i z_i^2/a_0^2|D)|^2$$
$$+3|(A|\sum_i x_iy_i/a_0^2|D)|^2+3|(A|\sum_i y_iz_i/a_0^2|D)|^2$$
$$+3|(A|\sum_i z_ix_i/a_0^2|D)|^2$$
$$-(A|\sum_i x_i^2/a_0^2|D)(A|\sum_i y_i^2/a_0^2|D)$$
$$-(A|\sum_i y_i^2/a_0^2|D)(A|\sum_i z_i^2/a_0^2|D)$$
$$-(A|\sum_i z_i^2/a_0^2|D)(A|\sum_i x_i^2/a_0^2|D)\}$$
$$+\sum_{E_G=E_A}{}'(G)4\pi|(A|\sum_{i>k}a_0/r_{ik}|G)|^2, \quad (3)$$

where $$(A|F|N)=\int\Psi_A^*F\Psi_N d\tau.$$

Ψ_A is the wave function of the atom in state A. The integration has to be carried out over the coordinates of all the atomic electrons. The first two terms in the expression (3) are the contributions to the level widths due to radiative transitions, dipole and quadrupole, respectively;[5] the last that due to Auger jumps; $\alpha=2\pi e^2/(ch)$ is the fine structure constant; $a_0=h^2/(4\pi me^2)$, the radius of the Bohr orbit for normal hydrogen; and the subscripts i and j refer to the number of the atomic electrons.

The above formula is greatly simplified if we treat all of the electrons of the atom as moving in the same central field. We may then represent the atomic wave-function by a determinant[6] of

[4] G. Wentzel, *Handbuch der Physik*, Vol. 24, part 1 (1931): p. 779 for the dipole component and p. 783 for the quadrupole component of the radiative transitions; p. 736 for the Auger effects.

[5] The formula given assumes real wave functions.

[6] The sums of the squared absolute values of the matrix elements over the magnetic quantum numbers of states C, D and G pertaining to given n_i, l_i, j_i are invariant under unitary transformations of the wave functions, so that this simplest form of an antisymmetrical wave function leads to the correct result.

individual electronic wave functions characterized by the quantum numbers n, l, j, m_j:

$$\Psi_A=\begin{vmatrix}\psi_1(1) & \psi_1(2) & \cdots & \psi_1(z-1)\\ \cdots & \cdots & \cdots & \cdots\\ \psi_{A-1}(1) & \psi_{A-1}(2) & \cdots & \psi_{A-1}(z-1)\\ \psi_{A+1}(1) & \psi_{A+1}(2) & \cdots & \psi_{A+1}(z-1)\\ \cdots & \cdots & \cdots & \cdots\\ \psi_z(1) & \psi_z(2) & \cdots & \psi_z(z-1)\end{vmatrix}/((z-1)!)^{\frac{1}{2}}, \quad (4)$$

where $$\psi_i(1)=P_{l_ij_i}^{m_{ji}}(\vartheta_1, \varphi_1, \mu_1)f_i(r_1)/r_1 \quad (5)$$

and $$\int\psi_i(1)\psi_j(1)d\tau=\delta(i, j). \quad (6)$$

In greater detail the angular function (with spin) is given by[7]

$$P_{lj}^{m_j}=\{\pm(l\pm m_j+\tfrac{1}{2})^{\frac{1}{2}}P_l^{m_j-\frac{1}{2}}(\vartheta, \varphi)\delta(\tfrac{1}{2}, \mu)$$
$$+(l\mp m_j+\tfrac{1}{2})^{\frac{1}{2}}P_l^{m_j+\frac{1}{2}}(\vartheta, \varphi)\delta(-\tfrac{1}{2}, \mu)\}/(2l+1)^{\frac{1}{2}} \quad (7)$$

for $j=l\pm\frac{1}{2}$, P_l^m being the associate Legendre function of order l and degree m normalized to 1. μ indicates the spin of the electron. The angular function has the following property:

$$\sum_{\mu=\pm\frac{1}{2}}\int_0^{2\pi}\int_0^{\pi}P_{lj}^{*m_j}(\vartheta, \varphi)P_{l'j'}^{m_j'}(\vartheta, \varphi)\sin\vartheta d\vartheta d\varphi$$
$$=\delta(l, j, m_j; l', j', m_j'). \quad (8)$$

If we substitute wave functions of the form (5) in the formula for the level width (3) we obtain:

$$\Gamma_A/R=\sum_{E_C<E_A}(\alpha^3/3)(\nu_{AC}/R)^3a(l_Aj_A; l_Cj_C)$$
$$\times\left|\int_0^{\infty}f_A(r/a_0)f_Cdr\right|^2+\sum_{E_D<E_A}(\alpha^5/240)(\nu_{AD}/R)^5$$
$$\times b(l_Aj_A; l_Dj_D)\left|\int_0^{\infty}f_A(r/a_0)^2f_Ddr\right|^2$$
$$+4\pi\sum_{\substack{k,\ j,\ li\\ E_i=-E_A+E_k+E_m\geqq 0}}\sum_{\kappa,\ \kappa'}\{c(l_kj_k, l_mj_m; l_ij_i, l_Aj_A; \kappa\kappa')$$
$$\times(kmG^{\kappa}iA)(kmG^{\kappa'}iA) \quad (9)$$
$$-d(l_kj_k, l_mj_m; l_ij_i, l_Aj_A; \kappa\kappa')(kmG^{\kappa}iA)(kmG^{\kappa'}Ai)$$
$$+e(l_kj_k, l_mj_m; l_ij_i, l_Aj_A; \kappa\kappa')(kmG^{\kappa}Ai)(kmG^{\kappa'}Ai)\}.$$

Here A refers to the initial vacancy; C, D, k and m to the vacancies in the several final states of the atom; and i to the expelled electron in the case of an Auger transition. Furthermore

$$(kmG^{\kappa}iA)=\int_0^{\infty}\int_0^{\infty}f_k(1)f_m(2)$$
$$\times(a_0r_a^{\kappa}/r_b^{\kappa+1})f_i(1)f_A(2)dr_1dr_2 \quad (10)$$

with $r_a=r_1$, $r_b=r_2$ for $r_2>r_1$,
$r_a=r_2$, $r_b=r_1$ for $r_2<r_1$.

If we sum over the j values pertaining to a given value of l_C we find for the angular coefficients in the first sum

$$a(l_A; l_C)=\sum_{jc}a(l_A, j_A; l_C, j_c)$$
$$=(1\pm1/(2l_A+1))\delta(l_C, l_A\pm1)/2. \quad (11)$$

Similarly, summing over j_D we find for

$$b(l_A; l_D)=\sum_{jD}b(l_A, j_A; l_D, j_D)$$

the values given in Table I. To obtain the angular coefficients a and b for specific j values recourse must be had to the sum rules and the formulas of A. Rubinowicz[8] for relative quadrupole intensities.

The angular coefficients c, d and e, finally, may be evaluated for each special case by the formulas for integrals over three associated spherical harmonics given by Gaunt.[9] The number of terms in the last sum increases rapidly with the azimuthal quantum number of the initial vacancy, l_A; for $l_A=0$ it reduces to three terms for given l and j values; for $l_A=1$ to eight terms. Thus for $l_A=0$ we can write for the contribution to Γ_A/R of the transition $A\rightarrow k, m; i$:

$$\Delta\Gamma_A/R=4\pi\{c(l_m, l_m)(kmG^{l_m}iA)^2$$
$$-d(l_m, l_k)(kmG^{l_m}iA)(kmG^{l_k}Ai)$$
$$+e(l_k, l_k)(kmG^{l_k}Ai)^2\}. \quad (12)$$

TABLE I. *Values of the coefficients* $b(l_A; l_D)$.

$l_A=$	0	1	2	3
l_D				
0			1/5	
1		2/5		3/35
2	1		2/7	
3		3/5		

[7] J. H. Bartlett, Jr., Phys. Rev. **35**, 230 (1930).

[8] A. Rubinowicz, Zeits. f. Physik **65**, 662–676 (1930).

[9] J. A. Gaunt, Phil. Trans. Roy. Soc. London **228**, 192 (1929); see also L. Pincherle, Nuovo Cimento **12**, 85–86 (1935).

The arguments of the coefficients indicate the values of κ and κ' in (9). Similarly for $l_A=1$ the contribution to the width is given by

$$\begin{aligned}\Delta\Gamma_A/R=4\pi\{&c(l_m-1,l_m-1)(kmG^{l_m-1}iA)^2\\&+c(l_m+1,l_m+1)(kmG^{l_m+1}iA)^2\\&-d(l_m-1,l_k-1)(kmG^{l_m-1}iA)(kmG^{l_k-1}Ai)\\&-d(l_m-1,l_k+1)(kmG^{l_m-1}iA)(kmG^{l_k+1}Ai)\\&-d(l_m+1,l_k-1)(kmG^{l_m+1}iA)(kmG^{l_k-1}Ai)\\&-d(l_m+1,l_k+1)(kmG^{l_m+1}iA)(kmG^{l_k+1}Ai)\\&+e(l_k-1,l_k-1)(kmG^{l_k-1}Ai)^2\\&+e(l_k+1,l_k+1)(kmG^{l_k+1}Ai)^2\}.\end{aligned}\tag{13}$$

The calculated values of the coefficients for these two cases are tabulated in Tables II and III, respectively. Where two j values are indicated for a given state the coefficients pertaining to the separate j values have been added.

III. Calculation of the Radial Wave Functions and Matrix Elements

Having decided to make use of electronic wave functions calculated for a common central field it became necessary to determine what field might be most suitable. The Thomas-Fermi field for doubly ionized thallium, $Tl^{++}(81)$, was chosen since, for Auger electrons, it simulated most closely the field of a gold atom with two internal vacancies. For the most tightly bound electrons the error in the effective field is greatest. At the same time the fact that the atomic field itself is very strong makes this error relatively unimportant.

The Thomas-Fermi field for $Tl^{++}(81)$ was obtained by numerical integration of the Thomas-Fermi equation, applying the boundary conditions for the ion prescribed by Sommerfeld.[10] The integration was performed inward, the ionic radius being adjusted until the boundary condition at the nucleus (the existence of a Coulomb field corresponding to a nuclear charge 81) was fulfilled. The effective ionic radius was found to be 4.61 a_0.

With the potential field V thus determined the wave functions of all the electrons of the gold atom ($1s$, $2s$, $2p$, $3s$, $3p$, $3d$, $4s$, $4p$, $4d$, $4f$, $5s$, $5p$, $5d$, $6s$) were calculated by integrating the equation

$$(d^2/dr^2+E+2V-l(l+1)/r^2)f=0,\tag{14}$$

the energy parameter E being adjusted so as to satisfy the boundary conditions, in the manner suggested by Hartree.[11] In addition continuous

[10] A. Sommerfeld, Zeits. f. Physik **78**, 283–308 (1932), Eqs. (1) to (3a).

[11] D. R. Hartree, Proc. Camb. Phil. Soc. **24**, 89 (1928).

Table II. *Angular coefficients of Auger effect contributions to level width for $l_A=0$.*

l_k	j_k	l_m	j_m	l_i	κ	κ'	$c(l_m, l_m)$	$d(l_m, l_k)$	$e(l_k, l_k)$
0	1/2	0	1/2	0	0	0	1	1	1
1	3/2	0	1/2	1	0	1	4	4/3	4/9
	1/2		1/2				2	2/3	2/9
1	3/2	1	3/2	0	1	1	8/27	4/27	8/27
	1/2		3/2				4/27	8/27	4/27
	3/2		1/2				4/27	8/27	4/27
	1/2		1/2				2/27	−2/27	2/27
1	3/2	1	3/2	2	1	1	16/27	20/27	16/27
	1/2		3/2				8/27	4/27	8/27
	3/2		1/2				8/27	4/27	8/27
	1/2		1/2				4/27	8/27	4/27
2	5/2	0	1/2	2	0	2	6	6/5	6/25
	3/2		1/2				4	4/5	4/25
2	5/2	1	3/2	1	1	2	24/45	12/75	24/125
	3/2		3/2				16/45	28/75	16/125
	5/2		1/2				12/45	24/75	12/125
	3/2		1/2				8/45	−4/75	8/125
2	5/2	1	3/2	3	1	2	12/15	16/25	36/125
	3/2		3/2				8/15	4/25	24/125
	5/2		1/2				6/15	2/25	18/125
	3/2		1/2				4/15	8/25	12/125
2	5/2	2	5/2	0	2	2	18/125	6/125	18/125
	3/2		5/2				12/125	24/125	12/125
	5/2		3/2				12/125	24/125	12/125
	3/2		3/2				8/125	−4/125	8/125
2	5/2	2	5/2	2	2	2	36/175	24/175	36/175
	3/2		5/2				24/175	36/175	24/175
	5/2		3/2				24/175	36/175	24/175
	3/2		3/2				16/175	4/175	16/175
2	5/2	2	5/2	4	2	2	324/875	500/875	324/875
	3/2		5/2				216/875	56/875	216/875
	5/2		3/2				216/875	56/875	216/875
	3/2		3/2				144/875	288/875	144/875
3	7/2	0	1/2	3	0	3	8	8/7	8/49
	5/2		1/2				6	6/7	6/49
3	7/2	1	3/2	2	1	3	16/21	12/49	48/343
	5/2		3/2				4/7	20/49	36/343
	7/2		1/2				8/21	16/49	24/343
	5/2		1/2				2/7	−6/343	18/343
3	7/2	1	3/2	4	1	3	64/63	88/63	64/343
	5/2		3/2				16/21	8/49	48/343
	7/2		1/2				32/63	8/147	32/343
	5/2		1/2				8/21	16/49	24/343
3	7/2	2	5/2	1	2	3	216/875	72/1225	216/1715
	5/2		5/2				162/875	306/1225	162/1715
	7/2		3/2				144/875	288/1225	144/1715
	5/2		3/2				108/875	−36/1225	108/1715
3	7/2	2	5/2	3	2	3	32/125	80/525	32/245
	5/2		5/2				24/125	88/525	24/245
	7/2		3/2				64/375	80/525	64/735
	5/2		3/2				16/125	32/525	16/245
3	7/2	2	5/2	5	2	3	16/35	24/49	80/343
	5/2		5/2				12/35	4/49	60/343
	7/2		3/2				32/105	8/147	160/1029
	5/2		3/2				8/35	16/49	40/343
3	7/2	3	7/2	0	3	3	32/343	8/343	32/343
	5/2		7/2				24/343	48/343	24/343
	7/2		5/2				24/343	48/343	24/343
	5/2		5/2				18/343	−6/343	18/343
3	7/2	3	7/2	2	3	3	24/343	0	24/343
	5/2		7/2				32/343	56/343	32/343
	7/2		5/2				32/343	56/343	32/343
	5/2		5/2				128/1029	56/1029	128/1029
3	7/2	3	7/2	4	3	3	576/3773	72/539	576/3773
	5/2		7/2				432/3773	72/539	432/3773
	7/2		5/2				432/3773	72/539	432/3773
	5/2		5/2				324/3773	36/539	324/3773
3	7/2	3	7/2	6	3	3	3200/11319	5000/11319	3200/11319
	5/2		7/2				800/3773	200/3773	800/3773
	7/2		5/2				800/3773	200/3773	800/3773
	5/2		5/2				600/3773	1200/3773	600/3773

wave functions (with positive values for E, corresponding to the kinetic energy of the ejected Auger electron) were calculated from the differential equation and normalized by comparison with the asymptotic form of the wave function given by Kramers:[12]

$$f=(2/\pi)^{\frac{1}{2}}(E+2V-l(l+1)/r^2)^{-\frac{1}{4}}$$
$$\times\cos\left\{\int_R^r(E+2V(\rho)-l(l+1)/\rho^2)^{\frac{1}{2}}d\rho\right\}. \quad (15)$$

The lower limit of the integral was chosen so as to obtain coincidence of the zero points of the numerically integrated function and those of the asymptotic form. From a certain value of r on, i.e., where the variation of

$$(E+2V-l(l+1)/r^2)^{-\frac{1}{4}}$$

was slow compared to that of the cosine, it proved to be convenient and sufficiently accurate to calculate the wave function from this asymptotic expression.

The energy parameter of the Auger electron was set equal to the difference between the measured x-ray term value of the initial vacancy

[12] H. A. Kramers, Zeits. f. Physik **39**, 828 (1926).

TABLE III. *Angular coefficients of Auger-effect contributions to level width for* $l_A=1$.

j_A	l_k	j_k	l_m	j_m	l_i	$c(l_m-1, l_m-1)$	$c(l_m+1, l_m+1)$	$d(l_m-1, l_k-1)$	$d(l_m-1, l_k+1)$	$d(l_m+1, l_k-1)$	$d(l_m+1, l_k+1)$	$e(l_k-1, l_k-1)$	$e(l_k+1, l_k+1)$
3/2	0	1/2	1	3/2	0	2			2/3				4/27
		1/2		1/2									2/27
1/2		1/2		3/2									4/27
		1/2		1/2		2			2/3				2/27
3/2	0	1/2	1	3/2	2		2/25				2/15		8/27
		1/2		1/2			2/25				2/15		4/27
1/2		1/2		3/2			4/25				4/15		8/27
		1/2		1/2									4/27
1/2	1	3/2	1	3/2	1		16/125				4/125		16/125
		1/2		3/2			8/125			4/5		4	
		3/2		1/2		4			4/5				8/125
		1/2		1/2		2		2				2	
1/2	1	3/2	1	3/2	3		24/125				36/125		24/125
		1/2		3/2			12/125						
		3/2		1/2									12/125
		1/2		1/2			0						0
1/2	0	1/2	2	5/2	1								4/15
		1/2		3/2			6/49				2/7		32/105
1/2, 3/2	0	1/2	1	1/2, 3/2	0	2			2/3				2/9
					2		4/25				4/15		4/9
1/2, 3/2	1	1/2, 3/2	1	1/2, 3/2	1	6	24/125	2	4/5	4/5	4/125	6	24/125
					3		36/125				36/125		36/125
1/2, 3/2	2	3/2, 5/2	1	1/2, 3/2	0		4/25						
					2	10	8/35	4/3	6/7	4/15	4/15	4/9	
					4		72/175				12/245	8/9	54/343
											72/245		72/343
1/2, 3/2	3	5/2, 7/2	1	1/2, 3/2	1		36/125			36/125		36/125	
					3	14	112/375	6/5	8/9	24/125	10/189	54/125	32/243
					5		8/15				8/27		40/243
1/2, 3/2	0	1/2	2	3/2, 5/2	1	4/9			4/9				4/9
					3		6/49				2/7		2/3
1/2, 3/2	2	3/2, 5/2	2	3/2, 5/2	1	8/9	54/343	4/35	12/35	12/35	18/1715	8/9	54/343
					3	4/3	8/49	4/5	8/35	8/35	48/735	4/3	8/49
					5		100/343				100/343		100/343
1/2, 3/2	3	5/2, 7/2	2	3/2, 5/2	0		6/49			6/35		6/25	
					2	4/3	8/49	4/35	10/63	64/343	4/441	60/49	80/567
					4	16/9	108/539	24/35	40/189	36/245	40/539	108/175	800/6237
					6		220/637				220/819		220/1053

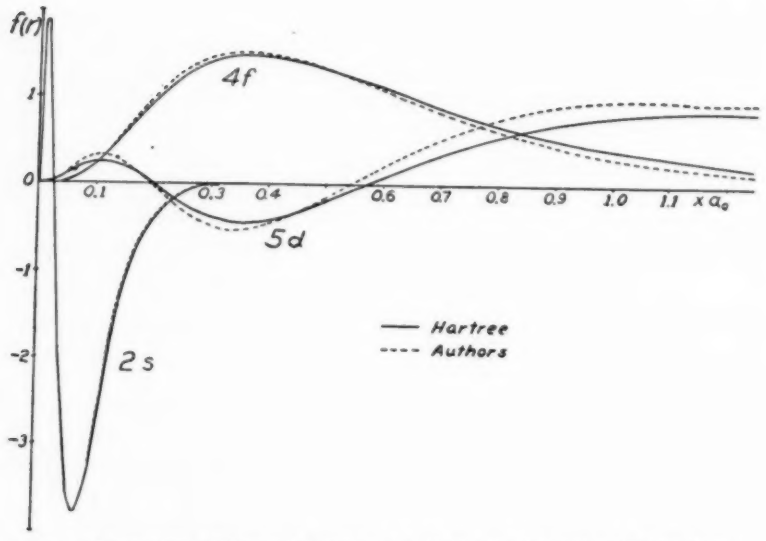

FIG. 1. Comparison of Hartree's functions for Hg^{++} with the authors' calculations.

for Au and the sum of the term value for the inner final vacancy for Au and that for the outer final vacancy for the next higher element, Hg. Since the value of the interaction matrix elements is in general not very sensitive to small changes in the energy parameter of the continuous function, only a limited number of continuous wave functions was calculated for a given azimuthal quantum number and that one was used whose energy parameter was closest to the prescribed value, as shown in Table V. In calculating the contribution to the width of the radiative transitions the actual line frequencies were substituted in the coefficients of the coordinate matrix elements (Eq. 9) in preference to the differences between the calculated energy parameters.

IV. SOURCES OF ERROR

Before giving the results of the calculations it is pertinent to summarize the principal sources of error. Perhaps the major defect, especially influential in the case of the radiation widths of the deepest energy levels, lies in the fact that the treatment given is nonrelativistic. Added to this is the practically unavoidable approximation that all the electrons move in a common central field. A comparison with Hartree's functions[13] for Hg^{++} in Fig. 1 makes it likely that the use of a common statistical field for all of the electron functions is not a major source of error.

For transitions involving the outermost levels the circumstance that in our observations we are dealing with atoms bound in a crystal lattice rather than with free atoms should lead to appreciable discrepancies owing to the modification of the electronic wave functions by the fields of the neighboring atoms. The widths of the electronic energy bands in the metal themselves are, it is true, negligible. Taking into account the twelve nearest neighbors of any one atom in a face-centered cubic structure, the width of the energy band becomes equal to 12 times the exchange integral A where[14]

$$A=\int \psi_0^*(\mathbf{r}-\mathbf{N})(V(\mathbf{r})-U(\mathbf{r})\psi_0(\mathbf{r})d\tau. \quad (16)$$

Here $\mathbf{r}$ is the coordinate vector; $\mathbf{N}$ the radius vector from the origin of r (the nucleus of the atom considered) to one of the nearest neighbors; and $V(\mathbf{r})-U(\mathbf{r})$ the difference between the lattice potential and that of the free atom. We can obtain an estimate of A by replacing the difference $V(\mathbf{r})-U(\mathbf{r})$ simply by $U(\mathbf{r})$. We then find

[13] D. R. Hartree and W. Hartree, Proc. Roy. Soc. London **A149**, 210 (1935).

[14] A. Sommerfeld and H. Bethe, *Handbuch der Physik*, Vol. 24, part 2 (1933), p. 397.

for the width of the energy band of the 5*s* electrons of Au(79):

$$12A = 0.002 \text{ Rydberg (0.03 volt)}, \quad (17)$$

which is negligible compared with the observed line and level widths.

V. Results for the Radiation Transition Probabilities

In Table IV are collected the calculated contributions $\Delta\Gamma_R$ of the various radiation transitions to the energy widths Γ_R of the several energy levels of gold, the unit for Γ_R and $\Delta\Gamma_R$ being the electron volt, corresponding to

$$(600\pi^2me^3/h^2)\Gamma/R = 13.54\Gamma/R.$$

For comparison, there are given in parentheses the relative transition probabilities deduced from the measurements by A. Jönsson,[15] Duane and Stenström[16] and others reported by Compton and Allison.[17] In every case the probability of the strongest transition to a given level has been set equal to the calculated value and is indicated by a dash in parenthesis. It is seen that there is agreement between the present calculations and experiment as far as order of magnitude of the relative transition probabilities is concerned. It is equally evident that, except for the *K* level, the radiation widths of the levels are materially smaller than the observed widths, tabulated at the bottom of the table. These latter data are taken from RBR, with the exception of that for the *K* level which was extrapolated from the measurements of Richtmyer and Barnes[18] for W(74) assuming proportionality of the width with Z^4.

[15] A. Jönsson, Zeits. f. Physik **36**, 426 (1926).

[16] Duane and Stenström, Proc. Nat. Acad. Sci. **6**, 477 (1920).

[17] *X-Rays in Theory and Experiment*, p. 645.

[18] F. K. Richtmyer and S. W. Barnes, Phys. Rev. **46**, 352 (1934).

Table IV. *Relative probabilities of radiation transitions.**

Initial Vacancy	K	L_{I}	L_{II}	L_{III}	M_{I}	M_{II}	M_{III}	M_{IV}	M_{V}	N_{I}	N_{II}	N_{III}	N_{IV}	N_{V}	N_{VI}	N_{VII}
Final Vacancy	$A=5942$ $B=5597$	1057 934	1011.4 896.8	877.7	252.2 221.8	231.8	201.9 204.5	168.6	162.2 172.6	55.8 50.85	47.3	39.9 43.5	25.8	24.5 30.03	6.2	5.8←A 11.95 ←B
L_{II}	16.63	0.0003														
L_{III}	36.0	.0014														
M_{I}			0.048 (.078)	0.027 (.050)												
M_{II}	3.44	.41 (.57)		.001	0.0002											
M_{III}	6.98	.92 (—)	.003	.001	.0058											
M_{IV}	.11	.020 (.007)	2.328 (—)	.138 (.145)		0.0081	0.0001									
M_{V}	.17	.031 (.013)		1.283 (—)			.0018									
N_{I}			.012	.008 (.015)		.0066	.0038									
N_{II}	.83	.11 (.14)			.0186					0.0001						
N_{III}	1.66	.22 (.19)			.0414	.0001		0.0003	0.0015	.0008						
N_{IV}	.03	.01	.465 (.429)	.030	.0001	.0646	.0040	.0012			0.00222	0.00006				
N_{V}	.04			.272 (.253)			.0371					.00073				
N_{VI}			.003			.0007	.0004	.0706	.0030				0.00145	0.00006		
N_{VII}				.001					.0600					.00119		
O_{I}			.003	.002 (.002)		.0015	.0009				.00050	.00027				
O_{II}	.16	.02			.0040			.0002		.0006			.00014	.00001		
O_{III}	.32	.04			.0081				.0003	.0011				.00011		
O_{IV}	.01		.051 (.041)	.003		.0082	.0005				.00054	.00003			0.00002	0.000001
O_{V}				.030 (.013)			.0049					.00029				.000015
P_{I}			.000	.000		.0002	.0001				.00006	.00003				
Total Radiation Width	66.38	1.78	2.913	1.796	.0782	.0900	.0536	.0723	.0648	.0026	.00332	.00141	.00159	.00137	.00002	.00002
Observed Width (RBR)	54.	8.7	3.7	4.4	15.5	10.7	12.1	4.2	3.5	11.7	8.5	6.5	6.8	5.9	5.4	

* At the top of the table line *A* gives the observed term value of the initial ionized state; and line *B* gives the calculated energy parameter—both in Ry. The data in the body of the table give, in electron volts, the computed contfributions $\Delta\Gamma_R$ to the width of the initial state arising from the several radiation transitions. The summation of each column gives, at the bottom of the table, the total computed radiation width Γ_R of the state. For comparison there are given the observed widths as reported by RBR.

TABLE V. *Contribution of the Auger effect to the level widths.*

Initial Vacancy	Final Vacancies		Ejected Electron l_i	Ejected Electron $E_{i_{Ry}}$ calc.	Ejected Electron $E_{i_{Ry}}$ used	Contribution to Width: Present Calc. Ev.	Contribution to Width: With Hydrogen Functions[23]
K	L_I	L_I	0	3785.6	3729.5	0.055	0.068
	L_I	$L_{II, III}$	1	3831.6 3974.1	3766.5	.193	.239
	$L_{II, III}$	$L_{II, III}$	0	3877.4 4019.9	3803.5	.039	.051
			2	4155.8	3803.5	.485	.610
				Auger width contribution		>.772	
				Radiation width contribution		66.38	
				Calculated width of K level		>67.15	
				Observed width of K level		54	
L_I	L_{III}	$M_{IV, V}$	1	3.7 10.5	6.97	.827	
			3		6.97	7.77	
	L_{III}	N_I	1	120.5	152.4	.147	
	L_{II}	N_{III}	0	3.4	5.35	.066	
			2		5.35	.130	
	L_{III}	$N_{II, III}$	0	129.3 137.1	130.0	.188	
			2		130.0	.047	
	L_{II}	$N_{IV, V}$	1	17.9 19.4	6.97	.200	
			3		6.97	.023	
	L_{III}	$N_{IV, V}$	1	151.6 153.1	152.4	.172	
			3		152.4	.758	
	L_{III}	$N_{VI, VII}$	2	171.9 172.3	197.9	.005	
			4		197.9	.698	
	L_{II}	$N_{VI, VII}$	2	38.2 38.6	25.05	.015	
			4			.555	
	L_{II}	O_I	1	37.1	27.98	.047	
	L_{III}	O_I	1	170.8	175.0	.032	
	L_{II}	$O_{II, III}$	0	41.0	30.46	.042	
			2		30.46	.046	
L_I	L_{III}	$O_{II, III}$	0	174.6	197.9	.015	
			2		197.9	.001	
	L_{II}	$O_{IV, V}$	1	45.3	34.46	.024	
			3		34.46	.002	
	L_{III}	$O_{IV, V}$	1	179.0	175.0	.014	
			3		175.0	.090	
				Auger width contribution		>11.91	
				Radiation width contribution		1.78	
				Calculated width of L_I level		>13.69	
				Observed width of L_I level		8.7	
M_I	M_{III}	N_{II}	0	0.2	5.35	.098	
			2		5.35	.466	
	M_{III}	N_{III}	0	8.0	10.76	.397	
			2		10.76	.668	
	M_{III}	$N_{IV, V}$	1	22.5 24.0	24.0	.817	
			3		24.0	.249	
	M_{II}	$N_{VI, VII}$	2	12.9 13.3	10.76	.496	
			4		19.17	.365	
	M_{III}	$N_{VI, VII}$	2	42.8 43.2	46.66	.490	
			4		46.66	.829	
	M_{II}	O_I	1	11.8	8.28	.207	
	M_{III}	O_I	1	41.7	42.66	.154	
	M_{II}	$O_{II, III}$	0	15.7	10.76	.120	
			2		10.76	.433	

TABLE V.—*Continued.*

Initial Vacancy	Final Vacancies		Ejected Electron l_i	Ejected Electron $E_{i\,Ry}$ calc.	Ejected Electron $E_{i\,Ry}$ used	Contribution to Width: Present Calc. Ev.	Contribution to Width: With Hydrogen Functions[21]
	M_{III}	$O_{II,\,III}$	0	45.6	40.18	.101	
			2		40.18	.257	
M_I	M_{II}	$O_{IV,\,V}$	1	20.0	14.76	.123	
			3		14.76	.331	
	M_{III}	$O_{IV,\,V}$	1	49.9	42.66	.149	
			3		42.66	.089	
	M_{II}	P_I	1	20.4	15.965	.013	
	$M_{IV,\,V}$	N_I	2	24.7	25.05	.670	
				31.1			
	$M_{IV,\,V}$	$N_{II,\,III}$	1	33.5	42.66	.162	
				41.3			
			3	39.9	42.66	.098	
				47.7			
	$M_{IV,\,V}$	$N_{IV,\,V}$	0	55.8	55.0	.095	
				57.3			
			2	62.2	60.0	.148	
				63.7			
			4		60.0	.726	
	$M_{IV,\,V}$	$N_{VI,\,VII}$	1	76.1	80.0	.048	
				76.5			
			3	82.5	80.0	.426	
				82.9			
			5		80.0	.451	
	$M_{IV,\,V}$	O_I	2	75.0	85.0	.112	
				81.4			
	$M_{IV,\,V}$	$O_{II,\,III}$	1	78.9	80.0	.028	
				85.3			
			3		80.0	.016	
	$M_{IV,\,V}$	$O_{IV,\,V}$	0	83.2	85.0	.013	
				89.6			
			2		85.0	.020	
			4		85.0	.077	
	$N_{VI,\,VII}$	$N_{VI,\,VII}$	0	238.5	197.9	.003	
				238.9			
			2	239.3	197.9	.007	
			4		197.9	.125	
			6		197.9	.157	
				Auger width contribution		>10.234	
				Radiation width contribution		.078	
				Calculated width of M_I level		>10.31	
				Observed width of M_I level		15.5	
M_{II}	M_V	N_I	1	0.9	1.87	.048	
			3		1.87	.046	
	M_{III}	O_I	0	11.5	10.76	.005	
			2		10.76	.978	
	M_{III}	$O_{II,\,III}$	1	15.4	14.76	.760	
			3		14.76	.034	
	$M_{IV,\,V}$	$N_{II,\,III}$	0	3.3	10.76	.562	
				11.1			
			2	9.7	10.76	1.767	
				17.5			
			4		19.17	.023	
	$M_{IV,\,V}$	$N_{IV,\,V}$	1	25.6	37.25	.728	
				27.1			
			3	32.0	37.25	.040	
				33.5			
			5		37.25	.005	
	$M_{IV,\,V}$	$N_{VI,\,VII}$	0	45.9	55.0	.002	
				46.3			
			2	52.3	46.66	.440	
				52.7			
			4		46.66	6.05	
			6		46.66	.001	

TABLE V—*Continued.*

Initial Vacancy	Final Vacancies		Ejected Electron l_i	Ejected Electron $E_{i\,Ry}$ calc.	Ejected Electron $E_{i\,Ry}$ used	Contribution to Width: Present Calc. Ev.	Contribution to Width: With Hydrogen Functions[8]
				Auger width contribution		>11.49	
				Radiation width contribution		.09	
				Calculated width of M_{II} level		>11.58	
				Observed width of M_{II} level		10.7	
M_{III}	$M_{IV,V}$	$N_{VI,VII}$	0	16.0	19.95	.011	
				16.4			
			2	22.4	19.95	.031	
				22.8			
			4		19.95	4.41	
			6		19.95	.000	
				Auger width contribution		>4.45	
				Radiation width contribution		.05	
				Calculated width of M_{III} level		>4.50	
				Observed width of M_{III} level		12.1	
N_I	$N_{II,III}$	$N_{VI,VII}$	2	1.0	5.35	.296	
				1.4			
			4	8.4	5.35	2.451	
				8.8			
	N_{III}	O_I	1	7.3	6.97	.357	
	N_{II}	$O_{II,III}$	0	3.8	5.35	.107	
			2		5.35	1.091	
	N_{III}	$O_{II,III}$	0	11.2	10.76	.196	
			2		10.76	1.331	
	N_{II}	$O_{IV,V}$	1	8.1	6.97	.135	
			3		6.97	2.128	
	N_{III}	$O_{IV,V}$	1	15.5	14.76	.140	
			3		14.76	1.565	
	$N_{IV,V}$	$N_{IV,V}$	0	2.2	5.35	.016	
				3.7			
			2	5.0	5.35	.055	
			4		5.35	.122	
	$N_{IV,V}$	$N_{VI,VII}$	1	22.5	24.0	.005	
				22.9			
			3	23.8	24.0	.049	
				24.2			
			5		24.0	.458	
	$N_{IV,V}$	O_I	2	21.4	25.05	.495	
				22.7			
	$N_{IV,V}$	$O_{II,III}$	1	25.3	24.0	.095	
				26.6			
			3		24.0	.314	
	$N_{IV,V}$	$O_{IV,V}$	0	29.6	30.46	.018	
				30.9			
			2		30.46	.051	
			4		25.05	.038	
	$N_{VI,VII}$	$N_{VI,VII}$	0	42.1	40.18	.00004	
				42.5			
			2	42.9	40.18	.00002	
			4		46.66	1.156	
			6		46.66	.129	
N_I	$N_{VI,VII}$	O_I	3	41.2	42.66	.463	
	$N_{VI,VII}$	$O_{II,III}$	2	45.1	46.66	.034	
			4		46.66	.251	
	$N_{VI,VII}$	$O_{IV,V}$	1	49.4	42.66	.009	
			3		42.66	.011	
			5		37.25	.035	
				Auger width contribution		>13.601	
				Radiation width contribution		.003	
				Calculated width of N_I level		>13.60	
				Observed width of N_I level		11.7	

TABLE VI. *Comparison of Pincherle's computed values of widths of L levels with the observed values of RBR. Widths are given in electron volts.*

LEVEL	PINCHERLE'S COMPUTED WIDTHS			OBSERVED BY RBR	AUTHORS' VALUE FROM TABLE V
	Radiation	Auger	Total		
L_{I}	1.0	5.5	6.5	8.7	13.7
L_{II}	0.9	2.2	3.1	3.7	—
L_{III}	1.6	2.6	4.2	4.4	—

VI. RESULTS FOR THE AUGER EFFECT PROBABILITIES

Owing to the rapidly increasing complexity, mentioned in Section II, of the calculation with increasing azimuthal quantum number of the initial vacancy, extensive calculations have been made only for the s states, L_{I}, M_{I} and N_{I} in particular. For the K and $M_{\mathrm{II,\,III}}$ levels the contributions of only a few Auger effects were calculated which, owing to the relative closeness of the coupling of the participating electrons as well as the low velocity of the ejected electron, could be expected to be relatively probable. In Table V are given in the several columns, the level symbols of the initial vacancies, those for the two final vacancies, the azimuthal quantum number characterizing the state of the ejected Auger electron, its correct energy in Rydbergs,[19] the energy parameter of the continuous wave function used in the calculation, and finally the calculated contribution to the width in electron volts. All the calculated Auger contributions for a given initial state are added together and, augmented by the radiation width given in Table IV, are compared with the experimental data of RBR.

VII. DISCUSSION AND COMPARISON WITH EARLIER WORK

An inspection of Table V reveals that the Auger effect is responsible for the great discrepancy between the observed level widths and the calculated radiation widths. The credit for first suggesting that the Auger effect is primarily responsible for this discrepancy and for applying Wentzel's[20] considerations regarding the variation of the Auger-effect probabilities with atomic number belongs to L. Pincherle.[21] In a later paper[22] the same writer has given numerous Auger effect probabilities for initial vacancies in the K, L_{I} and $L_{\mathrm{II,\,III}}$ shells computed with hydrogenic wave functions without screening; in this approximation the probability of a given Auger transition becomes independent of the nuclear charge of the emitting element. Values thus obtained are given for comparison in the last column of Table V in the case of the K shell Auger effects. In a final paper, on the intensity of the L lines of gold,[23] Pincherle examines the factors determining the observed line intensities making use of radiation widths calculated with relativistic wave functions and the previously reported Auger transition probabilities. He compares the results with measurements of Jönsson[24] and RBR and concludes that the agreement between theory and experiment is satisfactory. Pincherle's computed values are shown in Table VI along with the observed values of RBR and the value for L_{I} from Table V. Pincherle's values for total width are smaller than the observed values of RBR; the reverse is the case throughout in the present calculations.

A further treatment of the Auger effect, for silver with the initial vacancy in the K shell, has been given by E. H. S. Burhop.[25] Burhop uses hydrogenic wave functions with effective nuclear charges determined by Slater.[26] The calculations are carried out rigorously for the cases in which the two final vacancies are in the L shell. The

[19] These values have been determined with the aid of the tables of term values in M. Siegbahn, *Spektroskopie der Röntgenstrahlen* (Springer, 1932).

[20] G. Wentzel, Zeits. f. Physik **43**, 524 (1927).

[21] L. Pincherle, Atti Accad. Lincei (Ser. VI) **20**, 29–35 (1934). Pincherle's papers did not come to the attention of the authors until the calculations here reported were practically completed. The present work, however, does not involve a duplication of Pincherle's calculations, since the latter obtained Auger effect probabilities for the K and L shells only. His calculations furthermore were carried out by means of hydrogenic wave functions, while the present ones are based on wave functions calculated from a statistical field approximating the real field of the gold atom.

[22] L. Pincherle, Nuovo Cimento (N.S.) **12**, 81–92 (1935).

[23] L. Pincherle, Nuovo Cimento (N.S.) **12**, 162–170 (1935); Physica **2**, 596–605 (1935).

[24] A. Jönsson, Zeits. f. Physik **36**, 426 (1926).

[25] E. H. S. Burhop, Proc. Roy. Soc. London **A148**, 272 (1935).

[26] J. C. Slater, Phys. Rev. **36**, 57 (1930).

remaining K Auger effect probabilities are calculated making use of a plane wave for the ejected electron. As the behavior of the wave function of the latter in the interior of the atom is of primary importance, the figures thus obtained give at best the order of magnitude of the transition probabilities.

The relativistic theory of Dirac and Møller has been applied by Massey and Burhop[27] to the calculation of K Auger effect probabilities and radiative transition probabilities for gold, using screened hydrogen wave functions. In Table VII we compare their results calculated relativistically and nonrelativistically, with the values obtained in the present work. Our values are in approximate agreement with the nonrelativistic results of Massey and Burhop, though they are somewhat smaller throughout. The relativistic treatment evidently increases the contribution of the Auger effects and decreases that of the radiation transitions. This need not apply generally, however; in particular not to the complex transitions (involving higher azimuthal quantum numbers) which, according to Table V, contribute the largest share to the width of the higher levels.

Apart from the fact that, except for the K level, the Auger effect appears to be the primary factor determining the level widths our calculations indicate the following:

(1) The widths of the L_{I}, M_{I}, and N_{I} levels[28] are found to lie between 10 and 15 electronvolts, in good agreement with the measurements of RBR. In general the calculated contributions appear to be too large. It should also be pointed out that any revision of measured line and level widths[29] would probably be in the direction of a decrease in observed widths.

(2) Comparing the relative probabilities of individual Auger processes, we find that, in general, those are most probable for which the ejected electron has a relatively low energy. For very high energies of the latter—high compared to its potential energy in the region where the wavefunctions of the remaining electrons participating in the transition are large—the Auger probability must necessarily be small due to the oscillatory character of the wave function of the ejected electron in this region.

TABLE VII. *Contributions to the width of the K level, in electron volts.*

Radiation Transition	Massey and Burhop		Authors Nonrelativistic
	Relativistic	Nonrelativistic	
$K \rightarrow L_{\mathrm{III}}$	28.7	37.6	36.0
$K \rightarrow L_{\mathrm{III}}$	13.4	18.8	16.6
$K \rightarrow L_{\mathrm{I}}L_{\mathrm{III}}$	0.249	0.156	0.129
$K \rightarrow L_{\mathrm{I}}L_{\mathrm{II}}$	0.258	0.078	0.064
$K \rightarrow L_{\mathrm{I}}L_{\mathrm{I}}$	0.047	0.069	0.055

(3) Comparing different levels having the same total quantum number, we should expect a considerable decrease in width with increasing azimuthal quantum number. Thus in passing from M_{I} to M_{II}, several transitions which contribute substantially to the width of M_{I} drop out—for example, transitions of the type $M_{\mathrm{I}} \rightarrow M_{\mathrm{II}}N_{\mathrm{VI,\,VII}}$ and $M_{\mathrm{I}} \rightarrow M_{\mathrm{II}}O_{\mathrm{I}}$. (See Table V.) The relatively small decrease in mean kinetic energy of the electrons expelled by the remaining Auger processes does not appreciably increase their respective probabilities and their contributions to the width of M_{II}.[30]

(4) No commensurate decrease in width should be expected in passing from the lower to the higher level of a relativistic doublet—for example from M_{II} to M_{III} or from M_{IV} to M_{V}, since in such cases the angular coefficients ($c(0, 0)$ in Table III) of the largest interaction integrals vanish.

These indications are in accord with observation.

The present results, being confined to a single element, give no immediate information about the variation of the line widths or level widths with atomic number, Z. This variation will be determined by (1) the approximate constancy of Auger-transition probabilities with change of Z and (2) the proportionality of the radiation-

[27] H. S. W. Massey and E. H. S. Burhop, Proc. Roy. Soc. London **A153**, 661 (1936).

[28] The uncalculated Auger effects for these levels correspond to ejected electrons of high energy (for $L_{\mathrm{I}} > 540$ Ry). Such transitions have very low probability and contribute very little to the level widths.

[29] For recent work on this subject see L. G. Parratt, Rev. Sci. Inst. **6**, 387 (1935).

[30] This slightly higher probability arises from the fact that Auger electrons expelled with M_{II} ionization as the initial state have, for a given final state of double ionization, a somewhat lower kinetic energy than if M_{I} ionization be the initial state. See the immediately preceding paragraph.

transition probabilities with Z^4.[20] For Kr(36) Auger observed that, for the K shell, the probability of radiation transitions is approximately equal to that for Auger transitions. This leads to a theoretical curve giving level widths as a function of atomic number, of substantially the same character as the curve given by Zinn for the variation of absorption-limit widths.[21] Zinn finds approximate constancy of the K widths for elements below Ge(32) and near fulfilment of a fourth power law for the heavier elements.

The principal conclusion of the work here reported is that we feel justified in stating that within the present accuracy of experimental and theoretical studies, the widths of the principal x-ray lines of the heavier elements may be regarded as having a purely atomic origin with the Auger effect playing a dominant role for all but the K series.

[21] W. H. Zinn, Phys. Rev. **46**, 659 (1934), Fig. 6.

JUNE 1, 1937 PHYSICAL REVIEW VOLUME 51

Satellite Structure of $L\alpha$ and $L\beta_2$ of Au(79)

F. K. RICHTMYER* AND E. G. RAMBERG†
Cornell University, Ithaca, New York

(Received April 7, 1937)

Assuming the correctness of Coster and Kronig's hypothesis of the origin of the satellites accompanying $L\alpha$ and $L\beta_2$, the separations and relative intensities of these satellites are calculated for Au(79) by means of the theory of complex spectra. Making use of data on the mean life of the states involved in the transitions and on the probability of the Auger effect producing the initial state for the satellite emission, contours of the satellite structure are obtained and compared with patterns previously measured with the two-crystal spectrometer. Within the limitations of the theoretical treatment as well as the experimental material the agreement, both with regard to intensity distribution and relative intensity of parent lines and satellites, is satisfactory and confirms Coster and Kronig's theory.

COSTER and Kronig[1] have suggested the following sequence of processes for the production of x-ray satellites, such as those accompanying $L\alpha$ ($L_{III}\rightarrow M_{IV,V}$) or $L\beta_2$ ($L_{III}\rightarrow N_{IV,V}$), the intensity of which varies rapidly with atomic number in certain atomic number ranges:

(1) By electron or x-ray bombardment, the atom is initially ionized by the expulsion of an electron from the L_I shell (in the case of the satellites of $L\alpha$, for example).

(2) By a radiationless transition (Auger effect) the atom passes over into a doubly-ionized state, with one vacancy in the L_{III} shell and another in the $M_{IV,V}$ shell.

(3) The vacancy in the L_{III} shell is then filled by an electron from the $M_{IV,V}$ shell (or from the $N_{IV,V}$ shell for the satellites of $L\beta_2$). The radiation emitted by this transition has a slightly higher frequency than $L\alpha$ (or $L\beta_2$) on account of the diminution of screening occasioned by the absence of the $M_{IV,V}$ electron expelled by the Auger transition.

Auger transitions $L_I\rightarrow L_{III}M_{IV,V}$ are possible only when the energy difference between the L_I and the L_{III} levels exceeds the energy of the $M_{IV,V}$ level (for the element of next higher atomic number). But when there is such excess energy, the transitions have a high probability. A study of x-ray term tables shows that within the atomic number range $52<Z<73$, approximately,[2] the Auger transitions $L_I\rightarrow L_{III}M_{IV,V}$ cannot occur. Both above and below this range, they are possible.

It is within this range of atomic numbers that the satellites of both $L\alpha$ and $L\beta_2$ are so weak as

* This research was made possible by a grant from the American Philosophical Society. F. K. R.

† At present with Electronic Research Laboratory, RCA Manufacturing Company, Camden, New Jersey.

[1] D. Coster and R. de L. Kronig, Physica **2**, 13 (1935).

[2] "Approximately," because the screening effect of an L_{III} electron on the $M_{IV,V}$ shell is somewhat less than unity.

TABLE I. *Calculated separations and relative intensities of the satellites of Lα.*

No.	Transition ($2p3d \rightarrow 3d^2$) Initial state	Final state	Separation from L_{III}	Relative Intensity*
	$(j_1, j_2)J \rightarrow$	$(j_1, j_2)J$	Ry	
1	(3/2, 5/2)4	(3/2, 5/2)4	−4.75	22.5
2	(3/2, 3/2)1	(3/2, 3/2)0	−4.44	6.67
3	(3/2, 5/2)2	(3/2, 5/2)1	−4.08	7
4	(3/2, 5/2)2	(3/2, 5/2)2	−3.76	.20
5	(3/2, 5/2)4	(3/2, 5/2)3	−3.60	7.5
6	(3/2, 3/2)2	(3/2, 3/2)2	−3.24	13.33
7	(3/2, 5/2)3	(3/2, 5/2)4	−3.16	7.5
8	(3/2, 5/2)2	(3/2, 5/2)3	−2.99	9.47
9	(3/2, 5/2)3	(3/2, 5/2)2	−2.76	9.48
10	(3/2, 3/2)3	(3/2, 3/2)2	−2.58	9.33
11	(3/2, 3/2)1	(3/2, 3/2)2	−2.56	10.67
12	(3/2, 5/2)1	(3/2, 5/2)1	−2.37	3
13	(3/2, 5/2)1	(3/2, 5/2)2	−2.06	7
14	(3/2, 5/2)3	(3/2, 5/2)3	−1.99	6.35
15	(3/2, 3/2)2	(5/2, 3/2)1	2.24	.5
16	(3/2, 5/2)2	(5/2, 5/2)2	2.33	20
17	(3/2, 5/2)4	(5/2, 5/2)4	2.37	15
18	(3/2, 5/2)1	(5/2, 5/2)0	2.39	6.67
19	(3/2, 3/2)2	(5/2, 3/2)2	2.55	5.83
20	(3/2, 3/2)3	(5/2, 3/2)4	2.84	30
21	(3/2, 3/2)0	(5/2, 3/2)1	2.91	5
22	(3/2, 3/2)1	(5/2, 3/2)1	2.92	4.5
23	(3/2, 3/2)3	(5/2, 3/2)2	3.22	.33
24	(3/2, 3/2)1	(5/2, 3/2)2	3.24	10.5
25	(3/2, 3/2)2	(5/2, 3/2)3	3.33	18.67
26	(3/2, 5/2)3	(5/2, 5/2)2	3.34	4
27	(3/2, 5/2)3	(5/2, 5/2)4	3.99	45
28	(3/2, 3/2)3	(5/2, 3/2)3	3.99	4.67
29	(3/2, 5/2)1	(5/2, 5/2)2	4.04	9.33
				300.00

* The absolute units of intensity here used are arbitrary and are so chosen as to minimize the occurrence of fractions in the component intensities. Under the circumstances the sum rules necessarily make the total intensity of the whole group a large, round figure −300, in this case.

to be experimentally unobservable. Above and below it they are relatively prominent.[3] The theory of Coster and Kronig seemed at once to clarify this rather puzzling situation.

In a later paper, Coster, Kuipers and Huizinga[4] give additional support to the theory by demonstrating that, in the case of Nb(41), the excitation potential of the satellites (more exactly of the major portion of the satellite structure) corresponds to the ionization potential of the L_I level rather than to the lower ionization potential required to create vacancies simultaneously in the L_{III} and $M_{IV, V}$ shell. Furthermore Hirsh[5] has found the theory applicable to a number of other satellites of the M and L series.

It is now possible to calculate approximately both the position and relative intensities of satellites[6] as well as to determine relative probabilities of Auger effects[7] and of ionization of different shells.[8] Accordingly, it seemed to be of interest to subject the Coster-Kronig theory to quantitative test by comparing the satellite structure which it would predict with that which has been observed experimentally. Au(79) was selected as the element to be studied, since experimental curves for the satellite structures accompanying $L\alpha$ and $L\beta_2$ had been obtained;[9] and further, electronic wave functions and preliminary calculations[8] were available for this element.

To simplify the calculations pure (j, j) coupling was assumed for the electrons participating in the transitions. In the notation corresponding to this type of coupling the first problem was to find the separations of all the lines making up the transition $(2p\ 3/2)3d \rightarrow 3d^2$ from $(2p\ 3/2) \rightarrow (3d\ 5/2)$, or $L\alpha_1$; and similarly the separations of the lines due to the transition $(2p\ 3/2)3d \rightarrow 4d\ 3d$ from $(2p\ 3/2) \rightarrow (4d\ 5/2)$, or $L\beta_2$. The figures in parenthesis indicate in each case the total electronic quantum number, n, of an electron hole; its azimuthal quantum number, l; and its j value in this order. Every energy level of a doubly ionized state (in the absence of a magnetic field) is characterized in addition by the total J value of the state considered, which may be conveniently written after the two groups of symbols in parentheses; thus: $(n_1 l_1 j_1)(n_2 l_2 j_2)J$.

In order to determine the separations between satellites and parent lines Slater's theory of complex spectra[10] was applied: the identical

[3] F. K. Richtmyer and R. D. Richtmyer, Phys. Rev. **34**, 574 (1929); R. D. Richtmyer, Phys. Rev. **38**, 1802 (1931); F. R. Hirsh, Jr. and F. K. Richtmyer, Phys. Rev. **44**, 955 (1933); F. R. Hirsh, Jr., Phys. Rev. **48**, 722 (1935); Anna W. Pearsall, Phys. Rev. **46**, 694 (1934); F. K. Richtmyer and Sidney Kaufman, Phys. Rev. **44**, 605 (1933); Sidney Kaufman, Phys. Rev. **45**, 385 and 613 (1934).

[4] D. Coster, H. H. Kuipers and W. J. Huizinga, Physica **2**, 870 (1935).

[5] F. R. Hirsh, Jr., Phys. Rev. **50**, 191–197 (1936).

[6] E. H. Kennard and E. Ramberg, Phys. Rev. **46**, 1040–1046 (1934).

[7] H. Bethe, Ann. d. Physik **5**, 325–400 (1930).

[8] E. G. Ramberg and F. K. Richtmyer, Phys. Rev. **51**, 913 (1937).

[9] F. K. Richtmyer, S. W. Barnes and E. Ramberg, Phys. Rev. **46**, 843–860 (1934): Figs. 6 and 7.

[10] J. C. Slater, Phys. Rev. **34**, 1293–1322 (1929).

orthogonal electronic wave functions were used for the calculation of the initial and the final energy states of both parent and satellite lines. The separation between the two is given by

$$h\nu_s - h\nu_p = W_{is} - W_{fs}$$

where ν_s is the frequency of a satellite line, ν_p that of the parent line and W_{is} and W_{fs} are

TABLE II. *Calculated separations and relative intensities of the satellites of $L\beta_2$.*

No.	Transition ($2p3d \rightarrow 4d3d$) Initial State	Final State	Separation from $L\beta_2$	Relative Intensity*
	$(j_1, j_2)J \rightarrow (j_1, j_2)J$		Ry	
1	(5/2, 3/2)4	(5/2, 3/2)4	5.90	27
2	(5/2, 3/2)4	(5/2, 3/2)3	6.16	9
3	(5/2, 3/2)2	(5/2, 3/2)1	6.44	8.4
4	(3/2, 3/2)2	(3/2, 3/2)2	6.45	8
5	(3/2, 3/2)1	(3/2, 3/2)0	6.52	4
6	(5/2, 3/2)2	(5/2, 3/2)2	6.62	.22
7	(5/2, 3/2)2	(5/2, 3/2)3	6.77	11.38
8	(3/2, 3/2)3	(3/2, 3/2)2	7.12	5.6
9	(3/2, 3/2)1	(3/2, 3/2)2	7.13	6.4
10	(5/2, 3/2)4	(5/2, 5/2)4	7.16	9
11	(3/2, 3/2)2	(3/2, 3/2)3	7.32	5.6
12	(3/2, 3/2)2	(3/2, 3/2)1	7.32	6.4
13	(5/2, 3/2)3	(5/2, 3/2)4	7.51	9
14	(5/2, 3/2)2	(5/2, 5/2)2	7.54	12
15	(5/2, 3/2)3	(5/2, 3/2)2	7.62	11.38
16	(5/2, 3/2)4	(5/2, 5/2)5	7.67	44
17	(5/2, 3/2)3	(5/2, 3/2)3	7.78	7.62
18	(5/2, 3/2)4	(5/2, 5/2)3	7.81	1
19	(3/2, 3/2)2	(3/2, 5/2)1	7.87	.6
20	(3/2, 3/2)3	(3/2, 3/2)3	7.98	22.4
21	(3/2, 3/2)0	(3/2, 3/2)1	7.99	4
22	(3/2, 3/2)1	(3/2, 3/2)1	8.00	1.6
23	(3/2, 3/2)2	(3/2, 5/2)2	8.05	7
24	(5/2, 3/2)1	(5/2, 3/2)1	8.14	3.6
25	(3/2, 3/2)2	(3/2, 5/2)3	8.20	22.4
26	(5/2, 3/2)2	(5/2, 5/2)1	8.22	3.6
27	(5/2, 3/2)1	(5/2, 3/2)2	8.32	8.4
28	(5/2, 3/2)2	(5/2, 5/2)3	8.42	14.4
29	(3/2, 3/2)0	(3/2, 5/2)1	8.54	6
30	(5/2, 3/2)3	(5/2, 5/2)2	8.55	2.4
31	(3/2, 3/2)1	(3/2, 5/2)1	8.55	5.4
32	(3/2, 3/2)3	(3/2, 5/2)4	8.60	36.0
33	(5/2, 3/2)1	(5/2, 5/2)0	8.70	4
34	(3/2, 3/2)3	(3/2, 5/2)2	8.71	.4
35	(3/2, 3/2)1	(3/2, 5/2)2	8.73	12.6
36	(5/2, 3/2)3	(5/2, 5/2)4	8.78	27
37	(3/2, 3/2)3	(3/2, 5/2)3	8.87	5.6
38	(5/2, 3/2)1	(5/2, 5/2)2	9.25	5.6
39	(5/2, 3/2)3	(5/2, 5/2)3	9.42	12.6
40	(5/2, 3/2)1	(5/2, 5/2)1	9.93	8.4
				400.0

* See footnote, Table I.

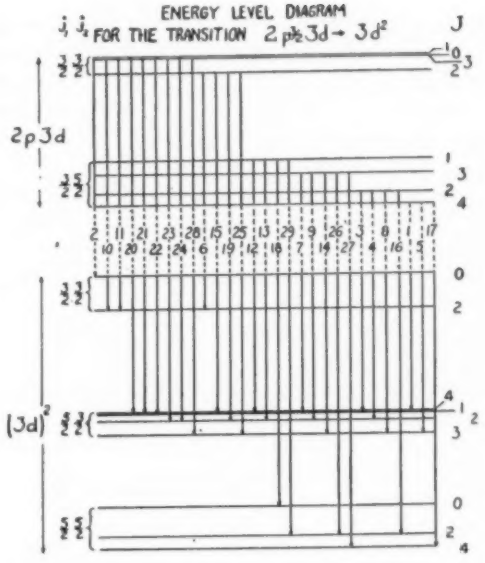

FIG. 1. Energy level diagram showing transitions between the doubly ionized states, $2p_{\frac{1}{2}}3d \rightarrow 3d^2$, these being the initial and the final states for the production of satellites accompanying $L\alpha$. The several transitions are numbered as in Table I.

the interaction energies of the corresponding additional vacancy (in our case in the $M_{IV, V}$ or $3d$ shell) with the vacancies in the initial and final states of the parent line ($2p$ and $3d$ or $4d$), respectively. The proper form of the wave functions as well as the angular factors of the interaction integrals for (j, j) coupling have been given by Inglis.[11] Making use of them, expressions in terms of Coulomb and exchange integrals and of the spin-doublet separations for the individual vacancies, were found for all the energy levels under consideration. Finally, by subtracting the energy difference for the initial and final state of the parent line from the corresponding differences for the satellite transitions, the separations of the satellites from the parent line were derived. These separations are listed in Tables I and II. The radial interaction integrals were calculated by use of wave functions found by numerical integration of the Schrödinger equation with the Thomas-Fermi field for Tl^{++} as potential, as reported in reference 8. Fig. 1 shows the energy level diagram for the satellites accompanying $L\alpha$,

[11] D. R. Inglis, Phys. Rev. **38**, 862–872 (1931).

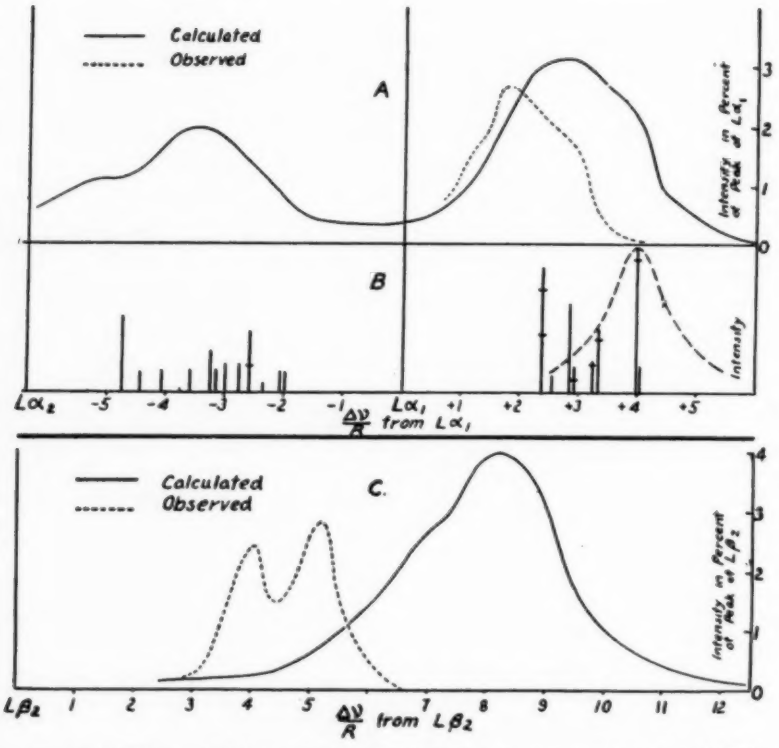

FIG. 2. (A) Observed and computed satellite "structure" accompanying $L\alpha$ of Au(79). (B) Predicted fine structure of the satellites of $L\alpha$. Data from Table II. (C) Observed and computed satellite structure accompanying $L\beta_2$ of Au(79).

the transitions shown being those given in Table I.

Having found the separations, relative intensities were next determined. For this purpose Bartlett's formulas for the relative intensities of supermultiplet lines were used.[12] The relative intensities so calculated are given in the last column of Tables I and II. The satellite components accompanying $L\alpha$ are shown graphically in (B) of Fig. 2.

Tables I and II, and Fig. 2(B) show at a glance that the satellite structure consists of a very large number of components lying much too close to each other to be resolved experimentally. To find the probable appearance of the structure we must treat each component as spread out over a certain frequency range according to the formula

$$J_\nu = 2A/\{\pi\Gamma(1+[2\nu/\Gamma]^2)\}, \qquad (1)$$

where[13] A is the calculated total intensity of the line; Γ the width of the component at half-maximum; and ν is measured from the calculated position of the component as origin.

We estimate Γ for the satellite component in the following manner. For an $L\alpha$ satellite the width of the initial state $L_{III}M_{IV,V}$ is approximately equal to the sum of the widths of L_{III} and $M_{IV,V}$, since the absence of a single other electron is not likely to influence materially the probability per unit time that either one of these vacancies will be filled; similarly, we may expect that the level width of the final state, $M_{IV,V}M_{IV,V}$, will be equal to about twice the width of an $M_{IV,V}$ state. Finally, the width of

[12] J. H. Bartlett, Phys. Rev. **35**, 229–234 (1930).

[13] This equation is identical with Eq. (1) of reference 8 if we set

$A=1$, $J=J_{AB}(\nu)$, $\nu=(\nu_{AB}-\nu)$ and $\Gamma=(\Gamma_A+\Gamma_B)$

the latter being the widths of the initial and final states of the satellite.

the line should be equal to the sum of the widths of the initial and final states. According to Table V in reference 9 the widths of the L_{III} state and of the $M_{IV,V}$ states are, each, approximately 4 ev. Thus we set $h\Gamma = 16$ ev (1.18 Ry)—about twice the width of the parent line. Similarly the width of an $L\beta_2$ satellite component should be about 19 ev (1.40 Ry). In Fig. 2(B) there is shown at (a) a plot of Eq. (1) for a satellite having a width of 1.18 Ry.

We can now superpose the energy distribution (1) for all of the components and thus obtain a contour for the satellite structure. We can determine the approximate height of this contour relative to that of the parent line if we estimate the ratio of the over-all intensities of the satellite structure to that of the parent line in the following manner.

The ratio of the probability of excitation of the satellite of $L\alpha$ to the probability of excitation of $L\alpha_1$ itself is equal to the product of the following four factors:

1. The ratio of the probability of the ionization of the L_I shell to that of the L_{III} shell.
2. The ratio of the probability of the Auger effect $L_I \rightarrow L_{III}M_{IV,V}$ to the sum of the probabilities of all possible Auger and radiation transitions from L_I.
3. The ratio of the mean life (or reciprocal width) of the state $L_{III}M_{IV,V}$ to that of the state L_{III}.
4. The ratio of the probability of an electron transition from either the M_{IV} or the M_V shell into a vacancy in the L_{III} shell to that of a transition from the M_V shell into a similar vacancy.

The first factor can be calculated from Bethe's[14] formula (78) and becomes 0.48. The second factor may be estimated from Table V in reference 8 to be about 2/3—demonstrating the very high probability of Auger transitions of the type $L_I \rightarrow L_{III}M_{IV,V}$. The third factor we have just seen to be equal to about 1/2. Finally x-ray data as well as the intensity rules give for the last ratio approximately 1.1. We thus find the ratio of the total $L\alpha$ satellite intensity to the intensity of $L\alpha_1$ to be equal to 0.18. Knowing the width of $L\alpha_1$ to be about 8 ev we can plot calculated satellite intensities in terms of the peak intensity of $L\alpha_1$. Fig. 7 in reference 9 permits us to do the same for the experimentally determined satellite structure. Fig. 2(A) shows the experimental and calculated structures plotted to the same scale. The similarity of the two structures on the short wave-length side of $L\alpha_1$ as well as the agreement in intensity relative to the parent line is surprising in view of the crudeness of the calculations. The less pronounced structure on the long wave-length side of $L\alpha_1$ would be scarcely observable owing to the proximity of $L\alpha_2$.

The fact that the calculated satellite structure is too far separated from the parent line is inherent in the present naive application of the theory of complex spectra to the calculation of satellite separations. Actually the contraction of the electron cloud when a vacancy is produced in the interior of the atom acts so as to reduce the difference between the interaction energy of the additionally removed electron in the $M_{IV,V}$ shell for the initial and final state of the parent line.

An analogous calculation for the $L\beta_2$ satellites gives for the ratio of total satellite intensity to parent line intensity 0.15. The contour is shown in Fig. 2(C). Here again we see that the calculated separations exceed the observed.

With due regard to the imperfections of the calculations it can be said that the present results support the theory of the origin of the $L\alpha$ and $L\beta_2$ satellites proposed by Coster and Kronig.

[14] Reference 7. The exciting voltage used in obtaining the experimental curves given in reference 9 was about 50,000 volts.

On the Analysis of Molecular $^3\Pi$ States with Application to AlH, OH^+, and BH

C. N. CHALLACOMBE AND G. M. ALMY
Department of Physics, University of Illinois, Urbana, Illinois

(Received January 28, 1937)

The molecular constants λ, B, D for the $^3\Pi$ states of BH, AlH, and OH^+ have been calculated by the method of Gilbert, based on Van Vleck's solution of the case of intermediate coupling, but including a more accurate consideration of the rotational D terms. A graphical method of obtaining λ has also been developed based on Budó's series expansion solution of the Hill and Van Vleck energy equation for the intermediate $^3\Pi$ state. A graph shows, for a given K, the variation in multiplet splitting as the coupling constant λ is varied from -8 to $+10$. Graphs are plotted for $K=2$, 3, 4, 5, and application is made to the $^3\Pi$ states of BH, AlH, OH^+ and NH. New data for AlH for lines with K less than 6 are given. A comparison of corresponding electronic *ls* coupling coefficients in molecule and atom is made.

THE energy levels of a $^3\Pi$ molecular state having a coupling intermediate between Hund's cases *a* and *b* are given by the solutions of a third-order equation proposed by Hill and Van Vleck.[1] This equation was obtained by starting with a system representing Hund's case *b* type of coupling and applying a perturbation towards case *a*. Later, Van Vleck[2] derived the same equation by setting up a system representing case *a* and perturbing towards case *b*. In a recent paper, Budó[3] has discussed the analysis of such $^3\Pi$ states using the equation of Hill and Van Vleck. Still more recently, Gilbert[4] has extended the treatment by Van Vleck to include the effect of the D terms, i.e. the terms in $J^2(J+1)^2$, in the expression for the rotational energy.

An analysis of a multiplet state involves the determination of the rotational constants B and D, and of the constant, $\lambda=A/B$, which appears implicitly in the equations of Hill and Van Vleck, Van Vleck, and Gilbert. It is the purpose of this paper to apply the method outlined by Gilbert to obtain the constants B, D, and λ of the $^3\Pi$ states of AlH, OH^+ and BH; to present a graphical method of determining λ which has certain advantages over previous methods in the region near case *b*; and to compare the values of λ obtained by the graphical method with those obtained by Gilbert's method.

GILBERT'S THEORY OF $^3\Pi$ STATES

The energy levels, $W_1(J)$, $W_2(J)$ and $W_3(J)$, of $^3\Pi$ states having intermediate coupling are given by the solution of Van Vleck's equation

$$|(W/B)\delta(\Sigma,\Sigma')-H_a(\Sigma,\Sigma')|=0, \qquad \Sigma,\Sigma'=1,0,-1, \quad (1)$$

where $\delta(\Sigma,\Sigma')$ is a unit matrix and $H_a(\Sigma,\Sigma')$ represents the energy matrix, the elements of which, as given by Gilbert, contain the rotational D terms.

Determination of B and D

Gilbert obtains the expression

$$\Sigma\Delta_2 W_i(J)/6(2J+1)=B+4D+2DJ(J+1).^5 \quad (2)$$

To compute B and D, one plots the average $\Delta_2 W(J)$ for the three substates, divided by $4J+2$, against $J(J+1)$. If the plot is a straight line, the slope is $2D$ and the intercept is $B+4D$. If the plot departs slightly from a straight line, an appreciable term in $J^3(J+1)^3$ is present in the rotational energy and $3FJ^2(J+1)^2$ may be added to the right side of Eq. (2).

On account of Λ type doubling, there are two sets of energy levels. These levels have been distinguished as *c* and *d* levels according to rules given by Mulliken.[6] However, Hebb[7] has shown that if one sets up the problem, including

[1] E. L. Hill and J. H. Van Vleck, Phys. Rev. **32**, 250 (1928).
[2] J. H. Van Vleck, Phys. Rev. **33**, 467 (1929).
[3] A. Budó, Zeits. f. Physik **96**, 219 (1935) and **98**, 437 (1936).
[4] Cecil Gilbert, Phys. Rev. **49**, 619 (1936).

[5] In Gilbert's equation, $6D$ appears in place of $4D$. Associated with this change we find $\frac{1}{3}$ Spur $H_a=J(J+1)-\frac{1}{3}+\mu[J^2(J+1)^2+2J(J+1)+1]$ instead of Gilbert's expression for this quantity. This discrepancy will not materially affect the values obtained for B and D.
[6] R. S. Mulliken, Rev. Mod. Phys. **3**, 89 (1931).
[7] M. H. Hebb, Phys. Rev. **49**, 610 (1936).

the Λ type doubling and spin-spin interaction, and solves for the energies of the $^3\Pi$ state, they fall naturally into two sets: (1), what may be called W^+ levels, which are + or − depending upon whether J is even or odd, and (2), what may be called W^- levels, which are − or + depending upon whether J is even or odd. One can keep the two sets of levels of different symmetry separate by using in Eq. (2) the combination differences,

$$\Delta_2 W^+(J)=\Delta_2 W_{1c}(J)+\Delta_2 W_{2d}(J)+\Delta_2 W_{3c}(J),$$
$$\Delta_2 W^-(J)=\Delta_2 W_{1d}(J)+\Delta_2 W_{2c}(J)+\Delta_2 W_{3d}(J). \quad (3)$$

The combination differences on the right side of these equations can be obtained as differences between the wave numbers of branch lines appropriately chosen from the branches of the transition being considered.

Determination of λ

Upon making the transformation

$$E=W/B-\tfrac{1}{3}\ \text{Spur}\ H_a, \quad (4)$$

Gilbert obtains Eq. (1) in the form

$$-E^3+\alpha E+\beta=0, \quad (5)$$

where

$$\alpha(J)=\lambda^2-4\lambda+(4/3)+4J(J+1)+8J(J+1)\{2J(J+1)+1\}\mu-4\{2J(J+1)-1\}\lambda\mu+16J^2(J+1)^2\{J(J+1)+1\}\mu^2, \quad (6)$$

$$\beta(J)=-(4/3)\lambda^2+(4/3)\lambda+(16/27)+(8/3)J(J+1)+(\text{terms in }\mu). \quad (7)$$

In Eqs. (6) and (7), $\lambda=A/B$, $\mu=D/B$. To obtain λ, Gilbert uses the identity

$$\tfrac{3}{4}(E_1-E_3)^2+\tfrac{1}{4}\{(E_1-E_2)-(E_2-E_3)\}^2=3\alpha, \quad (8)$$

which gives the relation

$$\tfrac{3}{4}B^{-2}[W_1(J)-W_3(J)]^2+\tfrac{1}{4}B^{-2}\{[W_1(J)-W_2(J)]-[W_2(J)-W_3(J)]\}^2=3\alpha(J). \quad (9)$$

For a given J, the differences on the left are obtained from the data and the equation is solved for λ. The value of λ should be the same for each J.

Again there are two sets of levels, W^+ and W^-, and, as in the formation of $\Delta_2 W_1(J)$, one must cut across the c, d classification to form J multiplets of levels having the same symmetry. Thus, we have

$$W_1^+(J)-W_2^+(J)=W_{1c}(J)-W_{2d}(J),$$
$$W_1^-(J)-W_2^-(J)=W_{1d}(J)-W_{2c}(J),$$
$$W_2^+(J)-W_3^+(J)=W_{2d}(J)-W_{3c}(J),$$
$$W_2^-(J)-W_3^-(J)=W_{2c}(J)-W_{3d}(J). \quad (10)$$

The differences on the right can be expressed in terms of band lines appropriate to the transition involved.

Neither set of levels is given exactly by Eq. (8). In general, both are slightly perturbed by the spin-spin interaction and the Λ type doubling, the latter effect depending upon the position and multiplicity of the Σ states of the molecule. Hebb[8] has developed a complete expression of the form of Eq. (8) which takes account of these small effects. They will not, however, be included in the applications to be made in this paper. In the case of OH^+, however, λ will be calculated independently for W^+ and W^- levels.

Graphical Determination of λ

The computation of λ by the above method is rather tedious. It requires, moreover, that the rotational constants be first accurately determined. This is because the splitting of a J triplet is largely rotational energy, especially near case b. The coupling energy, measured by λ, can be estimated accurately only if the rotational energy in the multiplet is precisely known. Therefore, it is advantageous to compute λ from a K multiplet in which no rotational energy is involved. The expressions necessary to solve for λ in terms of K multiplet intervals are very complex. However, a graphical method has been developed which, for any $^3\Pi$ state having a value of λ in the range considered, will yield the value of λ upon inspection, as soon as the quantum assignments are made and B is approximately known. The principal advantage of the method is its directness. The spectrum triplet splitting in the main branches (if due entirely to a $^3\Pi$ state) immediately gives the K multiplet splitting for three levels of the same rotational symmetry. A correction can be made for the splitting of the combining state (usually $^3\Sigma$) if it is appreciable. One set of graphs cannot be applied to all $^3\Pi$ states if the D term is included. It is therefore omitted and the method is applied

[8] Private communication.

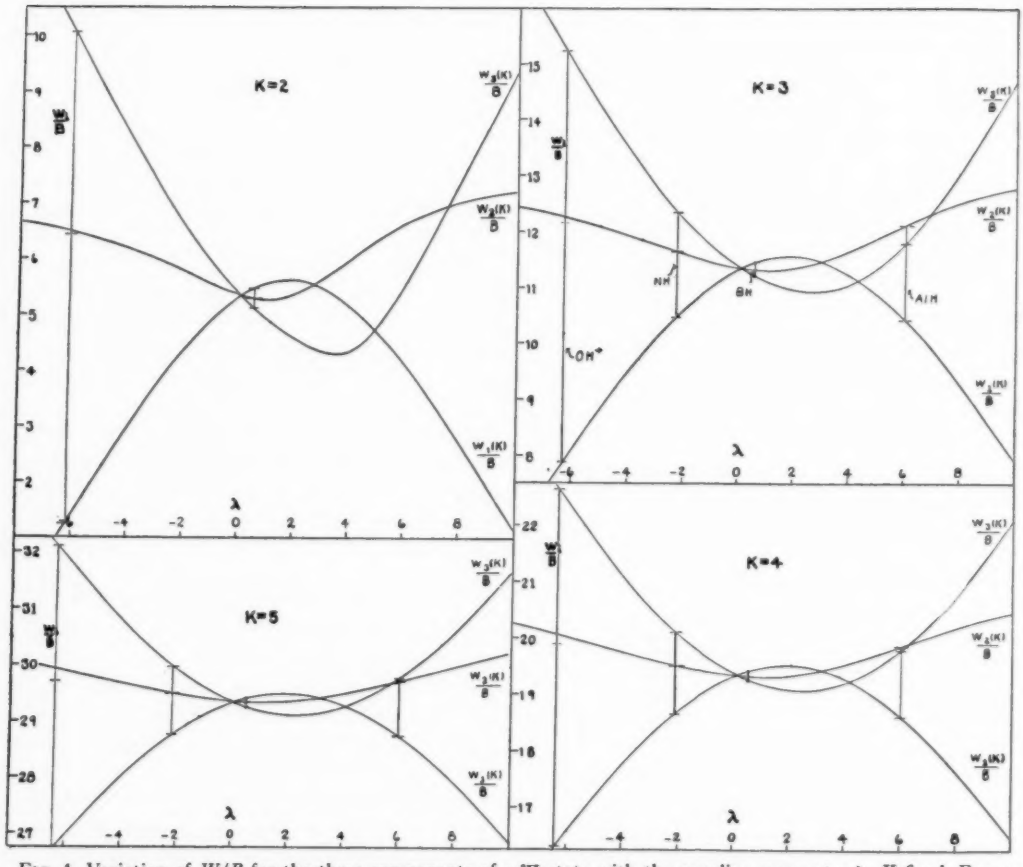

FIG. 1. Variation of W/B for the three components of a $^3\Pi$ state with the coupling parameter λ, K fixed. For any $^3\Pi$ state, λ can be determined by fitting the observed K multiplet intervals (in cm^{-1}), divided by B_v, to the graphs. The observed intervals for OH^+, NH, BH and AlH, as fitted to the graphs for the determination of λ, are shown.

only for low values of K where the D term is unimportant. The graphically obtained values of λ are probably as reliable as those obtained by the analytical method unless one wishes to extend the latter method to include the effect of Λ type doubling.

Finally, the graphs are useful in making the analysis of a band having a value of λ in the range from $+2$ to $+7$ where the spectrum triplets appear to behave in an anomalous manner. In fact, we were led to draw the graphs by the peculiar behavior of the $^3\Sigma \rightarrow {}^3\Pi$ band of AlH at low values of K.

By expanding the trigonometric solutions[9] of Eq. (5), one obtains

$$\begin{aligned} E_3(J) &= \alpha^1 + \tfrac{1}{2}\beta/\alpha - \tfrac{3}{8}\beta^2/\alpha^{5/2} + \tfrac{1}{2}\beta^3/\alpha^4 + \cdots, \\ E_2(J) &= \quad -\beta/\alpha \qquad\qquad - \beta^3/\alpha^4 + \cdots, \\ E_1(J) &= -\alpha^1 + \tfrac{1}{2}\beta/\alpha + \tfrac{3}{8}\beta^2/\alpha^{5/2} + \tfrac{1}{2}\beta^2/\alpha^4 + \cdots. \end{aligned} \quad (11)$$

By omitting the terms involving μ in Eqs. (6) and (7), one can calculate values of $E_i(J)$ as functions of λ and J, but independent of the rotational constant B. When the μ term and a constant term $-\frac{1}{3}$ are dropped, $\frac{1}{3}$ Spur $H_a = J(J+1)$ and Eq. (4) gives the relations

$$\begin{aligned} (W_1(K))/B &= (K+1)(K+2) + E_1(K+1), \\ (W_2(K))/B &= K(K+1) + E_2(K), \\ (W_3(K))/B &= (K-1)K + E_3(K-1). \end{aligned} \quad (12)$$

Fixing $K=2$, the values of $W_i(K=2)/B$ were

[9] These solutions are given by Budó (reference 3). His Eq. (3) is identical with Eq. (5) if μ is set equal to zero.

computed for values of λ from $+10$ to -8. This calculation was repeated for $K=3$, 4, 5 and 10. In every case the last term given in each of Eqs. (11) may be neglected. Fig. 1 shows the relative separations of the K multiplet levels of the $^3\Pi$ state for the values, $K=2$, 3, 4 and 5. To find λ, one divides the experimentally obtained separations, $W_i(K)-W_j(K)$ by B and fits these quotients on the graph for the corresponding value of K. It is interesting to note the peculiar behavior of the multiplet levels having values of λ between 0 and $+8$. For example, if $\lambda=6$; $W_3>W_2>W_1$ for $K\geq 5$; $W_2>W_3>W_1$ for $K\leq 4$. In the case of $^2\Pi$ states, one can theoretically predict pure case b coupling for $\lambda=0$, 4. For $^3\Pi$ states, one observes pure case b coupling for $\lambda=0$, but for $\lambda=4$ there is an appreciable splitting. As K increases, this splitting diminishes and the graph for $K=10$ shows the three levels almost meeting in a point at $\lambda=4$. The general trend towards case b with increasing values of K may also be noted by comparing the multiplet separations of the different graphs.

The $^3\Sigma\rightarrow{}^3\Pi$ Band of AlH at λ3800

This band, analyzed by Holst,[10] consists of almost headless P and R branches and superimposed Q branches so that only the P and R branches are usable for the determination of the constants, B, D and λ, of the $^3\Pi$ state. Holst makes assignments for the P and R branch lines from $K=6$ to $K=20$ and, from a consideration of the intensities, believes the $^3\Pi$ state to be inverted. Budó, using Holst's data, concludes that $\lambda=+6.0$ and, therefore, the state is regular.

To extend the band to lower K, the most important region for deciding whether the state is inverted or regular, and for determining λ, the spectrum was photographed in the first order of a 21-foot grating with a dispersion of 1.25 A/mm, using a Schüler lamp as a source. The new data on the P and R branches are given in Table I.

Table I. *Data on P and R branches of band of AlH at λ3800.*

K	R_1(cm^{-1})	R_2(cm^{-1})	R_3(cm^{-1})
3	26,283.09	26,271.49	26,273.73
4	295.40	287.28	287.54
5	308.38	302.00	301.70
K	P_1(cm^{-1})	P_2(cm^{-1})	P_3(cm^{-1})
3	26,188.60	26,176.97	26,179.14
4	173.98	165.92	166.26
5	160.35	153.86	153.59

[10] W. Holst, Zeits. f. Physik **86**, 338 (1933).

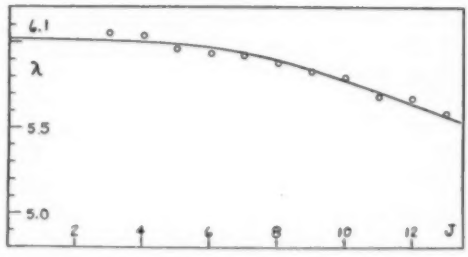

Fig. 2. λ for AlH by Gilbert's method.

The data of Table I were combined with those of Holst for $K>5$ to compute B, D and λ. Since only the P and R branches are resolved, $\Sigma\Delta_2W_{id}$[11] was used instead of $\Sigma\Delta_2W_i^+$ or $\Sigma\Delta_2W_i^-$ in Eq. (2) to obtain B and D. Also, in computing λ by Eq. (9), the small second term on the left side of the equation was first omitted since it involves Q branches. The differences $W_{1d}(J)-W_{3d}(J)=R_1(J-1)-P_3(J+1)$ were computed and an approximate λ was obtained using values of J from 3 to 13. With this λ, the omitted term was calculated from a relation which follows from Eqs. (11), namely,

$$B^{-1}[(W_1-W_2)-(W_2-W_3)] = (E_1-E_2)-(E_2-E_3)=\frac{\beta}{\alpha}+\frac{\beta^3}{\alpha^4} \quad (13)$$

and a second approximation to λ was made. The results are contained in Table III and Fig. 2. λ does not remain strictly constant with increasing J. This may be because no account is taken of Λ doubling and because of an unobserved splitting in the $^3\Sigma$ state. The latter is certainly small since $\Delta_2W_1'=\Delta_2W_2'=\Delta_2W_3'$ within the errors of measurement, but, as Gilbert has shown in the case of NH, a very small $^3\Sigma$ splitting may cause a pronounced depression of λ with increasing J.

To obtain λ from the graphs, W^-, K'' triplet separations averaged from the P and R branches and divided by B'', were fitted to the graphs in

[11] A consideration of the states of separated and united atom configurations indicates that the upper state is probably $^3\Sigma^+$ and, therefore, that the P and R branches involve the d levels.

Fig. 1 for $K=3, 4, 5$. The average value, $\lambda=+6.0$, is in good agreement with Budó and with the method applied above. The accuracy of the graphical method in this critical region is shown in Table II where the observed separations are compared with those obtained from Eqs. (12) in computing the graphical points for $\lambda=+6$.

In obtaining the value of λ analytically, one must solve an equation which is quadratic in λ. In this particular case, values of λ are obtained which must either be in the neighborhood of $\lambda=-2$ or $\lambda=+6$. By an inspection of the graphs, it is readily seen that it is impossible to fit the observed separations to the curves at $\lambda=-2$ and, therefore, one must conclude that the $^3\Pi$ state is regular.

The $^3\Sigma\rightarrow{}^3\Pi$ Band of BH at λ3690

This band is the analog of the band of AlH just discussed. It was discovered and partially analyzed by Lochte-Holtgreven and van der Vleugel.[12] Almy and Horsfall[13] have recently resolved the band more completely and established the nature of the transition. The upper state is very probably $^3\Sigma^+$ with a splitting too small to be estimated from a comparison of the values of $\Delta_2 W'$.

The $^3\Pi$ state is very near case *b*. The *P* and *R* branches form close triplets whose seaprations, divided by B'', fit the graphs of Fig. 1 approximately at -0.4 but better at $+0.5$. The observed separations obtained from the *Q* branches will not fit the graphs for any value of λ. The latter separations give the $W^+(K)$ multiplets while the *P* and *R* triplets correspond to the $W^-(K)$ multiplets. In this case, it appears that the $W^-(K)$ levels are less affected by Λ type doubling.

Because of the lack of resolution in the *Q* branches, only the *P* and *R* branches were used in obtaining *B*, *D* and λ by Gilbert's method. The procedure was the same as in the case of AlH and the results are given in Table III and Fig. 3. A very small error in *B* or *D* or an unobservable splitting in the $^3\Sigma$ state would account for the decrease of λ which occurs with increasing *J*.

Table II. *Comparison of observed separations and those computed graphically.*

		$\frac{W_{2d}''(K)-W_{1d}''(K)}{B''}$		$\frac{W_{3d}''(K)-W_{2d}''(K)}{B''}$	
K	λ	obs.	graph	obs.	graph
5	+6.0	0.96	0.97	0.04	0.05
4	+6.0	1.20	1.15	−0.04	−0.05
3	+6.0	1.73	1.70	−0.33	−0.32

The $^3\Pi\rightarrow{}^3\Sigma$ Band of NH at λ3360

The graphical method for the determination of λ of the $^3\Pi$ state has been applied to some recent data on lines of low *K* of the (0, 0) band, published by Funke.[14] Gilbert has calculated the value, $\lambda=-2.20$, for the $^3\Pi$ state using the data of Pearse and Batsch and Budó has computed the value $\lambda=-2.14$ using the data of Batsch. The writers obtain the graphical value, $\lambda=-2.18$, as an average of the values obtained from the W^+ and W^- levels.

The $^3\Pi\rightarrow{}^3\Sigma$ Band System of OH^+

The vibrational and rotational analysis of this system has been carried out by Loomis and Brandt.[15] Two vibrational levels of the $^3\Pi$ state were observed and the data of the (0, 0) band at λ3565 and the (1, 0) band at λ3332 were used in the present calculation of the constants. In addition to the nine strong branches, several satellite branches were photographed which pro-

Table III. *Values of constants B, D, and λ (Gilbert's method).*

Molecule	B cm^{-1}	D cm^{-1}	λ(graph)	λ(calc.)	Remarks
AlH($v''=0$)	6.704	-4.00×10^{-4}	+6.0	+6.02	λ = +6.0, (Budó)
BH($v''=0$)	12.667	-1.22×10^{-3}	+0.5	+0.47	
OH^+($v'=0$)	13.333	-2.15×10^{-3}			
W^+levels			−6.3	−6.35	
W^-levels			−6.0	−6.03	
OH^+($v'=1$)	12.488	-2.10×10^{-3}			
W^+levels			−6.8	−6.76	λ = −6.64, −6.82, −7.18, (Kovner)
W^-levels			−6.5	−6.53	
NH($v'=0$			−2.18		λ = −2.14 (Budó) λ = −2.20 (Gilbert)

[12] W. Lochte-Holtgreven and E. S. van der Vleugel, Zeits. f. Physik **70**, 188 (1931).

[13] G. M. Almy and R. B. Horsfall, Jr., Phys. Rev. **51**, 491 (1937).

[14] G. W. Funke, Zeits. f. Physik **96**, 787 (1935) and **101**, 104 (1936).

[15] F. W. Loomis and W. H. Brandt, Phys. Rev. **49**, 55 (1936).

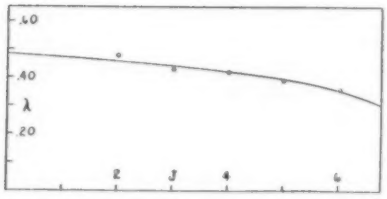

FIG. 3. λ for BH by Gilbert's method.

vide a more direct measurement of the intervals involved (particularly the correction for the $^3\Sigma$ splitting) than was possible in the other cases considered.

In their analysis of the bands, Loomis and Brandt did not compute λ, or $A=B\lambda$, except by the rough, pure case *a* method of extrapolating the observed K multiplet intervals to $K=1$. At $K=1$, $A=^3\Pi_2-^3\Pi_1=-97$ cm^{-1} or $A=^3\Pi_1-^3\Pi_0=-66$ cm^{-1}. During the course of this investigation, a note by Kovner[16] has appeared discussing the solution of the Hill and Van Vleck equation for the $^3\Pi$ state with an application to the OH^+ bands. He has used the Cardan formula to find the roots of the cubic energy equation and, by making use of a graphical interpolation, found that the states $v=1$, $K=10$ and $v=1$, $K=11$ led to values of A between -82.2 and -88.9 cm^{-1} depending upon the multiplet interval used.

The OH^+ bands presumably correspond to the similar transitions of the isoelectronic molecule NH and to the triplet bands of PH. Mulliken[17] concludes that the $^3\Sigma$ states of NH and PH are $^3\Sigma^-$. We assume therefore that the lower state of the OH^+ bands is $^3\Sigma^-$, which determines the order of the W^+ and W^- levels in the $^3\Pi$ state. The data on these bands are sufficient to carry the calculations of B, D, and λ through for both

TABLE IV. *Comparison of electronic coupling coefficients in molecule and atom.*

Molecule	Configuration and State	$A(v=0)$	a_{MH}	a_M	$\frac{a_{MH}}{a_M}$
BH	$2p\sigma 2p\pi\ ^3\Pi$	5.96	10.92	10.3	1.16
AlH	$2p\sigma 3p\pi\ ^3\Pi$	40.2	80.4	74.7	1.08
NH	$2p\sigma(2p\pi)^3\ ^3\Pi$	−35.6	71.2	83.1	.86
OH^+	$2p\sigma(2p\pi)^3\ ^3\Pi$	−80.4	160.8	180.0	.89
PH	$3p\sigma(3p\pi)^3\ ^3\Pi$	−115.4	230.8	297.7	.77

[16] M. Kovner, Phys. Rev. **50**, 188 (1936).
[17] R. S. Mulliken, Rev. Mod. Phys. **4**, 6 (1932).

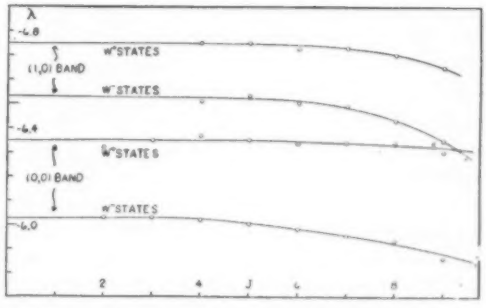

FIG. 4. λ for OH^+ by Gilbert's method, calculated independently for states of + and − symmetry.

the W^+ and W^- levels. This has been done and the results are shown in Table III and Fig. 4. As already mentioned in the general discussion, the correction for Λ doubling is neglected in the formulas used to determine λ. By calculating λ independently for W^+ and W^- levels, one obtains two values whereas one value should be obtained if the correction for the Λ doubling is included. The values of λ found by fitting the various separations to the graphs are also recorded in Table III.

The more nearly constant λ is obtained with the W^+ levels. However, Hebb[8] predicts that, if the interaction producing Λ doubling is with a $^1\Sigma^+$ and a $^3\Sigma^-$ state, as is probably the case in OH^+, the W^- levels are less perturbed, at least for low values of J. The decrease in λ with increasing J cannot be ascribed to unresolved $^3\Sigma$ splitting in this case since the latter is accurately determined by the use of satellite lines and has been taken into account in the calculations.

COMPARISON OF ELECTRONIC COUPLING COEFFICIENTS

Mulliken[18] has compared the spin multiplet separations in various molecular states with those of the constitutent atoms. In hydrides (MH) he finds, as a general rule, that the molecular coupling coefficient a_{MH} of l and s of the important electron is about 0.9 of the corresponding atomic coefficient a_M in the atom M.

The $^3\Pi$ state of NH is derived presumably from $(2p)^3\ ^2D$ of N plus normal H but in the

[18] R. S. Mulliken, Rev. Mod. Phys. **4**, 34 (1932).

molecular field the coupling is broken down and replaced by separate λ-quantization in the configuration $2p\sigma(2p\pi)^3\ ^3\Pi(2p\sigma$ is the promoted H electron). In this case a_{MH} may be compared with a_M of a $2p$ electron in the N atom as observed in the state $(2s)^2(2p)^2 3s\ ^2P$. The calculation on this basis made by Mulliken for NH and PH can be refined with the more accurate determinations of the molecular coefficients,[4] and the case of OH^+ included. The results are in Table IV. The value for OH^+ supports the assumption that the OH^+ bands are analogous to the NH and PH bands.

No comparison of coupling coefficients for a $\sigma\pi$ configuration seems to have been made. The $^3\Pi$ states of BH and AlH provide such a case. Following Mulliken we put $a_{MH}=2A$ and $a_M=(2/3)\Delta\nu$ where $\Delta\nu$ is the doublet interval in the ^2P state from which the molecular $^3\Pi$ is derived. a_{MH}/a_M is greater than one for both molecules. This calculation, however, supposes the molecular splitting to be due entirely to the ls interaction of the $p\pi$ electron and neglects the interaction of l of $p\pi$ with the spin of the $p\sigma$ electron.

JUNE 1, 1937 PHYSICAL REVIEW VOLUME 51

Low Voltage Proton Sources*

E. S. LAMAR, W. W. BUECHNER AND K. T. COMPTON
Massachusetts Institute of Technology, Cambridge, Massachusetts
(Received February 27, 1937)

Further experiments have been carried out with a view towards increasing the proton percentage obtainable from capillary arc sources previously described. The collision method of breaking up molecular ions has been investigated. Although no difficulty was experienced in refocusing the scattered ions, no evidence was found for break-up in the absence of magnetic fields. Rather than investigate these possibilities further, a quartz capillary was tried, using a simple beveled outlet. This eliminated the rapid disintegration of the quartz by secondary electrons from any probe electrode, but there was still evidence of gradual disintegration of the quartz by low speed electrons in the discharge. The absence of excessive heating indicated that the capillary might as easily be made of Pyrex. A Pyrex capillary source was therefore tried. In a 3.5 mm capillary, heating was not excessive at arc currents below 0.3 ampere. The proton percentages ranged up to 20 percent. Following the experience of Wood, water vapor was introduced, and resulted in a marked increase in the proton percentage (a factor of about 4). This source possesses the advantages of slightly greater ion current efficiency, requires no cooling, is easily constructed, and is free from impurities.

INTRODUCTION

IN view of the rapidly increasing number of high voltage installations for nuclear research, it has become desirable to develop more adequate sources of positive ions, particularly protons. Since, in most of these installations, both space and total power output are limited, the ideal source should require a minimum of space and power. To this end, the fraction of the total gas flow which is ionized should be as high as possible to minimize the pumping requirements. In addition, artificial cooling should not be required, since this would necessitate auxiliary equipment. The source should give high ion purity, so that the available power will not be wasted in accelerating objectionable ions. The source described by Lamar and Luhr[1] possesses the advantage of high ion purity and requires no cooling. Its successful operation, however, necessitates extreme care in experimental technique. Moreover, the current densities obtainable are small. The capillary type ion source,[2,3] although giving high ion current density, requires cooling, and does not give high ion purity. The object of the present investigation has been to reduce the discrepancies between the ideal source and the present existing types.

* A preliminary report of this work was presented at the Washington Meeting of the American Physical Society, May, 1936.

[1] Lamar and Luhr, Phys. Rev. **46**, 87 (1934).
[2] Tuve, Dahl and Hafstad, Phys. Rev. **48**, 241 (1935).
[3] Lamar, Samson and Compton, Phys. Rev. **48**, 886 (1935).

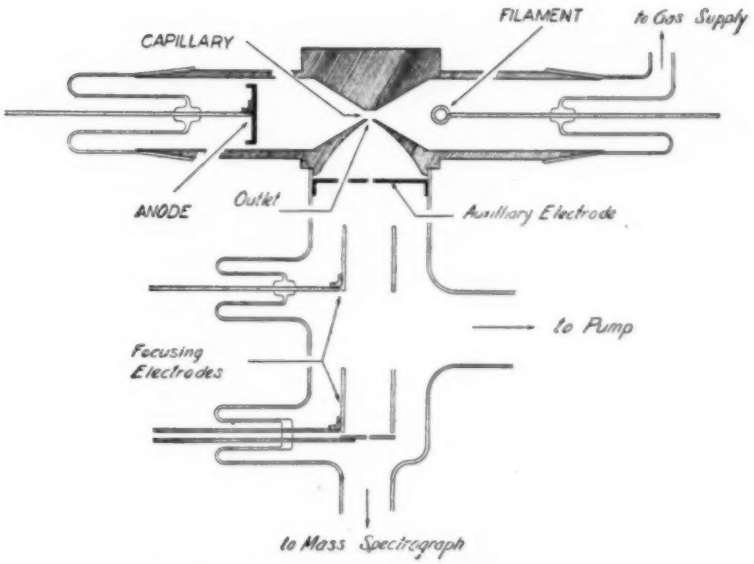

FIG. 1. Metal capillary source showing break-up electrode.

METAL CAPILLARY SOURCES

In the work of Lamar, Samson and Compton,[3] some hope for increased proton percentages was offered by the fact that heavy ions at high speeds break up, on collision with gas molecules, into protons and neutral particles. This effect had been observed previously by Smyth[4] and others. In the paper mentioned above in the third reference, a tentative design for a break-up chamber was proposed. Following this suggestion, such a chamber was built. A diagram of the experimental arrangement is shown in Fig. 1. The source itself was exactly the same as the one previously described. The enclosing wall for the break-up chamber consisted of a metal plate, with a central hole 3 mm in diameter. The potential of this plate could be controlled independently of the other circuit elements. It was found that, with increasing voltages, more and more of the total output of the source could be focused through the hole, until at 5800 volts, 60 percent of the total output was realized. The pressure in the chamber could be varied by varying the pressure in the arc. In the paper mentioned in the third reference, limits were set on the efficiencies of ion break-up, the upper limit agreeing in order of magnitude with that calculated by Smyth. In the present work, the pressure in the break-up chamber was kept sufficiently high to insure the number of collisions required on the basis of these efficiency calculations. The fraction of the current getting through the hole did not depend to any marked degree upon the pressure in the chamber.

The ions were focused into a mass spectrograph for analysis. Various arrangements of accelerating potentials were tried. Although peaks in the mass-spectrograph curves were found identifiable as broken up ions, in every case they corresponded with ions which had fallen through the entire potential difference. They were, therefore, ions which were produced by break-up in the region immediately above the spectrograph, and not in the break-up chamber. Since the solid angle subtended by the slit of the spectrograph at the hole in the plate was small, it was believed at first that the apparent absence of broken up ions from the chamber was due to small angle scattering in the chamber. In order to refocus these scattered ions, the potential between the plate and the lower electrodes was made large in comparison with the potential

[4] H. D. Smyth, Phys. Rev. **25**, 452 (1925).

between plate and source. The failure to observe broken up ions from the chamber under these conditions indicated that the process did not take place in the break-up chamber. Considerable care was exercised in the establishment of this negative result. To quote a particular set of experiments, with 1000 volts on the break-up electrode and 5000 volts over-all, primary protons plus protons resulting from break-up were expected, ranging in voltage between 4300 and 5000. The width of the proton peak measured in units of magnet current should then have 7.1 percent of the magnet current at the peak. The observed width, even at pressures in the source as high as 0.55 mm, was only 5 percent, which is approximately the resolving power of the spectrograph. Furthermore, an increase in the ratio of proton current to H_3^+ current was expected, but not observed. The possibility that these protons appeared as a highly spread background was ruled out by the fact that the background was less than 0.2 percent of the height of the H_3^+ peak. The only apparent difference between the break-up chamber and the region immediately above the spectrograph was the presence of a stray magnetic field in the latter. Hence, it would appear that ion break-up, although a collision process, for voltages below 5000 volts, takes place only in the presence of a magnetic field. This rather surprising indication, although interesting as a subject for further research, seems less promising at present than other possibilities for the development of an improved ion source.

A significant result of the experiments with the break-up chamber was the lack of difficulty experienced in the refocusing of the ions scattered in the high pressure region. If one is interested in high total ion currents, one is faced with the necessity of handling large gas flows. To do this in a single pumping stage requires an extremely fast system. The flow of gas into the main high voltage tube, however, can be reduced appreciably by differential pumping from the high pressure region formed by the introduction of the additional electrode. For the particular case of the tube shown in Fig. 1, one may calculate from the geometry what decrease in gas leakage one may expect with intermediate pumping. Pumping through the annular ring separating the electrode from the source, one might hope to gain a factor of the order of 100 in reduction of gas leakage, since the ratio of the areas of the hole and the ring is 200. Since, for electrode potentials as low as 5800 volts, 60 percent of the ion current from the source was focused through the hole, the above calculation represents a gain in available ion current, for a given gas leakage, of a factor of approximately 100. Suitable design with this in mind could be made to give even higher factors of gain, particularly since, at 5800 volts, the indications were that higher voltages would focus a larger fraction of the current.

Quartz Capillary Source

Rather than investigate the break-up mechanism further, a source was constructed having the capillary of quartz. Quartz capillary sources had been tried previously by Mohler and by Tuve and his collaborators. In their sources, rapid disintegration of the quartz resulted from bombardment by secondary electrons from the high voltage probe used for drawing the ions out of the arc. Since, in our case, a simple beveled hole was used as an outlet, allowing the ions to drift out into the nearly field free space of relatively high vacuum in the discharge tube before attempting to focus them into a beam, it was hoped that this disintegration would be avoided. Furthermore, it was believed that the clean quartz surfaces would be less effective as a catalyst for the recombination of atomic hydrogen than the metal or the disintegrated quartz surfaces in the sources that had been tried previously. This source is shown in Fig. 2.

Mass-spectrograph analysis of the ions obtained with this source, however, showed a proton percentage little or no better than that obtained from the metal sources. In addition, investigation of the capillary after some hours of use showed a gradual disintegration of the quartz, presumably by low speed electrons in the discharge. In operation, there was no apparent overheating of the capillary, indicating that the source might as easily be made of Pyrex, with the attendant elimination of graded seals and other inconveniences connected with the use of quartz.

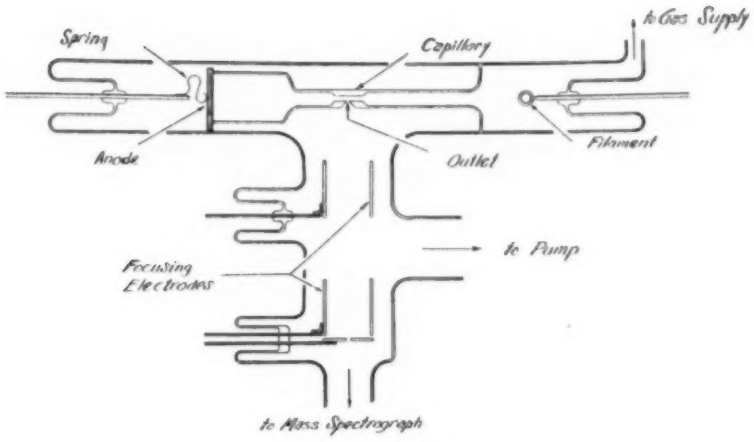

FIG. 2. Typical nonmetal capillary source.

PYREX CAPILLARY SOURCE

A Pyrex capillary source was constructed, therefore, in the manner indicated in Fig. 2. For the 3.5 mm diameter capillary used, no undue heating of the capillary occurred for arc currents below 0.3 amp. The spectrum of the discharge was viewed through a transmission grating, and was predominantly that of atomic hydrogen up to arc currents of 0.3 amp., above which the atomic spectrum increased in intensity along with the appearance of the sodium D lines, indicating that the capillary was beginning to overheat. With this source, proton percentages were found ranging up to 20 percent. Following the experience of Wood, water vapor was introduced into the tube, in an attempt to increase the atomic hydrogen present in the discharge. This resulted in a marked increase in the intensity of the atomic spectrum. It might be of interest to remark in passing that it was feared that the water vapor might have a deleterious effect upon the oxide coated filament used for a cathode. It was found, however, that, instead of being harmed by the water, the filament actually seemed benefited by its presence. This, of course, is contrary to usual experience with gases other than hydrogen. The water vapor was introduced into the discharge by having saturation vapor pressure in the hydrogen reservoir, the percentage of water vapor used being controlled by varying the hydrogen pressure. Typical mass-spectrograph curves taken with this source are shown in Fig. 3. The bottom curve shows the beam constitution with no water vapor in the source, and it is seen that the protons amount to about 18 percent of the total ion current. The middle curve was taken with a hydrogen pressure in the reservoir of 4 cm, the arc pressure being 0.04 mm. It is seen that the proton percentage in this case has increased to approximately 58 percent. The top curve was taken at an arc pressure of 0.18 mm, and here the proton percentage is 80 percent. No attempt was made to increase this last figure, but it is probable that further adjustment of the water vapor concentration would allow even higher percentages. A search was made for water vapor and for atomic oxygen ions, and none were found. It was not convenient to look for molecular oxygen ions. However, the lack of water vapor ions, atomic oxygen ions, and the purity of the atomic hydrogen spectrum make it improbable that any molecular oxygen ions were present.

It was found that the source operated quite satisfactorily using hollow cathodes made of stainless steel, a potential of approximately 600 volts being necessary for an arc current of 0.2 ampere. The power input for a given arc current is, of course, increased by the amount of the increase in cathode fall. In particular, the total arc drop with a hot cathode was approximately 150 volts, deviating from this value slightly with

changes in pressure; whereas, with the hollow cathode, the total arc drop for the same current was about 600 volts. With a hot cathode, the arc was quite stable at pressures as low as 0.04 mm; whereas, with a hollow cathode, it was difficult to maintain a discharge at pressures below 0.2 mm. This minimum could be reduced, of course, by increasing the dimensions of the hollow cathode, since the indications are that the minimum pressure at which a hollow cathode will operate depends upon its diameter measured in mean free paths. The hollow cathode used in

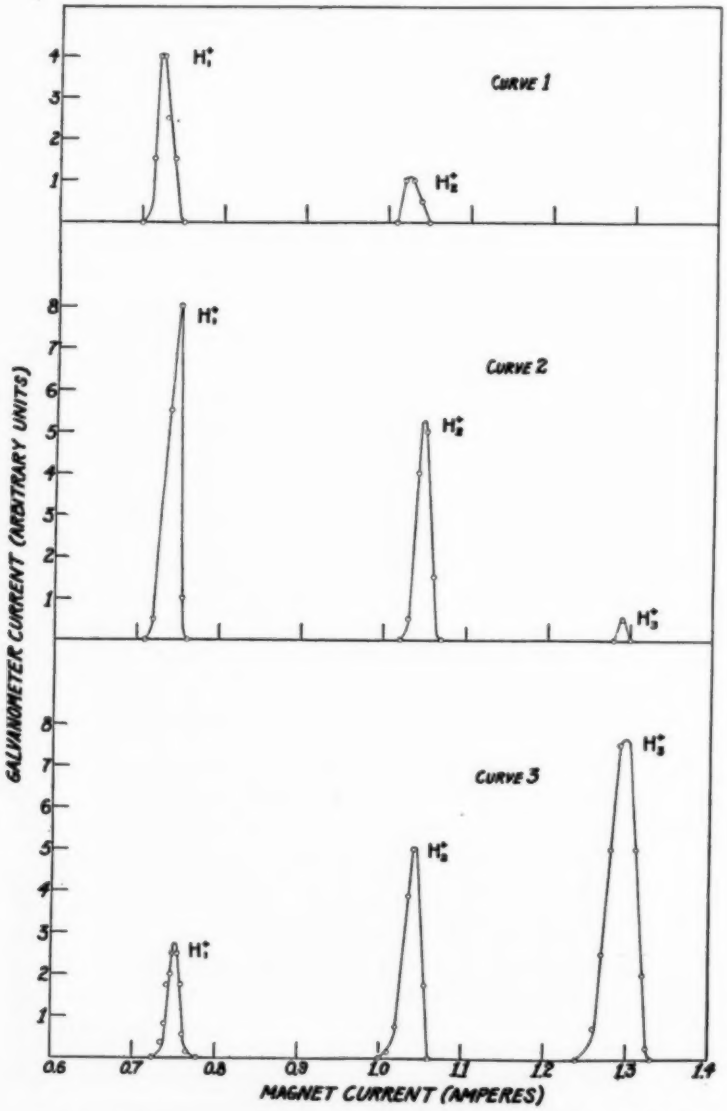

FIG. 3. Mass-spectrograph curves for Pyrex capillary source. Curve 1: Arc pressure of 0.18 mm, arc current 0.2 amperes, 30 percent water vapor in reservoir. Curve 2: Arc pressure 0.04 mm, arc current 0.2 ampere, 45 percent water vapor in reservoir. Curve 3: Typical curve with no water vapor in reservoir.

TABLE I. *Typical performances of M. I. T. proton sources. A is the source utilizing accommodation coefficients to achieve high percentage of hydrogen dissociation. B is metal capillary source with hydrogen. C is the Pyrex source with moist hydrogen.*

	A	*B*	*C*
Pressure in arc	0.23–0.60 mm	0.04–0.49 mm	0.04–0.45 mm
Arc current	1.00 amp.	0.1–5 amp.	0.1–0.3 amp.
Total power used	61–97 watts	60–550 watts	68–101 watts
Ion current density	1.4–10.5 milliamps/cm²	7–1000 milliamps/cm²	21–46 milliamps/cm²
Percentage of protons	98–100*%	5–20%	58–80%
Percent useful ionization†	0.0021–0.04%	0.0003–2.21%	0.012–0.41%

† The percent useful ionization is the ratio of the number of protons to the number of gas molecules leaving the outlet per second expressed in percent.
* Lower values if metal surfaces are not clean.

these experiments was already one inch in diameter. It seems out of the question, therefore, to hope to better this by another order of magnitude.

In the Pyrex source, ion currents of 60 microamperes were obtained with an arc current of 0.2 ampere in a 3.5 mm capillary with an outlet hole 0.5 mm in diameter. With the Pyrex source, as with the metal source, the ion current per unit effective outlet area is proportional to total arc current, as is described in detail in the third reference. For a given outlet area, the ion current per unit arc current in the case of the Pyrex source is slightly in excess of that reported for the metal source. Heating of the Pyrex capillary limits the arc current in the present source to 0.3 ampere. This limitation is partly compensated for by the increased ion purity. The presence of insulating, rather than conducting, walls makes for ease of starting and stability of operation. Since the ion current obtainable is adequate for most requirements, and since it requires no cooling, this source compares favorably with other types, even in its present form. Obviously, the direction in which to seek improvement lies in providing some convenient means for cooling the capillary. This might be accomplished by first coating the capillary with some conducting film, such as Aquadag, and then depositing, by means of electroplating, a heavy coating of copper, thus providing a low resistance path for the flow of heat away from the capillary.

In conclusion, a rough comparison between the sources tested at M. I. T. is given by Table I.

The authors wish to acknowledge their indebtedness to Dr. C. M. Van Atta for helpful advice and criticism.

On the Matrix Element in Fermi's Theory of β-Decay

L. W. NORDHEIM AND F. L. YOST
Purdue University, Lafayette, Indiana
(Received March 22, 1937)

It is investigated how the Fermi theory of β-decay has to be formulated for a complex nucleus containing many particles. By symmetrizing the problem in all particles (neutrons and protons) a general prescription is obtained which would allow one to calculate the transition probabilities when the wave functions for the nucleus in its initial and final state are known. The discussion of the heavy particle matrix element which is involved shows that a considerable decrease of the transition probability with the complexity of the nucleus is to be expected. A new reduction of the empirical data shows that the influence of the Coulomb field on the β-disintegration probability is larger than heretofore assumed. The difference obtained in reduced lifetimes of light and heavy nuclei (of the order of a factor 50 to 100) is of the same order of magnitude as estimated from the theoretical considerations.

1. INTRODUCTION

IN the Fermi theory of β-decay the probability for a definite disintegration process contains besides other factors a matrix element depending on the wave functions of the heavy particle which goes over from a neutron to a proton state or *vice versa*. Hitherto one has assumed that this matrix element, whose square enters in the total transition probability, should be of the order unity for the so-called allowed transitions.[1] This was suggested by the fact that the lifetimes of different elements with approximately the same maximum energy are of the same order of magnitude. (See Table I.) However, a more careful consideration of the theory shows that this apparent equality in the lifetimes for heavy and light nuclei actually means a considerable variation of the matrix element. This is due to the large influence of the Coulomb field on the electronic density near the nucleus.[2] We have made a new calculation of this effect (see §2) and we have found it considerably larger than heretofore assumed. In fact, the reduced lifetimes between light and heavy elements differ by a factor of the order of 100.

The only possible explanation for this effect seems to be that it is due to the above mentioned matrix element of the heavy particles. We have investigated, therefore, whether one can make any statements concerning this matrix element from theoretical considerations. The first question is then, how one can take into account the fact that we have many particles in the nucleus which virtually can make the neutron-proton transition. It seems to us that a unique formulation of the Fermi theory for this case can be obtained which would make it possible to calculate the matrix element if the correct wave functions were known. From the form of this matrix element one would expect rather large individual deviations and it seems to be a natural consequence that the matrix element becomes smaller with increasing complexity of the nucleus.

2. EFFECT OF THE COULOMB FIELD

In the Fermi theory of β-decay the probability that an electron is emitted by a nucleus with total energy between ϵ and $\epsilon+d\epsilon$ (in units mc^2) is

$$wd\epsilon=\frac{|M|^2}{\tau_0}F(Z,\epsilon)(\epsilon_0-\epsilon)^{2n}(\epsilon^2-1)^{\frac{1}{2}}\epsilon d\epsilon, \quad (1)$$

if the mass of the neutrino is taken to be zero. In (1) ϵ_0 is the upper limit of the energy. The exponent n depends on the basic assumption regarding the interaction, n being 1 for Fermi's original form and 2 for the one used by Konopinski and Uhlenbeck,[3] which gives a better agreement with the experimental distribution curves. τ_0 is a universal constant of the dimension

[1] We say that a transition is an allowed one when the corresponding element belongs to the group which shows the shortest reduced life times among all elements of comparable atomic weight.

[2] The influence of the Coulomb field has already been included in Fermi's original treatment (Zeits. f. Physik **88**, 161 (1934)) and H. A. Bethe and R. F. Bacher, Rev. Mod. Phys. **8**, 82 (1936) give an estimate similar to ours, but they obtain much smaller differences between heavy and light nuclei.

[3] E. J. Konopinski and G. E. Uhlenbeck, Phys. Rev. **48**, 7 (1935).

TABLE I. *Lifetimes, maximum energies and comparative values for the heavy particle matrix elements for β radioactive nuclei.*

Nucleus	±	τ(sec.)	$(\epsilon_0-1)(mc^2)$	f_F	f_{KU}	$10^5\times 1/\tau f_F$		$10^5\times 1/\tau f_{KU}$	
$_6C^{11}$	+	1,200	2.5	11	29	8.0		29	
$_7N^{13}$	+	660	2.8	17	57	8.9		26	
$_8O^{15}$	+	150	3.9	63	360	11		19	
$_9F^{17}$	+	70	4.9	170	1,400	8.6		9.9	
$_{12}Mg^{27}$	−	620	(3.9)	110	620	1.5		2.6	
$_{14}Si^{27}$	+	150	3.9	54	300	12		22	
$_{45}Rh^{105}$	−	44	5.5	1600	18,000	1.5		1.3	
$_{47}Ag^{105}$	−	22	5.5	1700	19,000	2.7		2.4	
$_{49}In$	−	13	6.3	3200	46,000	2.4		1.7	
$_{49}In$	−	3,240	2.5	83	230	.37		1.3	
$_{81}AcC''^{207}$	−	410	2.7	750	2,700	.33	(.20)	.91	(.44)
$_{81}ThC''^{208}$	−	275	3.6	2200	12,000	.17	(.11)	.32	(.18)
$_{82}ThB^{212}$	−	55,000	0.7	8.2	2.4	.22	(.05)	7.7	(.79)
$_{82}RaB^{214}$	−	2,300	1.3	54	48	.81	(.33)	9.1	(2.3)
$_{91}UX_2^{234}$	−	94	4.5	7100	57,000	.15	(.11)	.19	(.12)

of a time which determines the absolute magnitude of the interaction.

$$\frac{1}{\tau_0}=\frac{G}{(2\pi)^3}\frac{mc^2}{\hbar};\quad G\sim 10^{-13}.$$

M is the matrix element of the wave functions of proton and neutron which can be factored out under the assumption that the electron and neutrino functions can be taken as constant over the nucleus (allowed transitions).

$$M=\int \Phi^*(x)O\Psi(x)dx, \tag{2}$$

where Ψ and Φ are the wave functions for the initial and final state and where x stands for spin and space variables. O might be an operator acting on the spin variable depending on the special form of the interaction Hamiltonian.

$F(Z,\epsilon)$, finally, is a factor expressing the dependence on the Coulomb field of the nucleus. Its physical meaning is the change in the electronic density $|\psi|^2$ at the nucleus, introduced by the Coulomb field and obtained by summing over all electronic s states in the interval $d\epsilon$. The relativistic s functions, of course, diverge at the center of the field. However, as the field in a nucleus with finite range will not increase infinitely, the electronic density inside of it will not vary rapidly and we can use for the β-decay the value at the border of the nucleus. The expression for $F(Z,\epsilon)$ already determined by Fermi[2] is then

$$F(Z,\epsilon)=\frac{4}{[\Gamma(1+2s)]^2}\left(\frac{2(\epsilon^2-1)^{\frac{1}{2}}}{\hbar}mcR\right)^{2s-2}\times e^{\pi\gamma\epsilon(\epsilon^2-1)^{-\frac{1}{2}}}|\Gamma(s+i\gamma\epsilon(\epsilon^2-1)^{-\frac{1}{2}})|^2 \tag{3}$$

with Z being the nuclear charge, $\alpha=1/137$, $\gamma=\alpha Z$, $s=(1-\gamma^2)^{\frac{1}{2}}$ and R the nuclear radius.[4] The quantity γ is positive for electron emitters and negative for positron emitters. For $Z\to 0$, i.e., $\gamma\to 0$, $s\to 1$, we obtain $F\to 1$ as it should be. Even for the largest Z, $x=s-1\sim-\gamma^2/2$ and $y=\gamma\epsilon(\epsilon^2-1)^{-\frac{1}{2}}$ will be <1 (excluding the smallest values of ϵ which do not contribute much to (1)). We can therefore use the evaluation of the complex Γ function:[5]

$$|\Gamma(s+i\gamma\epsilon(\epsilon^2-1)^{-\frac{1}{2}})|^2=|\Gamma(1+x+iy)|^2\sim\left[\frac{\pi^2(x^2+y^2)}{\sin^2\pi x+\sinh^2\pi y}\cdot\frac{(1-x)^2+y^2}{(1+x)^2+y^2}\right]^{\frac{1}{2}},$$

which, if terms of the order x^2 are neglected, reduces to

$$\frac{2\pi|y|(1-2x)}{|e^{\pi y}-e^{-\pi y}|}.$$

Approximately, therefore,

$$F(Z,\epsilon)=\frac{2^{2s}}{(2s!)^2}\frac{2\pi|\gamma|(1+\gamma^2)}{|1-e^{-2\pi\gamma\epsilon(\epsilon^2-1)^{-\frac{1}{2}}}|}\left(\frac{mcR}{\hbar}\right)^{2s-2}\times\epsilon(\epsilon^2-1)^{s-\frac{1}{2}}. \tag{4}$$

For not too small ϵ the denominator can be developed

[4] We take $R=1.5\times 10^{-13}A^{\frac{1}{3}}$ (A = atomic weight). The new slightly larger values of H. A. Bethe, Phys. Rev. **50**, 977 (1936), would increase our final values for the matrix elements by a factor 1.2 for the heaviest nuclei, which is not important.

[5] Compare Jahnke-Emde, second edition (Teubner, 1933), p. 87.

$$|1-e^{-2\pi\gamma\epsilon(\epsilon^2-1)^{-\frac{1}{2}}}|^{-1}$$

$$\sim\frac{1}{|1-e^{-2\pi\gamma}|}\left[1-\frac{2\pi|\gamma|}{|e^{2\pi\gamma}-1|}\cdot\frac{1}{2\epsilon^2}\right], \quad (5)$$

and (4) and (5) can be used for the whole range of γ, i.e., Z.

(4) is easily seen to give a factor ~ 50 between heavy and light elements, as, e.g., for $Z\sim 90$, the factors become

$$\frac{2^{2s}}{(2s!)^2}\sim 1.6, \quad \frac{2\pi\gamma(1+\gamma^2)}{|1-e^{-2\pi\gamma}|}\sim 6, \quad \left(\frac{mcR}{\hbar}\right)^{2s-2}\sim 5.$$

With the help of (4) and (5) one can integrate (1) over the energy to obtain the average lifetime

$$\frac{1}{\tau}=\int_1^{\epsilon_0} w d\epsilon=\frac{|M|^2}{\tau_0}f(\epsilon_0), \quad (6)$$

where

$$f(\epsilon_0)=\frac{2^{2s}}{(2s!)^2}\frac{2\pi|\gamma|(1+\gamma^2)}{|1-e^{-2\pi\gamma}|}\left(\frac{mcR}{\hbar}\right)^{2s-2}\times$$

$$\int_1^{\epsilon_0}\left[1-\frac{2\pi|\gamma|}{|e^{2\pi\gamma}-1|}\cdot\frac{1}{2\epsilon^2}\right](\epsilon_0-\epsilon)^{2n}(\epsilon^2-1)^{s-1}\epsilon^2 d\epsilon. \quad (7)$$

Replacing the slowly varying factor $(\epsilon^2-1)^{s-1}$ by $(\bar{\epsilon}^2-1)^{s-1}$ where $\bar{\epsilon}$ is the mean value of ϵ, we obtain for the integral in (7) for $n=1$ (Fermi)

$$(\bar{\epsilon}^2-1)^{s-1}\left[\frac{\epsilon_0^5}{30}-\frac{\epsilon_0^2}{3}+\frac{\epsilon_0}{2}-\frac{1}{5}\right.$$

$$\left.-\frac{2\pi|\gamma|}{|e^{2\pi\gamma}-1|}\frac{(\epsilon_0-1)^3}{6}\right] \quad (8a)$$

and for $n=2$ (Konopinski-Uhlenbeck)

$$(\bar{\epsilon}^2-1)^{s-1}\left[\frac{\epsilon_0^7}{105}-\frac{\epsilon_0^4}{3}+\epsilon_0^3-\frac{6}{5}\epsilon_0^2+\frac{2}{3}\epsilon_0-\frac{1}{7}\right.$$

$$\left.-\frac{2\pi|\gamma|}{|e^{2\pi\gamma}-1|}\frac{(\epsilon_0-1)^5}{10}\right]. \quad (8b)$$

As τ_0 is assumed to be constant, the product $1/\tau f(\epsilon_0)$ is proportional to the square of the matrix element. In Table I we give the relevant data for all the elements with allowed transitions, for the Fermi as well as for the Konopinski-Uhlenbeck case. The last two columns give relative values for M^2 for the different elements.

For the maximum energies ϵ_0 we have taken the values extrapolated from Konopinski-Uhlenbeck plots, as far as they are known. Though it seems to be agreed now that the Konopinski-Uhlenbeck plots give too high values for ϵ_0 it seems still to be reasonable to use this method of reduction as otherwise the form of the electronic distribution agrees so well with the Konopinski-Uhlenbeck formulae. A possible error introduced by this choice of ϵ_0 would also enter similarly for all elements.

For the heavy radioactive elements, on the other hand, only Sargent's values which have been obtained by inspection are available. This means probably that the ϵ_0 used for the heavy elements are systematically too low compared with those for the lighter elements. To see the possible influence of this effect we have given in brackets other reduced values which are obtained when one increases Sargent's ϵ_0 arbitrarily by 0.2 MV $\sim 0.4\ mc^2$ which is of the order of the observed difference between the Konopinski-Uhlenbeck and the inspection values. From the table we see, besides individual fluctuations, chiefly a systematic decrease of the matrix elements with increasing mass number. M^2 decreases from the group of the light positron emitters of the type ${}_6C^{11}$ to the elements with medium weight as In and Ag by a factor ~ 10 and to the heavy elements by a factor 50 to 100.

Only the two heavy elements with very low maximum energy, Th B and Ra B fall somewhat out of line with the rest but owing to the much smaller ϵ_0 they are not directly comparable with the others.[6] The empirical corrections, introduced above, already reduce the matrix elements sufficiently to remove the anomaly. A further interesting remark is, that the values for M^2 straggle decidedly less if the Fermi coupling is taken instead of the Konopinski-Uhlenbeck one. This might suggest that the latter gives too strong a dependence of the life times on the maximum energy which again would explain the anomalous behavior of Th B and Ra B.

[6] The integral in (7) has been more accurately evaluated for these elements than in (8a) and (8b).

3. General Formulation of the Fermi Theory

The matrix element (2) is defined only for a single particle which makes the proton-neutron transition. We have to investigate how M is to be generalized for a nucleus with many particles.

According to our present knowledge, a nucleus containing k neutrons and l protons can be described by a wave function

$$\Psi(\{x_1\cdots x_k\}\{x_{k+1}\cdots x_{k+l}\})$$

which has to be antisymmetrical in the protons and neutrons separately as indicated by bracketing the corresponding variables. (x representing again space and spin variables). Similarly, after a β transformation, the nucleus in its final state can be described by a function

$$\Phi(y_1\cdots y_{k-1}, y_k\cdots y_{k+l})$$

in which we have one neutron less and one proton more. The problem is to find the matrix element for the Fermi theory, when these two functions are known. It is clear that the theory has to be formulated so that one cannot distinguish the particle which makes the neutron-proton transition. For this reason we can give no elementary correlation between the variables x and y, and it is therefore not possible to take over the matrix element (2) simply summing it over the initial neutrons.

Considering that it has no meaning to ascribe the neutron or proton property to a definite group of particles as soon as there are processes involved in which a particle changes its character, it is evident that the theory has to be formulated completely symmetrical in all particles. Such a symmetrization[7] can be carried out most conveniently by introducing a new fifth coordinate for each particle. This coordinate determines the neutron or proton characteristics of the particle to which it refers. We designate the proper functions in the neutron or proton states by n and p, respectively. With this the totally antisymmetrized wave function (which is necessary to fulfill the Pauli principle) can be written as

$$\Psi_i=\left[\frac{k!\,l!}{(k+l)!}\right]^{\frac{1}{2}}\sum_I\Psi(\{x_1\cdots x_k\}\{x_{k+1}\cdots x_{k+l}\})\eta_I \times n(1)\cdots n(k)p(k+1)\cdots p(k+l),$$

$$\Phi_f=\left[\frac{(k-1)!(l+1)!}{(k+l)!}\right]^{\frac{1}{2}}\sum_I\Phi(\{x_1\cdots x_{k-1}\}\{x_k\cdots x_{k+l}\}) \times\eta_I n(1)\cdots n(k-1)p(k)\cdots p(k+l).$$

The sums are extended over all interpermutations I between the neutrons and protons, $\eta_I=\pm1$ depending whether the permutation is even or odd. We can use now in both functions the same variables x. The radicals serve for normalization, i.e., the functions Ψ_i, Φ_f are normalized provided the original Ψ and Φ were.

The natural generalization of the matrix element (2) will then be

$$M=\sum_m\int\Phi_f^*[F_m\Psi_i]dx_1\cdots dx_{k+l} =(k+l)\int\Phi_f^*[F_k\Psi_i]dx_1\cdots dx_{k+l}, \quad (9)$$

where the sum is to be extended over all particles. The transformation operator F_m signifies that in Ψ_i $n(m)$ has to be replaced by $p(m)$. (The terms of Ψ_i which already contain $p(m)$ give automatically no contribution to M). All terms in the sum over m give the same contribution due to the complete symmetrization so that one obtains the above final form. In this we attribute the $n\rightarrow p$ transition to the definite particle k and multiply then by the total number $k+l$ of all the particles. The summation over the character coordinates can be carried out with the help of the orthogonality and normalization relations

$$\sum n^2(m)=\sum p^2(m)=1, \qquad \sum p(m)n(m)=0. \quad (10)$$

Introducing now the full expressions Ψ_i and Φ_f in (9) we see with the help of (10): Firstly, all interpermutations in $F_k\Psi_i$ which involve the particle k are orthogonal to Φ_f as the number of protons is different. Secondly, all interpermutations in Φ_f which involve the particle k are orthogonal to $F_k\Psi_i$ as they contain $n(k)$. Therefore all interpermutations which involve k drop out. The remaining interpermutations are then the same for both wave functions and only corresponding terms give a contribution owing to (10). As these terms differ only by the designation of the integration variables, all the integrals are identical, their total number being the number of inter-

[7] G. Breit and E. Feenberg, Phys. Rev. **50**, 850 (1936); B. Cassen and E. U. Condon, Phys. Rev. **50**, 846 (1936).

permutations with the exception of k, i.e., $(k+l-1)!/(k-1)!l!$, and we obtain finally

$$M=(k+l)\frac{(k+l-1)!}{(k-1)!\,l!}\left[\frac{k!\,l!}{(k+l)!}\right]^{\frac{1}{2}}\left[\frac{(k-1)!(l+1)!}{(k+l)!}\right]^{\frac{1}{2}}\times\int\Phi^*\Psi dx_1\cdots dx_{k+l}$$

$$=[k(l+1)]^{\frac{1}{2}}\int\Phi^*(\{x_1\cdots x_{k-1}\}\{x_k\cdots x_{k+l}\})\times O_k\Psi(\{x_1\cdots x_k\}\{x_{k+1}\cdots x_{k+l}\})dx_1\cdots dx_{k+l}, \quad (11)$$

where Ψ and Φ are the original wave functions for the initial and final state for the total nucleus which do not contain the character variables. In the final form we have reintroduced an operator O_k which might act on the spin or space variable of the particle k in case it is assumed to do so in the original interaction.

Naïvely one would perhaps have expected the result (11) only with the numerical factor k(=number of initial neutrons) instead of the factor $[k(l+1)]^{\frac{1}{2}}$ which is symmetric in the number of neutrons in the initial and protons in the final state.

4. Discussion of the Matrix Element

To get an idea of the meaning of our prescription (11), especially the factor $[k(l+1)]^{\frac{1}{2}}$, we evaluate M under the assumption that Ψ and Φ are Hartree-Fock wave functions, i.e., can be written as determinants of individual particle wave functions. We develop these functions in the minors of the particle assumed to make the transition, i.e.,

$$\Psi=\frac{1}{(k)^{\frac{1}{2}}}\sum\psi_{ni}(x_k)R_{in},$$
$$\Phi=\frac{1}{(l+1)^{\frac{1}{2}}}\sum\phi_{pf}(x_k)R_{fp}, \quad (12)$$

where ψ_n and ϕ_p are the individual particle wave functions for the initial neutrons and final protons and R_n and R_p, respectively, the normalized wave functions of the rest nuclei.

Inserting (12) into (11) we get simply

$$M=\int\sum_{nipf}\phi_{pf}^*(k)(O_k\psi_{ni}(k))R_{ni}R_{pf}^*d\tau. \quad (13)$$

We obtain therefore as a prescription for the case of Hartree-Fock wave functions the following one: Take an arbitrary initial neutron state and final proton state, assign them to the particle which makes the transition, multiply them with normalized wave functions for the rest nucleus, sum over all possible combinations and integrate. The numerical factor is then exactly unity.

If we assume furthermore that the individual particle wave functions are practically the same for neutrons and protons and in both nuclei, and that they form an orthogonal set, (13) will give unity for M if we have in the initial and final nucleus just one corresponding neutron proton state with the rest nuclei identical. In all other cases we would obtain zero. According to this oversimplified picture we would get the result that M would be ~ 1 for the radioactive nuclei of the type ${}_6C^{11}$ in which just one surplus neutron or proton would be present which could then go over into the corresponding state of opposite character. In all other cases M would be very small.

This result shows again that the Hartree-Fock approximation is inadequate for heavier nuclei. According to the considerations of Feenberg and Wigner[8] and Bethe and Rose[9] we can, however, expect to obtain reasonable approximations to the true many-body wave functions by the superposition of a number of such configurations. In using such a development

$$\Psi_i=\sum a_r\psi_r, \quad \sum a_r^2=1,$$
$$\Phi_f=\sum b_s\phi_s, \quad \sum b_s^2=1 \quad (14)$$

the matrix element M will be

$$M=\sum a_rb_r^*, \quad (15)$$

where the sum is over all identical spin and space configurations which occur both in the initial and final nucleus. (15) will give again unity for the light positron emitters of the group ${}_6C^{11}$, as here initial and final nuclei are built up with the same configurations and approximately the same coefficients. However, we have to expect, firstly that the number of configurations necessary for a good approximation increases considerably with the complexity of the nucleus; secondly, that in

[8] E. Feenberg and E. Wigner, Phys. Rev. **51**, 195 (1937).
[9] H. A. Bethe and M. E. Rose, Phys. Rev. **51**, 205 (1937).

case the numbers of neutrons and protons differ by more than 1, only a fraction of the configurations will occur in both Ψ_i and Φ_f with large coefficients.

We can illustrate this behavior by the following simple consideration. Let us assume that for the function Ψ_i a set of f configurations and for the function Φ_f another set of g configurations is important so that only part of them, in number h, occur in both sets. In the average over all possible distributions of the coefficients, that means all directions of the unit vectors Ψ and Φ in their respectively f and g dimensional spaces, we obtain

$$(M^2)_{Av}=(a\cdot b)^2=h(a_x^2)_{Av}(b_x^2)_{Av}=h/fg, \quad (16)$$

where x designates an arbitrary component of the corresponding vector.

It seems not possible at the present stage to obtain estimates of the number of configurations which are necessary to give a good approximation for higher nuclei. But we think that the empirical behavior of the matrix elements as found in §2 gives a definite indication about the nature of the wave functions in heavy nuclei. From the crude estimate (16) one would conclude that the number of configurations required for a fair approximation will increase more than linearly with the mass number. A factor of the order 1/100 for the heavy elements would be given by some such values as $f\sim g\sim 20$ of which $h\sim 4$ would coincide, which means that a rather large number of configurations would be necessary as would seem to be required by our other knowledge of the constitution of heavy nuclei.

JUNE 1, 1937 PHYSICAL REVIEW VOLUME 51

On the Structure of Nuclei Beyond Oxygen

E. WIGNER
University of Wisconsin, Madison, Wisconsin
(Received March 16, 1937)

An attempt is made to correlate the kinks in the mass defect curve with the energy differences between isobars, both as obtained from direct measurements and also from the shift of the isotopic number to higher values with increasing number of particles. Since the single-particle picture is known to be an insufficient approximation, the symmetry property of the wave function, resulting from the use of a symmetric Hamiltonian is utilized. The average interaction between symmetrically and antisymmetrically coupled particles ($L+L'$ and $L-L'$) is determined mainly from the kinks in the mass defect curve and enables one to calculate the energy differences between isobars. The energy change at the end of the shell is obtained from experimental data. It should enable one to get some idea of the probabilities with which the particles are in excited configurations. For heavier elements, the formula obtained here should naturally be identical with Weizsäcker's semi-empirical formula and the connection between both is discussed.

(1)

THE extension of the calculations of E. Feenberg and the present author[1] on the spectroscopic characteristics of the normal state and the low excited states to higher elements encounters great computational difficulties. With the one-particle picture, after the $2p$ shell is completed at O^{16}, the $3d$ and $2s$ shells begin to be built up probably simultaneously. Even the normal states of these elements will contain wave functions from several configurations ($3d^n$, $3d^{n-1}2s$, $3d^{n-2}2s^2$, $\cdots$) with about equal coefficients. But even the d^n configuration alone gives rise to a large number of terms with the lowest partition and the explicit calculation of all the matrix elements between these states becomes increasingly difficult. Table I shows[2] the "low terms" of the d^n configurations up to d^4, together

[1] E. Feenberg and E. Wigner, Phys. Rev. **51**, 95 (1937); also H. A. Bethe and R. F. Bacher, Rev. Mod. Phys. **8**, 82 (1936), and F. Hund, Zeits. f. Physik, to appear soon.

[2] For the preparation of Table I, cf. E. Wigner, Phys. Rev. **51**, 106 (1937), F. Hund, ref. 1. The terms for Table I have been first determined by E. Feenberg (private communication).

with the corresponding partition. In addition to the terms of the d^n configuration, one would have to take into account the terms from the $d^{n-1}s$, $d^{n-2}s^2$ etc. configurations, which are the same as those of the d^{n-1}, d^{n-2}, etc. configurations. Even for Ne^{20} one would have three S terms already. On the basis of the calculations of reference 1, one would expect that the term with the lowest azimuthal quantum number would be the lowest —that is, in all cases an S term. This, however, is certainly not correct for Na^{23}, which has a spin of $\frac{3}{2}$, although it is probably correct for the majority of nuclei.

It is well known also that the single-particle picture is not as good an approximation for nuclei as it is for atomic spectra.[3] Although it is probably at least a useful guiding principle for the determination of the lowest term[4] it may be that even for a light element like B^{10} or N^{14} it leads to erroneous results.[5] The greatest difference between nuclear and atomic spectra in this respect is doubtless the fact that while the terms of a configuration in atomic spectra are rather close together and more or less well separated from other configurations, the situation is exactly opposite in nuclear spectra. Even the lowest configuration spreads out its terms from low energy values to large, positive values. An example of this is given in reference 1, Table V, in the case of Li^6 where all terms (not only the "low terms") of the configuration p^2 are listed. The potential energy of the terms extends from $-12.7\ mc^2$ to $+5.5\ mc^2$, giving an actual repulsion in the latter case. This great difference between atomic and nuclear spectra is due to the fact that the interaction between nuclear constituents is not only a function of the distance but is for the same distance

TABLE I. *Low terms of the d^n configurations.*

	d	d^2	d^3	d^4
Terms	D	SDG	$SDFGI$	$SDDGGHIK$
Partition	$4+\cdots+4+1$	$4+\cdots+4+2$	$4+\cdots+4+3$	$4+\cdots+4+4$

[3] This point has been especially emphasized lately by N. Bohr, Nature **137**, 344 (1936). Cf. also S. Flügge, C. F. v. Weizsäcker, W. Heisenberg, Zeits. f. Physik **96**, 459, 431, 473 (1935) also M. Ostrofsky, G. Breit, D. P. Johnson, Phys. Rev. **49**, 22 (1936).

[4] W. Elsasser, Phys. Rev. **51**, 144 (1937).

[5] According to E. Feenberg and M. Phillips, Phys. Rev. **51**, 597 (1937) the ground states of B^{10} and N^{14} are possibly D states, instead of S states as one would expect on the basis of the single particle picture (reference 1).

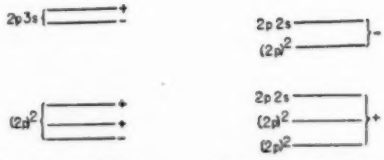

Spectrum of O^{++} Spectrum of Li^6 nucleus

FIG. 1. In atomic spectra, the states with the same configuration are usually close together while the effect of the symmetric (+) or antisymmetric (−) character of the wave function is comparatively unimportant. In nuclear spectra, the symmetry character of the wave function is much more important than the configuration. Observed values for O^{++}, crude estimates for the Li nucleus.

negative or positive according to the symmetric or antisymmetric character of the wave function for an interchange of the two particles. In consequence hereof, those configurations which give the strongest binding, give the strongest repulsion between the particles also. While in atomic spectra the terms of the same configuration are close together, in nuclear spectra this is much rather true of terms of the same symmetry character with respect to permutations, though, of course, for *extremely high* configurations (kinetic energy) the terms of every symmetry class become extremely high. The situation is schematically illustrated in Fig. 1. It is evident from this picture also that the configurations will be least mixed up for the ground state and the shell structure will be most noticeable for this state.

(2)

Since a calculation of the potential energies on the basis of the one particle picture is hardly practicable, a calculation on the more general lines of reference 1, Eqs. (4)–(8), suggests itself. Neglecting again spin dependent forces and differences between proton-proton, proton-neutron, and neutron-neutron forces (approximation 1 of reference 2) the wave functions belong to irreducible representations $D(R)$ of the whole permutation group. Consequently, if P_R is the permutation R of the coordinates[6]

$$P_R\psi_\kappa(x_1, \cdots, x_n) = \sum_{\lambda=1}^{f} D(R)_{\lambda\kappa}\psi_\lambda(x_1, \cdots, x_n), \quad (1)$$

[6] Cf. reference 1, Eq. (6). The + sign in this equation is a misprint and should be replaced by an = sign. There is an error also in Table VIII, p. 104 of this paper, insofar as the experimental energy differences are too small by 1 mc^2 throughout the table, excepting the pair H^3-He^3.

where x_i always stands for the three positional coordinates of the ith particle. The ψ are supposed to be orthogonal and normalized and κ, λ take on the values 1, 2, $\cdots$, f.

The potential energy is symmetric in the n particles in approximation 1. Hence, it will be the same[7] for all f wave functions $\psi_1, \cdots, \psi_f$ and we can use instead of the potential energy of any of them, the mean value of all of them. Assuming only Majorana interaction, the potential energy V will be

$$V=\sum_{\alpha<\beta}^{n}(\psi_\kappa, J(x_\alpha-x_\beta)P_{\alpha\beta}\psi_\kappa)$$
$$=(1/f)\sum_{\kappa=1}^{f}\sum_{\alpha<\beta}(\psi_\kappa, J(x_\alpha-x_\beta)P_{\alpha\beta}\psi_\kappa), \tag{2}$$

where $\alpha\beta$ is the transposition of α and β so that:

$$P_{\alpha\beta}\psi(x_1, \cdots, x_\alpha, \cdots, x_\beta, \cdots)$$
$$=\psi(x_1, \cdots, x_\beta, \cdots, x_\alpha, \cdots).$$

Because of (1) the $(\psi_\kappa, J(x_\alpha-x_\beta)P_{\alpha\beta}\psi_\kappa)$ can be all expressed by the $(\psi_\lambda, J(x_1-x_2)P_{12}\psi_\mu)$

$$\begin{aligned}(\psi_\kappa, J(x_\alpha-x_\beta)P_{\alpha\beta}\psi_\kappa)&=(P_{(\beta 2)(\alpha 1)}\psi_\kappa, P_{(\beta 2)(\alpha 1)}J(x_\alpha-x_\beta)P_{\alpha\beta}\psi_\kappa)\\&=(P_{(\beta 2)(\alpha 1)}\psi_\kappa, J(x_1-x_2)P_{12}P_{(\beta 2)(\alpha 1)}\psi_\kappa)\\&=\sum_{\lambda,\mu=1}^{f}D((\beta 2)(\alpha 1))_{\lambda\kappa}{}^{*}D((\beta 2)(\alpha 1))_{\mu\kappa}\\&\quad\times(\psi_\lambda, J(x_1-x_2)P_{12}\psi_\mu),\end{aligned} \tag{3}$$

where $(\beta 2)(\alpha 1)$ denotes two simultaneous transpositions of β with 2 and of α with 1. This inserted back into (2) gives, because of the unitary character of the representation

$$V=(1/f)\sum_{\alpha<\beta}\sum_{\lambda\mu}\delta_{\lambda\mu}(\psi_\lambda, J(x_1-x_2)P_{12}\psi_\mu)$$
$$=[n(n-1)/(2f)]\sum_{\lambda}(\psi_\lambda, J(x_1-x_2)P_{12}\psi_\lambda). \tag{4}$$

This transformation can be performed with an arbitrary interaction of the form $\sum H_{\alpha\beta}$.

Using (1) again, to expand $P_{12}\psi_\lambda$ one obtains

$$V=[n(n-1)/(2f)]\sum_{\lambda\kappa}D(12)_{\kappa\lambda}(\psi_\lambda, J(x_1-x_2)\psi_\kappa). \tag{5}$$

[7] Cf. e.g., E. Wigner, *Gruppentheorie*, etc. (Braunschweig 1931), p. 124–125.

In reference 1, in order to make qualitative estimates of the integrals occurring on the right side of (4), $J(x_1-x_2)$ was assumed to extend over a region which is large compared with nuclear dimensions. Then $J(0)$ could be taken out of the integral and this vanished for $\kappa\neq\lambda$. However, this can be done only for purposes of qualitative estimates, since the range of forces is certainly not very large compared with nuclear diameter.

There is a certain arbitrariness in the ψ_κ since all the matrices of the representation can be subjected to a common similarity transformation $D(R)\rightarrow SD(R)S^{-1}$. This will amount to a new choice of the set of wave functions $\psi_1, \cdots, \psi_f$. It is in particular possible in this way to make all ψ either symmetric, or antisymmetric in the first two particles, while still maintaining their orthogonality. Supposing that the first s wave functions $\psi_1, \psi_2, \cdots, \psi_s$ are symmetric in x_1 and x_2 and the rest are antisymmetric, then $D(12)_{\kappa\lambda}$ will be $\delta_{\kappa\lambda}$ if $\kappa\leq s$ and $-\delta_{\kappa\lambda}$ if $\kappa>s$. Thus (5) will become

$$V=[n(n-1)/(2f)]\Big[\sum_{\kappa=1}^{s}\int|\psi_\kappa|^2J(x_1-x_2)$$
$$-\sum_{\kappa=s+1}^{f}\int|\psi_\kappa|^2J(x_1-x_2)\Big]. \tag{6}$$

The integrals in this expression can be interpreted in the following way:

$$g_s(x_1-x_2)=(1/s)\sum_{\kappa=1}^{s}\int|\psi_\kappa|^2dx_3\cdots dx_n \tag{7a}$$

is the probability of the distance $|x_1-x_2|$ for two symmetrically coupled particles and

$$g_a(x_1-x_2)=(1/(f-s))\sum_{\kappa=s+1}^{f}\int|\psi_\kappa|^2dx_3\cdots dx_n \tag{7b}$$

is the probability of the distance $|x_1-x_2|$ for two antisymmetrically coupled particles. The expression

$$-\int g_s(x)J(x)dx=L+L' \tag{8a}$$

is the mean interaction for the former, and

$$-\int g_a(x)J(x)dx=L-L' \tag{8b}$$

is the mean interaction for the latter. Necessarily,

both $L+L'$ and $L-L'$ are positive. L and L' will be positive themselves for smoothly varying functions, J having the same sign throughout. In order to obtain s, we can remember that the matrix $D(12)_{\alpha\alpha}$ contained $+1$ in the main diagonal s times, -1 it contained $f-s$ times. The trace of any matrix corresponding to a transposition is therefore

$$\chi(T)=s-(f-s)=2s-f. \tag{9}$$

The whole potential energy thus reduces to

$$\begin{aligned} V&=-\Xi L-(n(n-1)/2)L', \\ \Xi&=n(n-1)\chi(T)/2f. \end{aligned} \tag{10}$$

For ordinary forces, the potential energy will have the same form (10), only the role of L and L' will be interchanged. Henceforth, L and L' will mean that combination of the left sides of (8a) and (8b) which enter into (10) allowing for ordinary forces. For Wheeler's velocity dependent forces,[8] (10) remains formally valid also, however $L=L'$ in this case. The approximation consisting in using linear combinations of Slater determinants with wave functions belonging to one configuration is a special case of (10) if one drops all small integrals (the K of reference 1) and keeps only the large ones (corresponding to L of reference 1).

Of course, (10) is only a formal expression for the potential energy in nuclei, since L will vary with atomic mass and will be different for different terms of the same element. However, the variation of L and L' can be reasonably assumed to be a smooth function of the number of particles and also of the excitation energy so that the rapid irregular variations may be attributed to Ξ. We shall be confined, thus, in our discussions to the comparison of the binding energies and stability of isobars and the kinks in the mass defect curve. It may be expected that the smoothness of the variation of L will be the better the more the configurations are mixed with each other. It will not be attempted in this paper to use (10) for the total binding energy.

The kinetic energy is usually estimated on the basis of the statistical model. This estimate is certainly too low since the wave function of the statistical model gives the smallest possible kinetic energy for a given radius r of the nucleus. This energy is

$$K=(9/20)(3^{\frac{1}{3}}\pi^{\frac{1}{3}}/2^{\frac{1}{3}})(\hbar^2/(Mr^2))(n_p^{5/3}+n_n^{5/3}), \tag{11}$$

where n_p is the number of protons, n_n the number of neutrons, r is the nuclear radius. Setting $n_n=\frac{1}{2}n+T_\zeta$ and $n_p=\frac{1}{2}n-T_\zeta$ and developing into a power series of T_ζ, this gives

$$K=[7.05n^{5/3}+15.7T_\zeta^2/n^1+\cdots]mc^2(r/r_e)^{-2}. \tag{12}$$

where $r_e=e^2/mc^2$ is the electronic radius.

If we confine ourselves again to the discussion of isobars and kinks in the mass defect curve, only the second term will be of importance. This gives us the increase in kinetic energy if the number of neutrons is greater than that of the protons. Although there is not much reason to expect that this term is correct in (12), it is not possible to tell whether it is too great or too small and it will therefore be used below.

The second part of (12) will be used as it stands for even n_n and n_p. If n_n or n_p is odd, it seems more appropriate to use the mean value of the corresponding expression for the adjoining even elements. This whole term will be only a small correction for most of the present paper.

The third important quantity for the nuclear binding energy is the electrostatic interaction of the protons. It will be dealt with in detail in Section 4.

(3)

The wave functions discussed so far contain only the positional coordinates of the particles. In order to form the complete wave function they must be completed[2] by functions of the ordinary and isotopic spin coordinates s and τ.

$$\Psi(x_1, s_1, \tau_1, \cdots, x_n, s_n, \tau_n)$$

$$=\sum_{\kappa=1}^{f}\psi_\kappa(x_1, \cdots, x_n)F_\kappa(s_1, \tau_1, \cdots, s_n, \tau_n) \tag{13}$$

and Ψ will be antisymmetric if F_κ belongs to the κ row of the representation $\epsilon_R D(R)$, adjoint to $D(R)$; ($\epsilon_R=1$ for even and -1 for odd permutations R). In general there are several such sets

[8] J. A. Wheeler, Phys. Rev. **50**, 643 (1936).

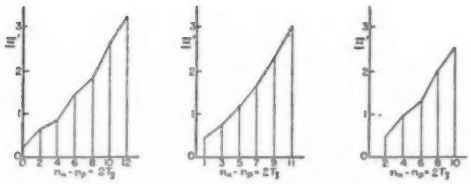

FIG. 2. The coefficient Ξ' of L as function of the difference between the number of protons and neutrons for the three types of nuclei with masses $4k$, $4k\pm1$, $4k+2$. The plots for $4k$ and $4k+2$ show breaks, the plot for odd nuclei not.

of F_κ, which can be distinguished by three indices S_z, T_ξ, Y_ξ.

$$\begin{aligned}
&\tfrac{1}{2}(s_{z1}+\cdots+s_{zn})F_{\kappa M}=S_zF_{\kappa M},\\
&\tfrac{1}{2}(\tau_{\xi 1}+\cdots+\tau_{\xi n})F_{\kappa M}=T_\xi F_{\kappa M},\\
&\tfrac{1}{2}(s_{z1}\tau_{\xi 1}+\cdots+s_{zn}\tau_{\xi n})F_{\kappa M}=Y_\xi F_{\kappa M}.
\end{aligned}\tag{14}$$

M stands for $S_zT_\xi Y_\xi$ and even for given S_z, T_ξ, Y_ξ there may be several sets[9] of F_κ. As long as the ψ_κ are unchanged, all the wave functions (13) with the different S_z, T_ξ, etc., indices for F_κ have the same energy in our approximation 1, which neglects all spin forces, and form a multiplet if one introduces them. The character of the multiplet is determined by the representation $D(R)$ of the original wave functions ψ_1, $\cdots$, ψ_f. From the partition characterizing $D(R)$, the partition $\Lambda_4+\Lambda_3+\Lambda_2+\Lambda_1$ characterizing the adjoint representation $\epsilon_R D(R)$ can be obtained (Eq. (17), reference 2) and the latter partition can be replaced by the (STY) symbol (Eq. (11), reference 2). The S in this latter is the greatest value of S_z for which functions of the s and τ can be found belonging to $\epsilon_R D(R)$; T is the greatest value of T_ξ compatible with the greatest value S of S_z for such functions; and Y is the greatest value of Y_ξ compatible with both. Since the possible sets of $S_zT_\xi Y_\xi$ are the same as the possible sets of $T_\xi S_z Y_\xi$ or of any permutation of these numbers, S is at the same time also the greatest value of T_ξ (or also of Y_ξ) for which functions F_κ can be found such that (13) becomes antisymmetric.

The (STY) symbol has thus a more immediate physical significance than the partition by which the representation $D(R)$ usually is characterized and will be used instead of the latter henceforth.

The quantity $\Xi=n(n-1)\chi(T)/2f$ can be obtained either using Frobenius' character formula or by an argument similar to that of Dirac for atomic spectra which is given in the appendix.[10] It is

$$\begin{aligned}
\Xi &= -n^2/8+2n+5/2-\Xi',\\
\Xi' &= \tfrac{1}{2}\{(S+2)^2+(T+1)^2+Y^2\}.
\end{aligned}\tag{15}$$

Again, the first part of the expression for Ξ can be omitted for most applications because it is the same for all isobars. The restrictions on the S, T, Y are the following: $S\geq T\geq Y$, $T+Y\geq 0$. All three are integers for even n, half-integers for odd n; the sum $S+T+Y$ is even if n is a multiple of 4, it is odd if n has the form $4k+2$, it has in general the form $2k'-\frac{1}{2}n$ (k and k' are integers).

Since the quantity L in (10) is necessarily positive, the binding energy of a term will be the greater, the smaller Ξ' is. The stablest nucleus with given isotopic spin $\frac{1}{2}(n_n-n_p)=T_\xi$ is obtained, therefore, by giving S its minimum value $S=T_\xi$ and besides making T and Y as small as possible; for by doing so one gives to Ξ' its minimum value. Fig. 2 gives the smallest value of Ξ' for given n_n-n_p. The curve is smooth for odd masses, because T and Y can be $\frac{1}{2}$ and $\pm\frac{1}{2}$, respectively, which gives 5/4 for the sum of the last two terms of Ξ' throughout. The curves for

[9] The number of such sets of F_κ for given S_z, T_ξ, Y_ξ is given by the numbers in the circles of Fig. 1, reference 2. The middle number in the figure for $(STY)=(110)$ (partition $2+1+1+0$, page 113) should be a 3 instead of a 2. The last sentence in the legend was meant to correct this mistake. There are two errors in Fig. 4 also. One is in the figure for the masses $4n+2$ for $(STY)=(210)$ where the point on the top should be a line, extending from $T_\xi=-1$ to $T_\xi=+1$, and the point below should have a 1 to the left, rather than a 0, denoting that the total ordinary spin momentum is 1 for this term. The other mistake is in the figure for the masses $4n$: for $(STY)=(200)$ a point is missing which should have a 0 to the left, denoting that the term is a singlet.

[10] Formulas similar to (10) and (15) can be derived on the basis of the Hartree model also. This was pointed out in reference 1, p. 100, bottom of first column, and also Proc. Nat. Acad. **22**, 662 (1936), last paragraph. The calculation on this basis has been performed recently by D. R. Inglis and L. A. Young, Phys. Rev. **51**, 525 (1937). In this paper, for sake of further simplification, the orbital and spin degeneracy is neglected also, although they will occur, of course. The argument in references 1, 2 shows that not only the orbital and spin degeneracy does not matter but also that the results are valid also outside the limits of the Hartree scheme. The condition $g<g_m$, derived by Inglis and Young for the instability of odd-odd nuclei should read $g+2g_\sigma<g_m$.

The kinetic energy is, of course, the same for all terms of the same (STY) multiplet. Hence, the quantity which enters into (12) should not be T_ξ but rather the highest T_ξ of the multiplet, i.e. the S of the (STY).

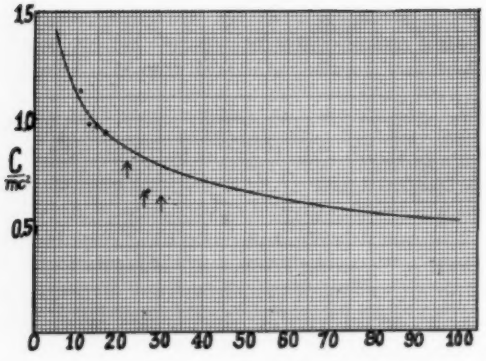

FIG. 3. The coefficient C in the expression (16) for the Coulomb energy as function of the total number n of the particles. The points result from the comparison of pairs of isobars in which the number of protons and neutrons is interchanged.

even masses show breaks, because for masses of the form $4k+2$, for even $S=T_t$ the $T+Y$ must be odd and $T=1$, $Y=0$ is the best choice, while for odd $S=T_t$, the $T+Y$ must be even and both T and Y can be 0. Thus the last two terms of Ξ' give 2 in the former, $\frac{1}{2}$ in the latter case. For masses of the form $4k$ it is the other way around. The breaks in the two latter curves will be made responsible for the instability of nuclei with odd number of protons and neutrons, i.e., of elements with masses $4k+2$ and even T_t and elements with masses $4k$ and odd T_t.

(4)

The last important term in the Hamiltonian is the Coulomb energy. This is supposed, at present, to represent the only difference between protons and neutrons in the Hamiltonian.[11] The Coulomb energy will be assumed to have the form

$$E_c=\tfrac{1}{2}Cn_p(n_p-1)=\tfrac{1}{2}C(\tfrac{1}{2}n-T_t)(\tfrac{1}{2}n-T_t-1)$$
$$=C(n^2-2n)/8-\tfrac{1}{2}C(nT_t-T_t(T_t+1)). \qquad (16)$$

If we approximate the charge distribution in a nucleus by assuming it to be uniform within a sphere of radius r and zero outside, the significance of C is $C=1.2e^2/r$. Actually the exchange energy should be substracted from this. We shall assume C to be proportional to n^{-1} which corresponds to neglecting the exchange energy and assuming a constant density for the nuclei. The latter approximation probably introduces a greater error than the former, and there is a considerable uncertainty in the values of C assumed here. This will affect the values of L as well. Since L/C is less sensitive under a change of C than L itself, the latter quantity will be used in most cases.

C can be determined experimentally almost directly by comparing the binding energies of two nuclei[1] with $T_t=\pm\frac{1}{2}$. The difference in binding energy is according to Heisenberg's hypothesis, only the Coulomb energy, which can be expressed by (16) and the resulting C plotted against n. The plot is given in Fig. 3, the solid curve is $2.4n^{-1}$, the energies are given in mc^2.

Unfortunately, most of the points are at low n. Only one is as high as $n=27$, corresponding to the transition from $_{14}Si^{27}$ to $_{13}Al^{27}$ and this one falls off the curve. This would indicate that the radius increases more quickly than with the $\frac{1}{3}$ power of n, or that the energy of the transition is greater than the value measured by I. Curie and Joliot[12] for the limit of the β-ray spectrum. The latter alternative is rendered probable by the energy differences[13] $_{11}Na^{22}-{}_{10}Ne^{22}$ and $_{15}P^{30}-{}_{14}Si^{30}$. Assuming a symmetric Hamiltonian there will be a term of Na^{22} equal to every term of Ne^{22}, even using "approximation 3" of reference 2, i.e., taking ordinary spin forces into account. The term of Na^{22} which has in approximation 3 equal

[11] The hypothesis that the proton-proton interaction differs only by the electrostatic energy from the neutron-neutron interaction was first introduced by W. Heisenberg, Zeits. f. Physik **77**, 1 (1932) and has not been questioned seriously so far. The most direct experimental verification for the H^3-He^3 pair leads to a moderate agreement only: S. Share's calculation (Phys. Rev. **50**, 488 (1936)), yields 1.37 mc^2 or the electrostatic energy in He^3, the experimental difference in the binding energies is 1.58 according to the most recent masses of H. A. Bethe and M. S. Livingston (cf. reference 18). The experimental energy difference would be even much greater, 2.0 mc^2, on the basis of the masses of S. Flügge and A. Krebs (Physik. Zeits. **38**, 13 (1937)). These are thus definitely in contradiction to Heisenberg's hypothesis.

Another piece of evidence pointing in the direction that the difference between neutron-neutron and proton-proton interaction is greater than the electrostatic energy, is given in Table VIII, reference 1, if the experimental values are increased by 1 mc^2 (cf. reference 6). In order to eliminate the discrepancy here, it was necessary to decrease the radii to $\frac{3}{4}$ of the values assumed in reference 1. For the present considerations this is not very important if one considers (16) as the total difference between proton-proton and neutron-neutron interaction.

[12] I. Curie and F. Joliot, J. de phys. et rad. **5**, 153 (1934).

[13] L. Meitner, Naturwiss. **22**, 420 (1934); C. D. Ellis and W. J. Henderson, Proc. Roy. Soc. **A152**, 714 (1935).

binding energy to that of Ne^{22} can be the ground state or an excited state of Na^{22}. The latter possibility is the more probable one, on account of the Heisenberg forces which have a similar effect in the nuclei Li^6, B^{10}, N^{14}. At any rate, the binding energy of Na^{22} is at least equal to that of Ne^{22} in approximation 3. If the departure from the symmetric Hamiltonian is caused by the electrostatic forces alone, these must be at least equal to the experimental binding energy difference of 8·1 mc^2 between Ne^{22} and Na^{22}. This gives $10C > 8{\cdot}1\ mc^2$ or $C > .81\ mc^2$ for $n=22$. The $P^{30}-Si^{30}$ pair gives in the same way $14C > 9\ mc^2$. The corresponding points are inserted as small arrows in Fig. 3 and render the value obtained directly for $n=27$ improbable. Further experiments would be needed, however, to definitely settle this point.

(5)

In the following we shall assume $C = 2{\cdot}4\ mc^2/n^{\frac{1}{3}}$ which leads to $r = n^{\frac{1}{3}} r_e/2$, a radius for the nucleus which is much smaller than that obtained by Bethe.[14] It must be remembered, however, that our radius is the distance over which the wave function extends while Bethe's radius is the distance in which the electrostatic repulsion on an α-particle becomes as strong as the attraction due to specifically nuclear forces. It is natural that Bethe's radii are greater than ours.

The value of r can be inserted into (12), the second part of which becomes $(63T_t^2/n)\ mc^2$. This value for the change in kinetic energy with increasing isotopic number is too high within a shell and too low at the end of the shell. In Hartree's model, the kinetic energy of all isobars is the same, as long as all the particles can be in the same shell; it is very different, however, if one particle is forced out of the shell. This will not be true actually, of course, but it is to be expected that our expression is too high in the middle of the shell. At the end of the shells, there will be an additional decrease in binding energy for all particles which are outside the shell. This decrease, on the other hand, will not be as great as one would expect on the basis of Hartree's model.[15]

The energy difference between a particle in the $2p$ and $3d$ shells should be, according to the central field model,[15] about 41 mc^2, while it actually is only[16] about 10 mc^2. The energy change at the end of the $(3d)(2s)$ shell should be according to Hartree's model[15] about 17 mc^2 while the experiments indicate about 3 mc^2. It seems that roughly $\frac{1}{3}$ of the increase in kinetic energy is concentrated at the end of the shells, the rest is probably rather uniformly distributed all over the shell. We shall decrease, hence, the expression for increase in kinetic energy with isotopic number to $(50T_t^2/n)\ mc^2$.

The final expression for the binding energy $-E$ will be, hence,[16a]

$$-E = -E_0(n) - \Xi' L + \tfrac{1}{2}C(n - T_t - 1)T_t - (50T_t^2/n)mc^2$$

$$C = 2{\cdot}4mc^2/n^{\frac{1}{3}}, \qquad (17)$$

where Ξ' is defined in (15), plotted for the lowest state in Fig. 2. $E_0(n)$ is a smooth function of n which contains all terms omitted and is responsible for the greatest part of the binding. L will be supposed also to depend mainly on n, and a smooth function of this.

According to (17), there are (apart from the small mass difference between neutron and H^1) two causes which tend to keep T_t small: the potential energy and the kinetic energy. For small T_t the former one will be more effective, for large T_t their values will be in a constant ratio. The Coulomb energy is the only term which tends to increase the isotopic spin.

The following sections will be devoted to a comparison of (17) with experiment. The only unknown quantity in (17) is L. This L will be derived from the kinks in the mass defect curve,

[14] H. A. Bethe, Phys. Rev. **50**, 977 (1936).

[15] W. Elsasser, J. de phys. et rad. **4**, 549 (1933); **5**, 389, 635 (1934); cf. also K. Guggenheimer, J. de phys. et rad. **5**, 253, 475 (1934). What is called central field model here is really only a somewhat crude potential well picture, without direct interactions between the particles. Also the term Hartree's approximation, as used in papers dealing with nuclei, often refers only to the kind of conclusions which one can draw, according to Slater, (Phys. Rev. **34**, 1293 (1929)), for the relative positions of terms, without a detailed knowledge of the wave functions. The direct interaction between the particles is taken into account here at least in first approximation.

[16] According to E. O. Lawrence, E. McMillan and M. C. Henderson, Phys. Rev. **47**, 273 (1935) and to J. D. Cockcroft and W. B. Lewis, Proc. Roy. Soc. **A154**, 261 (1935) there is an excited state of N^{16} in this height above the normal state.

[16a] In the last term of (17), it would be more logical to write S instead of T_t (cf. footnote 10). However, the S of the lowest term of a nucleus is T_t.

from the energy difference between isobars, and from stability conditions for isobars; the results then compared.

(6) Kinks in the Mass Defect Curve

Through the work of Brasefield and Pollard and of Aston[17] the masses of most stable elements up to 40 are known with sufficient accuracy to make a comparison with (17) possible.

Formula (17) written for the atomic mass M instead of the binding energy reads (electronic mass units)

$$M(n)=M_0(n)+\Xi' L-\tfrac{1}{2}C(n-T_t-1)T_t +50T_t^2/n+1.4T_t \quad (18)$$

(1.4 is the difference between the mass of H^1 and the neutron). Fig. 4 contains the difference between the actually observed masses[17] and the next integer number, multiplied by 1825. The points for the three kinds of masses, $4k$, $4k\pm1$, $4k+2$ are connected by broken lines. Around $n=30$, the line for the $4k+2$ type of masses runs just in the middle between the lines for the two other types. Using this as an empirical fact, one obtains

$$15L/8-C(n-\tfrac{3}{2})/4+50/(2n)+0.7 =2(5L/2-C(n-2)/2+50/n+1.4)$$

or $L/C=4.7$; $L=3.5\ mc^2$.

Some corrections, applied by Bethe[18] on the masses[17] make the lines for $4k$ and $4k+2$ just cross at $n=28$ and we obtain $5L/2-C(n-2)/2+50/n+1.4=0$, or the somewhat smaller values $L/C=4.0$; $L=3.15$. This is as accurate a value as can be expected with the present masses.

At lower masses, one can make a calculation for individual points also. It gives for $n=13$, 14, 15 the values $L/C=4.6$, 4.5, 4.4, respectively, with an average error of 0.3 each. For $n=21$, 22, 23, one obtains $L/C=4.2$, 4.8, 4.0, respectively; the average error is here 0.5.

From the value of L at 28 or 30, one can calculate the actual distance of the broken lines for the elements $4k$ and $4k\pm1$. The result is 2 mc^2 (with $L=3.15\ mc^2$) or 3 mc^2 (with the original values, $L=3.5\ mc^2$). This is in fair agreement with the "observed" 3 mc^2 (corrected masses) and 2 mc^2 (original values).

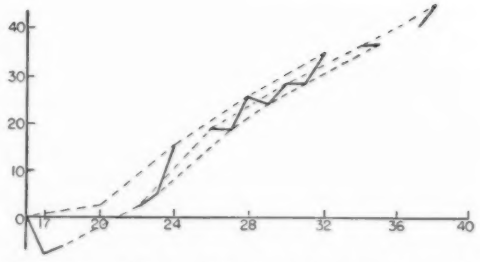

Fig. 4. The difference between n times one-sixteenth of the mass of oxygen and the mass of the stable element with n particles, given in units of the electronic mass. Experiments of Aston and Pollard and Brasefield.[17]

The increase of isotopic number with nuclear mass will be discussed in more detail later. However, the change from $\frac{1}{2}$ at $n=35$ to $\frac{3}{2}$ at $n=37$ may be treated here. The condition for the stability of $_{17}Cl^{35}$ against electron emission is

$$35L/8-C(n-\tfrac{3}{2})/4+50/(2n)+0.7 <59L/8-C(n-5/2)/(\tfrac{3}{4})+(50/n)/(5/2)+2.1,$$

which gives $L/C>3.4$ for $n=35$. The condition that Cl^{37} be stable against the capture of an extranuclear electron is the opposite of this inequality. This gives $L/C<3.8$.

A knowledge of the masses of S^{33}, A^{36}, K^{39} would be very valuable for a further comparison. The values of L obtained in this section are plotted in Fig. 5.

(7) Differences Between Masses of Isobars

The previous section yielded values for the quantity L which should enable us to calculate the differences between isobaric masses from about $n=12$ to $n=40$. The value of L obtained in the previous section decreases a little less strongly than with the inverse first power of n. This is indeed what would be expected as soon as the nuclear dimension exceeds the range of forces.

For elements of the form $4k$, the (STY) symbol for the lowest state with isotopic spin 1 is (110). The difference in potential energy between this state and the lowest state of the element with isotopic spin zero $[(STY)=(000)]$ is $4L$. The

[17] E. Pollard and C. J. Brasefield, Phys. Rev. **51**, 8 (1937); F. W. Aston, Nature **138**, 1094 (1936).

[18] I am much indebted to Professor H. A. Bethe for communicating to me his results before publication.

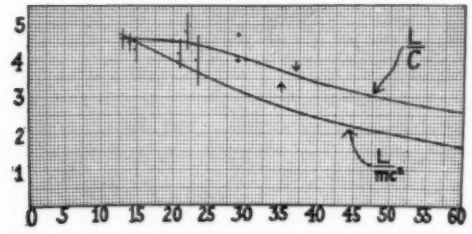

FIG. 5. L/C and L as function of the number of particles. The experimental points (with mean errors for the light elements) all refer to L/C. The higher point at $n=29$ refers to the original measurements,[17] the lower one to the corrected ones.[18]

difference between the mass defects is, therefore, in units of the electronic mass

$$4L-C(n-2)/2+100/n+1.4.$$

The expression for the mass difference for odd elements with isotopic spin $\frac{3}{2}$ and $\frac{1}{2}$ is

$$3L-C(n-3)/2+100/n+1.4.$$

The theoretical and experimental values are collected in Table II. Except for F^{20}, the agreement is quite satisfactory. For F^{20} one may infer the existence of γ-radiation. The disintegrations in which a neutron outside the $3d2s$ shell is transformed into a proton within this shell, are excluded from this comparison (Cl^{38}, A^{41}, K^{42}).

(8) Stable Isobars

The first important change in the isotopic number occurs, as we saw, at Cl^{37} where it becomes $\frac{3}{2}$. We know, however, that K^{39} has $T_t=\frac{1}{2}$ again. This can be attributed only to the closing of a shell, since the Coulomb energy is certainly even more effective in $_{19}K^{39}$ than in $_{17}Cl^{37}$. The instability of $_{18}A^{39}$ can be explained by assuming that one of its 21 neutrons is outside a closed shell and its transformation into a proton which can be inside the shell represents a large energy decrease. One is thus led to the assumption that a shell is closed with 20 neutrons, or 10 orbital states. This agrees with the calculations of Margenau[19] with the potential well picture.

It is possible to determine the magnitude of the increase X in kinetic energy of a particle lifted from the $3d2s$ shell into the next one from the energies of the $_{17}Cl^{38}$, $_{18}A^{41}$ and $_{19}K^{42}$ nuclei which are known from β-disintegration, if one assumes that they are not accompanied by γ-rays. In both cases a neutron outside the ds shell is transformed into a proton inside this shell. The change in potential and Coulomb energy can be calculated for the disintegrations if one extrapolates the value of L in Fig. 5, assuming that one is already in the region where L is inversely proportional to n and L/C to n^1. For $_{17}Cl^{38}$ and $_{19}K^{42}$ the formula $5L-C(n-4)/2+4.50/n+1.4$ yields 6.9 and 4 mc^2, respectively; for $_{18}A^{41}$ $4L-C(n-5/2)+4.50/n+1.4=3$. The experimental values[20] are 9.4, 7.2 and 5.8 mc^2, respectively. This gives approximately $X=3$ mc^2 for the energy difference between the sd shell and the next shell. (Cf. Section 5.)

Assuming this value, $_{19}K^{39}$ is by 1.5 mc^2 more stable than $_{18}A^{39}$, which explains the curious backward movement of the isotopic spin.[19] It has been pointed out before[2] that simultaneously with the first change in isotopic spin for odd elements there should be a change for the $4k$ elements also. The following Table III gives for $n=36$, 40, 44 the calculated mass differences between the elements with isotopic number 1 and 2 on the one hand and the element with $T_t=0$ on the other hand, in units of the electronic mass. One sees, first of all, that all the nuclei with isotopic spin 1 (proton and neutron number both odd) are unstable, for $n=36$ and 40 even against both $T_t=0$ and $T_t=2$. From the nuclei with equal

TABLE II. *Theoretical and experimental values of the mass difference for odd elements with isotopic spin 3/2 and 1/2 (electronic mass units).*

n	calc.	observed
12	24	21.5
20	14.4	9.8
24	10.7	9.8
27	4.6	4.0
28	7.7	6.4
31	3.2	3.45
32	5.1	4.3
36	2.7	?

Sources for the experimental results: For $n=12$ and 20: W. A. Fowler, L. A. Delsasso and C. C. Lauritsen, Phys. Rev. **49**, 561 (1936). For $n=24$ E. O. Lawrence, Phys. Rev. **47**, 17 (1935) and N. D. Kurie, J. R. Richardson and H. C. Paxton, Phys. Rev. **49**, 368 (1936). For $n=27$ M. C. Henderson, Phys. Rev. **48**, 855 (1935). For $n=28$ E. McMillan and E. O. Lawrence, Phys. Rev. **47**, 343 (1935). For $n=31$ and 32 Kurie, Richardson and Paxton, reference 20, and E. M. Lyman, Phys. Rev. **51**, 1 (1937).

[19] H. Margenau, Phys. Rev. **46**, 613 (1934); H. A. Bethe and R. F. Bacher, Rev. Mod. Phys. **8**, 82 (1936), § 32.

[20] F. N. D. Kurie, J. R. Richardson and H. C. Paxton, Phys. Rev. **49**, 368 (1936); J. Ambrosen, Zeits. f. Physik **91**, 43 (1934).

number of protons and neutrons, masses 36 and 40 are stable, 44 unstable, in agreement with experiment. However, all three isobars 36, 40, 44 with $T_t=2$ should be stable against the emission of an electron.[21] The first one, S^{36}, is not known (S^{35} is, of course, unstable).

The next change in the isotopic number of odd elements occurs at $n=49$, where it changes to 5/2. Using further the extrapolated value of L along the curve $L=96/n$, one obtains that the mass difference between the isobars with isotopic spin $\frac{3}{2}$ and 5/2

$$4L-C(n-5)/2+200/n+1.4$$

becomes just 0 at $n=47$, while the latter should be by about 1.2 mc^2 more stable than the former for $n=49$. In fact, the element $T_t=5/2$ is the stable one for $n=49$ while only $T_t=\frac{3}{2}$ is stable for $n=47$.[22]

It has been pointed out before[2] that simultaneously with this jump in isotopic number, that of the elements $4k+2$ should increase by 2. Table IV gives in units of electronic mass the calculated mass differences between the elements $T_t=2$, 3 on one hand and $T_t=1$ on the other hand, according to the formulae

$$5L-C(n-4)/2+200/n+1.4$$
$$8L-C(n-5)+400/n+2.8.$$

The situation is very similar to that of Table III. Again, all odd-odd elements are unstable, $_{21}Sc^{46}$ even against disintegration into both $_{20}Ca^{46}$ and $_{22}Ti^{46}$. The elements $n=42$, 46, 50 with $T_t=1$ are stable, in agreement with experiment. From the elements with isotopic spin 3, the mass number 42 should be unstable, the rest stable against transformation into the element with isotopic spin 2. Again, one of the elements which should be stable, $_{20}Ca^{46}$, is not known. In additon to this, the element with mass 54 and $T_t=1$ is stable. Probably, L is somewhat larger than the extrapolated curve (Fig. 5) would indicate.

TABLE III. *Calculated mass differences between elements with isotopic number 1 and 2 and the element with $T_t=0$ (electronic mass units).*

n	$T_t=1$	$T_t=2$
36	2.3	0
40	$0+X$	$-4.1+2X$
44	−2.2	−8

[21] M. Goeppert-Mayer, Phys. Rev. **48**, 512 (1935) has shown that this means an enormously long lifetime even if the nucleus is unstable against the emission of two electrons or positrons.

[22] The stability or instability of a nucleus depends often on mass differences of less than the electronic mass. Certainly none of the formulas of this paper is accurate to that amount.

(9)

It is hardly necessary to mention that the somewhat surprising agreements between the rather rough theory given in this paper and the experimental findings must be partly fortuitous.[22] Approximation 1 is certainly very crude around $n=50$ and it would be desirable to take into account the Heisenberg force at least in first approximation and, what is probably even more important, the second approximation for the Coulomb force. Also, the shells become probably even less important for higher masses and the factor 50 should be somewhat increased in (17). All these factors work for a decrease of the isotopic spin and, indeed, they seem to be noticeable already in the region of Table IV.

For very large nuclei, the probabilities $g_s(x)$ and $g_a(x)$ of a distance x between two particles will be inversely proportional to the volume of the nucleus as long as x is small compared with the nuclear diameter. This follows from the assumption that the $g(x)$ approach limiting functions with increasing number of particles.[23] In the region in which this is true, L and L' will be inversely proportional to the total number n of the particles, since $V(x)$ will extend over a region which is small compared with the nuclear diameter. For nuclei with about 30 or 40 particles, this limiting case will not yet be reached, because the surface effects are still appreciable. Their gradual disappearance will cause L to decrease more slowly than indicated in Fig. 5. This point

TABLE IV. *Mass differences between elements with $T_t=2$, 3 and with $T_t=1$ (electronic mass units).*

n	$T_t=2$	$T_t=3$
42	4.4	5
46	2	0.7
50	0.1	−3.6
54	−2	−6.9

[23] In metals, where the situation is very similar from the mathematical point of view, the existence of such a limiting function is quite obvious.

has been fully discussed by Weizsäcker[24] into whose well-known quasiempiric formula (18) should go over for high n.

Since for heavy nuclei Ξ' is proportional to T_ξ^2, and L to $1/n$, the term $\Xi' L$ is proportional to 50 T_ξ^2/n. As far as the experimental values for heavy nuclei are concerned, the factor of T_ξ^2/n could be changed if the magnitude of L is changed also to compensate for it. For light nuclei, the other terms in Ξ' are important also and keep the possibility of a change of the numerical value of L within certain limits.

It is a pleasure to remember the interesting conversations I had on the subject of this paper with Drs. Breit, Feenberg and Wheeler.

Appendix

Formula (15) is of course, an immediate consequence of the character formulas of Frobenius.[25] There seems to be a general desire, however, for a derivation which does not make use of the whole theory of representations of the symmetric permutation group. The derivation to be given here is a generalization of that given by Dirac[26] for the theory without isotopic spin which is used in atomic and molecular problems.

Instead of considering the positional part of the wave function, one may consider the spin function alone. Since the corresponding representations are adjoint, the respective values of $n(n-1)\chi(T)/(2f)$ have opposite signs.

There are several sets of spin functions for every representation which may be distinguished, e.g., by the total S_z, T_ξ, and Y_ξ. The value of Ξ depends, however, only on the representation which is specified by S, T, Y. It is thus immaterial which S_z, T_ξ, Y_ξ one takes, and the highest set will be taken here: $S_z = S$, $T_\xi = T$, $Y_\xi = Y$.

Consider the operators is_x, is_y, is_z, $i\tau_\eta$, $i\tau_\xi$ and the nine products $s_x\tau_\xi$, $s_x\tau_\eta$, $\cdots$ etc., acting on the spin variables of one particle. These 15 matrices, taken with both $\pm$ signs, together with the unit matrix, taken again with both signs, form a group of the order $h=32$. It is the same irreducible group which is generated by Dirac's α matrices. These α have the important property which will be repeatedly used later that the trace of every element is zero, except that of ± 1. This follows from the fact that they can be transformed into their negative values.

The interchange R_{12} of the spin coordinates $s_1\tau_1$ and $s_2\tau_2$ is identical with the following sum over the whole group.

$$R_{12} = (2h)^{-1}\sum_i \alpha_{i1}\alpha_{i2}^{-1}, \tag{I}$$

where α_{i1} acts on the spin of the first, α_{i2} on the spin of the second particle. Eq. (I) will be proved by showing that $R_{12}^2 = 1$ and then that $R_{12}\alpha_{k1}R_{12}^{-1} = \alpha_{k2}$. This proves that R_{12} is to within a sign the interchange of the spin 1 with spin 2. The sign can be obtained by considering the trace of R_{12}, which, according to (I), is positive. If R_{12} were the negative of an interchange, its trace would be negative, since the number of symmetric linearly independent spin functions is greater than the number of antisymmetric spin functions. We have

$$R_{12}^2 = (2h)^{-1}\sum_{ij}\alpha_{i1}\alpha_{i2}^{-1}\alpha_{j1}\alpha_{j2}^{-1}.$$

Setting $\alpha_{j2}\alpha_{i2} = \alpha_{l2}$, $\alpha_{j1}\alpha_{i1} = \alpha_{l1}$ we have $\alpha_{i2}^{-1}\alpha_{j2}^{-1} = \alpha_{l2}^{-1}$ and similarly $\alpha_{i1} = \alpha_{j1}^{-1}\alpha_{l1}$,

$$R_{12}^2 = (2h)^{-1}\sum_{jl}\alpha_{j1}^{-1}\alpha_{l1}\alpha_{j1}\alpha_{l2}^{-1}.$$

Now $\sum_j \alpha_{j1}^{-1}\alpha_{l1}\alpha_{j1}$ commutes with all α_{k1} and is, hence, a multiple of the unit matrix. Since its trace is h times the trace of α_{l1} it is different from zero only for $\alpha_{l1} = \pm 1$. Hence

$$R_{12}^2 = (2h)^{-1}[h\cdot 1 + (-h)\cdot(-1)] = 1. \tag{II}$$

Furthermore we have to show that

$$R_{12}\alpha_{k1}R_{12}^{-1} = R_{12}\alpha_{k1}R_{12} = \alpha_{k2}.$$

We have

$$R_{12}\alpha_{k1}R_{12} = (2h)^{-1}\sum_{ij}\alpha_{i1}\alpha_{i2}^{-1}\alpha_{k1}\alpha_{j1}\alpha_{j2}^{-1}.$$

Setting again $\alpha_{j2}\alpha_{i2} = \alpha_{l2}$, $\alpha_{j1}\alpha_{i1} = \alpha_{l1}$, we have

$$R_{12}\alpha_{k1}R_{12} = \sum_{jl}(2h)^{-1}\alpha_{j1}^{-1}\alpha_{l1}\alpha_{k1}\alpha_{j1}\alpha_{l2}^{-1}.$$

The sum over j is again different from zero only if $\alpha_{l1}\alpha_{k1} = \pm 1$ in which case it is $\pm h$. Hence

$$R_{12}\alpha_{k1}R_{12} = (2h)^{-1}\{h\alpha_{k2} + (-h)(-\alpha_{k2})\} = \alpha_{k2}.$$

This proves Eq. (I). Dirac's equation for ordinary spin $Q_{12} = \frac{1}{2}(1 + s_{x1}s_{x2} + s_{y1}s_{y2} + s_{z1}s_{z2})$ is a special case hereof, for $h=8$.

We shall consider now the operators for the "total spin."

$$A_i = \sum_{\kappa=1}^{n}\alpha_{i\kappa}. \tag{III}$$

Since the α are unitary,

$$A_i^\dagger = \sum_{\kappa=1}^{n}\alpha_{i\kappa}^{-1}. \tag{IIIa}$$

We shall calculate now the sum of all $n(n-1)/2$ interchange operators $R_{\kappa\lambda}$. We shall denote this sum by Ξ because it will turn out that, if applied to a function F belonging to a definite multiplet system, it merely multiplies this F with $n(n-1)\chi(T)/(2f)$ where $\chi(T)$ is the trace of the matrix $D(R)$ in (1) corresponding to a transposition.

[24] C. F. v. Weizsäcker, Zeits. f. Physik **96**, 431 (1935).

[25] G. Frobenius, Berl. Ber. (1900) p. 516. F. Hund (ref. 1) has derived the very simple formula for

$$\Xi = \tfrac{1}{2}[\lambda_1(\lambda_1-1) + \lambda_2(\lambda_2-3) + \lambda_3(\lambda_3-5) + \cdots].$$

$(\lambda_1 \geq \lambda_2 \geq \lambda_3 \geq \cdots.)$

[26] P. A. M. Dirac, *The Principles of Quantum Mechanics*, second edition (Oxford 1935), § 61.

We have

$$\Xi=\sum_{\kappa<\lambda}R_{\kappa\lambda}=\tfrac{1}{2}\sum_{\kappa\lambda}R_{\kappa\lambda}-\tfrac{1}{2}\sum_{\kappa}R_{\kappa\kappa}$$
$$=\tfrac{1}{2}(2h)^{-1}\sum_{\kappa\lambda}\sum_{i}\alpha_{i\kappa}\alpha_{i\lambda}^{-1}-\tfrac{1}{2}(2h)^{-1}\sum_{\kappa}\sum_{i}1$$
$$=\tfrac{1}{2}(2h)^{-1}\sum_{i}A_iA_i^{\dagger}-\tfrac{1}{2}nh(2h)^{-1}. \qquad \text{(IV)}$$

So far, the first index of α referred in an arbitrary way to the elements of the group generated by Dirac's α matrices. In the following, however, we shall use single indices for Dirac's original four matrices α_1, α_2, α_3, α_4 only, and write $\alpha_{12}=\alpha_1\alpha_2$, $\alpha_{123}=\alpha_1\alpha_2\alpha_3$, etc. The notation for the A will be changed in a similar way. The A with one or four indices will be Hermitean, those with two or three indices skew-Hermitean. Hence (IV) will read (in the summation in (IV), A_i occurred with both signs; $h=32$)

$$\Xi=-2n+(1/8)\{n^2+A_1^2+A_2^2+A_3^2+A_4^2$$
$$-A_{12}^2-A_{13}^2-A_{14}^2-A_{23}^2-A_{24}^2-A_{34}^2$$
$$-A_{123}^2-A_{124}^2-A_{134}^2-A_{234}^2+A_{1234}^2\}. \qquad \text{(V)}$$

The S_z, T_ζ are, apart from a trivial factor, two commuting A's. Perhaps the most symmetric choice is

$$S_z=\tfrac{1}{2}iA_{12}; \qquad T_\zeta=\tfrac{1}{2}iA_{34}; \qquad \text{then} \qquad Y_\zeta=-\tfrac{1}{2}A_{1234}.$$

Let us consider now the functions F which belong to a certain multiplet system (STY) and let us assume that they have definite "magnetic quantum numbers" S_z, T_ζ, Y_ζ. This is always possible since iA_{12}, iA_{34}, $-A_{1234}$ commute. Since Ξ is a sum over all elements of a class, it follows from the general theory that it is a constant within the multiplet. One can convince oneself also directly with the help of (V) and the commutation relations that it commutes with all A and thus, if applied to the functions F of an (STY) multiplet, it merely multiplies them with the same number. This number is, according to (IV), $n(n-1)/2$ times the mean value of the diagonal elements of the interchange operator $R_{\kappa\lambda}$. Since the latter quantity is $\chi(T)/f$ it was justified to denote the sum in (IV) by Ξ.

In order to find another expression for the value of Ξ, we apply it to the F with the highest set of magnetic quantum numbers $S_z=S$, $T_\zeta=T$, $Y_\zeta=Y$. For this F_{STY} we have

$$iA_{12}F_{STY}=2SF_{STY}, \quad iA_{34}F_{STY}=2TF_{STY},$$
$$-A_{1234}F_{STY}=2YF_{STY}. \qquad \text{(VI)}$$

Repeated use will now be made of the fact that for every equation giving the commutator of two α, there is a similar equation for the A. Thus

$$[\alpha_1,\alpha_2]=2\alpha_{12}; \quad [A_1,A_2]=2\sum\alpha_{1\kappa}\alpha_{2\kappa}=2A_{12}.$$

From $[iA_{12}, A_1-iA_2]=2(A_1-iA_2)$ it follows that

$$iA_{12}(A_1-iA_2)F_{STY}=2(S+1)(A_1-iA_2)F_{STY},$$

so that the S_z of $(A_1-iA_2)F_{STY}$ is $S+1$. Since no F exists with a higher S_z than S, this must be zero. In this way we obtain the equations

$$(A_1-iA_2)F_{STY}=0, \quad (A_{12}-iA_{23})F_{STY}=0,$$
$$(A_{14}-iA_{24})F_{STY}=0, \quad (A_{134}-iA_{234})F_{STY}=0. \qquad \text{(VII)}$$

A_3-iA_4 commutes with iA_{12} and it does not change thus the value of S_z. However, $[iA_{24}, A_3-iA_4]=2(A_3-iA_4)$ so that the T_ζ of $(A_3-iA_4)F_{STY}$ is $T+1$. Therefore $(A_3-iA_4)F_{STY}$ must be zero, since the highest T_ζ for all the F with $S_z=S$ is T. In this way one obtains

$$(A_3-iA_4)F_{STY}=0, \quad (A_{123}-iA_{124})F_{STY}=0. \qquad \text{(VIII)}$$

We can rewrite now (V)

$$\Xi=-2n+(1/8)\{n^2+(A_1+iA_2)(A_1-iA_2)+(A_3+iA_4)$$
$$\times(A_3-iA_4)-A_{12}^2-(A_{13}+iA_{23})(A_{13}-iA_{23})$$
$$-(A_{14}+iA_{24})(A_{14}-iA_{24})-A_3{}^2-(A_{123}+iA_{124})$$
$$\times(A_{123}-iA_{124})-(A_{134}+iA_{234})(A_{134}-iA_{234})$$
$$+A_{1234}{}^2\}+(1/8)\{2iA_{12}+2iA_{34}+2iA_{12}+2iA_{12}$$
$$+2iA_{34}+2iA_{12}\}. \qquad \text{(IX)}$$

This gives with (VI), (VII) and (VIII)

$$\Xi F_{STY}=\{-2n+(1/8)(n^2+4S^2$$
$$+4T^2+4Y^2+16S+8T)\}F_{STY} \qquad \text{(X)}$$

for the Ξ of the representation of the spin functions. Taking into account the change of sign in passing to space functions this proves (15) of the text.

Geiger-Müller Counter Measurements of Reflected Mo $K\alpha$ X-Rays from Powdered Zinc

R. D. MILLER
Wayman Crow Hall of Physics, Washington University, St. Louis, Missouri
(Received April 7, 1937)

Volz has used the formula $n=n_0 \exp(-n_0/2.78n_m)$ where n is the observed counting rate of the system, n_0 is the rate of production of pulses in the counter and n_m is the maximum possible random counting rate. It was found that n_0, calculated from n and corrected for background count, varied as the inverse square of the distance from a gamma-ray source. Further, the absorption coefficient of Mo $K\alpha$ rays in aluminum was found to have the correct value when measured by means of this formula. Thus the formula was satisfactory. The absolute F values were obtained by comparison of the $(11\bar{2}2)$ reflection from zinc with the (420) reflection from KCl. This gives $F(11\bar{2}2)=13.9$. Brindley, using Cu $K\alpha$ rays, obtains $F(11\bar{2}2)=12.0$. The difference is caused by dispersion. The F values for other reflections very closely agree with those found by Brindley for Cu $K\alpha$ rays, when his values are corrected for dispersion. The very weak (0004) reflection, which was not obtained by Brindley, was found to have an F value of about 10.6. Jauncey and Bruce's values of the amplitudes of the thermal vibrations parallel and perpendicular to the c axis fit these results better than do Brindley's.

1. INTRODUCTION

THE problem of the anisotropy of the thermal vibrations of the atoms in zinc crystals has recently been studied by Brindley,[1] Jauncey and Bruce[2] and Zener.[3] Brindley measured the reflection of Cu $K\alpha$ rays ($\lambda=1.54$A) from powdered zinc, Jauncey and Bruce measured the diffuse scattering of x-rays (average $\lambda=0.435$A) from single zinc crystals at different orientation angles, while Zener made a theoretical investigation of the Debye-Waller temperature factor for zinc. Since Jauncey and Bruce's experiments were made with wave-lengths on the short wave-length side of the Zn K absorption edge ($\lambda=1.28$A) while Brindley's experiments were made on the long side, it was considered worthwhile to obtain F values for powdered zinc on the short wave-length side of the Zn K edge. For this purpose Mo $K\alpha$ rays ($\lambda=0.71$A) were used. Moreover, in Zener's formula[3]

$$M=(a\cos^2\psi+b\sin^2\psi)\cdot\frac{\sin^2\phi/2}{\lambda^2}. \qquad (1)$$

Brindley uses the values[4] $a=1.27$A^2 and $b=0.495$A^2, whereas Jauncey and Bruce prefer the respective values 2.34 and 0.68. This situation gave further reason for this present research, and especially so since Jauncey and Bruce were forced to correct Brindley's values for dispersion. Still again Brindley used a photographic method and it was thought worthwhile to make the measurements by another method. On account of the recent success of Locher, LeGalley[5] and others in using Geiger-Müller tubes for x-ray measurements, it was decided to use the G-M tube in the present research.

2. APPARATUS

The Geiger-Müller tube which was used had a 100-mesh stainless steel screen cathode of 1.5 cm diameter and 15.0 cm length and was filled with methyl bromide at 8 cm pressure. The anode wire was made of 22-mil nickel. The x-rays entered the tube through a thin glass window whose effective area was defined by means of a slit in a lead sheet. The rays passed along the tube at a small angle with the anode wire and crossed this wire. A lead cylinder 1.5 cm thick surrounded the tube to reduce the number of stray counts. Methyl bromide was found to be quite sensitive to x-rays, but to deteriorate with use so that the counter had to be refilled daily. The anode was held at 1400 volts, about 175 volts above the threshold.

[1] G. W. Brindley, Phil. Mag. [7] **21**, 789 (1936).
[2] G. E. M. Jauncey and W. A. Bruce, Phys. Rev. **50**, 408 (1836).
[3] C. Zener, Phys. Rev. **49**, 122 (1936).
[4] The English have lower room temperatures than we do. These values of a and b are for 290°K. Calculated for 298°K they become $a=1.29$A^2 and $b=0.51$A^2.
[5] G. L. Locher and D. P. LeGalley, Phys. Rev. **46**, 1047 (1934); D. P. LeGalley, Rev. Sci. Inst. **6**, 279 (1935).

The circuit described by Neher and Harper[6] was used, because of the lower resistances necessary, and because the counting rate is independent of the supply voltage over a range greater than in the conventional circuit. The voltage supply was a conventional one with a Medicus[7] control. For recording the counts, the frequency meter described by Hunt[8] was tried, but was found unsatisfactory for slow counting rates, even when using the tank circuit described by Gingrich, Evans and Edgerton.[9] A mechanical counter consisting of a stopwatch actuated by a magnetic relay was finally used. The over-all resolving time of the system (amplifier plus counter) for irregularly spaced pulses was found to be of the order of 0.1 second.

3. Tests of Counting System

The observed counting rate of the mechanical counter is only proportional to the rate of production of pulses in the G-M tube when the rate is small. For brevity we shall call the rate of production of pulses in the G-M tube the true counting rate.

Volz[10] has used the formula

$$n = n_0 e^{-n_0/n_m}, \tag{2}$$

where n and n_0 are the observed and true counting rates, respectively, and the parameter n_m is the maximum random counting rate which can be recorded by the mechanical counter. n_m can be easily determined by bringing a source of gamma-rays up to the G-M tube; it is found that the counting rate increases to a maximum and then diminishes as the distance between the gamma-ray source and the G-M tube is lessened. For this apparatus, $n_m = 670$ counts per minute.

Formula (2) was subjected to the following tests: (a) A source of gamma-radiation was placed at various distances from the tube, and it was found that, correcting for the background counts, the true counting rate as obtained by (2) from the observed counting rate[11] was proportional to the inverse square of the distance from the counter. (b) The $(10\bar{1}1)$ reflection from zinc of Mo $K\alpha$ rays, which is relatively very intense, was allowed to enter the G-M tube. In order to remove the Mo $K\beta$ rays a ZrO_2 screen was placed over the counter window admitting the x-rays. This screen also removed the fluorescent zinc radiation. Various thicknesses of aluminum were placed in the beam and it was found that when $\log n_0$ is plotted against thickness, a reasonably good straight line was obtained. The value of the mass absorption coefficient of Mo $K\alpha$ rays in aluminum was found to be 5.30. This is in good agreement with the value 5.22 given by Compton and Allison.[12] (c) With the $(10\bar{1}1)$ reflection entering the window of the G-M tube, first the upper half and then the lower half of the window was closed. The sum of the observed counting rates was found to be considerably greater than the counting rate for the completely open window. When the corresponding true counting rates were found by means of (2), the sum of the true rates for the two halves was equal to the true rate for the whole window.

In order to measure the intensity of a zinc reflection at one setting of the G-M tube, it was necessary to make the width of the window admitting the rays of the reflection to the tube wide enough to take account of the angular divergence of the beam. With a wide window it was further necessary to measure the sensitivity of the G-M tube to rays entering various parts of the window. This was done by placing a fixed slit one-quarter the width of the window just in front of the window and measuring the counting rate as the tube with its window was moved across the beam. Such a test showed that the tube was equally sensitive to rays entering all parts of the window.

4. Experimental Arrangement

The collimating slit and the G-M tube window were each placed at 16.8 cm from the powdered crystal so that partial focusing was obtained. The collimating slit was 0.1 cm wide and 0.8 cm high. The tube window was 0.2 cm wide by 0.5 cm high. The ZrO_2 filter was placed in front

[6] H. V. Neher and W. W. Harper, Phys. Rev. **49**, 940 (1936).
[7] G. Medicus, Zeits. f. tech. Physik **8**, 304 (1933).
[8] F. V. Hunt, Rev. Sci. Inst. **6**, 43 (1935).
[9] N. S. Gingrich, R. D. Evans, H. E. Edgerton, Rev. Sci. Inst. **7**, 450 (1936).
[10] H. Volz, Zeits. f. Physik **93**, 540 (1935).
[11] It is not possible to express n_0 explicitly in terms of n so a graph of n *versus* n_0 was plotted. From this, n_0 corresponding to a given value of n can be obtained immediately.
[12] Compton and Allison, *X-Rays in Theory and Experiment* (1935).

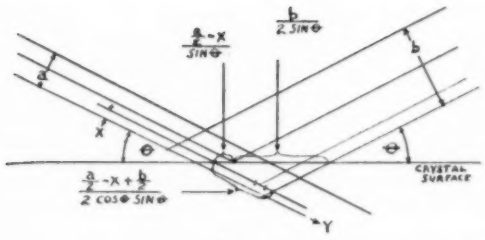

FIG. 1.

of the counter window to absorb the Mo $K\beta$ line and the zinc fluorescent radiation.

The zinc powder was prepared by the sublimation of zinc filings heated in vacuum, as described by Brindley and Spiers.[13] The x-ray tube with a water-cooled molybdenum target was operated at 32 kv peak and 28 ma. The briquet of zinc powder was always placed so that α, the angle between the primary beam and the briquet face, was equal to the angle between the reflected beam and the face.

For convenience the notation used in Brindley's[13] paper will be followed. The quantity I/A is the intensity for a given reflection when corrected for background. Values of I/A were determined on both sides of the primary beam and the average taken. Each of the reflections was compared with the $(11\bar{2}2)$ reflection as a standard. Ten minute readings were taken in the order—standard reflection, standard background, test reflection and test background. A total of two hours of observation was taken for the stronger reflections. The weaker ones were observed for a total of three hours. As an example of the number of counts recorded, the $(11\bar{2}2)$ reflection will serve. The true background (counter plus x-rays) rate was about 80 per minute, while that of the reflections was 115 per minute.

To get the absolute value of the $(11\bar{2}2)$ reflection, it was compared with the (420) reflection of KCl. The KCl was finely powdered and passed through a 200-mesh screen. The comparison was made by alternately taking readings, first from a KCl briquet and then from the zinc. A comparison was tried with MgO, but because of its very small density, when powdered, and its small absorption coefficient, the x-ray beam penetrated the briquet a considerable distance. The scattered beam was so broad that accurate measurements were impossible. The same effect occurs to a much smaller degree with KCl, and it becomes necessary to find a formula which will indicate the inaccuracy due to this effect.

In Fig. 1, let $\phi=2\theta$ be the scattering angle, a be the width of the incident x-ray beam, b the width of the detector window, μ' the effective linear absorption coefficient of the powder, and let y be measured from the crystal surface along the direction of propagation of the x-rays. Let $P(x)dx$ be the intensity distribution across the beam between x and $x+dx$. We shall consider the case of no angular divergence. When the incident and reflected beams are at the same angle, the fraction of the rays traveling between x and $x+dx$ which are scattered by an element dy at y and which emerge from the crystal in the direction of the detector window is $\exp(-2\mu' y)s'dy$, where s' is a linear scattering coefficient. By reference to Fig. 1, it is seen that the total intensity scattered is

$$\int_0^a P(x)dx \int_0^{(a-2x+b)/(4\cos\theta\sin\theta)} e^{-2\mu' y} s'dy. \quad (3)$$

For a beam of uniform cross-sectional intensity $P(x)dx=I_0dx/a$. In this case the total intensity becomes $s'I_0/2k\mu'$, where

$$k=\frac{1}{1-(\sin\phi/2a\mu')\left[e^{-\mu'(b-a)/\sin\phi}-e^{-\mu'(a+b)/\sin\phi}\right]}. \quad (4)$$

The final result is that μ' in Eq. (2) of Brindley and Spiers' paper[13] must be replaced by $k\mu'$. When the method of standardization by separate powders is used, μ_1 and μ_2 in Brindley and Spiers' Eq. (5) must be replaced by $k_1\mu_1$ and $k_2\mu_2$ where the subscripts refer to the two powders. For MgO this correction amounted to about 30 percent. In the case of KCl, however, it was less than $\frac{1}{2}$ percent and so was neglected.

From data given by James and Brindley[14] the absolute F value for the (420) reflection from KCl was estimated to be 13.5. From this it

[13] G. W. Brindley and F. W. Spiers, Phil. Mag. [7] **20**, 865 (1935).

[14] R. W. James and G. W. Brindley, Proc. Roy. Soc. **A121**, 154 (1928).

We have

$$\Xi=\sum_{\kappa<\lambda}R_{\kappa\lambda}=\tfrac{1}{2}\sum_{\kappa\lambda}R_{\kappa\lambda}-\tfrac{1}{2}\sum_{\kappa}R_{\kappa\kappa}$$
$$=\tfrac{1}{2}(2h)^{-1}\sum_{\kappa\lambda}\sum_{i}\alpha_{i\kappa}\alpha_{i\lambda}^{-1}-\tfrac{1}{2}(2h)^{-1}\sum_{\kappa}\sum_{i}1$$
$$=\tfrac{1}{2}(2h)^{-1}\sum_{i}A_iA_i^{\dagger}-\tfrac{1}{2}nh(2h)^{-1}. \qquad \text{(IV)}$$

So far, the first index of α referred in an arbitrary way to the elements of the group generated by Dirac's α matrices. In the following, however, we shall use single indices for Dirac's original four matrices α_1, α_2, α_3, α_4 only, and write $\alpha_{12}=\alpha_1\alpha_2$, $\alpha_{123}=\alpha_1\alpha_2\alpha_3$, etc. The notation for the A will be changed in a similar way. The A with one or four indices will be Hermitean, those with two or three indices skew-Hermitean. Hence (IV) will read (in the summation in (IV), A_i occurred with both signs; $h=32$)

$$\Xi=-2n+(1/8)\{n^2+A_1^2+A_2^2+A_3^2+A_4^2$$
$$-A_{12}^2-A_{13}^2-A_{14}^2-A_{23}^2-A_{24}^2-A_{34}^2$$
$$-A_{123}^2-A_{124}^2-A_{134}^2-A_{234}^2+A_{1234}^2\}. \qquad \text{(V)}$$

The S_z, T_ζ are, apart from a trivial factor, two commuting A's. Perhaps the most symmetric choice is

$$S_z=\tfrac{1}{2}iA_{12}; \qquad T_\zeta=\tfrac{1}{2}iA_{34}; \qquad \text{then} \qquad Y_\zeta=-\tfrac{1}{2}A_{1234}.$$

Let us consider now the functions F which belong to a certain multiplet system (STY) and let us assume that they have definite "magnetic quantum numbers" S_z, T_ζ, Y_ζ. This is always possible since iA_{12}, iA_{34}, $-A_{1234}$ commute. Since Ξ is a sum over all elements of a class, it follows from the general theory that it is a constant within the multiplet. One can convince oneself also directly with the help of (V) and the commutation relations that it commutes with all A and thus, if applied to the functions F of an (STY) multiplet, it merely multiplies them with the same number. This number is, according to (IV), $n(n-1)/2$ times the mean value of the diagonal elements of the interchange operator $R_{\kappa\lambda}$. Since the latter quantity is $\chi(T)/f$ it was justified to denote the sum in (IV) by Ξ.

In order to find another expression for the value of Ξ, we apply it to the F with the highest set of magnetic quantum numbers $S_z=S$, $T_\zeta=T$, $Y_\zeta=Y$. For this F_{STY} we have

$$iA_{12}F_{STY}=2SF_{STY}, \quad iA_{34}F_{STY}=2TF_{STY},$$
$$-A_{1234}F_{STY}=2YF_{STY}. \qquad \text{(VI)}$$

Repeated use will now be made of the fact that for every equation giving the commutator of two α, there is a similar equation for the A. Thus

$$[\alpha_1,\alpha_2]=2\alpha_{12}; \quad [A_1,A_2]=2\sum\alpha_{1\kappa}\alpha_{2\kappa}=2A_{12}.$$

From $[iA_{12}, A_1-iA_2]=2(A_1-iA_2)$ it follows that

$$iA_{12}(A_1-iA_2)F_{STY}=2(S+1)(A_1-iA_2)F_{STY},$$

so that the S_z of $(A_1-iA_2)F_{STY}$ is $S+1$. Since no F exists with a higher S_z than S, this must be zero. In this way we obtain the equations

$$(A_1-iA_2)F_{STY}=0, \quad (A_{13}-iA_{23})F_{STY}=0,$$
$$(A_{14}-iA_{24})F_{STY}=0, \quad (A_{134}-iA_{234})F_{STY}=0. \qquad \text{(VII)}$$

A_3-iA_4 commutes with iA_{12} and it does not change thus the value of S_z. However, $[iA_{34}, A_3-iA_4]=2(A_3-iA_4)$ so that the T_ζ of $(A_3-iA_4)F_{STY}$ is $T+1$. Therefore $(A_3-iA_4)F_{STY}$ must be zero, since the highest T_ζ for all the F with $S_z=S$ is T. In this way one obtains

$$(A_3-iA_4)F_{STY}=0, \quad (A_{123}-iA_{124})F_{STY}=0. \qquad \text{(VIII)}$$

We can rewrite now (V)

$$\Xi=-2n+(1/8)\{n^2+(A_1+iA_2)(A_1-iA_2)+(A_3+iA_4)$$
$$\times(A_3-iA_4)-A_{12}^2-(A_{13}+iA_{23})(A_{13}-iA_{23})$$
$$-(A_{14}+iA_{24})(A_{14}-iA_{24})-A_{3}^2-(A_{123}+iA_{124})$$
$$\times(A_{123}-iA_{124})-(A_{134}+iA_{234})(A_{134}-iA_{234})$$
$$+A_{1234}^2\}+(1/8)\{2iA_{12}+2iA_{34}+2iA_{12}+2iA_{12}$$
$$+2iA_{34}+2iA_{12}\}. \qquad \text{(IX)}$$

This gives with (VI), (VII) and (VIII)

$$\Xi F_{STY}=\{-2n+(1/8)(n^2+4S^2$$
$$+4T^2+4Y^2+16S+8T)\}F_{STY} \qquad \text{(X)}$$

for the Ξ of the representation of the spin functions. Taking into account the change of sign in passing to space functions this proves (15) of the text.

Geiger-Müller Counter Measurements of Reflected Mo $K\alpha$ X-Rays from Powdered Zinc

R. D. MILLER
Wayman Crow Hall of Physics, Washington University, St. Louis, Missouri
(Received April 7, 1937)

Volz has used the formula $n=n_0 \exp(-n_0/2.78n_m)$ where n is the observed counting rate of the system, n_0 is the rate of production of pulses in the counter and n_m is the maximum possible random counting rate. It was found that n_0, calculated from n and corrected for background count, varied as the inverse square of the distance from a gamma-ray source. Further, the absorption coefficient of Mo $K\alpha$ rays in aluminum was found to have the correct value when measured by means of this formula. Thus the formula was satisfactory. The absolute F values were obtained by comparison of the $(11\bar{2}2)$ reflection from zinc with the (420) reflection from KCl. This gives $F(11\bar{2}2)=13.9$. Brindley, using Cu $K\alpha$ rays, obtains $F(11\bar{2}2)=12.0$. The difference is caused by dispersion. The F values for other reflections very closely agree with those found by Brindley for Cu $K\alpha$ rays, when his values are corrected for dispersion. The very weak (0004) reflection, which was not obtained by Brindley, was found to have an F value of about 10.6. Jauncey and Bruce's values of the amplitudes of the thermal vibrations parallel and perpendicular to the c axis fit these results better than do Brindley's.

1. INTRODUCTION

THE problem of the anisotropy of the thermal vibrations of the atoms in zinc crystals has recently been studied by Brindley,[1] Jauncey and Bruce[2] and Zener.[3] Brindley measured the reflection of Cu $K\alpha$ rays ($\lambda=1.54$A) from powdered zinc, Jauncey and Bruce measured the diffuse scattering of x-rays (average $\lambda=0.435$A) from single zinc crystals at different orientation angles, while Zener made a theoretical investigation of the Debye-Waller temperature factor for zinc. Since Jauncey and Bruce's experiments were made with wave-lengths on the short wave-length side of the Zn K absorption edge ($\lambda=1.28$A) while Brindley's experiments were made on the long side, it was considered worthwhile to obtain F values for powdered zinc on the short wave-length side of the Zn K edge. For this purpose Mo $K\alpha$ rays ($\lambda=0.71$A) were used. Moreover, in Zener's formula[3]

$$M=(a\cos^2\psi+b\sin^2\psi)\cdot\frac{\sin^2\phi/2}{\lambda^2}. \qquad (1)$$

Brindley uses the values[4] $a=1.27\text{A}^2$ and $b=0.495\text{A}^2$, whereas Jauncey and Bruce prefer the respective values 2.34 and 0.68. This situation gave further reason for this present research, and especially so since Jauncey and Bruce were forced to correct Brindley's values for dispersion. Still again Brindley used a photographic method and it was thought worthwhile to make the measurements by another method. On account of the recent success of Locher, LeGalley[5] and others in using Geiger-Müller tubes for x-ray measurements, it was decided to use the G-M tube in the present research.

2. APPARATUS

The Geiger-Müller tube which was used had a 100-mesh stainless steel screen cathode of 1.5 cm diameter and 15.0 cm length and was filled with methyl bromide at 8 cm pressure. The anode wire was made of 22-mil nickel. The x-rays entered the tube through a thin glass window whose effective area was defined by means of a slit in a lead sheet. The rays passed along the tube at a small angle with the anode wire and crossed this wire. A lead cylinder 1.5 cm thick surrounded the tube to reduce the number of stray counts. Methyl bromide was found to be quite sensitive to x-rays, but to deteriorate with use so that the counter had to be refilled daily. The anode was held at 1400 volts, about 175 volts above the threshold.

[1] G. W. Brindley, Phil. Mag. [7] **21**, 789 (1936).
[2] G. E. M. Jauncey and W. A. Bruce, Phys. Rev. **50**, 408 (1836).
[3] C. Zener, Phys. Rev. **49**, 122 (1936).
[4] The English have lower room temperatures than we do. These values of a and b are for 290°K. Calculated for 298°K they become $a=1.29\text{A}^2$ and $b=0.51\text{A}^2$.
[5] G. L. Locher and D. P. LeGalley, Phys. Rev. **46**, 1047 (1934); D. P. LeGalley, Rev. Sci. Inst. **6**, 279 (1935).

The circuit described by Neher and Harper[6] was used, because of the lower resistances necessary, and because the counting rate is independent of the supply voltage over a range greater than in the conventional circuit. The voltage supply was a conventional one with a Medicus[7] control. For recording the counts, the frequency meter described by Hunt[8] was tried, but was found unsatisfactory for slow counting rates, even when using the tank circuit described by Gingrich, Evans and Edgerton.[9] A mechanical counter consisting of a stopwatch actuated by a magnetic relay was finally used. The over-all resolving time of the system (amplifier plus counter) for irregularly spaced pulses was found to be of the order of 0.1 second.

3. Tests of Counting System

The observed counting rate of the mechanical counter is only proportional to the rate of production of pulses in the G-M tube when the rate is small. For brevity we shall call the rate of production of pulses in the G-M tube the true counting rate.

Volz[10] has used the formula

$$n = n_0 e^{-n_0/n_m}, \qquad (2)$$

where n and n_0 are the observed and true counting rates, respectively, and the parameter n_m is the maximum random counting rate which can be recorded by the mechanical counter. n_m can be easily determined by bringing a source of gamma-rays up to the G-M tube; it is found that the counting rate increases to a maximum and then diminishes as the distance between the gamma-ray source and the G-M tube is lessened. For this apparatus, $n_m = 670$ counts per minute.

Formula (2) was subjected to the following tests: (a) A source of gamma-radiation was placed at various distances from the tube, and it was found that, correcting for the background counts, the true counting rate as obtained by (2) from the observed counting rate[11] was proportional to the inverse square of the distance from the counter. (b) The $(10\bar{1}1)$ reflection from zinc of Mo $K\alpha$ rays, which is relatively very intense, was allowed to enter the G-M tube. In order to remove the Mo $K\beta$ rays a ZrO_2 screen was placed over the counter window admitting the x-rays. This screen also removed the fluorescent zinc radiation. Various thicknesses of aluminum were placed in the beam and it was found that when $\log n_0$ is plotted against thickness, a reasonably good straight line was obtained. The value of the mass absorption coefficient of Mo $K\alpha$ rays in aluminum was found to be 5.30. This is in good agreement with the value 5.22 given by Compton and Allison.[12] (c) With the $(10\bar{1}1)$ reflection entering the window of the G-M tube, first the upper half and then the lower half of the window was closed. The sum of the observed counting rates was found to be considerably greater than the counting rate for the completely open window. When the corresponding true counting rates were found by means of (2), the sum of the true rates for the two halves was equal to the true rate for the whole window.

In order to measure the intensity of a zinc reflection at one setting of the G-M tube, it was necessary to make the width of the window admitting the rays of the reflection to the tube wide enough to take account of the angular divergence of the beam. With a wide window it was further necessary to measure the sensitivity of the G-M tube to rays entering various parts of the window. This was done by placing a fixed slit one-quarter the width of the window just in front of the window and measuring the counting rate as the tube with its window was moved across the beam. Such a test showed that the tube was equally sensitive to rays entering all parts of the window.

4. Experimental Arrangement

The collimating slit and the G-M tube window were each placed at 16.8 cm from the powdered crystal so that partial focusing was obtained. The collimating slit was 0.1 cm wide and 0.8 cm high. The tube window was 0.2 cm wide by 0.5 cm high. The ZrO_2 filter was placed in front

[6] H. V. Neher and W. W. Harper, Phys. Rev. **49**, 940 (1936).
[7] G. Medicus, Zeits. f. tech. Physik **8**, 304 (1933).
[8] F. V. Hunt, Rev. Sci. Inst. **6**, 43 (1935).
[9] N. S. Gingrich, R. D. Evans, H. E. Edgerton, Rev. Sci. Inst. **7**, 450 (1936).
[10] H. Volz, Zeits. f. Physik **93**, 540 (1935).
[11] It is not possible to express n_0 explicitly in terms of n so a graph of n *versus* n_0 was plotted. From this, n_0 corresponding to a given value of n can be obtained immediately.
[12] Compton and Allison, *X-Rays in Theory and Experiment* (1935).

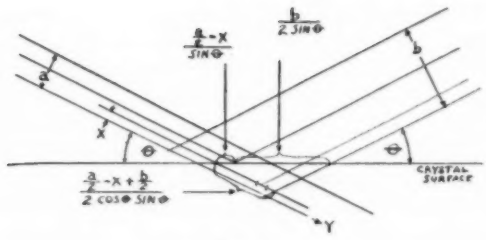

FIG. 1.

of the counter window to absorb the Mo $K\beta$ line and the zinc fluorescent radiation.

The zinc powder was prepared by the sublimation of zinc filings heated in vacuum, as described by Brindley and Spiers.[13] The x-ray tube with a water-cooled molybdenum target was operated at 32 kv peak and 28 ma. The briquet of zinc powder was always placed so that α, the angle between the primary beam and the briquet face, was equal to the angle between the reflected beam and the face.

For convenience the notation used in Brindley's[13] paper will be followed. The quantity I/A is the intensity for a given reflection when corrected for background. Values of I/A were determined on both sides of the primary beam and the average taken. Each of the reflections was compared with the $(11\bar{2}2)$ reflection as a standard. Ten minute readings were taken in the order—standard reflection, standard background, test reflection and test background. A total of two hours of observation was taken for the stronger reflections. The weaker ones were observed for a total of three hours. As an example of the number of counts recorded, the $(11\bar{2}2)$ reflection will serve. The true background (counter plus x-rays) rate was about 80 per minute, while that of the reflections was 115 per minute.

To get the absolute value of the $(11\bar{2}2)$ reflection, it was compared with the (420) reflection of KCl. The KCl was finely powdered and passed through a 200-mesh screen. The comparison was made by alternately taking readings, first from a KCl briquet and then from the zinc. A comparison was tried with MgO, but because of its very small density, when powdered, and its small absorption coefficient, the x-ray beam penetrated the briquet a considerable distance. The scattered beam was so broad that accurate measurements were impossible. The same effect occurs to a much smaller degree with KCl, and it becomes necessary to find a formula which will indicate the inaccuracy due to this effect.

In Fig. 1, let $\phi=2\theta$ be the scattering angle, a be the width of the incident x-ray beam, b the width of the detector window, μ' the effective linear absorption coefficient of the powder, and let y be measured from the crystal surface along the direction of propagation of the x-rays. Let $P(x)dx$ be the intensity distribution across the beam between x and $x+dx$. We shall consider the case of no angular divergence. When the incident and reflected beams are at the same angle, the fraction of the rays traveling between x and $x+dx$ which are scattered by an element dy at y and which emerge from the crystal in the direction of the detector window is $\exp(-2\mu' y)s'dy$, where s' is a linear scattering coefficient. By reference to Fig. 1, it is seen that the total intensity scattered is

$$\int_0^a P(x)dx \int_0^{(a-2x+b)/(4\cos\theta\sin\theta)} e^{-2\mu' y} s'dy. \quad (3)$$

For a beam of uniform cross-sectional intensity $P(x)dx = I_0 dx/a$. In this case the total intensity becomes $s'I_0/2k\mu'$, where

$$k=\frac{1}{1-(\sin\phi/2a\mu')\left[e^{-\mu'(b-a)/\sin\phi}-e^{-\mu'(a+b)/\sin\phi}\right]}. \quad (4)$$

The final result is that μ' in Eq. (2) of Brindley and Spiers' paper[13] must be replaced by $k\mu'$. When the method of standardization by separate powders is used, μ_1 and μ_2 in Brindley and Spiers' Eq. (5) must be replaced by $k_1\mu_1$ and $k_2\mu_2$ where the subscripts refer to the two powders. For MgO this correction amounted to about 30 percent. In the case of KCl, however, it was less than $\frac{1}{2}$ percent and so was neglected.

From data given by James and Brindley[14] the absolute F value for the (420) reflection from KCl was estimated to be 13.5. From this it

[13] G. W. Brindley and F. W. Spiers, Phil. Mag. [7] **20**, 865 (1935).

[14] R. W. James and G. W. Brindley, Proc. Roy. Soc. **A121**, 154 (1928).

follows that the F value for the standard $(11\bar{2}2)$ reflection from zinc is 13.9. The F values for all the zinc reflections are expressed in terms of this.

5. The Effect of Diffuse Scattering on the Background

During this work the question of the proper background from which to measure the reflection maxima arose. As a result of a discussion with Professor Jauncey, the following answer to this question is presented.

Diffuse scattering consists of a coherent and an incoherent part. When monochromatic rays fall upon a single crystal, reflections only occur at those values of θ which satisfy Bragg's law and nowhere else. The incoherent part of the diffuse scattering occurs at all except very small values of the scattering angle, while the coherent part occurs between the Bragg reflections. As a Bragg reflection is approached the coherent part changes into the Bragg reflection at a Bragg value of θ. Hence for a single crystal the background which must be subtracted from a reflection maximum is that due to the incoherent part of the diffuse scattering. In a recent experiment in this laboratory, the intensity of the (200) reflection of a slightly divergent beam of Mo $K\alpha$ rays from rock-salt was 2000 as against 1 for the diffuse scattering. Of the value of 1 for diffuse scattering, an amount 0.5 was probably due to the incoherent part. Whether one subtracts 1 or 0.5 from 2000 makes very little difference, and the subtraction of whatever background there is on either side of the reflection maximum for a single crystal gives a sufficiently accurate value of the true reflection intensity.

In the case of reflection from a powdered crystal the intensity of the background which is due to diffuse scattering and is on either side of the reflection is of the same order of magnitude as the intensity of the reflection itself. The probability that a crystallite of the powder[15] will be lined up to give a certain reflection of x-rays of a given wave-length depends upon the divergence of the primary beam and upon the values of $\cos\theta$ and of the multiplicity factor p. The fraction of the crystallites taking part in reflection is so small that almost 100 percent of these may be considered as giving rise to diffuse scattering. For this reason practically no error is made when the whole of the diffuse scattering background is subtracted from a reflection maximum in order to obtain the true intensity of the reflection.

Table I. *F values for various reflections of Mo Kα x-rays from powdered zinc.*

Reflection	$\sin\theta/\lambda$	ψ	$pS^2\phi(\theta)$	I/A	F
0002	0.203	0.0	375	212	22.3
$10\bar{1}0$	.218	90.0	242	161	24.2
$10\bar{1}1$	.240	65.0	1187	630	22.0
$10\bar{1}2$	.298	47.0	251	100.1	18.7
$10\bar{1}3$	.374	35.6	455	217	15.9
$11\bar{2}0$	.378	90.0	303		
0004	.406	0.0	85	11	10.6
$11\bar{2}2$	.428	61.7	454	100	13.9
$20\bar{2}1$	.447	76.9	309	68	13.9
$20\bar{2}3$	.532	55.0	206	24.5	10.2
$10\bar{1}5$	.552	23.2	189	33.5	8.2
$11\bar{2}4$	.554	42.8	250		
$21\bar{3}1$	.584	80.0	328	34.9	9.7
0006	.609	0.0	32.8	9.2	7.85
$21\bar{3}2$	.611	70.6	98.5		

These values of I/A have been corrected for the $K\beta$ ray which was 0.0075 times the intensity of the $K\alpha$. The only value which it changes is the $(10\bar{1}0)$ reflection.

6. Discussion of Results

The final results are shown in Table I. By comparison with Brindley's F values for Cu $K\alpha$ rays it is seen that the above F values are all larger than his values. This is because of dispersion. According to Hönl[16] the difference of f values for $\lambda/\lambda_K=1.20$ and $\lambda/\lambda_K=0.55$ is 2.36. By comparison with the (220) and (311) reflections from aluminum Brindley obtained $F=12.0$ for the standard $(11\bar{2}2)$ reflection from zinc. The value of F for the $(11\bar{2}2)$ reflection from zinc found by the author was 13.9. The relation between Δf and ΔF is

$$\Delta f=\Delta F e^{-M}, \qquad (5)$$

provided that F and $F-\Delta F$ refer to the same temperature. From diffuse scattering measurements, Jauncey and Bruce[2] find $a=2.34\text{A}^2$ and

[15] Compton and Allison, *X-Rays in Theory and Experiment* (1935), pp. 415–420.

[16] H. Hönl, Ann. d. Physik **18**, 625 (1932).

$b=0.68\text{A}^2$. Using these values in (1), we find from (5) that $\Delta f=1.9e^{0.193}=2.31$. This is remarkably close to the Hönl value of 2.36. This excellent agreement is probably more fortuitous than real.

The experimental values of F are shown as hollow circles in Fig. 2. The same main features are found with Mo $K\alpha$ rays as Brindley finds with Cu $K\alpha$ rays, *viz.*, the zigzag at the last four points and also the anomalous behavior of the first two points. This anomalous behavior of the first two points, the (0002) and (10$\bar{1}$0) reflections, has been previously verified by Miller and Foster.[17] It has been suggested as being due to distortion of the electron atmosphere of the zinc atoms. That the zigzag of the last four points is due to anisotropy in the vibrations of the atoms is shown by the fact that, when the f values are calculated by means of

$$f=Fe^{M},$$

and when Jauncey and Bruce's values of a and b are used, the resulting f points fall upon a curve in which the zigzag has been almost entirely smoothed out. The black circles in Fig. 2 show the f values for this case. The crosses show the f values as calculated when Brindley's values[4] of a and b are used in the calculation.

In addition to the F values found by Brindley it was estimated that the F value for the (0004) reflection is 10.6. This is not to be taken as accurate because the counting rate for this reflection is very small, but it does show that it is another low point on Fig. 2. Evidently the F values for $\psi=0°$ are low and the amplitude of vibration along the c axis is large. This shows that a in (1) must be large.

It is believed that after correcting for the atomic vibrations the f values fall upon a smooth curve at large values of $(\sin\theta)/\lambda$ but that at small values of $(\sin\theta)/\lambda$ the f values fall between two curves, one for $\psi=0°$ and the other for $\psi=90°$, the particular position for an f point depending upon the value of ψ. The forking f curve is shown in Fig. 2. This phenomenon is caused by electron distortion. Since by reference to Fig. 2 it is seen that for large values of $(\sin\theta)/\lambda$ the black circles fall somewhat better on a smooth curve than do the crosses it seems that Jauncey and Bruce's values of a and b are better than Brindley's. Jauncey and Bruce's values correspond to 0.172A and 0.093A for the root-mean-square displacements parallel and perpendicular to the c axis.

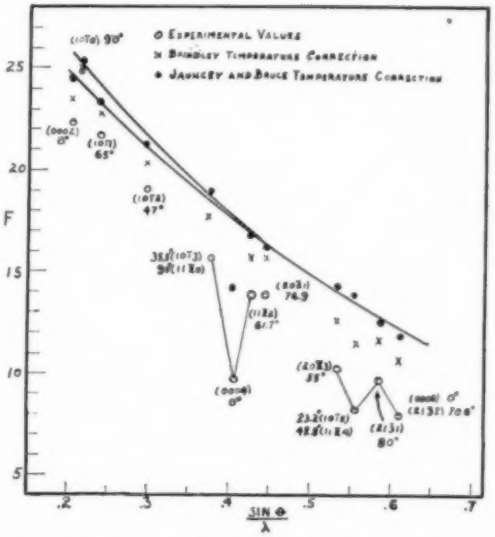

FIG. 2. Experimental F values and temperature corrections. (A better value for the (0004) reflection seems to be 10.6 instead of the value 9.6 indicated in the figure.)

The author wishes to thank Professor Jauncey for his untiring encouragement and help in the working out of this problem.

[17] R. D. Miller and E. S. Foster, Jr., Phys. Rev. **50**, 417 (1936).

Built-Up Films of Barium Stearate and Their Optical Properties

KATHARINE B. BLODGETT AND IRVING LANGMUIR
Research Laboratory, General Electric Company, Schenectady, New York

(Received March 20, 1937)

The technique of depositing successive single layers of molecules of various stearates on a solid surface is described. Films containing 3001 layers have been built of barium-copper stearate. A photograph shows films built in a series of steps having intervals of 2 molecular layers. The contrast of the steps is plainly visible when the slide is illuminated by polarized light at angles near grazing incidence. By measuring the angles at which films containing known numbers of layers reflect minimum intensity of monochromatic light for the first five interference fringes, the thickness per layer and refractive index can be calculated with great accuracy. The thickness per layer of barium stearate was found to be 24.40A. The presence of traces of foreign substances in the water affect the spacing by 1 to 3 percent. The films are uniaxial crystals, the optic axis being perpendicular to the surface on which the films are built. The refractive index of the ordinary ray, n_1, and of the extraordinary ray in a direction perpendicular to the axis, n_3, are $n_1=1.491$, $n_3=1.551$. Equations are given which describe the refraction of the extraordinary ray, the intensity of the rays reflected from the upper surface and from the film solid boundary, the phase change at the boundaries, Brewster's angle, and other special properties of birefringent films. The intensity of the light and dark fringes reflected by films built on a series of glasses of known refractive indices is used as a measure of n_1. *Skeleton films.* Barium stearate films built at $p\mathrm{H}<7.0$ are composed of a mixture of stearic acid and neutral stearate. The stearic acid can be dissolved by benzene leaving a skeleton of stearate which is birefringent and has refractive indices much lower than those of the normal film. Measurements are given of a skeleton for which $n_1=1.30$, others for which $n_1=1.32$, $n_3=1.39$. Skeletons have been built having $n_1=1.25$ and 1.22. The skeleton for which $n_1=1.30$ had 99.2 percent of the thickness of the original film, although only 63.7 percent of its density.

A METHOD for depositing many successive single layers of molecules on glass or metal has been described in a previous paper.[1] A monolayer of stearic acid was spread on the surface of water containing barium salts, or salts of other bivalent metals, and was transferred to the solid by a process of dipping, the stearic acid film being kept under suitable 2-dimensional pressure.

Stearic acid spreads on a water surface with the carboxyl group of each stearic acid molecule in contact with the water while the hydrocarbon chain is nearly vertical.[2] The monolayer therefore consists of a sheet having carboxyl groups on the under surface and CH_3 groups on the upper surface, the thickness of the sheet being determined by the length of the molecular chain and the tilt of the chain with respect to the surface. In the dipping process the first layer attaches itself by its carboxyl groups to a clean solid surface when the solid is raised out of the water, causing the surface to be dry when it emerges. The second layer attaches itself as the solid is lowered into the water, the third layer as it is raised again, and so on. Thus the dipping process serves to fold the monolayer back and forth on itself so that the molecules in successive layers are oriented in opposite directions.

When the water on which the stearic acid spreads contains barium salts, the barium combines with the carboxyl groups of the molecules forming barium stearate. X-ray diffraction studies[3] of built-up films of this type have confirmed the evidence that the $(-COO)_2Ba$ groups lie in planes having a spacing which is twice the length of the molecular chain.

Three methods have been used for measuring the spacing of the molecular layers. (a) An optical method based upon the interference of light from the upper and lower surfaces of the film. This was described in the previous paper and will be further described in this paper. This method employs films having less than 500 layers, and requires a knowledge of the refractive index of the film. (b) A second optical method which has been used by Professor A. H. Compton and C. Holley to measure films built by Dr. Blodgett. A film containing a known number of layers, in the range 1000 to 3000 layers, was built on an optical

[1] K. B. Blodgett, J. Am. Chem. Soc. **57**, 1007 (1935).
[2] I. Langmuir, J. Am. Chem. Soc. **39**, 1848 (1917).
[3] Clark, Sterrett and Leppla, J. Am. Chem. Soc. **57**, 330 (1935); Holley and Bernstein, Phys. Rev. **49**, 403 (1936).

flat adjacent to a film containing 100 layers, and the difference in thickness of the two films was measured with an interferometer. The method is independent of the refractive index of the film. (c) The methods of x-ray diffraction spectra.

Films containing 100 layers may be built of the stearates of Ba, Ca, Mg, Pb, Zn and other metals, or of stearic acid. Barium-copper stearate is the only substance with which it has been possible to build 1000 layers successfully; films have been built containing 3000 layers of this substance. Success in building large numbers of layers depends on properties of the film which are determined by the nature and concentration of salts dissolved in the water, the temperature of the water and the hydrogen ion concentration as determined by pH. Formulae of solutions used in film-building are given in a later section. The following properties of films affect the processes of building.

(1) Initial Layer

The problem of depositing the initial layer on a clean metal or glass surface is distinct from the problem of building successive layers. The first problem requires a molecular sheet having an under surface which will adhere well to the solid; the second requires a sheet which adheres to a similar sheet.

In the case of a glass surface the initial layer is deposited more readily from alkaline water, $p\text{H} \geqq 8.5$ than from acid or neutral water. In the case of metal the best initial layers are usually obtained at $p\text{H} = 6$ to 7.5. The glasses of high refractive index which we have used take up initial layers at $p\text{H} = 7.0$ far more readily than ordinary glass (microscope slides).

In many experiments it is not essential that the initial layer be of the same material as succeeding layers, and in these cases the following method has proved very useful. The solid surface is coated with molten paraffin wax, or preferably with molten ferric stearate, and is rubbed vigorously with a cloth until every visible trace of the coating has disappeared. This treatment leaves the slide covered with a monomolecular layer of wax to which layers of barium stearate will attach themselves in the same way as to an initial layer of stearate. Built-up films of barium stearate can also be rubbed down and provide a very good foundation on which new films can be built.

When the experiments require that the initial layer be built in the same manner as the rest of the layers, the glass or metal can be cleaned by using the metallographic polish Shamva. The surface is scoured with Shamva, rinsed and swabbed under running water, and plunged wet into the water bath used for film building. Glass can also be cleaned with a hot concentrated solution of $K_2Cr_2O_7$ and H_2SO_4, but the acid is apt to attack glass of high refractive index, and affects the surface of certain kinds of glass microscope slides in such a way that a layer will not adhere to the glass. Metal can be cleaned by being made cathode in an electrolytic bath of caustic soda, water and alcohol, but the treatment usually etches the metal slightly.

When an initial layer of wax or other substance is used to coat the slide this is called a "1st layer," meaning that the barium stearate which attaches itself to the wax has the molecular orientation characteristic of the 2nd layer of barium stearate built on a clean surface. Only layers of odd number exist out of water, layers of even number exist under water. The numbers 100, 200, etc. which are given in the text are round numbers.

(2) Speed

After an odd number of layers have been deposited, the surface consists of close packed CH_3 groups and so sheds water. When this slide is dipped into water covered by a barium stearate monolayer under pressure the next layer is transferred to the slide even if the slide is lowered very rapidly. To form the next odd layer by withdrawing the slide it is important not to raise the slide faster than the rate at which the water peels back from the slide. This peeling back is not caused by gravity but by a strong adhesion (between the hydrophilic sides of the two outer layers) which acts along the line of contact and so drives out the water film. When the slide is slowly withdrawn a large contact angle is observed between the water surface and the slide. The rate at which films can be built is thus limited by the rate at which the ascending slide sheds water, and the term "speed" refers to this limiting rate, not to the actual rate of building. A "fast

film" is one which can be built in successive layers at a rate 20 or more layers per minute.

Speed is commonly the greatest for the first layers which are deposited, and gradually slackens as more layers are added. Films of magnesium stearate begin to lose speed after about 50 layers have been deposited and at about 200 layers the process is virtually brought to a halt; films of barium-copper-stearate retain their initial speed up to more than 1000 layers. Loss of speed is due to disorder in the molecular orientation of successive layers. Several different causes may contribute to produce a disordered arrangement, the chief cause being severe mechanical strains to which the films are subjected during the building process which many types of film are unable to withstand without sustaining injury. Traces of some impurities in the water may also greatly affect the speed.

(3) Mechanical Properties

A monolayer of a stearate on a water surface may be liquid or solid. Most of the factors which determine the state originate in the water on which the film lies. Langmuir and Schaefer[4] have shown that when the water contains barium carbonate in a concentration 10^{-4} molar, and the pH is adjusted by adding either ammonium hydroxide or hydrochloric acid, 21 percent of the stearic acid is converted to barium stearate at $p\text{H}=5.0$, 88 percent at $p\text{H}=9.0$. For purposes of film building a barium stearate film built with a solution 3×10^{-5} M barium carbonate at $p\text{H}\leqq6.5$ is slow, and becomes progressively slower at 20°C; the initial speed is maintained for a much greater number of layers at 15°C than at 20°C. A barium stearate film at $p\text{H}=7.0$ is fast. These results show that an increase in rigidity of structure obtained by lowering the temperature or increasing the pH results in a more ordered arrangement of the CH_3 groups in the successive layers laid down on the solid.

Barium stearate films are faster at $p\text{H}=7.5$ than at $p\text{H}=7.0$, but the greater rigidity at $p\text{H}=7.5$ is not desirable. Very rigid films give unsatisfactory results for the following reason. A slide commonly picks up many specks of dust or tiny crystals of stearic acid, and the manner in which succeeding layers are affected by these specks is very important. The trough used in the present experiments was covered by glass as a necessary protection from dust falling from the air upon the water surface; extreme precautions to obtain dust-free air were not attempted. After a particle of dust has attached itself to a slide, a series of layers of a tough viscous film will coat the particle so successfully that after four or six layers have been added the particle sheds water as readily as does the rest of the slide. This occurs although a particle 0.2 mm in thickness has 80,000 times the thickness of a monolayer. A weak film coats the particle so unsuccessfully that a small mound of soft barium stearate soon piles up on the particle and serves as a center from which disorder in successive layers spreads out over the slide, and water recedes more and more slowly from that area. Layers of rigid film tend to be broken by a projecting particle so that hundreds of minute bits of broken film collect around the particle, and although these areas shed water rapidly they spoil the uniformity of the film. Observation of the water meniscus, as water is shed by an ascending slide, shows that the meniscus travels over dust particles with a "chattering" motion in the case of a rigid film, a lagging motion in the case of a weak film.

Monolayers can be formed on a water surface which are so rigid that they cannot be used to build films. When a slide is raised and lowered through a surface of this type the layer of stearate does not attach itself to the slide, i.e., the layer "slips" instead of adhering at the boundary edge where the layer meets the slide. In many cases of slipping a few initial layers can be built up, then subsequent layers fail to adhere to the slide and the slipping of these layers is recognized by a characteristic very noticeable chattering motion of the water meniscus. In other cases no initial layers adhere. Films having this great rigidity are obtained with barium solutions at $p\text{H}=7.0$ which contain copper salts in a concentration 10^{-5} M, or aluminum salts in a concentration 10^{-6} M.

(4) Fogging

After a number of layers have been built the film begins to have a fogged appearance. This occurs at 50 to 500 layers, depending on the type

[4] I. Langmuir and V. J. Schaefer, J. Am. Chem. Soc. **58**, 284 (1936).

of stearate which is used. Examination under a microscope shows that a myriad of tiny specks of approximately uniform size are built into the film. Nearly always the number per unit area is uniformly graded from top to bottom of the slide (the slide is held in a vertical position during dipping), and is greatest at the bottom of the slide. As more layers are deposited the specks increase in size and density until they cause the water to recede so slowly that the progress of film building is halted. The only substance which thus far has successfully prevented fogging is copper, a copper salt being added in a concentration 2 to 3×10^{-6} M to water containing barium salts.

(5) Cracking

A film of barium stearate built at pH = 7.0 and having a large number of layers invariably cracks in hundreds of fine lines. The tendency to crack increases with increasing thickness, cracking usually commencing at 300–500 layers. Films built on chromium crack more readily than films built on glass. At lower values of pH a greater number of layers can be deposited before the film commences to crack. Usually a cracked film curls upward slightly along the edges of the cracks. Water often works its way under a cracked film and loosens the film from the slide. Copper dissolved in the water is the only substance which has been found which will prevent cracking.

Good films can be built with the following two solutions:

Solution (a)

0.3×10^{-4} M $BaCl_2$ (or other soluble barium salt)
4.0×10^{-4} M $KHCO_3$
pH = 7.0 to 7.2. Temp $\leqq$ 22°C.

The water used in making the solution should be conductivity water having a specific resistance of 700,000 to 1,000,000 ohms-cm. If a brass or aluminum trough is used it should be lined with paraffin wax, and the floor of the trough should be covered with glass. Many solutions dissolve sufficient copper from a brass trough to affect the experimental results to a marked degree when the brass is coated with paraffin but is not covered with glass.

Films built with solution (a) are fast, reliable, and easily built. The solution is recommended for building films having less than 200 layers. A larger number of layers will become fogged or cracked, even 100 layers sometimes crack.

Solution (b)

0.3×10^{-4} M $BaCl_2$
2.0×10^{-4} M $KHCO_3$
0.02×10^{-4} M $CuCl_2$ (or other soluble copper salt)
pH = 6.8, temp < 22°C (temp < 20°C preferred).

The stearate should be left on the water surface for 5 min. before it is used for building, to allow time for copper to diffuse to the surface. Films built with solution (b) do not fog or crack at 1000 layers and can be built with fair success to 3000 layers. At thicknesses of 500 or more layers they have a faint green color, showing that the film contains copper stearate.

The problem of holding the copper concentration constant will be apparent from the following considerations. The trough used in the experiments contained 5000 cc of water and the area of water covered by a surface film was 3300 cm². Therefore the number of copper ions in the water, in a concentration 2×10^{-6} M was 7.36 times the number of pairs of stearate molecules on the surface, the molecules having an area per molecule 20×10^{-16} cm². The built-up films were not analyzed for copper content, but the results of analyses of similar films make it appear probable that not more than 25–50 percent of the stearic acid placed on the water surface was converted to copper stearate. Therefore each time a film was spread the concentration of copper ions in the water was reduced by 3 to 6 percent of the initial concentration.

In some experiments copper was introduced by covering the bottom of the trough with a clean sheet of copper. Under these conditions the rate at which copper was removed from the bath by surface films when new films were spread every 20 minutes was balanced fairly satisfactorily by the rate at which copper went into solution. Whenever the sheet was left in the trough for more than about 10 hrs. and no copper was removed, the resulting concentration of copper was much too high. It was pointed out in Section (2) that a concentration of copper 10^{-5} M causes films to slip completely; they frequently slip at $5\times$ 10^{-6} M.

Good results were obtained for 1000-layer films by scattering 100 small lumps of copper sulfide in the bottom of the trough. The copper sulfide contained 70.3 percent of copper. This method gave a concentration of copper which was never too high, even after standing in a solution for two weeks. The concentration was a little lower than was needed to build 3000 layers.

The amount of copper in water can be roughly estimated if one spreads a surface film on the water, then shoves all the film to one end of the trough, where it can be easily skimmed off the surface and dried on a porcelain slab in an oven at 95°–100°C. The green color of the film can be compared with the color of films skimmed from baths containing known concentrations of a copper salt. The film should be left on the water for at least 5 min. before it is skimmed. The method readily shows the presence of 10^{-6} M copper and can show less than this amount.

Optical Properties of Films

Built-up films of barium stearate are uniaxial crystals. The optic axis of the film is perpendicular to the surface on which the film is built. The birefringence is readily demonstrated by placing a 1000-layer film, built on glass, between crossed Nicol prisms or crossed Polaroid screens, the film being placed at azimuthal angle 45°. The film restores the light when the angle of incidence i of the light on the film is large; at $i=0$ it restores no light. The intensity of the restored light increases with increasing angle i.

Dr. L. Navias has investigated for us the birefringence of a 1000-layer film of barium stearate, employing a I red gypsum plate in the usual way and found that the film behaves as a positive uniaxial crystal.

Refractive Index

The previous paper described a method of determining the refractive index n of the films[5] by measuring Brewster's angle i_B for monochromatic light reflected from films of Ba stearate, Ca stearate, and stearic acid. Values of n were given which were derived from the relationship

$$n=\tan i_B. \qquad (1)$$

[5] The symbol n for refractive index is used in the present paper in place of μ in the previous paper.

For barium stearate films the refractive index was found to be $n=1.462$. This method was employed before the experiments were made which showed that the films were birefringent and that the ray used to measure i_B was the extraordinary ray for which Eq. (1) is not applicable. The film thickness measurements of the previous paper were made by optical methods which employed the ordinary ray. These should be corrected by using the proper refractive index for the ordinary ray.

In any uniaxial crystal two of the three principal refractive indices, n_1, n_2 and n_3 are equal, so we may put $n_2=n_1$. Since the film is a positive uniaxial crystal, n_3 must be greater than n_1. For rays parallel to the optic axis the crystal behaves as an isotropic medium of refractive index n_1.

Since the barium stearate film lies in a plane perpendicular to the optic axis, the plane of incidence of oblique rays is parallel to the optic axis. The plane of the electric vector of the ordinary ray R_s is perpendicular to the plane of incidence while that of the extraordinary ray R_p is parallel to the axis. For ordinary rays at any angle the film behaves as an isotropic body having the refractive index n_1, but for extraordinary rays the refractive index, n, varies with the angle of refraction r, according to the equation

$$1/n^2=\cos^2 r/(n_1)^2+\sin^2 r/(n_3)^2. \qquad (2)$$

According to the Fresnel theory, the amplitude of the light reflected at normal incidence from an interface between two isotropic media of refractive indices n_a and n_b is given by

$$\rho=(n_a-n_b)/(n_a+n_b), \qquad (3)$$

the amplitude of the incident light being unity. If ρ is negative; i.e., when $n_b>n_a$, the phase of the light waves is reversed by reflection, but it is not reversed if ρ is positive.

Let us consider the interference of light reflected from the top and bottom surfaces of a film (on glass) consisting of N monolayers each of which has a thickness t. Let λ be the wave-length of the light, r the angle of refraction corresponding to the wave normal of the light (direction of ray in case of ordinary ray) and n be the refractive index for these waves. Interference occurs as a result of a phase difference between the ray which is reflected from the upper surface, and the

ray which travels from the upper to the lower surface and is reflected at the lower surface and travels back to the upper surface. The condition that the two rays shall differ in phase by an integral multiple of 180° is given by

$$nNt \cos r = m\lambda/4 \tag{4}$$

where m is an integer.

Since the refractive index of the film is greater than that of air the light reflected from the upper surface of the film always suffers a phase reversal. If the light reflected from the interface between the film and the glass also undergoes a phase reversal, the interference fringes produced by the film have minimum intensity for odd values of m, maximum intensity for even values of m. If, however, the light reflected from the lower surface is not reversed in phase the intensity minima correspond to even values of m.[6]

If films are built on glass in a series of steps having thicknesses equal to $m\lambda/4n$, where m represents successive integers, they will give at normal incidence a series of interference fringes of maximum contrast. These may be classified as belonging to series A or B defined by Table I.

Series A occurs when there is a phase reversal in the reflection of light at the interface, while for series B there is no reversal. For light at normal incidence this means that if the fringes correspond to series A the refractive index of the film must be less than that of the glass.

Let B be the value of ρ as given for example by Eq. (3), for the light reflected from the upper surface of the film, and let C be the value of ρ for the reflection from the interface. Let us now consider films forming steps whose thicknesses have been chosen by Eq. (4) to give a series of fringes of maximum contrast. The theory of interference, allowing for multiple reflections within the film, then gives for the amplitude ρ_M of the total light reflected from the film

$$\rho_M = (B \pm C)/(1 \pm BC). \tag{5}$$

The two extreme values of ρ_M are thus found by taking the + and the − signs in Eq. (5).

If we calculate the values of B and C by Eq. (3) and introduce them into Eq. (5), taking the positive sign in the numerator and denominator, we find

$$\rho_+ = (n_0 - n_g)/(n_0 + n_g) \tag{6}$$

where n_g and n_0 refer to the glass and to air. With the negative sign we get

$$\rho_- = (n_0 n_g - n_1^2)/(n_0 n_g + n_1^2). \tag{7}$$

The contrast between the steps of maximum and minimum brightness may be conveniently measured in terms of a quantity K, defined by

$$K = (\rho_+^2 - \rho_-^2)/(\rho_+^2 + \rho_-^2). \tag{8}$$

The ratio of the intensities I_+ and I_- of the light from the successive steps is thus

$$I_+/I_- = (1+K)/(1-K). \tag{9}$$

Let us put

$$n_1 = n_g - \Delta n. \tag{10}$$

Then if Δn is so small that we can neglect terms of higher order than the first we find by combining Eqs. (6), (7), (8) and (10) that

$$K = 4n_0 \Delta n/(n_g^2 - n_0^2). \tag{11}$$

The refractive index n_1 of the film was determined by the relative intensities of the interference fringes produced on glasses having nearly the same refractive index as the film. All observations were made with the light from a 6000-lumen sodium vapor lamp ($\lambda = 5893$A). Preliminary experiments had shown that 162 layers of barium stearate had a thickness equal to λ/n. Therefore a series of steps having 41, 81, 121 and 161 layers were built on three types of glass. Glass (1) (fused quartz) had a refractive index[7] 1.459 and glass (2) and glass (3), according to the manufacturer (Jena Glassworks, Schott and Gen. Jena), had indices of 1.4937 and 1.7854. To prevent reflection from the back of the glass the back was coated with black paint.

The films built on glass (2) when viewed by light at normal incidence were found to belong

TABLE I. *Sequence of interference fringes. Step films of thicknesses* $= m\lambda/4n$; $\lambda = 5893A$.

$m=$	1	2	3	4
$N=$	41	81	121	161 layers
Series A ($n_g > n_1$)	dark	bright	dark	bright
Series B ($n_g < n_1$)	bright	dark	bright	dark

[6] R. W. Wood, *Physical Optics*, second edition, p. 155.

[7] *International Critical Tables*, Vol. 6, p. 342.

TABLE II. *Effect of underlying glass on interference fringes seen with the extraordinary ray R_p at various angles of incidence i. Measured for films of barium stearate built by using solution (a).*

i	(1) Series seen on glass (1) $n_g=1.459$	(2) Series seen on glass (2) $n_g=1.4937$	(3) Series seen on glass (3) $n_g=1.7854$	Contrast of bright and dark fringes (1), (2) and (3) refer to the 3 glasses
0	*B*	*A*	*A*	(1) Moderately strong contrast (2) Barely visible contrast (3) Strong contrast
45°±3	*B*	*A*	*A*	(1) Less than at $i=0$ (2) Greater " " " " (1) and (2) about equal
53° 20′	*B*	*A*	*A*	(1) Barely visible
55° 20′±1	–	–	–	Brewster's Angle observed best with (3). No fringes with any glass
56° 50′	*B*	*B*	*B*	(1) Just begin to be visible
70°	*B*	*B*	*B*	(2) Greater than (1)

to series A, the contrast between the bright and dark fringes being 1.5 to 2 percent. The films built on glass (1) belonged to series B and at normal incidence much more contrast was seen than with glass (2). The refractive index n_1 of the film is therefore slightly lower than that of glass (2). Taking $K=0.0090$ corresponding to 1.8 percent contrast, we then find from Eq. (11) that $\Delta n=0.0028$ and the refractive index of the film for rays at normal incidence is thus

$$n_1=1.491. \tag{12}$$

For the films on glass (1) we should then have $\Delta n=-0.032$ and by Eq. (11) $K=-0.113$. The ratio of intensities of the bright and dark fringes should thus be 1.26 in agreement with a rough estimate of intensity.

Experiments with barium stearate films on glasses (1) and (2) using the ordinary ray at all angles of incidence gave fringes that indicated that n was constant and equal to n_1 in agreement with theory. Thus with glass (2) the faint fringes at all angles i belonged to series A while with glass (1) the fringes were of much greater contrast and belonged to series B.

With the extraordinary ray, however, very different results were obtained as shown in Table II.

The intensity of the light reflected from the upper surface of the film passes through zero and reverses in phase when i increases through Brewster's angle 55° 20′. The sequence of fringes should thus change from the A to B series (or *vice versa*) as i increases through Brewster's angle. The observations with glasses (2) and (3) are in accord with this theory. With glass (1), however, series B was obtained both at high and low angles. This must mean that at some angle of incidence between the limits of 53° 20′ and 56° 50′ the reflection from the interface between the film and glass (1) falls to zero and reverses in phase.

Analogy with the behavior of isotropic substances suggests that the disappearance of reflection from the interface on glass (1) should occur at an angle at which the refractive index n falls below 1.459. When this value of n is compared with the value $n_1=1.491$ it would indicate that the film is a crystal of negative character (a crystal is negative when $n<n_1$) whereas the direct optical tests have shown that it is positive. In a later section we shall show that these data are not inconsistent with values of n and n_3 which are greater than n_1.

Brewster's angle i_B was measured by a method which was described in a previous paper,[1] p. 1016. The films used for the measurements were built on glass (3) in steps which had maximum contrast at the angle i_B. These steps were 47, 95, 143 layers for films of barium stearate. At angles $i<i_B$ these steps form an A series for both R_p and R_s, at angles $i>i_B$ they form a B series for R_p (Table II) and an A series for R_s. The angle i_B at which the contrast between two neighboring steps reverses in intensity when the steps reflect the ray R_p of monochromatic light can be very accurately measured. It is essential that the Nicol prism which is used to furnish R_p should be turned so as to extinguish R_s completely, for if only a very small component of R_s be transmitted the angle at which the contrast reverses is greater than Brewster's angle. Under these conditions the contrast does not reverse until i increases to a value at which the B contrast supplied by R_p becomes greater than the A contrast supplied by the small component of R_s. The correct setting of the Nicol prism is found by determining the minimum angle at which the contrast reverses, this angle being i_B. The values $i_B=55°\,35'$ and 55° 40′ given in the previous paper were determined before the need for extin-

guishing R_s was fully appreciated. Recent measurements have given the result $i_B = 55° 20' \pm 1'$.

Measurements of the Spacing t of Molecular Layers on Chromium

By determining the values of N which correspond to the interference minima in light reflected from the film, it should be possible by Eq. (4) to calculate nt/λ and then from the known values of n and λ to obtain t.

Eq. (4), however, is based on the simple Fresnel theory according to which the reflection from a surface produces a phase change of 0° or 180°. The observed slight elliptic polarization of light reflected from transparent media and the much stronger elliptic polarization from metals shows that in general the phase change is not exactly 0° or 180°. This effect can be taken into account by making the following modification of Eq. (4).

$$N(n/n_1)\cos r - N_0 = m\lambda/4n_1t, \qquad (13)$$

where N_0 in general varies with r and is different for the ordinary and the extraordinary ray but otherwise does not depend upon m.

It will be convenient to represent the first term of this equation by a special symbol which may be defined by

$$N_N = N(n/n_1)\cos r. \qquad (14)$$

This is the value that N would have for normal incidence ($\cos r = 1$ and $n = n_1$) on the assumption that N_0 does not change with i. If it is found that N_0 does vary with i no error, however, will be introduced into our calculations; it merely changes our interpretation of the physical meaning of N_N. Eq. (13) thus becomes

$$N_N - N_0 = m\lambda/4n_1t. \qquad (15)$$

The uncertainties in the value of N_0 may be eliminated by determining N for the successive minima which correspond to a series of odd or of even values of m. If the measurements of the successive minima are made at approximately the same angles of incidence the values of N_0 are the same for the various minima and thus by Eq. (15) the increment in N_N in passing from any minimum to the next should be

$$\Delta N_N = \lambda/2n_1t. \qquad (16)$$

Since the thickness which a film must have in order to reflect minimum intensity of light depends on the angle i, values of N corresponding to various values of i were determined by the following method.

A slide was prepared with an initial series of several steps, $a, b, c, \cdots$, having $1, 3, 5 \cdots$ layers or any other chosen sequence; the process of building films requires that the films contain an odd number of layers. With such thin films no interference colors are seen. Additional layers were then applied to the whole of the slide covered by the initial layer until colors began to appear.

Let N_a, N_b, etc. represent the number of layers on the a, b, c steps at any stage of this process. When the number of layers is sufficiently increased, if the film is viewed by an ordinary ray using light from a sodium lamp a minimum appears at one of the steps at small angles of incidence. Further increases in layers permit this minimum to be observed at larger angles. On chromium the minima become sufficiently sharp for useful measurements only when i is greater than 68° while on glass of high refractive index much smaller angles can be used.

The angle of incidence is measured at which two adjacent steps, say a and b, are equally bright. The value of N which corresponds to the minimum is then halfway between N_a and N_b. The first line in Table III gives data for the first minimum obtained with films on chromium using the ordinary ray. The minimum is given as occurring at $N = 48$ when $i = 79° 7'$. This means that two adjacent steps $N = 47$ and 49 were found to match in intensity when viewed at that angle.

Additional layers were then applied until a minimum corresponding to $m = 2$ was observed with the extraordinary ray at a suitable angle of incidence. The data for this ray are given in the first three columns of Table IV. In this way by building N up to 518 all the minima up to $m = 10$ were studied. Only one pair of steps, a and b, were used for every determination of N given in Tables III and IV. By this procedure all the data in these tables referred to films built up from the same film chromium boundary. It was found useful to have steps c, d, e, on the same slide having 2, 4, 6 more layers than b, because

as progressive layers were applied to the entire slide the approaching minimum appeared first at the higher steps, and its position showed the precise number of layers which must then be added to the slide in order that the minimum should occur between a and b.

The procedure for measuring i consisted in mounting the slide on a spectrometer table with the film boundary between a and b situated in the axis of the table. The process of matching two steps was similar to the photometric matching of two fields of illumination. At angles greater than i, a was brighter than b, at angles less than i the contrast was reversed. There was no difficulty in measuring i with an accuracy which determined the thicknesses corresponding to successive light minima with a probable error of 0.1 molecular layer. With the ordinary ray satisfactory measurements could be made between 68 and 85°, but with the extraordinary ray because of the lower intensity and contrast the range was only from 77° to 85°.

Experiments were also carried out with films built on glass of very high refractive index, $n_g = 1.78$. Steps built on this glass showed great contrast when viewed by perpendicular light, the contrast diminishing with increasing i. The intensity of successive maxima and minima varied with the film thickness in accordance with a cosine curve.

In the case of films built on chromium the intensity distribution curve had very sharp minima, when the films were viewed at $i = 75° - 85°$, due to multiple reflections of light in the film. Fig. 1 is a photograph of a chromium slide 1×3 inches in size, on which 15 steps were built having 35, 37, 39, ··· 63 layers. The photograph was made by Mr. V. J. Schaefer using the ordinary ray R_s of sodium light. The upper photograph shows the appearance of the steps at an angle $i = 82°$. The intensity minimum which lay at $N = 49$ was sharply differentiated from the neighboring steps $N = 47$ and 51. The rest of the steps were all bright and had too little contrast to be visible in the photograph, most of them were not visible to the eye. In the lower photograph the same slide is shown illuminated at an angle $i = 75°$. The minimum then lay between $N = 47$ and $N = 49$ and was not so sharply defined. At $i = 80°$ there were 108 layers between successive minima, so that the series seen in the photograph would need to be extended for 54 steps before it would reach the next minimum. Therefore even in the lower photograph the minimum lay in a fairly narrow region, since the drop in intensity occurred in about 8 steps on either side of the minimum.

The data of Tables III and IV were obtained with barium stearate films on a slide of highly polished chromium plated brass which had

TABLE III. *Intensity minima with ordinary ray, R_s of wave-length $\lambda = 5893A$ at various angles of incidence i. Film of barium stearate pH = 7.0; $\Delta N_N = 81.00$; $N_0 = -4.30$; $n_1 = 1.491$.*

m	N'	i	$\cos r$	N_N obs.	N_N calc.
1	48	79° 7′	0.7525	36.13	36.20
3	150	68° 48′	.7804	117.06	117.21
	152	71 35	.7714	117.25	
	154	74 59	.7618	117.32	
	156	79 12	.7523	117.36	
5	254	68° 50′	.7803	198.20	198.21
	258	72 50	.7676	198.04	
	262	77 29	.7559	198.05	
	266	84 17	.7448	198.12	
7	356	67° 42′	.7842	279.18	279.21
	362	71 39	.7712	279.17	
	368	76 8	.7589	279.28	
	374	82 37	.7467	279.27	
9	460	67° 59′	.7831	360.23	360.22
	468	71 59	.7702	360.45	
	476	77 0	.7569	360.28	
	484	84 32	.7444	360.29	

TABLE IV. *Intensity minima with extraordinary ray, R_p of wave-length $\lambda = 5893A$ at various angles of incidence i. Same film as Table III. $\Delta N_N = 81.00$; $N_0 = -7.01$ (at $i = 80°$); $n_1 = 1.491$; $n_2 = 1.551$.*

m	N	i	N_N obs.	N_N calc.
2	95	82° 54′	73.78	73.90
4	200	78° 12′	155.14	155.04
	202	33 49	155.05	154.90
6	304	77° 58′	235.94	236.05
	306	81 11	235.85	235.95
8	408	77° 28′	317.06	317.07
	410	79 41	316.96	317.00
	412	82 23	316.89	316.93
10	512	77° 8′	398.22	398.08
	514	78 56	398.02	398.02
	516	80 51	397.96	397.96
	518	83 16	397.89	397.88

previously been ground to a plane surface. The chromium was cleaned by being made cathode in an electrolytic bath of NaOH, water and alcohol. The initial steps transferred to the plate had a 2-layer step rise similar to the steps of Fig. 1.

The stearic acid films were spread upon doubly distilled water of specific resistance greater than 10^6 ohms-cm, the second distillation having been made in Pyrex glass. Barium bicarbonate was added to this water in a concentration 5×10^{-5} M. The barium bicarbonate was prepared in more concentrated solution by dissolving 0.3 g $BaCO_3$ in 1000 cc of water saturated with CO_2 at a pressure of 1 atmosphere. After a suitable amount of the barium bicarbonate solution was added to the water bath, air was bubbled through the bath to remove excess CO_2 and bring the pH to the value 6.7 which corresponded to equilibrium with the CO_2 contained in ordinary air. Measurements of pH were made by using La Motte standard indicators. The data of Tables III and IV were taken prior to the use of the solutions (a) and (b) recommended in this paper. The barium bicarbonate solution gave the same type of film as solution (a) but was more troublesome to prepare. The stearic acid which was used in all the measurements described in this paper was prepared by Dr. R. E. Burnett. Tests showed that this stearic acid had a very high degree of purity. The test for purity was described in a previous paper,[1] p. 1010.

Measurements with Ordinary Ray R_s

In Table III the values of cos r in column 4 were calculated from i by means of the equation

$$\sin i = n \sin r, \tag{17}$$

placing $n=n_1=1.491$, as given by Eq. (12). The value of N_N in the 5th column is the product $N\cos r$ in accord with Eq. (14).

It is seen that for any value of m, N_N is constant. This proves by Eq. (13) that within the range from $i=67$ to 85° (or r from 38 to 42°) there is no appreciable variation in N_0. The values of N_N are found to vary linearly with m, as they should by Eq. (13) and are accurately represented by the equation

$$\text{For } R_s\text{: } N_N = 40.502m - 4.30. \tag{18}$$

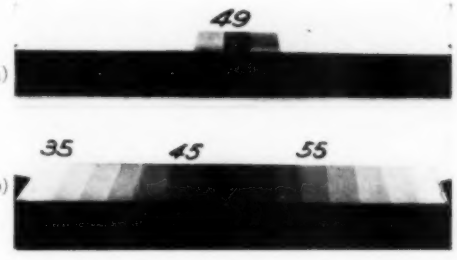

(a) $i=82°$. (b) $i=75°$.

FIG. 1. Interference fringe seen with 15 steps having 35, 37, . . . 63 layers of barium stearate built on polished chromium. Photographed with R_s ray of light $\lambda=5893$A.

The values of N_N in the last column of Table III have been calculated by this equation. A comparison of the observed values with the calculated (columns 5 and 6) shows that the probable error of the individual values of N_N is about ±0.07 layer. A comparison of Eqs. (18) and (13) gives

$$\text{For } R_s \text{ at } r=40°\text{: } N_0 = -4.30. \tag{19}$$

By Eqs. (12), (13), (16) and (18) we find taking $\lambda=5893$A.

$$\Delta N_N = 81.00 \text{ and } t=\lambda/2n_1\Delta N_N = 24.40\text{A}. \tag{20}$$

Measurements with Extraordinary Ray R_p

For R_p, n is a function of r according to Eq. (2). Since r is not directly observed it is convenient to eliminate r from this equation by using Eq. (17) and so obtain

$$(n/n_1)^2 = 1+(1/n_1^2-1/n_3^2)\sin^2 i. \tag{21}$$

Similarly r can be eliminated from Eq. (14) and then n can be eliminated by Eq. (21), so that

$$N_N^2 = N^2(1-\sin^2 i/n_3^2). \tag{22}$$

To calculate N_N from the data in columns 2 and 3 of Table IV we need to know n_3. To determine n_3 we make use of the fact that ΔN_N according to Eq. (16) must be the same whether R_s or R_p is used. Let ΔN_s and ΔN_p represent the increments in N between successive minima ($\Delta m=2$) which correspond to a particular value i (say i_M) for R_s and R_p, respectively. By interpolation in Tables III and IV for each value of m we obtain the value of N that corresponds to

$i_M=80°$ and by finding the successive intervals for $\Delta m=2$ we obtain:

$$\text{at } i_M=80° \quad \Delta N_s=107.89\pm0.05;$$
$$\Delta N_p=104.85\pm0.05.$$

From Eq. (22) we obtain

$$(\Delta N_N)^2=(\Delta N_s)^2[1-(\sin^2 i_M)/n_1^2]$$
$$=(\Delta N_p)^2[1-(\sin^2 i_M)/n_3^2]. \quad (23)$$

Introducing the values of ΔN_s, ΔN_p and $i_M=80$ we find

$$n_3^2=n_1^2/(1.0589-0.06073n_1^2). \quad (24)$$

If we take $n_1=1.491$ as in Table III we thus obtain

$$n_3=1.551\pm0.002. \quad (25)$$

The values of N_N obtained by Eq. (22) are given in column 4 of Table IV. There is a slight decrease in N_N as i increases. The values of N_N (calc.) in the last column were calculated by the empirical equation

$$\text{For } R_p\text{: } N_N=40.50m-7.01-0.03(i°-80), \quad (26)$$

where $i°$ is i expressed in degrees. The differences between the observed and calculated values of N_N correspond to a probable error of ±0.06 layer. The coefficient of m agrees with that of Eq. (18) because n_3 was chosen to make it do so. The other terms indicate that

$$\text{For } R_p \text{ at } i=80°\text{: } N_0=-7.01 \text{ layers.} \quad (27)$$

The difference between N_0 given by Eqs. (19) and (27) is associated with the marked elliptic polarization of the light reflected from films on chromium.

Birefringence Measured with Optical Compensator

The birefringence of films of barium stearate having a total thickness of 5752 layers built on glass (made by placing two slides face to face, coated with 2751 and 3001 layers) was studied with the aid of a quartz wedge compensator. The relative phase retardation of the two rays transmitted by the film was found to be 180° at $i=56°$ for sodium light.

The retardation in path of the extraordinary ray R_p' with respect to the ordinary ray R_s was

$$\Delta l=5752t[(n/\cos r_p-n_1/\cos r_s)$$
$$+(\tan r_s-\tan r_p)\sin i] \quad (28)$$
$$=2947\text{A}.$$

The terms in the first pair of brackets give the difference in optical path of the two rays in the film, and the terms in the second brackets the path difference in air after the rays leave the film. Values of n were calculated by means of Eq. (21) using $n_1=1.491$ from Eq. (12) and a series of values of n_3. Then r_s and $\cos r_p$ were calculated from n_1 and n and the value $i=56°$ by Eq. (17), and $t=24.40$A was substituted from Eq. (20). It was found that if n_3 was assumed to be greater than n_1 in accordance with the results given in the preceding section, the value which satisfied Eq. (28) was $n_3=1.5514$. This is in close agreement with the value obtained in Eq. (25).

Optical Properties of Chromium

Chromium has advantages as a surface on which to build films not only because it is nontarnishable but also particularly because it has a low reflectivity and so gives strong interference fringes. We see by Eq. (5) that a perfectly reflecting metal ($C=1$) would give no fringes. With silver the fringes are very faint except at nearly grazing incidence.

The reflection coefficients ρ_s and ρ_p for the rays R_s and R_p and the corresponding phase changes δ_s and δ_p can be calculated by the electromagnetic theory from the index of refraction n_m and the index of absorption k of the metal.

The dashed line curves given in Fig. 2 for bare chromium have been calculated using[8]

$$n_m=3.59; \quad k=1.26 \text{ for } \lambda=5893\text{A}$$

by the complicated equations given in convenient form by W. König.[9]

The full line curves have been calculated for the interface between chromium and an isotropic medium of refractive index $n_1=1.491$ and therefore should give accurate values of C_s and approximate values of C_p for the interface

[8] *International Critical Tables*, Vol. 5 (1929), p. 249. The equations for calculating ρ_s, ρ_p and Δ are also given.

[9] W. König, *Handbuch der Physik*, Vol. 20 (Julius Springer, 1928), p. 242.

between the chromium and the barium stearate films. These calculations gave the quantities δ_s and δ_p in terms of the angle of refraction r, but the data given in Fig. 2 have been expressed in terms of i, the angle of incidence in the air above the film. Thus with $i=90°$, $r=42°$ and the large changes in ρ_p and δ_p observed with bare chromium do not occur when the chromium is covered by the film.

The phase changes δ_s and δ_p are related to the quantities N_0 which we have found in our studies of films. Some part of N_0 may have its origin in a phase change at the upper surface of the film, but the extreme smallness of the elliptic polarization produced by reflection from transparent bodies would indicate that the larger part of N_0 should be due to the interface between the film and the metal. The addition of ΔN_s or ΔN_p layers, as given by Eq. (23) causes a phase retardation of 360° in the ray that traverses the film (down and back). Thus by proportion we find that

$$\text{For } R_s\text{:}\quad N_0=(\delta_s/360°)\Delta N_N/\cos r; \tag{29}$$
$$\text{For } R_p\text{:}\quad N_0^2=(\delta_p/360°)^2(\Delta N_N)^2/(1-\sin^2 i/n_3^2).$$

The values of N_0 have been calculated by these equations from the corresponding values of δ_s and δ_p in Fig. 2, using ΔN_N as given in Eq. (20). The results are shown in the two curves $(N_0)_s$ and $(N_0)_p$ in Fig. 3.

It is seen that $(N_0)_s$ is independent of i in agreement with the constancy of the calculated values of N_N in Table III for each value of m. The absolute value of $(N_0)_s$ is -5.28 which differs by one unit from the value -4.30 given in Eq. (18).

With the R_p ray, $-(N_0)_p$ increases with i and at $i=80°$ the rate of increase is 0.041 per degree, in reasonable agreement with the value 0.03 given by Eq. (26) as found from the variation of N_N with i in Table IV. The absolute value of $(N_0)_p$ at 80° in Fig. 3 is -9.10 which differs by 2 units from -7.01 given by Eq. (27).

In view of the fact that the values of n_m and k given for chromium in the I. C. T. are based on measurements of 1910, prior to the time that chromium plated surfaces were available, we should probably not expect better agreement. Perhaps the neglect of the anisotropic nature of the film for the R_p ray in the calculation of δ_p may account for the greater discrepancy in $(N_0)_p$.

The method that we have used to determine N_0 from molecular layers on metal makes it possible to find δ_s and δ_p separately, whereas the measurement of the ellipticity of the reflected light gives only Δ, the difference between δ_s and δ_p.

Films built on chromium in 2-layer steps show little contrast when seen by the R_s ray or the R_p ray at $i=45°$. If, however, the chromium slide is placed between crossed Polaroid screens and the plane of vibration of the incident light makes an angle of 45° with the chromium surface, great contrast in intensity is seen between the steps. Under these conditions the light reflected by the film is in general elliptically polarized, and the phase retardation of the resultant of the two R_s rays (reflected from the upper and lower surfaces of the film) with respect to the resultant of the two R_p rays is a function of the thickness of the film. If a quartz wedge compensator is introduced in the path of the light between the two Polaroid screens, the wedge being turned so that the dark band exhibited by the wedge traverses all the steps in the series, the variation of phase retardation with the thickness of the steps is beautifully demonstrated. The band of the wedge is seen as a sinusoidal wave having its steepest slopes at steps whose thicknesses correspond to intensity minima for the ray R_s or the ray R_p. The complete theory of the factors involved in the reflection of light by transparent films deposited on metal has been worked out by Hauschild.[10]

The Reflection of Light From the Upper and Lower Surfaces of Films on Glass

The general equations for the reflection of light from an interface between any crystal and an isotropic medium (both perfectly transparent) are very complicated but are given in convenient form by G. Szivessy[11] in the *Handbuch der Physik*.

For the case of a plane parallel plate of a uniaxial crystal (cut with surfaces perpendicular to the optic axis) lying between two isotropic media of refractive indices n_0 and n_e the equations

[10] H. Hauschild, Ann. d. Physik **63**, 816 (1920).
[11] Szivessy, *Handbuch d. Physik*, Vol. 20 (1928), pp. 635–726.

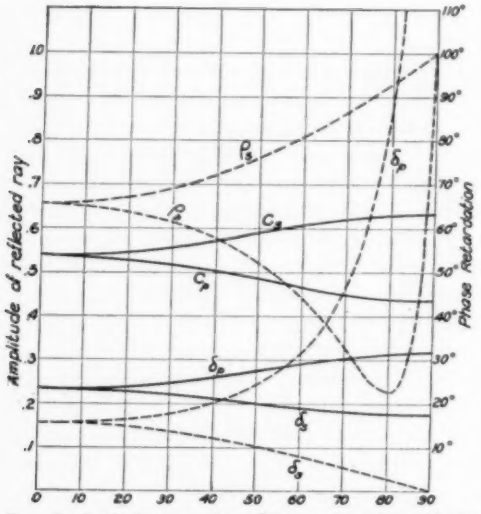

FIG. 2. Optical properties of bare chromium (dashed lines) and of the interface between chromium and a stearate film (solid lines). ρ_s and ρ_p are the amplitudes reflected from bare chromium for the R_s and R_p rays; C_s and C_p are the amplitudes reflected from the chromium-stearate interface. δ_s and δ_p are the phase retardations in degrees (beyond the normal 180° phase shift).

take the much simpler form:[12]

$$B_s=\frac{n_0\cos i-(n_1^2-n_0^2\sin^2 i)^{\frac{1}{2}}}{n_0\cos i+(n_1^2-n_0^2\sin^2 i)^{\frac{1}{2}}}, \tag{30}$$

$$B_p=\frac{n_0(n_3^2-n_0^2\sin^2 i)^{\frac{1}{2}}-n_1n_3\cos i}{n_0(n_3^2-n_0^2\sin^2 i)^{\frac{1}{2}}+n_1n_3\cos i}, \tag{31}$$

$$C_s=\frac{(n_1^2-n_0^2\sin^2 i)^{\frac{1}{2}}-(n_g^2-n_0^2\sin^2 i)^{\frac{1}{2}}}{(n_1^2-n_0^2\sin^2 i)^{\frac{1}{2}}+(n_g^2-n_0^2\sin^2 i)^{\frac{1}{2}}}, \tag{32}$$

$$C_p=\frac{n_1n_3(n_g^2-n_0^2\sin^2 i)^{\frac{1}{2}}-n_g^2(n_3^2-n_0^2\sin^2 i)^{\frac{1}{2}}}{n_1n_3(n_g^2-n_0^2\sin^2 i)^{\frac{1}{2}}+n_g^2(n_3^2-n_0^2\sin^2 i)^{\frac{1}{2}}}. \tag{33}$$

In these equations i is the angle of incidence in the medium of refractive index n_0; n_1 and n_3 are the refractive indices characteristic of the uniaxial crystal and n_g is that of the underlying glass. The quantities B and C are the amplitudes of the electric vectors of the reflected rays from the upper and lower surfaces, respectively, taking the amplitude of the light incident *upon that surface* as being unity.

It is evident from Eq. (5) that the interference fringes vanish if either B or C becomes zero. We see from Eqs. (30) and (32) that $B_s=0$ only when $n_1=n_0$, and $C_s=0$ only when $n_1=n_g$. There are, however, certain angles i_B and i_C at which B_p and C_p can vanish. These are given by:

$$\sin^2 i_B=n_3^2(n_1^2-n_0^2)/(n_1^2n_3^2-n_0^4) \tag{34}$$

and $$\sin^2 i_C=n_3^2n_g^2(n_1^2-n_g^2)/n_0^2(n_1^2n_3^2-n_g^4). \tag{35}$$

If n_3 and n_g differ only slightly from n_1, we may place

$$n_3^2=n_1^2+\Delta_3 \quad \text{and} \quad n_g^2=n_1^2+\Delta_g. \tag{36}$$

Then, neglecting terms involving Δ^2, we obtain (for $n_0=1$)

$$\tan i_B=n_1-\Delta_3/2n_1(n_1^2-1) \tag{37}$$

and $$\sin^2 i_C=n_1^2\Delta_g/(2\Delta_g-\Delta_3). \tag{38}$$

Thus Brewster's angle i_B decreases as n_3 increases above n_1, whereas with an isotropic substance the change with n is in the opposite direction. We can now understand the low value of i_B given in

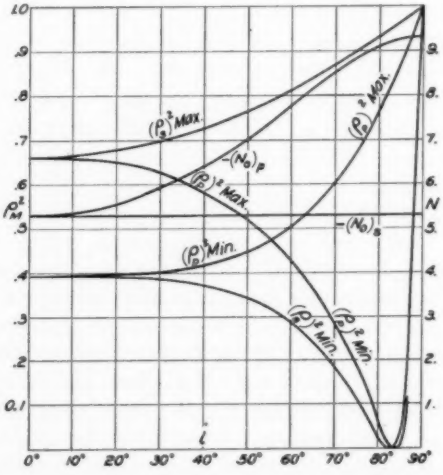

FIG. 3. Intensities of the interference fringes for barium stearate films on chromium and the value of N_0. $(\rho_s)^2$ and $(\rho_p)^2$ refer to the R_s and R_p rays. The values of (ρ) Max. and (ρ) Min. are the values given by Eq. (5) by taking the + and − signs. Note the different ordinate scales for $(\rho)^2$ and N_0.

[12] To obtain these equations from those given in the *Handbuch der Physik* many variables must be eliminated. Eqs. (189) to (192) on p. 718 give expressions for B_s and B_p in terms of i, r and ζ (the angle between the wave normal and the ray). Similar equations for C_s and C_p must be derived from Eqs. (181) to (184) and are then expressed in terms of ζ, r and r_g, the angle of the ray transmitted into the glass. The angle ζ can be eliminated by Eq. (147) on p. 689. Then r and r_g can be eliminated by using $n_0\sin i=n\sin r=n_g\sin r_g$ together with the value of n given by Eq. (145).

Table II. Taking $n_1=1.491$ and $i_B=55°\,20'$ we calculate by Eqs. (37) or (34) that $n_3=1.552$, while Eq. (1) gives $n=1.446$. The value $n_3=1.552$ is in agreement with the result given in Eq. (25).

Real values of i_C occur only when n_g lies within the range for which the 2nd member of Eq. (38) is between 0 and 1. When $n_3>n_1$ and $n_1>1.42$, n_g must be less than n_1 in order that there shall be any angle i_C at which C_p vanishes. This explains the fact that for films on quartz, Table II, column 3, series B was observed at large as well as at small angles.

If for a film on quartz we take $n_g=1.459$, $n_1=1.491$ and $n_3=1.551$ from Eq. (25) we find by Eq. (35) $i_C=50°\,18'$. The data shown in Table II give the result that for films built on quartz i_C had a value between $53°\,20'$ and $56°\,50'$. A mean of these angles, $i_C=55°\,5'$ corresponds to the values $n_1=1.491$, $n_3=1.535$. The discrepancy of about 4 degrees between the calculated and observed values of i_C suggests that conditions obtain at the boundary between the film and quartz which are not fully described by Eq. (35).

Intensity of Interference Fringes Produced by Films on Chromium and on Glass

The data for C_s and C_p in Fig. 2, together with B_s and B_p given by Eqs. (30) and (31) enable us to calculate the intensities ρ^2 of the maxima and minima of the interference fringes on chromium by Eq. (5). The results of such calculations using $n_1=1.491$ and $n_3=1.551$ are given in Fig. 3.

It is seen that at $i=0$ the ratio of the intensities of the maxima and minima is 1.68. With the R_s ray this contrast steadily increases until at about $82°\,30'$ the minima become completely black, while the maxima reflect about 95 percent of the incident light. With the R_p ray as i increases the contrast decreases until it disappears at Brewster's angle $55°\,20'$. The contrast then reverses and increases very rapidly, becoming infinite at about 84°. These results agree with the observations.

The upper part of Fig. 4 gives the maximum and minimum values of ρ calculated by Eq. (5) from the values of B_s, B_p, C_s and C_p given by Eqs. (30) to (33), using $n_1=1.491$ and $n_3=1.534$, which are the values of n_1 and n_3 which correspond to the observed value of i_C for films on quartz. The curves shown are for glass (1) (quartz, $n_g=1.459$) and for glass (3) ($n_g=1.7854$). The separation of the curves for ρ_s and ρ_p for glass (2) $n_g=1.4937$ is too small to be shown in Fig. 3. The mean value of ρ for this glass lies approximately midway between the two values shown for glass (1). The index of contrast, K, defined by Eq. (8), is shown for glasses (1) and (2) in the lower part of Fig. 4. We see that for glass (1) the contrast decreases slowly, while for glass (2) it increases rapidly when i increases and at 43° the contrasts are equal. These results are in complete agreement with the observations given in Table II. The observed points of disappearance and reappearance of fringes with glass (1) occur at $i=53°\,20'$ and $56°\,50'$. The contrast is about 1 : 1.15 at these points, so the fringes become invisible between these limits because of the low intensity of the reflected light (less than 0.04 percent). With glass (3), on the other hand, the intensity of the reflected light at Brewster's angle is 0.4 percent and in this neighborhood a relative change in intensity of 2 percent is caused by a change in i of a little less than 2'. Thus, the observed accuracy of measuring i_B on glass (3) and the inaccuracy with glass (1) is explained quantitatively.

The optical properties of the built-up films on chromium and on the several glasses are thus in accord with the theories given for uniaxial crystals with their optic axis perpendicular to the plane of the film. The analysis that we have made furnishes several independent methods by which n_1 and n_3 can be determined accurately. Thus with measurements of ΔN_N we have the possibility of precise measurements of t, the spacing of the layers. If then films are also used for x-ray diffraction measurements a direct comparison of optical and x-ray wave-lengths can be made.

Spacing Measurements for Films Built on Glass

When spacing measurements were made with films built on glass, the films had to be built with a greater step-rise than in the case of films on chromium since the minima were not so sharply defined. A step-rise of 10 layers was sufficient when the films were built on glass of refractive index $n=1.78$, when glass of lower refractive

index was used the step-rise had to be 16–20 layers.

The results which were obtained showed that measurements made with films on glass, $n_g = 1.78$ and a 10-layer step-rise, had the same probable error as with films on chromium having a 2-layer step-rise. The films on glass had the advantage that they could be measured at small angles of incidence and when i is small the calculated values of $\cos r$ are less affected by an error in the value of the refractive index than when i is large. With R_s accurate measurements could be made at angles up to about 50°, which was a greater range than for the case of chromium. The values of $n_s \cos r$ calculated from $n = 1.491$ were independent of the angle, as in the case of the data in Table III. When the glass was thoroughly cleaned by being scoured with Shamva the values of $-N_0$ obtained in accordance with Eq. (2) were $-N_0 = 0.2$ to 1.0 layer, the value commonly obtained being 0.7 layer. These relatively small values are in accord with the known small degree of elliptic polarization from transparent media.

Small variations in N_0 were attributed to the manner in which the glass was cleaned in successive runs. The glass $n_g = 1.78$ was visibly stained by dilute acid, also long exposure to the air produced a film on the surface which had a thickness of many stearate layers. Scouring the surface with Shamva removed films of stain and grease very satisfactorily, but the Shamva itself adhered to both glass and metal and could not be removed merely by rinsing the surface with a stream of running water. Even after thorough swabbing with cotton under water some traces of Shamva were frequently detected which were sufficient to account for small variations in N_0 of the magnitude which were observed. The values of N_0 obtained for chromium cleaned with Shamva were subject to similar variations within a range of approximately ± 0.2 layer. Chromium cleaned by being made cathode in an electrolytic bath showed an increase in $-N_0$ of 1 layer as a result of becoming slightly etched by being cleaned about 10 times.

Effect of Foreign Substances Dissolved in Benzene

The solution of stearic acid in benzene which was used to spread the monolayer on water in these experiments contained stearic acid in a concentration which was commonly 3×10^{-4} by weight. The benzene was "Benzene Merck" which was redistilled in this laboratory.

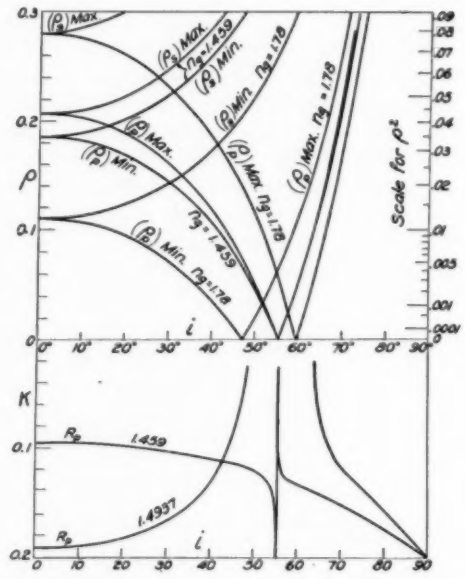

FIG. 4. Upper figure: intensities of interference fringes for films on three glasses. Ordinates with scale on left are the absolute values of ρ and with scale on right are intensities ρ^2. Lower figure: absolute values of index of contrast for films on two glasses. (0.2 on ordinate scale should be 0.)

The effect of the presence of a small amount of a dissolved oil in the benzene was demonstrated by adding mineral oil in a concentration 3×10^{-4} by weight to redistilled benzene containing a concentration 3×10^{-4} stearic acid. Films containing 200 layers were readily built on chromium with this mixture. They had a spacing approximately 80 percent greater than the normal spacing for barium stearate and were much less transparent, a large part of the light which fell on the film being reflected as scattered light. The appearance when seen in a microscope indicated that much of the oil had gathered into a myriad of droplets. When "Benzene Merck" was used without being redistilled a spacing 6 percent greater than normal was obtained, and films having more than 100 layers on chromium showed marked scattering of light.

Effect of Substances Dissolved in Water on Spacing of Layers and on the Refractive Indices

A large number of measurements have been made to determine the number of layers between successive minima, ΔN_N, for films of barium stearate built from many different solutions. The values were found to range from $\Delta N_N = 79$ to 82 for films which could be built in a satisfactory manner. Most of the values lay between $\Delta N_N = 81.2$ and 81.8. The values were independent of pH, temperature, and barium concentration, within the range in which these variables were commonly used for film building. This range was $p\text{H} = 6.5$–7.2, temperature 15°C–25°C, barium concentration 0.3×10^{-4} to 10^{-4} M. The presence of Cu in a concentration 2×10^{-6} did not affect the spacing. The differences obtained in values of ΔN_N were attributed to small amounts of foreign substances present in the water on which the films were spread. The belief that foreign substances were responsible for the variations was derived from data of the type shown in Table V. Water obtained from a still lined with tin was used to make up solutions on successive days, all the solutions being 0.3×10^{-4} M $BaCl_2$, 2×10^{-4} M $KHCO_3$, $p\text{H} = 6.8$. Some of these solutions produced films which gave data of the type shown in columns (*a*), Table V, whereas others gave data of the type in columns (*b*). In the type (*a*) ΔN_N increased steadily for each successive interval from the 1st to the 6th minimum. In every case when data of this type were obtained and a second series of measurements was made with films built from the same solution, the initial values obtained in the second measurements were similar to the final values of the first measurements. This made it appear very probable that the water used for the solution (specific resistance = 900,000 ohms-cm) contained a trace of some substance which was used up by the successive films. The series in columns (*b*) did not have this regular trend, the greatest departure from the mean value 81.6 being 0.2 layer.

Table V. *Films built on glass. Initial layer formed by rubbing down 50 layers of barium stearate.*

	(a)		(b)	
m	N_N	ΔN_N	N_N	ΔN_N
1	39.0		38.8	
3	118.6	79.6	120.4	81.6
5	199.2	80.6	201.9	81.5
7	280.0	80.8	283.7	81.8
9	361.1	81.1	365.1	81.4
11	442.3	81.2	446.8	81.7
13	523.5	81.2	528.4	81.6
				Mean 81.6

Mr. Schaefer has been conducting experiments which have shown that minute traces of tin, lead and silica in concentrations as low as 10^{-8} parts by weight in the water can produce effects of this kind. The effect on the 2-dimensional viscosity of the films[13] is a particularly sensitive indication of the presence of these impurities. The measurements given so far in this paper were made at a time when we had no knowledge of the nature of the foreign substances which may be responsible for changes in n and ΔN_N. Recently we have made a few observations with distilled water from various sources and have sometimes added small amounts of salts of divalent elements.

Using a laboratory supply of distilled water of specific resistance about 300,000 ohms-cm which had passed through tin lined lead pipe, we find with barium stearate films built up on quartz that with the extraordinary ray (compare with Table II) the B series is observed up to $i = 56°\,0'$ that there is then a range between $56°\,0'$ and $62°\,30'$ at which the A series is seen and at still larger angles the B series again appears. Thus for these films we may take $i_B = 56°\,0'$ and $i_C = 62°\,30'$. These values would indicate by Eqs. (34) and (35) that n_1 is about 1.515 and that n_3 is at least 1.56. These effects are probably due to traces of lead.

To investigate the effects produced by lead, $PbCl_2$ was added, sufficient to make the solution 3×10^{-6} molar with respect to Pb, the solution being 3×10^{-5} molar with respect to Ba. Films built from this solution on glass having a refractive index of 1.5106 showed at $i = 0$ a fairly strong B series, so that n_1 for this film must have been at least 1.52. Films built from this solution on quartz gave with R_p the B series for $i < 56°\,35'$ followed by the A series at $i > 56°\,35'$ with no return to the B series. The value of i_B for films

[13] I. Langmuir, Science **84**, 379 (1936).

built on glass $n=1.78$ was 56° 10′. With $n_1=1.52$ and $i_B=56°\ 10'$ we find by Eq. (34) $n_3=1.559$.

On doubling the amount of lead the films were more difficult to build, but a value of n_1 was found which was slightly less than 1.5106.

Films of pure stearic acid spread on distilled water pH = 5.8 without any added salts at $i=0°$ gave no observable fringes on glass of $n_g=1.5106$, so that we may take $n_1=1.510$.

Skeleton Films

When a slide coated with a film of barium stearate which has been built at pH = 6.5 is soaked for 1 to 10 sec. in benzene and is then withdrawn from the benzene, a striking change is observed in the interference color reflected by the film. The color of the soaked film corresponds to an optical thickness much less than that of the new film. Further soaking produces little or no change of color. The change is due to a large decrease in the refractive index of the film, the actual thickness being practically unaltered. Before the film is soaked it consists of a mixture of barium stearate and stearic acid,[4] the proportion of each component being determined by the barium concentration and pH of the water solution used in building the film. The benzene dissolves the stearic acid and leaves the barium stearate as a skeleton with air filling the spaces previously occupied by the stearic acid.

The data in Tables VI and VII refer to a film which had an initial refractive index $n_1=1.499$ and after soaking in benzene the refractive index of the skeleton was $n_W=1.30$. Several skeleton films have been built which had the value $n_W=1.25$, and in one case $n_W=1.22$. From the law of Clausius and Mosotti

$$(n^2-1)/(n^2+2)=k\times\text{density} \qquad (39)$$

we have the result that $n_W=1.30$ corresponds to a skeleton structure containing 63.7 percent of the material in the initial film. The values $n_W=1.25$ and $n_W=1.22$ correspond to 53.8 percent and 47.7 percent, respectively.

The removal of 35 to 40 percent of the material can be accomplished with practically no shrinkage in thickness of the film. Due to the decrease in refractive index vivid colors are obtained with skeleton films built on ordinary glass microscope slides, $n_g=1.51$ to 1.52, whereas normal films are barely visible on this glass. The air spaces in the film may be filled with oil by allowing a drop of mineral oil to travel across the film. The oil does not wet the film permanently but withdraws from the path which it has traveled, and this path is then seen to have the same color as that of the film before it was soaked. If a moderately volatile oil such as tetradecane or kerosene is used, the color gradually returns to that of the skeleton film as the oil evaporates.

When more than about 50 percent of the material of the film is removed, the skeleton commonly shows partial collapse and has a fogged appearance. Films which have collapsed completely, due to the removal of more than about 60 percent, are no longer transparent. The best skeleton films are obtained when the films contain less than 100 layers, for the reason that the water solutions which must be used to build films containing a large proportion of stearic acid are at pH = 6.5 which is a range of pH in which films are slower than at pH = 7.0 and become progressively slower as every successive 100 layers are added. A series of steps can be built in 50-layer intervals which appear perfectly transparent before the series is soaked, but when withdrawn from the benzene the higher skeleton steps are fogged in a manner which shows that the tendency to collapse is greatest for the films which are built at the lowest speed. A study of the skeleton of a film thus affords an important test of the building qualities of the material of which the film is composed.

A large part of the stearic acid is usually removed from the film by benzene in 10 to 60 sec., often it is removed in 1 sec. Prolonged soaking in

TABLE VI. *Intensity minimum $m=3$ with ordinary ray of wave-length $\lambda=5893A$ for normal and skeleton films of barium stearate built on glass.*

Film	N	i	cos r calc. for $n=1.499$	$N\cos r$	cos r calc. for $n=1.30$	$N\cos r$
Normal	124	17°57′	0.9786	121.35		
	134	38 55	.9079	121.66		
	144	53 40	.8433	121.44		
			Mean	121.48		
Skeleton	144	14°47′	0.9854	141.90	0.9805	141.19
	154	30 52	.9396	144.70	.9189	141.51
	164	41 20	.8977	147.22	.8613	141.25
	174	49 22	.8623	150.04	.8119	141.27
	184	57 0	.8288	152.50	.7640	140.58
Skeleton filled with Nujol	124	17°55′	.9787	121.36		
	134	38 32	.9096	121.89		

benzene frequently results in a gradual slow decrease in optical thickness, but this is usually accompanied by a slow collapse of the skeleton. In order to build a skeleton which will have a desired value of n_W the proportion of the film that is to be dissolved is fixed by the stearic acid content of the film. For example, the data in Table VI refer to a film built at pH = 6.4 which lost 36.3 percent of its initial material. Films built from a solution having the same barium content and pH = 7.0 lose practically no material when soaked in benzene for 1 min.

The amount of material which can be removed at a given pH value, and the amount which can be removed without causing collapse are both affected to a great extent by the presence of traces of foreign substances in the water. In recent experiments the skeleton films which have been built when using barium acetate have shown less tendency to collapse than those built with barium chloride. The presence of copper in the water usually causes the films to crack when skeletonized. A wide variety of effects produced by foreign substances in the water when building skeleton films is being studied by Mr. Schaefer.

The measurements given in Table VI were made with a film built on glass $n_g = 1.78$ in steps having 119, 129, $\cdots$ 229 layers. The water solution was 10^{-4} M barium acetate, 0.2×10^{-4} M $KHCO_3$, 10^{-5} M KCN. The KCN was added in order to remove traces of copper from the solution. The temperature was 19°–20°C, pH = 6.4. The initial layer was built from a solution containing the same concentration of barium, pH = 8.5.

The refractive index of the normal film was found by building steps on the standard glasses. Steps built on glass $n_g = 1.4937$ formed a B series which had a contrast about one-half as great as the A series exhibited by the steps on $n_g = 1.5106$.

TABLE VII. *Skeleton and normal films on chromium compared with R_r ray of white light.*

COLOR	N (NORMAL)	N_W (SKELETON)	$\frac{N}{N_W}$
2nd-order yellow	127	169	0.7515
2nd-order red	145	189	.7672
2nd-order blue	163	219	.7443
			Mean .7510

The refractive index was therefore $n = 1.499$. This value is higher than the usual value $n = 1.491$ obtained for films built at pH = 7.0 to 7.2 because of the greater percentage of stearic acid at pH = 6.4, the refractive index of pure stearic acid films being 1.51.

The data in column 5 for the normal film were calculated using $n = 1.499$. The resulting values of $N \cos r$ are in good agreement. After these measurements were made the film was soaked in benzene for 1 min. The values of $N \cos r$ in column 5 for the skeleton were calculated using $n = 1.499$, in column 7 using $n = 1.30$. The results in column 7 are reasonably constant whereas in column 5 they show a steep upward trend with increasing i. The refractive index of the skeleton was therefore 1.30.

All films which reflect minimum intensity corresponding to a particular value of m have a constant value of $nNt \cos r$ (by Eq. 4), if one neglects N_0 (Eq. (13)) which is a very small term in the case of films on glass. Therefore

$$t_W/t = nN \cos r/n_W N_W \cos r_W, \qquad (40)$$

where the subscript W refers to the skeleton film. Substituting $n = 1.499$, $n_W = 1.30$, $N \cos r = 121.48$, $N_W \cos r_W = 141.2$ (from Table VI) we have the result $t_W = 0.992t$. That is, the removal of 36.3 percent of the bulk of the film was accompanied by a shrinkage of only 0.8 percent in thickness.

When the skeleton was filled with Nujol the optical properties were nearly identical with those of the original film. Table VI gives the results of measurements of the oil-filled film. The refractive index of Nujol is 1.480 and of stearic acid is 1.51. The increase in the value of $N \cos r$ at $N = 134$ from 121.66 for the normal film to 121.89 for the oil-filled film is in accord with the lower mean value of refractive index.

During the process of building these films on glass a chromium slide was attached to the back of the glass slide. The films on the chromium were also skeletonized by being soaked for 1 min. in benzene. The colors of the steps were then compared with a standard color-scale made of normal films built on chromium in 18-layer intervals. The skeleton and the standard were viewed by the R_r ray of white light at $i = 80°$. The steps which matched most nearly in color

are listed in Table VII. Eq. (40) was applied to these data with the assumption that N_0 for skeleton films on chromium was the same as for normal films. The value of n_W which was required to satisfy Eq. (40) when $N/N_W=0.7510$ and $i=80°$ was $n_W=1.295$. Thus the method of building films simultaneously on glass and chromium affords a useful means of making two independent determinations of n_W which cover a range of i from 14° to 80°.

After the data given in Tables VI and VII were obtained, films were built on seven microscope slides, each film having steps of 333, 343, 353 layers. All were soaked in benzene for 1 min. Measurement of the angles i at which these films reflected the minimum $m=7$ gave the result $n_W=1.32$. It frequently happens that after a water solution has stood in a trough for several hours the values of n_W which are then obtained are slightly higher than the initial values. This is probably due to a gradual accumulation in the solution of substances dissolved from the trough or taken up from the air.

The slides were stacked in a pile and the birefringence of the total of the seven films was measured by means of a quartz wedge compensator using transmitted light. The relative phase retardation of the R_s and R_p rays corresponded to $\lambda/4$ for sodium light at $i=48°$ and $\lambda/3$ at $i=54°$. The total thickness Nt_W of the 2471 layers was 59,800A, taking $t_W=24.2$A. Therefore the factor $5752t$ in Eq. (28) was replaced by 59,800. For $\Delta l=1473$A at $i=48°$ it was found that when $n_1=1.32$ the value of n_3 which gave terms which satisfied Eq. (28) was $n_3=1.390$. For $\Delta l=1964$A at $i=54°$ the calculated value was $n_3=1.391$.

A measurement of Brewster's angle made after these films were built gave the result $i_B=51°\,17'$. Substituting $i_B=51°\,17'$ and $n=1.32$ in Eq. (34) we obtain $n_3=1.383$. The refractive indices of the normal films built at pH$=7.0$ were $n_1=1.491$, $n_3=1.551$ from Eqs. (12) and (25). The skeleton films having $n_1=1.32$ and $n_3=1.390$ or 1.383 have therefore approximately the same value of n_3-n_1 as the normal films.

JUNE 1, 1937 PHYSICAL REVIEW VOLUME 51

Properties of the Surface Magnetization in Ferromagnetic Crystals

W. C. ELMORE
Massachusetts Institute of Technology, Cambridge, Massachusetts
(Received March 22, 1937)

The magnetic powder patterns found on polished iron crystals (which may contain a few percent of silicon) have been studied more carefully by using a macroscopic model and by investigating the forces on the powder particles. Reasons are given for preferring one of two simple models to explain the patterns; some interesting implications of the proposed model are then considered. Experiments are described which indicate that the structures under discussion originate during the polishing operation, but that other than magnetic causes must be responsible for the remarkable regularity of the patterns.

A SMALL magnetic field applied normal to the *polished* surface of a silicon-iron single crystal will cause magnetic powder in a colloid suspension placed on it to collect into regular patterns related to the crystal symmetry. To explain these patterns, which resemble mazes with paths about 4 microns wide on a (100) surface but consist of lines parallel to a [110] axis on a $(1\bar{1}0)$ surface, McKeehan and Elmore[1] assumed the surface to contain blocks about 2 microns on a side spontaneously magnetized along <100> or <110> axes in the surface, with opposing magnetizations at about one-half

[1] L. W. McKeehan and W. C. Elmore Phys. Rev. **46**, 226 (1934) W. C. Elmore and L. W. McKeehan, Trans. A. I. M. E. **120**, 236 (1936).

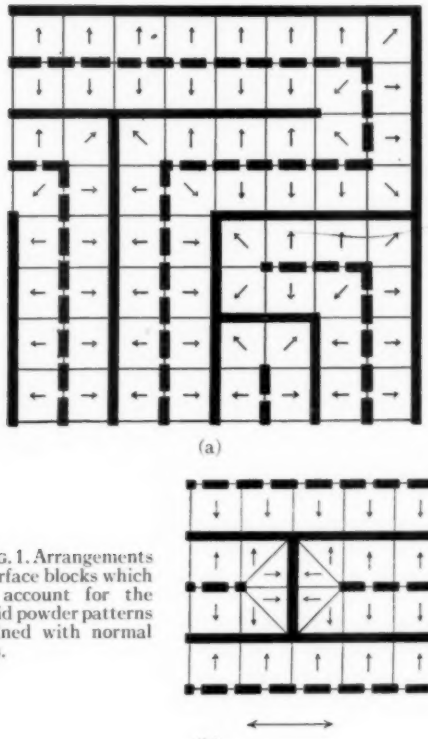

FIG. 1. Arrangements of surface blocks which will account for the colloid powder patterns obtained with normal fields.

of the block boundaries. The blocks with diagonal magnetizations were considered necessary to account for corners and for the abrupt endings of some of the maze pattern lines, illustrated in Fig. 1a. In this diagram, which shows a typical proposed arrangement of the block magnetizations, the heavy solid lines represent the colloid pattern which would be found upon applying a magnetic field normal to the specimen and directed outward. Upon reversing this field the colloid would migrate from the solid lines to the heavy broken lines. This change in pattern constitutes the shifting effect. It was also reported that a no-field pattern, less distinct than these patterns, appeared to be a *superposition of them*, that is, a double pattern of lines occurring at all of the block boundaries separating opposing magnetizations. Very careful observation under higher magnification (1500×) has since revealed that the no-field pattern lines always occur *halfway between those of the superposed double pattern*. Realization of this fact has led to a more careful analysis of the patterns, and to the construction of a macroscopic model. It is proposed to discuss this model, its connection with the iron patterns, and some interesting properties of the magnetic structure which seems best suited to account for the patterns. Brief mention will be made of a few points of experimental technique.

THE MACROSCOPIC MODEL

The model consisted of 100 one-half inch cubes of hardened steel packed together in square array. Each cube was permanently magnetized in one direction and various characteristic patterns simulated by suitably arranging the cubes. Exploration with iron filings of the field surrounding individual cubes indicated a satisfactory uniformity of magnetization. Fig. 2a shows a composite photograph of the simplest parallel line patterns for no field and for small normal fields of both signs. For this pattern the blocks were magnetized parallel to edges and arranged in rows which had the same polarity on adjacent faces. The no-field distribution of powder is seen to occur in lines along the middle of the blocks in the same position with respect to the field-selected lines as observed under high magnification for the colloid distributions.

That the no-field pattern does not occur at the block boundaries at first seemed puzzling, for intuition, confirmed by mathematical analysis of the field above the blocks (by the method of conformal mapping using the complex transformation $x+iy=-(id/\pi)\ \ln\ \mathrm{sn}(U+iV)$),[2] indicated that the force on a single powder dipole, $\mathbf{F}=\mathbf{M}\cdot\nabla\mathbf{H}=M(H)\mathbf{H}\nabla\cdot\mathbf{H}=\frac{1}{2}M(H)\nabla H^2$, would move it to the nearest block boundary. It is now realized that this discrepancy chiefly comes from neglecting the mutual magnetic interaction of large numbers of the powder particles. The following consideration will reveal the important part played by this interaction when there is no normal applied field.

Regardless of the actual distribution of surface magnetization responsible for the parallel line pattern, as long as it is periodic, the local field above the specimen can be derived from the

[2] J. J. Thomson, *Recent Researches in Electricity and Magnetism* (Oxford, 1893), p. 239.

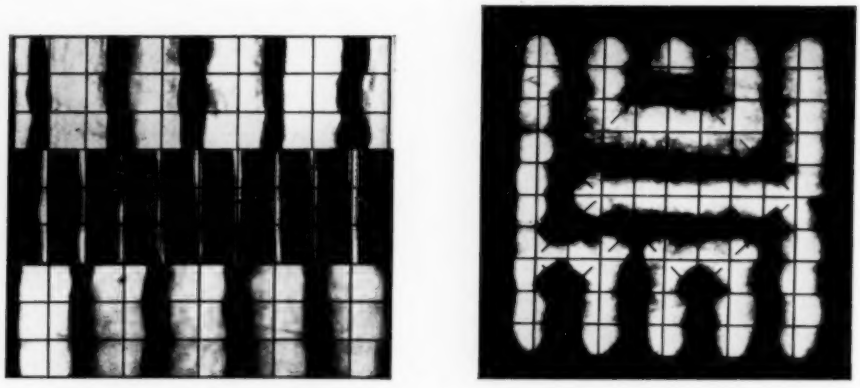

(a) (b)

FIG. 2. Patterns obtained with the steel cube model. (a) shows the no-field and the two normal field patterns of parallel lines; (b) shows a typical maze pattern obtained when diagonally magnetized blocks are used.

potential

$$V=\Sigma A_n e^{(-\pi n y)/d}\cos(\pi n x/d)$$
(summed with $n=1, 3, 5, \cdots$),

where x and y are distances measured in and normal to the surface, respectively; $2d$ is the smallest distance in which the surface distribution of magnetization does not repeat itself; the A_n are constants depending only upon the model of surface magnetization assumed, and, in general, decreasing with increasing n. For $y>0$ this series converges very rapidly, in fact the first term is a good approximation when $y \doteqdot d/2$. Consequently, the vector $\nabla H^2=\nabla\{(\partial V/\partial x)^2+(\partial V/\partial y)^2\}$ in the expression for $\mathbf{F}$, the force on a dipole, is nearly independent of x, that is, $\mathbf{F}$ is everywhere directed towards the surface. With the same approximation, however, the dipoles will make angles with the x axis given by $\theta=(\pi/d)(x+d/2)$. Fig. 3 shows schematically a cross section of the surface and the oriented particle dipoles. The layer L (drawn to be about 0.5 micron thick) represents a protective film of lacquer and a possible surface layer of the metal, damaged to such an extent by polishing that it does not take an active part in the production of surface stray fields. It is obvious from a simple consideration of energy that this arrangement of particles is not the most stable one. If the particles avoid positions near $x=0, \pm d, \pm 2d, \cdots$ and concentrate near $x=\pm d/2, \pm 3d/2, \cdots$ their mutual potential energy will be less, with little or no increase in their potential energy with respect to the local field. Accordingly, it is this latter arrangement which should be found, a result which does not depend upon a particular model of surface magnetization.

If a uniform magnetic field $\pm H_N$ normal to the surface is superposed on the unchanged local field H derived from V, then $\nabla H^2=\nabla\{(\partial V/\partial x)^2+(\partial V/\partial y)^2\}\pm 2H_N\nabla(\partial V/\partial y)$ in which the second term will correctly explain the shifting effect. It gives lines at $x=0, \pm 2d, \pm 4d, \cdots$ or at $x=\pm d, \pm 3d, \cdots$ depending on the sign of H_N. The mutual particle interaction, so important for the no-field pattern, simply tends to broaden these bands without affecting their mean position.

The above analysis shows, in addition, that there are many possible periodic magnetic structures which might account for the patterns.

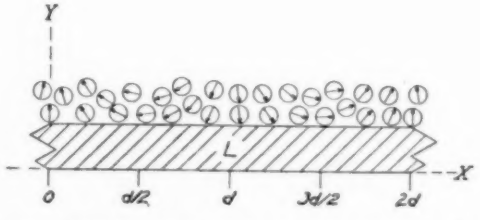

FIG. 3. Distribution of powder dipoles above the surface when mutual dipole interaction is neglected. An arbitrary periodic arrangement of surface magnetization is assumed.

Another *simple* structure is one in which blocks are magnetized normal to, rather than parallel to, the surface. Müller and Steinberg[3] proposed a somewhat similar model of layer magnetization for magnetite. Experiments with the macroscopic model have indeed shown that patterns similar to the three colloid patterns can so be obtained. The blocks were lined up with magnetization outward along the lines of one of the denser maze patterns, and inward along the lines of the corresponding reciprocal maze. The block boundaries then coincided with the less distinct no-field pattern. There are a number of reasons, however, for preferring the first model, in addition to some reasons to be discussed later in connection with diagonal magnetization. (1) The first model permits a qualitative interpretation of the effect on the patterns of preferential polish and of previous magnetic saturation. (2) The second model would seem to imply the frequent occurrence of patterns resembling a checkerboard. (3) The no-field patterns on iron have been compared with those on the basal plane of cobalt. The local stray fields of the latter crystal were found to be much greater than those of iron. Since the hexagonal axis in cobalt is the only direction of easy magnetization, it seems likely that the local magnetization must here be perpendicular to the basal plane. Consequently, the comparison of the stray fields favors the first model for iron. (4) Perhaps the best argument for the first model is the fact that only parallel line patterns are found on a polished (110) face with lines in the direction of traces of (001) planes. If the block magnetization were normal to the (110) surface or pointing out at an angle of 45°, there is no apparent reason why maze patterns should not be found. The first model can account for the (110) patterns very simply by employing block magnetizations in the surface parallel to the [001] axis. (5) Finally, the surface can have a small net residual magnetization parallel to itself if the surface magnetization resembles that of the first model.

An attempt has been made with the steel cube model to obtain ells, tees and other details of a maze pattern by using only blocks magnetized parallel to an edge and arranged in accordance with the first model. Additional short segments of powder and also gaps in the pattern lines appeared in a manner that has never been observed in hundreds of colloid patterns. When blocks more or less uniformly magnetized parallel to a diagonal were placed at appropriate positions in the model, the patterns were very similar to the colloid maze patterns, as may be judged from the photograph, Fig. 2b. The postulation of *uniformly* magnetized diagonal blocks, however, is open to question. It is well known that in iron axes of form <100> are directions of easiest magnetization; other directions in the crystal require more energy for magnetic saturation. Hence, instead of having the diagonal block uniformly magnetized, it seems better to have its magnetization divided between two <100> directions by a diagonal plane, as, for instance, in Fig. 1b. It would be difficult to decide between the two types of diagonal block by use of the macroscopic model; in what follows the second one will be assumed.

Some Properties of the Proposed Model

The model which is being proposed to account for the patterns on polished iron possesses a number of interesting properties. If patterns on paper are constructed by placing arrows indicating directions of magnetization in a network of squares, it is found that the arrows in the diagonal blocks must form continuous chains with pairs of arrows pointing to and from common corners (see Fig. 1a). The pattern lines change to their other possible direction as they pass such a chain. Accordingly, these chains of arrows (or the diagonal block divisions) divide the surface into a number of regions differing in the prevailing direction of magnetization. It is clear that the chains (or *diagonal lines*, as they will be called hereafter) must start at the edge of the pattern or close on themselves. Furthermore, they may be locally modified without changing the pattern other than locally. Geometrically, the diagonal lines completely determine the pattern.

Further analysis reveals that consecutive diagonal lines cutting any line in the surface cannot be chosen arbitrarily. The details of permitted choices, which depend essentially upon dividing diagonal lines into four classes and

[3] N. Müller and D. Steinberg, Tech. Phys. U. S. S. R. **1**, 205 (1934).

establishing a cyclic order for these classes, are easily worked out. Once the class of such a line is determined, its exact course is arbitrary with the exception that two diagonal lines cannot, in general, cross one another. The positions of the lines, however, determine the amount and direction of a small residual magnetization associated with the pattern. This remanence for any given pattern is easily computed.

The relation of magnetostriction to the patterns leads to an interesting speculation. The magneto-mechanical properties of iron crystals are well known and have been correlated by a formal theory.[4] For instance, an iron crystal magnetized along an axis of form <100> increases its length in that direction, and, conversely, the crystal can be magnetized most easily along a <100> axis which is, at the same time, the direction of an applied tension. If the tension is replaced by compression, then the other two axes of form <100> become directions of easiest magnetization. Since magnetostriction is essentially related to the spontaneous magnetization of the ferromagnetic, it is correct to apply these results to the magnetization of the blocks. Hence it is realized that the diagonal lines have more than a geometrical significance: they represent boundaries in the surface between regions in which the magnetostrictive strain axes, always lying in the surface, differ in direction by a right angle.

From the converse point of view it can be argued that, during the polishing operation, the surface is stretched or compressed in various places in a more or less random fashion. These regions of positive and negative strain must be distributed so that the distortion of the surface as a whole is small. From the brief discussion of the magneto-mechanical interaction it is clear that the resulting regional stresses must tend to control the direction (not the sense) of the local magnetization. If the proposed model is correct, the diagonal lines must be the approximate boundaries between these regions. To summarize, the magnetization of the blocks will arrange itself not only to produce a nearly complete demagnetization of the surface of the crystal, but in addition to decrease the magnitude of the stresses set up in the surface by the polishing operation. The diagonal lines have been drawn on several photomicrographs of which Fig. 4 is typical. One set of regions marked out by the lines has been shaded. The direction of magnetization in the shaded and in the unshaded parts differs by a right angle.

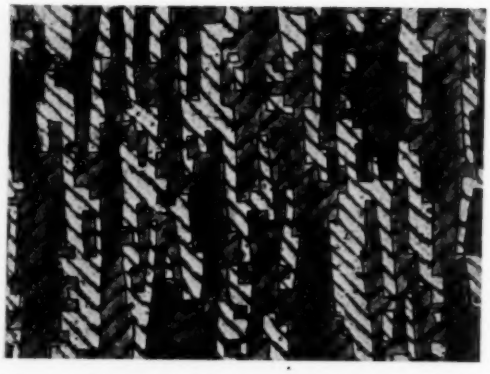

FIG. 4. A maze pattern in which the diagonal lines discussed in the text have been drawn. The direction of magnetization in the shaded parts is perpendicular to that in the unshaded parts.

The diagonal lines have further use in the interpretation of local pattern changes which occur upon the application and removal of a field parallel to the surface. These changes have already been sufficiently described[1] although they require subjective observation for a full appreciation. (Plans are under way to take motion pictures of these and other changes in pattern.) The local pattern changes were shown to be consistent with the view that the blocks retain their identity, with only their direction of magnetization changing. Such changes involve local modification of a diagonal line, in fact it can be considered that they consist of the motion of this line from one stable position to another. Only rotations of the net block magnetizations through angles of 45° would then be involved and the diagonal line boundary itself would progress by rotation of electron spins through angles of 90°. The following local pattern change which was observed on one specimen of silicon-iron is simple enough to be described in words. The cross bar of an "*H*" occurring in a maze pattern was found to be quite unstable with respect to the variation of a field applied parallel to the surface and to the sides of the "*H*."

[4] E. C. Stoner, *Magnetism and Matter*. (Methuen & Co., London, 1934), p. 395.

By slightly increasing and then decreasing the field, which was not very uniform, the cross bar could be made to run back and forth along the sides of the "*H*." The neighboring pattern showed no changes unless the field was considerably increased. Fig. 1b shows the arrangement of magnetization which will account for the pattern; the two-headed arrow indicates the motion of the cross bar.

Nature of the Block Structure

The analysis of the maze patterns presented so far has been based on the assumption of unit blocks, uniformly magnetized, uniform in size and geometrically fixed in the surface. The character of this structure requires further elucidation.

At first it was thought that the structure extended throughout the crystal in a manner suggesting Zwicky's regular secondary structure,[5] and not depending upon the presence of a polished surface layer. This conclusion was drawn chiefly from a study of patterns found on various cuts of the same crystal. It is now recognized that polishing plays an all-important role, and that the position of the block boundaries, as far as the patterns are concerned, is fixed during the polishing operation, but probably not by causes deriving from magnetism.

The evidence is fairly conclusive. Patterns formed on a very smooth unpolished strip of silicon-iron, as well as on unpolished pieces of Cioffi iron,[6] did not resemble the maze patterns under discussion. They resembled, rather, the more widely spaced parallel line patterns discovered by Bitter.[7] An entire set of these lines could be made to move continuously across the microscope field by changing the applied magnetic field which, for the effect, had a component parallel to the surface and perpendicular to the lines. No sign of the maze patterns could be found. The behavior of the colloid while the applied normal field was increasing from zero to a small value suggested that, if such a structure be present, it is too fine for resolution. Detailed study of the Bitter lines has been retarded by the difficulty of obtaining mirror-like surfaces suitable for high power microscopic examination, without recourse to mechanical polishing. This difficulty has been very recently met by extending to iron the Jacquet electrolytic method of polishing.[8] A specimen of silicon-iron polished by this method, which yields unstrained surfaces of extreme local smoothness, gave only the Bitter parallel line pattern. It is expected to continue the study of these patterns and their relation, if any, to the finer scaled maze patterns.

Further evidence about the maze patterns was obtained by making a broad shallow scratch on the Cioffi specimen. Colloid deposited by normal field formed a portion of a perfect maze on the scratched region, whereas the neighboring undamaged surface contained only a broadly spaced parallel line pattern, very sensitive to changes in magnetic field. In another experiment a piece of silicon-iron strip magnetized practically to saturation by a small Alnico horseshoe magnet was subjected to the customary metallurgical polishing. Upon removing the magnet and applying a normal field, the usual maze pattern was found. This experiment shows that magnetostrictive strains in undamaged demagnetized crystals probably do not play an important part in the origin of the maze structure during the cold working of the surface. To account for the regularity of the magnetic structure produced by polishing, it seems necessary to suppose that cold working of the surface merely serves to enhance some sort of nonmagnetic structure already present in the crystal, perhaps by the formation of block crystal fragments.

Electron diffraction[9] indicates that a polished surface consists of, first, an amorphous or microcrystalline layer 30 or 40A thick (the Beilby layer); next, a relatively thicker layer of larger crystal fragments; finally the parent crystals. A recent optical investigation of copper, polished mechanically and then electrolytically,[10] indicates that polishing cold work extends to a depth of 13 microns or more. Since silicon-iron is

[5] F. Zwicky, Phys. Rev. **43**, 270 (1933).
[6] P. P. Cioffi, Nature **126**, 200 (1930). The specimens used were kindly furnished by Mr. P. P. Cioffi and Dr. R. M. Bozorth of the Bell Telephone Laboratories, New York.
[7] F. Bitter, Phys. Rev. **38**, 1903 (1931); **41**, 507 (1932).
[8] P. Jacquet, Comptes rendus **201**, 1473 (1935); **202**, 403 (1936).
[9] For a general discussion see Trans. Faraday Soc. **31**, 1043 (1935).
[10] H. Lowery, H. Wilkinson and D. L. Smare, Phil. Mag. [7] **22**, 796 (1936).

harder than copper, it is likely that the depth of the damage in the former is more nearly comparable with the size of the magnetic blocks. With the addition of a block regularity to the crystal fragments underneath the Beilby layer, the present picture of a polished iron surface is consistent with these views. The aim of speculation and future experiment must be to account for the regularity in the cold worked crystal.

Before the part that polishing plays was realized, it was suggested that the magnetic structural regularity and stability might be due to the segregation of foreign atoms in the necessary planes. Such a segregation seems now to be a reasonable, if not the only, pre-polishing structure (assuming that such a structure is really necessary) which could lead to a regular fragmented block structure through cold working. If it be supposed that at high temperatures the foreign atoms are uniformly distributed in solid solution but that at lower temperatures they are most stably located as a two-dimensional array in <100> planes (rather than forming three-dimensional particles) the very regular distribution called for may represent an attained equilibrium. Only 0.02 atomic percent of impurity would be required to populate single planes at the observed intervals.

Notes on Technique

Colloid similar to that used to form patterns in this and in previous investigations may be prepared quite simply. The author is greatly indebted to Dr. O. Baudisch[11] for the following formula:

100 grams gamma Fe_2O_3, or siderac
200 grams white Schering-Kahlbaum dextrin (puriss)
0.66 grams HCl
1 liter distilled water.

These constituents are to be run through a colloid mill until the siderac is in a colloid state. If the colloid is to be kept for some time it will be found necessary to add a small amount of preservative to prevent bacterial action.

An improvement in the technique of producing patterns consists in coating the clean surface of the specimen with a thin layer of water-proof lacquer. For this purpose a small amount of lacquer dissolved in amyl acetate may be brushed on the surface which is then held in an air blast. The resulting film, thin enough to show interference colors, will prevent the colloid from sticking to the metal and will also protect the specimen from rusting. The sticking of the colloid, formerly prevented by a thin grease film, is no doubt due to the electrical discharge of the colloid particles by the metal surface. The layer of lacquer does not interfere with the formation of patterns.

In conclusion the author wishes to thank Professor F. Bitter and the Department of Mining and Metallurgy for placing at his disposal certain facilities for conducting the experimental part of this work. He is greatly indebted to Professor Bitter and to Professor L. W. McKeehan of Yale for discussing many of the ideas which have been presented. The colloidal siderac used in recent experiments was kindly furnished by Sharp and Dohme of Philadelphia.

[11] Director of Research, Saratoga Springs Authority. For a discussion of magnetic and other properties of iron oxides, see L. Welo and O. Baudisch, Chem. Rev. **15**, 45 (1934).

LETTERS TO THE EDITOR

Prompt publication of brief reports of important discoveries in physics may be secured by addressing them to this department. Closing dates for this department are, for the first issue of the month, the eighteenth of the preceding month, for the second issue, the third of the month. Because of the late closing dates for the section no proof can be shown to authors. The Board of Editors does not hold itself responsible for the opinions expressed by the correspondents.

Communications should not in general exceed 600 words in length.

Thermionic Emission into Dielectric Liquids

In a recent letter to the editor of *Physical Review* K. H. Reiss[1] has stated his belief that the "potential dissociation effect," rather than thermionic emission is the proper explanation of the authors' data,[2] as well as previous data obtained by Nikuradse,[3] which were used by Reiss[4] in support of the potential dissociation theory of conduction in pure liquids.

The two theories give identical current field strength relations with the exception of the manner in which the dielectric constant D appears. Thus:

(1) Reiss $I = I_0 \exp [\epsilon^{\frac{1}{2}} F^{\frac{1}{2}}/KTD^{\frac{1}{2}}]$.
(2) Baker and Boltz $I = I_0 \exp [\epsilon^{\frac{1}{2}} F^{\frac{1}{2}} D^{\frac{1}{2}}/KT]$.

The slope of the straight line $\log_{10} I$ *vs.* $F^{\frac{1}{2}}$ is *less* than the Schottky slope for a vacuum $\epsilon^{\frac{1}{2}}/2.3KT$ for formula (1) and *greater* for formula (2).

We wish to point out that the "theoretical" slopes in Reiss' paper[4] were *incorrectly calculated* and that the agreement with experiment which he obtained is *entirely spurious*. This may be seen from Table I. It will be observed that in each case the experimental slopes are *greater* than the Schottky slope for a vacuum and thus cannot possibly be explained by formula (1). In the case of the practically nonpolar liquids, hexane and toluene, the experimental slope is greater even than that given by our formula (2), which we interpret to mean the existence of sharp points on the cathode surfaces. In the case of polar chlorbenzene the lower value is to be interpreted as resulting from the smaller effective dielectric constant caused by dielectric saturation at high field strengths.

These data of Nikuradse were selected from others having lower slopes, according to Reiss.[4] We submit that no data for which this variation of slope is not understood nor under control can be safely used to check either formula.

TABLE I. *Slopes of the line* $\log_{10} I/I_0 = K\sqrt{F}$ *with* F *in volts/cm and* $T = 300°K$. *Here* $K_{vac} = \epsilon^{\frac{1}{2}}/2.3KT = 1.91/T = 0.00637$.

Liquid	Hexane	Toluene	Chlorbenzene
Dielectric constant D I. C. T.	1.874	2.39	5.44
$K_E = K_{vac} \cdot 1/D^{\frac{1}{2}}$	0.00465	0.00412	0.00273
$K_{BB} = K_{vac} \cdot D^{\frac{1}{2}}$	0.00872	0.00985	0.01486
Experimental slope of Nikuradse obtained from Fig. 2 of Reiss' paper, reference 4.	0.0177	0.0146	0.0078

Therefore even the qualitative variation of slope with D may not be determined from data selected *arbitrarily*. The authors, however, had a controllable and naturally explained basis of selection, and obtained exact quantitative agreement with formula (2) for toluene.

We realize the desirability of obtaining data for other pure liquids than toluene and intend to do this in future work. The case does not rest on this point, however, since the potential dissociation theory is unable to explain many other facts, such as the very great dependence of the current (and also the slope of $\log I$ *vs.* $F^{\frac{1}{2}}$) on the material and roughness of the cathode surface. As we have shown,[2] these may be varied in a known and reproducible manner to produce the results expected from the thermionic emission theory.

The potential dissociation theory has the unattractive feature of requiring the presence of ionizing impurities. We do not believe that sufficient impurities are present in a carefully purified liquid, at least one of low dielectric constant such as toluene, to produce this effect.

Reiss has also presented the argument that since theoretically one would expect a lowering of the work function in the presence of a dielectric liquid, and since his measurements[5] of the photoelectric cut-off with and without liquid are almost identical (and therefore, he concludes, there is no lowering of the work function), there can be no thermionic emission at room temperature into a liquid.

The authors believe that all of the photoelectric current in the presence of a liquid will not be collected, particularly near cut-off, since the free path of an electron in the liquid is only one or two hundred angstroms. Electrons released by light of wave-length near the cut-off will not have sufficient kinetic energy to escape the surface fields *in spite of collisions*, unless the extracting field is sufficiently great to neutralize the surface fields at a distance from the surface approximating the free path. If such an extracting field is applied, however, thermally emitted electrons will also be collected. We therefore believe that it is not possible to measure the true photoelectric work function in the presence of a liquid; a value greater than the true value will be found.

EDWARD B. BAKER
HOWARD A. BOLTZ

Research Department,
The Detroit Edison Company,
Detroit, Michigan,
May 12, 1937.

[1] K. H. Reiss, Phys. Rev. **51**, 781 (1937).
[2] E. B. Baker and H. A. Boltz, Phys. Rev. **51**, 275 (1937).
[3] A. Nikuradse, Ann. d. Physik **13**, 851 (1932).
[4] K. H. Reiss, Zeits. f. physik. Chemie **178**, 37 (1936).
[5] K. H. Reiss, Ann. d. Physik **28**, 325 (1937).

The Structure of Hα of Hydrogen

The structure of the lines of the Balmer spectrum of hydrogen was a subject of investigation in this laboratory some years ago. Recently we have attacked the problem again, using two Lummer plates, not "crossed" as in the paper of Kent, Taylor and Pearson,* but dispersing in the same plane. With this arrangement, the microphotometer curves of the resultant pattern reveal clearly four distinct components of Hα with intensities and positions roughly as given by theory. There are no ghosts in the Lummer plates and the interference of lines of the secondary spectrum of hydrogen has been eliminated.

We are now engaged in obtaining quantitatively the intensity and position of these components.

We feel that this method (new, as far as we know) may be of service in the study of the hyperfine structure of the spectrum lines of other elements.

NORTON A. KENT
ROYAL M. FRYE
WILLIAM H. ROBINSON

Boston University,
Boston, Massachusetts,
April 30, 1937.

* Kent, Taylor, and Pearson, Phys. Rev. **30**, 266 (1927).

The Velocity of Radio Waves Over Long Distances

Last year a system was developed in this laboratory for measuring the speed of radio waves over short distances.[1] Lately the writers have devised a new method for measuring the velocity of radio waves over long distances, which is fairly accurate provided the base line is several hundred miles long. In the short distance tests (20 km) the velocity of the waves (2398 kc frequency) was found to vary from 50 to 85 percent of the velocity of electromagnetic waves in a vacuum. It was desirable to make tests at greater distances than those used at first; but the difficulty involved in maintaining a fixed reference time at two widely separated locations was very great.

In overcoming the timing difficulty the new system makes it possible to record all measurements of velocity at the original transmitting station. Briefly the system involves a station B which is rebroadcasting the timing impulses sent from another station A so as to enable them to make a round trip. The path will be from A to B and then from B to A. If there were no time lag in the rebroadcasting system at B, the velocity would be equal to twice the distance between stations A and B divided by the total elapsed time required for the signal to travel from A to B and back to A, as measured at A by the use of a cathode-ray oscillograph. If station B consists of a standard receiver and transmitter the time required for a signal to pass through this station and be rebroadcast can easily be determined by the use of an oscillograph and a pulsating timing signal. The velocity corrected for rebroadcasting lag will then be the total distance traveled divided by the difference between the total elapsed time and the rebroadcasting time.

If stations A and B are less than 1500 miles apart the height of the ionospheric propagation path will have to be considered in calculating the distance traveled. At greater distances the error involved will not be of sufficient magnitude to influence the results. The rebroadcasting lag can also be neglected in most cases in a qualitative test if the total path is more than 2000 miles. The lag in a common type of communications receiver and low power transmitter was found to be 0.0011 second. Most similar systems should then have lags of from 0.0005 to 0.002 second.

On March 18, 1937 the first satisfactory experimental run was completed by using a pulse transmitter at West Virginia University (Morgantown, W. Va.) as the master station (A) and the station of Mr. J. R. Bouknight of Columbia, S. C., for the rebroadcasting station (B). Station A operated on a frequency of 14,160 kc while station B returned the signals on 14,186 kc. This test was made at 1:15 P.M. local time over a north and south path. The return signal was broken into two or more parts indicating return from both the E and F regions. Assuming the first return signal to come from the E region at a height of 100 km, the velocity calculated for this test was 165,500 km/sec., or 55.2 percent of the velocity of waves in vacuum. A second test on March 20, 1937 during severely fluctuating radio conditions gave velocities from 181,000 km/sec. to 235,500 km/sec. assuming E region transmission in all cases; this wide variation is possibly due to changing penetration in different ionospheric regions. The third run was made on March 23, 1937 and showed a velocity of 152,500 km/sec. for the E region path. Corrections for receiver and transmitter lag were made in these measurements and the accuracy may be taken as better than five percent. While these tests were conducted with an amateur station rebroadcasting the signals, later work will probably be performed by the use of two experimental stations.

The authors wish to thank Mr. J. R. Bouknight for his cooperation and the use of his station in returning the signals.

R. C. COLWELL
A. W. FRIEND

Department of Physics,
West Virginia University,
Morgantown, West Virginia,
May 6, 1937.

[1] Colwell, Friend, Hall and Hill, Phys. Rev. **50**, 4, 381 (1936); Colwell, Hall and Hill, J. Frank. Inst. **222**, 5, 551 (1936).

Additional Interaction of Protons with an Electromagnetic Field, Due to the Presence of the Electron–Neutrino Field

The electron–neutrino (e–n) field theory predicts that a proton (P), has a certain probability to dissolve into a neutron (N), positron (e^+), and neutrino (n^+).[1] Suppose this occurs in an external electromagnetic (e–m) field; then the P is dissolved a certain fraction of each second, (equal to T), and the interaction of the e–m field with the e^+, ($H_{e^+,\,e-m}$), changes the latter's state, and thus upon its subsequent absorption, the state of the P is changed as well. This change of state may be described by assigning to the P, an interaction with the e–m field, ($H'_{P,\,e-m}$), in addition to that given by the Dirac equation ($H_{P,\,e-m}$).

Thus we may expect the P to have an additional magnetic moment, (μ'_P), additional forces between P's and external electrons $(H'_{P,\ldots})$, additional Compton scattering, (σ'_C), radiative losses, (σ'_r), etc. Since the e–n field theory is symmetrical between the P and N, $H'_{P,\ e-m}$ is equal in magnitude, and opposite in sign to the total interaction of the N with the e–m field $(H'_{N,\ e-m})$.

The process, $P \rightarrow N+e^++\nu^+$, can be described theoretically, if an interaction, $H_{P,N,e,\nu}$, be introduced between the quantized wave fields which represent the particles. $H_{P,N,e,\nu}$ depends, in general, on the field scalars, Ψ, Φ, ψ, φ and their derivatives with respect to space and time coordinates.[2]

A serious objection to the introduction of derivatives into $H_{P,N,e,\nu}$ has been advanced by Fierz.[3] If $H_{P,N,e,\nu}$ depends on higher derivatives than the first of ψ, φ so will the wave equation for ψ, φ. Thus to specify ψ at time t, the essentially unspecifiable quantities, $(\partial^2\psi/\partial t^2)$, $\cdots$ $(\partial^k\psi/\partial t^k)$ must be given initially. Alternatively, the existence, of k time derivatives in the wave equation for ψ, implies the k-tuple multiplicity of every eigenfrequency of the ψ field, the ψ field thus possessing k different infinite sequences of states of excitation, and hence representing k different types of particles. In all calculations, including ours, $k-1$ of these types are unjustifiably ignored.

However, if several derivatives of ψ, φ do not appear in $H_{P,N,e,\nu}$ the e–n theory (with the magnitude of $H_{P,N,e,\nu}$ determined by mean lines of β-emitters), cannot account for the magnitude of the proton-neutron interaction, $(V_{NP}(r))$, and of μ'_P. Derivatives in $H_{P,N,e,\nu}$ permit the explanation of the magnitude and range of $V_{NP}(r)$[4] and of the magnitude and sign of μ'_P,[5] though the theory still does not imply a necessary connection between these quantities.

Using derivatives in $H_{P,N,e,\nu}$, we obtain the general result: $H'_{P,\ e-m}=T\{(H_{e^+,\ e-m})_{\text{average}}-H_{P,\ e-m}\}$, the average being taken over all states of the dissolved e^+. To fix $H_{P,N,e,\nu}$ assume for the moment, no derivatives. Then the most general relativistic invariant for $H_{P,N,e,\nu}$ is:[6]

$$G\int \sum_{j=1}^{j=5} C_j(\Phi^+A_j\Psi)(\varphi^+A_j\psi)d\tau$$

with $A_1=1$, $A_2=\gamma^l$, $A_3=\gamma^l\gamma^m$, $A_4=\gamma^l\gamma^m\gamma^n$, $A_5=\gamma^1\gamma^2\gamma^3\gamma^4$. The choice of the C_j determines the exchange character of $V_{NP}(r)$, and by a proper choice of the C_j one can obtain:[7]

$$V_{NP}(r)=f(r)P_H, \quad \text{or} \quad V_{NP}(r)=f(r)P_M,$$

or

$$V_{NP}(r)=f(r)\{(1-g)P_M+gP_H\}.$$

Upon introducing derivatives into $H_{P,N,e,\nu}$, we may arbitrarily restrict ourselves to the same five types of invariants, by imposing the limitation that $(\Phi^+\Psi)(\varphi^+\psi)$ be replaced by a scalar formed out of the derivatives. From our formula for $H'_{P,\ e-m}$, we have:[8]

$$\mu'_P \leqq T\left\{\frac{M}{m}\frac{(L_{Ns}+2S_{Ns})}{(p_{Ns}^2+1)^{\frac{1}{2}}}-1\right\} \text{ nucl. magn.}^9$$

$$\leqq \frac{T}{p_{Ns}}\frac{M}{m}(L_{Ns}+2S_{Ns})\text{n.m.},$$

the average magnetic moment of the dissolved e^+, being $(L_{Ns}+2S_{Ns})/(p_{Ns}^2+1)^{\frac{1}{2}}$ Bohr magn.[10] Now, $T \leqq$ ratio of mean lives of dissolved e^+ and P, $\leqq$ inverse ratio of corresponding energy uncertainties[11]

$$\leqq \frac{V_{NP}(0)}{p_{Ns}} \leqq V_{NP}(0)R_{NP}; \qquad \frac{T}{p_{Ns}}\frac{M}{m} \leqq V_{NP}(0)R_{NP}^2\frac{M}{m} \leqq 1,$$

from the relation between $V_{NP}(0)$ and R_{NP} demanded by a stable deuteron:[12] $(L_{Ns}+2S_{Ns}) \leqq (R_{NP}p_{Ns}+1) \leqq 2$. Hence, $\mu_P' \leqq 2$. Thus, if the e–n theory gives $V_{NP}(0)R_{NP}^2$ correctly, then it automatically predicts a μ'_P which is a pure number, independent of $V_{NP}(0)$, R_{NP}, i.e. of G and the number of derivatives, and, which is of the proper order of magnitude. The exact calculation gives

$$\mu'_P \leqq \frac{T}{p_{Ns}}\frac{M}{m}2\{C_2^2+C_4^2+C_1C_3+C_3C_4\}\text{n.m.}$$

$$\leqq 2\{C_2^2+C_4^2+C_1C_3+C_2C_4\}\text{n.m.}$$

and from the conditions on the C_j in reference 8, we see that, if $V_{NP}(r)=f(r)P_H$, $\mu'_P=0$, while if $V_{NP}(r)=f(r)P_M$, or $f(r)\{(1-g)P_M+gP_H\}$, then μ_P' may have any *positive* value from 0 to about 2 n.m. Also μ'_N is exactly $-\mu'_P$.

By quantizing the e–n field, as well, we obtain σ_C' and σ'_r. As might be expected, σ'_C and σ'_r are just due to μ'_P, and are thus of the same order of magnitude as the Compton and radiative cross sections due to the ordinary magnetic moment of the P.

Similarly we found $H'_{P,\ e^-}$, which consists of two parts, the first that due to μ'_P, the second an additional retarded interaction, $\leqq T\{(H^{\text{retarded}}{}_{e^+,\ e^-})-H^{\text{retarded}}{}_{P,\ e^-}\} \leqq H^{\text{retarded}}{}_{P,\ e^-}$[13] $\leqq$ energy of separation of hyperfine hydrogen levels, which depends only on the distance between the particles and the radial velocity of the electron.

H. PRIMAKOFF

New York University,
University Heights,
New York, N. Y.,
April 28, 1937.

[1] Fermi, Zeits. f. Physik **88**, 161 (1934).
[2] The notation and the units of length, mass, energy, used here, are the same as in Johnson and Primakoff, Phys. Rev. **51**, 612 (1937).
[3] Fierz, Helv. Phys. Acta, **10**, 2 (1937).
[4] Cf. Johnson and Primakoff, reference 2, p. 615, footnote 4a.
[5] Cf. below; experimental values of magnitude and sign of μ'_P, are due to Rabi *et al.*, Phys. Rev. **50**, 396, 472 (1936).
[6] Bethe and Bacher, Rev. Mod. Phys. **8**, 82 (1936), §40; Fierz, Zeits. f. Physik **104**, 553 (1937); G, the Fermi constant $\leqq 10^{-13}$, and C_j are arbitrary real constants $\leqq 1$.
[7] For $V_{NP}(r)=f(r)P_H$, we must have, $C_3=C_4=0$; for $V_{NP}(r)=f(r)P_M$, $C_1^2+C_5^2=C_2^2+C_4^2=\frac{1}{4}$; for $V_{NP}(r)=f(r)\{(1-g)P_M+gP_H\}$, $C_2^2+C_4^2=\frac{1}{4}(1+g)$, $C_2^2+C_4^2=\frac{1}{4}(1-g)$.
P_M and P_H are the Majorana and Heisenberg exchange operators; $g \leqq 0.2$. The conditions which the C_j must satisfy to give forces of various exchange types differ from those found by Fierz, reference 7. The discrepancy is due to the fact that we make the theory give a finite $V_{NP}(r)$, by use of a converging factor (cf. reference 2), our conditions on the C_j being strictly valid only for $r=0$; i.e. $V_{NP}(r)=V_{NP}(0)$, while Fierz uses the character of the force at large distances. Since it is probable that nuclear binding energies are not altogether determined by $V_{NP}(0)$, our conditions on the C_j are not rigorous.
[8] μ'_P has been found without the use of derivatives in $H_{P,N,e,\nu}$ by Fierz, reference 7, and von Weizsäcker, Zeits. f. Physik **102**, 512 (1936). As far as the dependence on the C_j our result for μ'_P (cf. below) agrees with Fierz.
[9] L_{Ns}, S_{Ns}, p_{Ns}, are the average orbital angular momentum, spin angular momentum, and linear momentum of the e^+. Also $\Delta p\Delta q \leqq 1 \leqq p_{Ns}R_{NP}$, whence $p_{Ns} \leqq 200$; M/m is the mass of the P, in our units, M and m being the masses of the P and e^-, in c.g.s. units.
[10] Bethe and Bacher, reference 6, §45, erroneously give the magnetic moment of the e^+, as $\frac{1}{2}$ Bohr magn. and, hence find μ'_P too large.
[11] The self-energy of the P due to the $e-n$ field is $V_{NP}(0)$. cf. reference 2, Eqs. (3), (5), (6).
[12] Cf. reference 2, Eq. (9) or Bethe reference 7, Eq. (40).
[13] Lowen, Phys. Rev. **51**, 190 (1937).

On the Theory of Neutron Scattering by Magnetic Substances

In a note submitted for publication to the *Physical Review* we have suggested a new method for detecting magnetic scattering of neutrons which is based on a comparative study of paramagnetic substances with identical nuclei but varying magnetic moments. As a theoretical basis we used a letter by Bloch[1] who was the first to point out and quantitatively describe the magnetic scattering of neutrons. His results were later rederived in a quantum-theoretical treatment by Schwinger.[2]

Both authors have essentially treated the magnetic atom as an external field which is uninfluenced by the collision process. A complete quantum-mechanical treatment leads to the following results which for clarity, we state for different special cases.

(A) Unmagnetized paramagnetic bodies (with the magnetic ion in an S state)

The magnetic cross section is

$$\sigma=(8\pi e^4/3m^2c^4)\gamma_n^2 j(j+1). \quad (1)$$

Wherein γ_n denotes the magnetic moment of the neutron in nuclear Bohr magnetons and the other symbols are self-explanatory. The result is independent of the spin-state of the incident neutron beam. It raises all values of the magnetic cross sections given in our previous note in the ratio $(j+1)/j$.

(B) Ferromagnetic bodies

Here the result depends on the energetic possibility of the atomic moment changing direction during the course of the collision. If this possibility is excluded the old result is obtained. If on the other hand the energy difference between the magnetic sublevels is small the total magnetic cross section of an unpolarized beam becomes

$$\sigma=(\pi e^4/m^2c^4)\gamma_n^2 j\{(j+\tfrac{1}{2})(3-\cos^2\Theta)+1+\cos^2\Theta\}. \quad (2)$$

In (2) Θ denotes the angle between the direction of the incident neutrons and the direction of magnetization; it is assumed that the scattering body is magnetically saturated.

Comparison of (2) with the old result

$$\sigma=(\pi e^4/m^2c^4)\gamma_n^2 j^2(3-\cos^2\Theta) \quad (3)$$

indicates (for sufficiently large magnetic cross section) a simple method of experimentally determining whether or not these transitions take place. The ratio of the scattering cross sections for magnetization parallel and normal to the direction of incidence is for (3) 2/3 whereas according to (2) it is very nearly one if j is less than 3/2. These transitions would reduce all polarization effects by the increase of the total scattering cross section (incoherent with the nuclear scattering). They also lead to polarization effects because the neutrons with spins antiparallel to the spin of the atom will be scattered more frequently. Whether this increases or decreases the total polarization depends on the sign of the phase of the nuclear wave and the sign of the neutron's magnetic moment.

The magnitude of the polarization effects is further reduced by the inelastic collisions involving atomic transitions to neighboring spectroscopic levels, the presence of isotopes and the existence of spin-dependent nuclear forces. The magnetic cross section on the other hand, is increased by transitions of the atoms to neighboring energy states.

In the above considerations we have refrained from including form factors which can considerably influence the results, even for thermal neutrons, but which are taken into account in our detailed calculations.

O. HALPERN
M. H. JOHNSON, JR.

New York University,
University Heights,
May 13, 1937.

[1] F. Bloch, Phys. Rev. **50**, 259 (1936).
[2] J. Schwinger, Phys. Rev. **51**, 544 (1937). Bloch's formula seems to be distorted by misprint; we could not verify the interpretive correction given by Schwinger.

The Ionosphere and Magnetic Storms*

It has been recognized for many years that there was some relation between magnetic storms and poor radio transmission conditions at high frequencies. It was believed that disturbances of the ionosphere produced both the magnetic storms and poor radio transmission conditions. The ideas concerning this relation were somewhat nebulous because of a lack of specific information concerning either normal or abnormal conditions of the ionosphere.

In two previous Letters to the Editor[1, 2] we have described in detail many of the specific effects which we have observed to occur in the ionosphere during and following magnetic disturbances. Our observations and conclusions have been confirmed by many other observations at the National Bureau of Standards and by published data,[3–7] from distant parts of the earth which have led us to believe that these effects can be observed over most of the earth.

The observations indicate that the ionosphere disturbances associated with magnetic storms occur principally in the night F and daytime F_2 layers, and to a lesser degree in the daytime F_1 layer. No such disturbances have been observed in the E layer. The principal effects are a marked increase of virtual heights, decrease of ionization densities and increased diffusion of the night F and daytime F_2 layers, an increased separation of the F_1 and F_2 layers and a sharpening of the F_1 critical frequency. This indicates an expansion and diffusion of the F and F_2 layers such as might be produced by heating. The ionization density of the daytime F_1 layer is also decreased. These effects are regularly observed during the night of and the day following a severe magnetic disturbance recorded at the Cheltenham observatory. Another effect which has been observed is an increase of ionization density of the F_2 layer during the beginning of or preceding the magnetic storm.

Ionosphere disturbances associated with magnetic storms are especially pronounced during the transition periods of spring and fall, somewhat less pronounced during the summer and least pronounced during the winter at Washington.

From April 24 to May 5, 1937, there was a series of very severe magnetic storms, during which the phenomena described above occurred to a greater degree than hereto-

fore observed. During some of these days the ionization densities of the night F and daytime F_2 layers were reduced to as little as 25 percent of normal, the virtual heights doubled and the layers were highly diffused. The ionization density of the F_1 layer was reduced to about 75 percent of normal with no marked change of virtual height.

The appearance of many fade-outs of the type known as the Dellinger effect,[8] during the recent series of magnetic storms was very striking. During the three months preceding April 21, only two small fade-outs were observed at Washington. From April 21 to May 4, 32 fade-outs were recorded by us. From this it would appear that the active sunspot areas which probably were the seat of phenomena which caused the magnetic storms, were also associated with the solar flares which produce the fade-outs. From the fact that in the past magnetic storms and fade-outs have usually occurred independently it seems that the agencies producing these two phenomena are different but that they are both associated with active sunspot areas.

S. S. KIRBY
N. SMITH
T. R. GILLILAND
S. E. REYMER

National Bureau of Standards,
Washington, D. C.,
May 8, 1937.

* Publication approved by the director of the National Bureau of Standards of the U. S. Department of Commerce.
[1] S. S. Kirby, T. R. Gilliland, E. B. Judson, and N. Smith, Phys. Rev. **48**, 849 (1935).
[2] S. S. Kirby, T. R. Gilliland, N. Smith, and S. E. Reymer, Phys. Rev. **50**, 258 (1936).
[3] Nature (London), **139**, 69 (1937).
[4] Zeits. f. tech. Physik **17**, 327 (1936).
[5] Hochf. tech. u. Elek. akus. **48**, 181 (1936).
[6] Terr. Mag. **41**, 407 (1936).
[7] Mimno, Joint meeting I.R.E.-U.R.S.I. (1937).
[8] J. H. Dellinger, Phys. Rev. **48**, 705 (1935).

Interferometer Measurements of Wave-Lengths in H_2 Bands

As part of a program of measurement of the bands due to H_2, HD and D_2 molecules, the wave-lengths of some of the stronger lines in the red and near infrared of the spectrum of H_2 have been measured with a Fabry-Perot interferometer. Auxiliary dispersion was obtained by means of a stigmatic grating spectrograph with a dispersion of 5.2 angstroms per millimeter. The source was a Pyrex discharge tube with large electrodes, and a flattened constriction from which the light was taken through the wall of the tube. The temperature of the interferometer was subjected to the usual controls, and the barometric pressure was observed. Five exposures using two etalon separators were measured and reduced in the usual manner, the red neon lines between 6304 and 8377 angstroms being used as standards.

The results of the measurements are given in Table I. Unless specified, the error is less than 0.002 angstrom, which is the average value of the mean error for all lines. The difference between the average values from the two etalons is less than 0.004 angstrom unless the error is followed by the letter h. Measurements are from four or five spectrograms unless the error is followed by the letter p. The fourth column in the table gives the fractional parts of the wave-lengths obtained for these lines by Gale, Monk, and Lee.[1] The differences between these new measures and those of Gale, Monk, and Lee are in some cases to be attributed to the presence of neighboring lines, although not in a sufficient number of cases to affect the mean difference between the two sets of measures. These new values indicate that the grating measures of Gale, Monk and Lee are systematically too low in the region between 6500 and 8500 angstroms.

TABLE I. *Wave-length intensities and comparison with previous values (G.M.L.) of lines in H_2 bands.*

WAVE-LENGTH	INT.	ERROR	G.M.L.	WAVE-LENGTH	INT.	ERROR	G.M.L.
6285.391	4		0.388	7295.433	5		0.42
6299.424	8		.420	7328.155	4		.12
6303.482	0		.485	7474.525	4		.51
6327.068	10	0.003	.063	7524.667	5		.64
6332.490	4		.486	7545.025	2		4.99
6340.580	5	.003	.574	7576.429	0	0.003	.41
6362.488	5		.483	7606.379	1		.36
6372.218	1		.209	7650.779	1	.005h	.75
6380.116	1	.004h	.110	7685.555	6	.004h	.53
6399.479	6		.475	7719.120	0	.003	.09
6428.127	5		.113	7789.811	2		.78
6441.517	2		.502	7875.465	1	.003h	.43
6517.696	2		.695	7900.305	2	.004	.24
6527.356	3		.355	7923.484	3		.44
6540.525	2	.003	.510	7953.495	1	.003	.44
6622.619	3		.590	7985.901	1	.004	.86
6696.767	2		.755	8018.761	2		.71
6701.893	1	.003h	.861	8164.697	2		.64
6806.447	1		.438	8222.933	3		.90
6840.900	0	.004p	.886	8240.798	1	.003	.75
6940.432	2		.421	8273.280	4		.26
6988.727	1	.003	.708	8330.441	3		.42
7049.616	1		.60	8349.547	10		.52
7112.658	2	.005h	.65	8366.938	2		.89
7168.822	3	.003	.81	8398.284	2		.26
7195.666	5	.004	.66	8486.081	2	.003	.08
7227.886	3		.88	8528.090	3		.11
7269.992	6		.96	8546.248	10	.002p	.27

H. LANDAHL
G. S. MONK

Ryerson Physical Laboratory,
University of Chicago,
May 2, 1937.

[1] Astrophys. J. **67**, 89 (1928).

Erratum: Nuclear Spins and Magnetic Moments in the Hartree Model

(Phys. Rev. **51**, 205 (1937))

Professor E. Wigner and Dr. E. Feenberg have called our attention to an error made in our paper of the above title. In considering the spin-orbit splitting of a multiplet in the case that this splitting is mainly due to a half-closed shell of protons or neutrons it is necessary to remember that the presence of the other particles influences the contribution of the half-closed shell whether these other particles are in a singlet state or not. For nuclei which are mirror images the spin-orbit interaction will, on "the theory of holes," have opposite sign. Therefore, we conclude that the ground states of B^{12}, B^{11} and C^{11} are $^3P_0$, $^2P_{\frac{1}{2}}$ and $^2P_{\frac{1}{2}}$, respectively (instead of $^3P_2$, $^2P_{\frac{3}{2}}$ and $^2P_{\frac{3}{2}}$). The magnetic moments of B^{11} and C^{11} are then -0.52 and 1.57 nuclear magnetons, respectively (instead of 3.50 and -1.65).

M. E. ROSE
H. A. BETHE

Cornell University,
Ithaca, New York,
May 15, 1937.

On the Magnetic Scattering of Neutrons. II

Some time ago[1] we have shown that the scattering of slow neutrons in magnetized matter should depend noticeably on their magnetic moment. In deriving a formula for this effect, it was assumed that the neutron could be treated as a true magnetic dipole; at present the interior properties of heavy particles are not known well enough to decide whether this assumption, or any other, is justified; but it is interesting to notice that the physical nature of the neutron moment has an influence on the magnetic scattering, marked enough to be decided experimentally.

To obtain a unique theoretical answer it is in fact not sufficient to treat the neutron as a mass point, carrying an angular momentum and a magnetic moment, since this would lead to a magnetic field of the neutron, singular at the position point in such a way as to make the result on that basis ambiguous. To illustrate the situation, let us consider a case in which the electron currents of the scattering atom are flowing only outside a closed surface S, surrounding the neutron. We shall see that the geometrical shape of this surface matters for the result even in the limit in which its linear dimensions are small compared to the wave-length of the neutron and the radius of the atom, both entering in a first-order treatment of the scattering process. This exclusion of the interior of S is, of course, not meant as a physical model; in fact with our present knowledge it is impossible to give such a model as soon as the linear dimensions of S become comparable to those of the neutron itself or to the electron radius. The exclusion is merely introduced as a device to separate the origin of any ambiguities from well-established facts.

In this case the force acting on a neutron at a position $\mathbf{r}_n$ is the negative gradient of a potential

$$U(\mathbf{r}_n) = -\int (\mathbf{H}_n(\mathbf{r}-\mathbf{r}_n)\cdot\mathbf{m}_e(\mathbf{r}))d\tau, \tag{1}$$

where $$\mathbf{H}_n(\mathbf{r}) = \text{curl}\ (\boldsymbol{\mu}_n\times\mathbf{r})/r^3$$

is the magnetic field of the neutron with magnetic moment $\boldsymbol{\mu}_n$ and where the integral is to be extended over the volume outside the surface S. $\mathbf{m}_e$ is the well-known polarization vector of Maxwell's theory, connected with the stationary current density $\mathbf{i}_e$ of the atomic electrons by the relation $\mathbf{i}_e = c\ \text{curl}\ \mathbf{m}_e$. Accepting the law of action and reaction between neutron and electrons the expression (1) follows immediately from the force $1/c(\mathbf{i}_e\times\mathbf{H}_n)d\tau$ acting on the volume element $d\tau$ of the atom. We notice further that the total magnetic moment of the atom is given by

$$(1/2c)\int(\mathbf{i}_e\times\mathbf{r})d\tau = \int\mathbf{m}_e d\tau. \tag{2}$$

The values of $\mathbf{i}_e$ and $\mathbf{m}_e$ are to be taken as the expectation values of the corresponding operators in a stationary state of the atom; the above equations are then just as valid as in classical theory.[2]

Treating the scattering of the neutron, due to the potential (1) by the usual Born approximation and assuming that the nuclear cross section σ_ω per unit solid angle is small compared to the square of the neutron wave-length the total cross section per unit solid angle is now easily found to be

$$\phi_\omega = \sigma_\omega\left|1\pm\frac{\gamma_n\gamma_e}{2(\sigma_\omega)^{\frac{1}{2}}}\frac{e^2}{mc^2}\left(\frac{q_z^2}{q^2}-C\right)\right|^2 \tag{3}$$

with $$C = (1/4\pi)\int(zds_z/r^3). \tag{4}$$

Here we have arbitrarily chosen as z axis the direction of the vector

$$\boldsymbol{\mu}_e(\mathbf{q}) = \int\mathbf{m}_e(\mathbf{r})e^{i(\mathbf{q}\mathbf{r})}d\tau.$$

γ_e and γ_n are the magnitudes of $\boldsymbol{\mu}_e$ measured in Bohr magnetons and $\boldsymbol{\mu}_n$ measured in nuclear magnetons, respectively; $\mathbf{q}$ is the difference between the vectors of propagation of the incident and scattered neutron wave, and the plus or minus sign in (3) is valid according to the two possible orientations of the neutron moment with respect to $\boldsymbol{\mu}_e$. The integral (4) is to be taken around the origin over the surface S, which is supposed here to extend over linear dimensions, small compared to $1/9$; ds_z is the z component of a vector in the direction of the external normal to S with magnitude equal to the surface element.

In the limit, where the neutron wave-length is large compared to the linear dimensions of the atom the quantity γ_e in (3) becomes simply the magnetic moment of the atom in Bohr magnetons and the z axis points in the direction of magnetization. The characteristic constant C depends then solely on the shape of the surface S: If, for example, one chooses S to be a sphere, one finds $C=\frac{1}{3}$;[3] choosing S as a cylinder with height h and radius R around the z axis, one has the two limiting cases

(a) $R\ll h$. This corresponds to treating the neutron as a true dipole and gives $C=0$, i.e., our result, obtained in I.

(b) $R\gg h$. This corresponds to treating the neutron as a little amperian current and gives $C=1$, i.e., Schwinger's result.[2]

An assumption about the interaction between nuclear magnetic moments and atomic electrons, analogous to the choice (b) underlies the usual calculations of hyperfine structures and is experimentally supported for the proton and the deuteron by the agreement of the results for their magnetic moments obtained by the Stern-Estermann and Rabi methods. What choice has to be made for the neutron is not *a priori* certain and therefore the value of the constant C should be left open. Since it appears in (3) together with a strongly angle dependent term, one may hope to determine this constant experimentally by directly measuring the angular distribution of slow neutrons, scattered in their passage through magnetized matter.

F. Bloch

Department of Physics,
Stanford University, California,
April 28, 1937.

[1] Bloch, Phys. Rev. **50**, 259 (1936). Here referred to as "I".

[2] If in the light of these considerations one examines a recent paper by J. S. Schwinger (Phys. Rev. **51**, 544 (1937)) one finds that his result for the magnetic scattering is not essentially based on the use of the Dirac operator for the electron current but on the assumption, implicit in the form chosen for the energy of the neutron in the magnetic field of the atomic electrons, that the neutron can be treated as a little amperian current.

[3] This result has been kindly communicated to me by Mr. M. Bronstein, who obtained it by introducing polar coordinates around the neutron and first integrating over the angles.

Proton Induced Radioactivity in Oxygen

As previously reported[1, 2] a large number of elements are found to become radioactive under bombardment by protons of energies up to 3.8 Mev. Two periods have been definitely established for oxygen, using targets of quartz and other solid oxides as well as a platinum foil in oxygen. The short period of 1.28 ± 0.10 min. is at once identified with the well-known F^{17} formed by the capture of a proton by O^{16}. The activity becomes detectable at a proton energy of 1.4 Mev rising rapidly to about 3 Mev and then more slowly (thick target).

The second period of 107 ± 4 min. is shown by chemical separation to be due also to an isotope of fluorine and is close to the 112 min. period found by Snell[3] for F^{18}. This period must be attributed to the reaction

$$O^{18}+H^1\rightarrow F^{18}+n^1$$
$$F^{18}\rightarrow O^{18}+e^+.$$

All other oxygen reactions lead either to stable isotopes or to known and much shorter periods. The presence of neutrons expelled during bombardment was proved by the activity induced in a silver plate imbedded in paraffin.

This proton-neutron type of reaction has not been previously reported since disintegration experiments with protons have hitherto been confined to energies below about 1.2 Mev. The above reaction sets in sharply at 2.6 Mev and rises so rapidly that at 3.8 Mev the F^{18} activity is much stronger than the F^{17} in spite of the low abundance of the O^{18} isotope. Rough calculations of the cross section give a value of 4×10^{-26} cm² which is 4000 times greater than for the O^{16} capture reaction.

It is easily seen that for any proton-neutron reaction of this type where the initial and final stable isotopes are the same, the reaction becomes energetically balanced for protons of energy given by

$$E_p=n^1-H^1+e^+(e^-)+E_++E_n,$$

where E_n is the kinetic energy of the neutron and E_+ the maximum energy of the positrons. For F^{18} the latter has been found to be about 0.6 Mev which gives for the threshold, assuming here the neutrons escape with negligible energy,

$$E_p=0.81+1.02+0.6=2.43 \text{ Mev}$$

in good agreement with the observed threshold of 2.6 Mev.

It seems probable that this type of reaction is taking place in a number of the other elements studied. In particular for the Mn reaction (90 min. period) previously reported[1] this appears to be the only possibility. The deuteron emission first suggested is energetically excluded in this case and subsequent chemical tests indicate the reaction

$$Mn^{55}+H^1\rightarrow n^1+Fe^{55}\rightarrow n^1+Mn^{55}+e^+.$$

Department of Physics,
University of Rochester,
Rochester, New York,
May 7, 1937.

L. A. DuBridge
S. W. Barnes
J. H. Buck

[1] Barnes, DuBridge, *et al*, Phys. Rev. **51**, 775 (1937).
[2] Washington Meeting, 1937.
[3] Snell, Phys. Rev. **51**, 143 (1937).

Scattering of Fast Neutrons

The elastic cross sections of heavy nuclei for beryllium-radon neutrons have been recalculated for the same approximate interaction between neutron and nucleus considered previously[1] using the larger value for the nuclear radius suggested recently by Bethe.[2] Fig. 1 shows

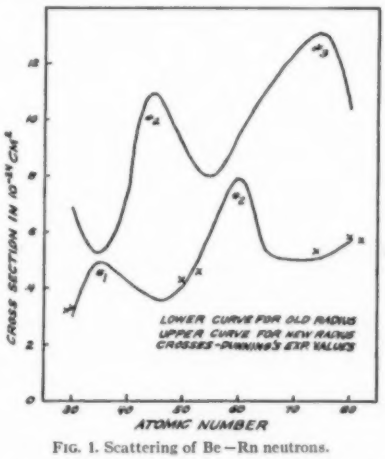
CROSS SECTION IN 10⁻²⁴ CM²
ATOMIC NUMBER
LOWER CURVE FOR OLD RADIUS
UPPER CURVE FOR NEW RADIUS
CROSSES - DUNNING'S EXP. VALUES

FIG. 1. Scattering of Be—Rn neutrons.

the results for both old and new radii. The partial cross sections responsible for the maxima are indicated.

The new radius is seen to give cross sections too high compared with the experimental values of Dunning.[3] If Bethe's larger radius is not to be rejected it must be shown that the polarization effects neglected in our treatment of the nucleus as a single particle operate consistently to reduce the cross section for fast neutron scattering. The Bohr "water-drop" model of the nucleus, so useful in affording a qualitative explanation of large capture cross sections for slow neutrons, does not appear to give an obvious answer to this question.

C. H. Fay

Research Laboratory of Physics,
Harvard University,
Cambridge, Massachusetts,
May 14, 1937.

[1] Fay, Phys. Rev. **50**, 560 (1936).
[2] Bethe, Phys. Rev. **50**, 1100(A) (1936).
[3] Dunning, Phys. Rev. **45**, 586 (1934).

Long Period Activity in Cadmium Irradiated with Neutrons

Recently Cork and Thornton[1] bombarded cadmium with 6.3 Mev deuterons and found two activities due to cadmium with periods of 4.3 hr. and 58 hr., respectively. The radioactive isotope of cadmium of 58 hr. period gives rise to a radioactive indium isotope of 2.3 hr. half-life. The two active cadmium isotopes are Cd^{115} and Cd^{117} which can be formed from Cd^{114} and Cd^{116} by neutron capture. Since no activity has thus far been produced in Cd by neutron bombardment, it was thought worthwhile to see if it would be possible to activate Cd in this manner.

A neutron source, consisting of 200 mC radium salt mixed with beryllium was surrounded by blocks of paraffin.

Two cadmium foils, 0.1 mm thick, were placed in the paraffin about 3 cm from the source. Paraffin was placed behind the detector as well as between it and the source. After irradiation for a week, the activity of the detectors was measured with the help of a tube counter and recording mechanism, the sensitivity of the counter being checked at the time of each measurement with the help of a standard uranium preparation. The material was rather weakly active, giving rise to a decay curve which showed two periods. The measurements on the longer period gave a value of 52 ± 5 hr., while the shorter period, determined by difference, was about 5 hr. The initial activity corresponding to the shorter period was about one-fifth of that for the longer period, under the conditions of the experiment.

Unfortunately, the activity was not strong enough to enable one to carry out a chemical analysis. In order to preclude the possibility of the activity being due to any surface contamination, one of the detectors was vigorously scoured during the course of the measurements with no resulting difference in the activity. It would appear from the weakness of the activity that neither activity is connected with the large capture cross section exhibited by Cd for slow neutrons. Furthermore, the activity on both sides of the detector was measured and no difference was found between them, lending support to the view that the capture cross section for the process is not exceedingly large. It would seem that the two periods obtained by neutron activitation are the same as those found by Cork and Thornton under deuteron bombardment. Further experiments are in progress from which it is hoped that a chemical identification of the active substance may be made.

The author wishes to express his thanks to the Penrose Fund of the American Philosophical Society for a grant which enabled him to carry out this work.

ALLAN C. G. MITCHELL

Physics Department,
New York University,
University Heights,
New York, N. Y.
May 14, 1937.

[1] J. M. Cork and R. L. Thornton, Phys. Rev. **51**, 608 (1937).

On Hard Gamma-Rays from Ra (C+C′+C″+D)

Danysz[1] first and later Rutherford and others[2] observed that Ra C emits hard beta-rays which are the internal conversion electrons of hard gamma-rays. However, Rutherford, Chadwick and Ellis[3] remark that these beta-rays may be nuclear disintegration electrons since according to the measurements of Yovanovitch and d'Espine[4] these beta-rays are not homogeneous but possess a wide range of energies.

I examined these gamma-rays with a Wilson chamber and found three gamma-rays of energies about 3.1, 4 and 4.9 Mev (recently by the absorption method, Devons and Neary[5] found Ra C″ emits one gamma-ray of energy (5 ± 1) Mev which may correspond to the observed 4.9 Mev). About 13 electron and positron tracks were observed in every 100 photographs. The source was 1.5 m from the chamber. Hence, it may be certain that Ra C emits hard gamma-rays but not such beta-rays as may be called abnormal decay electrons.

To explain the origin of these hard gamma-rays, and from a consideration of the recent experiments of W. Bothe and H. Maier-Leibnitz,[6] I suggest a scheme of levels from Ra C to Ra D as shown in Fig. 1. The total

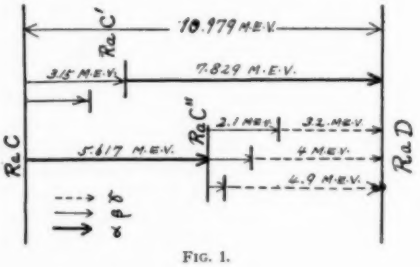

FIG. 1.

energy of disintegration Ra C→Ra C′→Ra D is 10.979 Mev. Therefore, the energy of disintegration Ra C″→Ra D must be 5.368 Mev. Then if we estimate the maximum energy of the beta-ray from Ra C″ to be 2.1 Mev,[7] the gamma-ray of energy 3.2 Mev is to be expected. The other gamma-rays of energies 4 and 4.9 Mev may be explained by assuming that they are emitted from the excited levels as shown in Fig. 1. This assumption is not in contradiction with any current views.

Details of the experiment and full discussions will be published in the *Proceedings of the Physico-Mathematical Society of Japan.*

SOTOHIKO NISHIDA

Hyogoken Mukogun Motoyamamura,
Konan-Koto-Gakko, Japan,
April 15, 1937.

[1] Danysz, Le Radium **10**, 4 (1913).
[2] Rutherford and Robinson, Phil. Mag. **26**, 717 (1913).
[3] Rutherford, Chadwick, and Ellis, *Radiations from radioactive substances.*
[4] Yovanovitch and d'Espine, J. de phys. **8**, 276 (1927).
[5] Devons and Neary, Proc. Camb. Phil. Soc. **33**, 154 (1937).
[6] W. Bothe and H. Maier-Leibnitz, Zeits. f. Physik **104**, 604 (1937).
[7] According to the result of Devons and Neary, the maximum energy is 1.95 Mev and from Sargent's curve about 2.3 Mev.

Proceedings of the American Physical Society

MINUTES OF THE WASHINGTON MEETING, APRIL 29, 30 AND MAY 1, 1937

THE 213th regular meeting of the American Physical Society was held in Washington, D. C., at the National Bureau of Standards on Thursday and Friday, April 29 and 30, 1937 and at George Washington University on Saturday, May 1, 1937. There were two parallel sessions for the reading of ten-minute contributed papers on Thursday morning, and three parallel sessions in the afternoon. On Friday morning there were two parallel sessions and in the afternoon three parallel sessions. At George Washington University on Saturday there were two sessions in the morning and afternoon. The presiding officers were H. M. Randall, President of the Society, L. J. Briggs, Vice President, H. L. Curtis, K. K. Darrow, W. P. Davey, L. A. DuBridge, Harvey Fletcher, R. C. Gibbs, G. F. Hull, A. E. Ruark, F. A. Saunders, P. I. Wold and John Zeleny. The attendance at the meeting was over five hundred.

On Friday morning Professor F. Simon of Oxford University gave an invited paper on "Magnetic Experiments at Very Low Temperatures." On Friday afternoon at the close of the regular sessions Professor R. W. Wood showed moving pictures of unique crystallization phenomena of protocatechnic acid in colors.

On Friday evening the Society held its dinner at the Raleigh Hotel. President H. M. Randall presided and called upon Editor John T. Tate to introduce Mr. David Sarnoff, President of the Radio Corporation of America. Mr. Sarnoff spoke on "Science and Society." There were three hundred and ten guests present.

Meeting of the Council. At its meeting held on Thursday, April 29, 1937 the deaths of two fellows (Elihu Thomson and Albert P. Wills) and of two members (Clete Adams and Wesley P. Coates) were reported. One candidate was elected to fellowship, four candidates were transferred from membership to fellowship and forty-six candidates were elected to membership. *Elected to fellowship:* Charles P. Smyth. *Transferred from membership to fellowship:* Gerhard Herzberg, P. Kapitza, Harold P. Knauss and J. C. Mouzon. *Elected to membership:* Stanley Anderson, Dennison Bancroft, Francis Breazeale, Allan R. Brown, J. C. Burnett, Walter D. Claus, Edward A. Coomes, Robert J. Dwyer, Lorenzo Emo, Marvin Evans, Florence L. Feicht, James E. Field, J. S. Foster, Francis E. Fox, Bernard Fried, Raymond M. Fuoss, Nelson Fuson, Marcel J. E. Golay, John P. Hervey, Robert B. Jacobs, Haydn Jones, Carlton V. Kent, William S. Lanterman, Jr., Vergil C. Lohr, Oscar E. McClure, Charles A. Mabey, W. B. Mann, John B. Merrill, Dan Moore, Henry Primakoff, Thomas A. Read, Nicholas A. Renzetti, E. W. Ritter, Julian Schwinger, Franz Simon, Albert E. Smith, Harold S. Stewart, Jr., Leo Szilard, Georgia A. Tapley, Charles Trilling, Ramond C. Waddel, J. H. Waggoner, J. S. Wang, Harold E. Way, H. J. Williams, and Marvin M. D. Williams.

The regular scientific program of the Society consisted of one hundred and sixty-one contributed papers of which numbers 143 and 144 were read by title. The abstracts of these papers are given in the following pages. An Author Index will be found at the end.

W. L. SEVERINGHAUS, *Secretary*

ABSTRACTS

1. A Simplified Method for Indexing Debye-Scherrer-Hull Patterns. LUDO K. FREVEL, *The Dow Chemical Company, Midland, Michigan.* (*Introduced by J. D. Hanawalt.*) —The feasibility of finding a solution for the quadratic form of powder patterns has been limited to cubic crystal and to the simpler structures with tetragonal or hexagonal symmetry. Mathematical methods have been proposed to solve the case of three or more parameters; however, practical efforts to apply these devices have proved laborious and unsatisfactory. Yet in view of the simplicity and general applicability of the powder method, it is worthwhile to simplify the indexing of powder photographs of tetragonal and hexagonal substances and, moreover, to extend the simplification to orthorhombic and monoclinic crystals. In order to supplement the information gained by accurate spacing measurements, one records on a single film a direct temperature shift[1] of the diffraction pattern of a substance by taking two successive exposures, each at a

constant temperature. An interval of 150°C or greater will generally suffice to produce easily measurable temperature shifts that can be related to the anisotropy of a crystalline substance. A systematic treatment of the various crystal systems has shown that the first four systems (cubic, tetragonal, hexagonal, and orthorhombic) can be indexed in a straightforward manner. Two cases of the monoclinic system: (1) $\partial\beta/\partial T=0$ and (2) $\alpha_b/2=(1/b)(\partial b/\partial T)>\alpha_a>\alpha_c>\cot\beta\cdot(\partial\beta/\partial T)$ can be solved without time-consuming mathematical calculations.

[1] L. K. Frevel, Rev. Sci. Inst. **6**, 214 (1935).

2. The Focusing of Electrons in an X-Ray Tube. N. C. BEESE, *Westinghouse Lamp Company, Bloomfield, N. J.*—A theory is proposed that accounts for the variations in the observed focal spot patterns on the anodes of x-ray tubes caused by changes in the geometry of the cathode structures. The focusing of electrons emitted by a helical filament within a focal cup can be explained qualitatively by elementary electrostatics. Data are presented to show the variations in size and energy distribution within the focal spots when changes are made in the dimensions of the focal cup mouth, throat, filament diameter and the mounting depth of the filament in the trough of the focal cup.

3. The Shape of the Density-Exposure Time Curve for X-Rays. F. R. HIRSH, JR., *Cornell University.*—Silberstein[1] has shown by a nuclear theory of photographic exposure that the probability of a quantum striking an active nucleus and reducing it to the latent image stage is $p_\lambda=(1-e^{-cE})$ where c is a constant and E is the "exposure"; this is of the same type of function as deduced by quantum theory. It may be shown that the slope of the density-exposure time curve is given by $D/t=k_1n_0(1-e^{-k_2n_0\lambda p_\lambda t})$ where k_1 and k_2 are constants, and n_0 is the number of quanta of energy $h\nu$ incident on unit area of emulsion per second. It will be shown that for x-ray quanta of sufficient energy, p_λ, the probability function rises sharply to 1.0 as t increases. Thus only a small "foot" appears on density-exposure time curves for $\lambda\sim5.0$A; these curves appear to be straight lines passing through the origin.[2] For x-ray quanta of small energy, the probability function, p_λ, rises slowly to 1.0 as t increases, and a large "foot" should appear on the density-exposure time curve. A large "foot" is observed experimentally for curves taken with $\lambda\sim12.0$ to 14.0A.

[1] L. Silberstein, Phil. Mag. **5**, 464 (1928).
[2] F. R. Hirsh, Jr., J. O. S. A. **25**, 229 (1935).

4. Fourier Analysis of Liquid Methyl Alcohol. G. G. HARVEY, *Massachusetts Institute of Technology.*—The x-ray diffraction curve for liquid methyl alcohol at a temperature of about −75°C has been obtained with monochromatic Mo $K\alpha$ radiation out to $\sin\theta/\lambda=1.2$. At this temperature, which is about 22° above the freezing point, there is much greater detail in the diffraction curve than is observable at ordinary temperatures. Five diffraction rings are visible on the film whereas at higher temperatures it is difficult to distinguish a second one. It has consequently been possible to carry through a Fourier analysis and obtain a radial electron distribution function showing more distinct peaks than Zachariasen[1] was able to obtain from Stewart and Morrow's[2] data taken at room temperature. The results are, however, in substantial agreement with Zachariasen's conclusions with the addition that the present curve shows a very definite peak corresponding to oxygen-oxygen linkages, whereas at room temperature this peak is practically washed out. The distribution curve shows five well-defined peaks.

[1] Zachariasen, J. Chem. Phys. **3**, 158 (1935).
[2] Stewart and Morrow, Phys. Rev. **30**, 232 (1927).

5. The Crystal Structure of Potassium Tetrachloriodide. R. C. L. MOONEY, *Newcomb College, Tulane University.*—In connection with a study of the configuration of the polyhalogen anions of alkali metal salts, the crystal structure of a pentahalide, namely, potassium tetrachloriodide, has been determined by means of x-rays. The data, consisting of intensities observed photographically for more than two hundred planes, were obtained by the usual single crystal oscillation method. The crystal is monoclinic, and has the symmetry of $P2_1/n(C^5_{2h})$. There are four molecules in a unit cell of dimensions: $a=12.89$A, $b=14.18$A, $c=4.17$A, Angle $\beta=95.7°$. The location of atomic positions involved the determination of eighteen parameters. Values for these have been found such that the calculated structure amplitudes of the proposed structure agree well with observations. No assumptions were made as to grouping or expected interatomic distances; the positions of the iodines were found from intensity considerations; the chlorine and potassium atoms were first approximately located from two dimensional Fourier analyses, and then fixed by intensity calculations. It is found that the halogens form a planar group, consisting of a central iodine surrounded by four chlorines at the corners of a square. The iodine to chlorine distances in a group are 2.3A and the chlorine to chlorine distances in different groups are more than 3.5A. There is a coordination sphere of eight chlorines about each potassium.

6. X-Ray Investigations of the Structure of Wood. W. I. CALDWELL AND K. LARK-HOROVITZ, *Purdue University.*—Preliminary experiments[1] have shown that wood, regardless of the appearance, exhibits x-ray diffraction patterns ranging from perfect fiber structure to almost completely homogenous diffraction rings. Extraction treatment did not change the cellulose pattern of the samples investigated. Even wood deteriorated under prolonged x-ray treatment yields the characteristic diffraction pattern. Systematic investigations have been carried out recently with wood samples graded according to origin, conditions of growth, mechanical properties and of known fibril angle.[2] Monochromatic Cu K radiation and a vacuum camera were used. Only cellulose patterns have been obtained. Lignin, investigated separately, gives a "liquid" pattern ($\sin\theta/\lambda$ corresponding to 0.045, 0.113, 0.222),[3] but no indication of it was found in any of the wood samples investigated so far. The results show that the presence or absence of fiber structure depends on the fibril angle: small fibril angle corresponds to fiber pattern, large fibril angles are accompanied by more homogenous pattern. These results are

checked also by heat conductivity determination normal and parallel to grain (isotherm method).[4] Compression and spring wood have less pronounced fiber structure than summer wood.

[1] K. Lark-Horovitz, W. I. Caldwell, Phys. Rev. **15**, 749 (1934).
[2] We are indebted to Dr. A. Koehler and Mr. H. Y. Pillow, Forest Products Laboratory, Madison, Wisc., for selecting the samples and the information regarding mechanical and microscopical investigations.
[3] Experiments with Dr. E. P. Miller and Mr. G. C. Danielson.
[4] K. Lark-Horovitz, Nature **137**, 663 (1936).

7. X-Ray Diffraction Patterns from Crystalline Substances at Very High Hydrostatic Pressures. ROBERT B. JACOBS,* *Harvard University.* (*Introduced by W. L. Severinghaus.*)—An apparatus has been constructed which enables one to take Debye-Scherrer type x-ray spectrograms of substances under pure hydrostatic pressures as high as 4000 atmospheres. The usual comparatively soft x-rays useful for crystal work are employed (Cu K_α $\lambda=1.539$A). The x-ray beam enters the high pressure steel chamber through a small beryllium window; it there encounters the specimen and is diffracted to a photographic film which is bent inside the inner cylinder wall. The compressive medium is helium gas, which even at these pressures does not absorb the x-ray beam excessively. The quality of the diffraction lines obtained compares favorably with similar ones taken with a conventional camera at atmospheric pressure. Thus far the apparatus has been employed in the study of crystallographic changes which accompany polymorphic changes under pressure. KNO_3, $CsClO_4$, and AgI have been successfully studied in the pressure range 3000–4000 atmospheres. However, only the structure of the latter has been completely solved to date. At 3700 atmospheres, and at 25°C, it is found to have an NaCl type of cubic structure with unit edge 6.070 ± 0.010A with a corresponding density of 5.72.

* This work began while author was a National Research Fellow.

8. X-Ray Measurement of the Effect of Temperature on the Atomic Vibrations in Single Crystals of Zinc. G. E. M. JAUNCEY AND W. A. BRUCE, *Washington University.*—The investigations of the previous paper have been extended to temperatures of 100°, 200°, 298°, 370°, and 550°K for the scattering angle $\phi=30°$. Curves of $S\rho/\mu$ against the orientation angle ψ for these temperatures were obtained. In the front face method of measuring diffuse scattering it is very necessary to remove pits and other irregularities in the surfaces of the specimens. This was done by careful polishing, annealing, and etching. A theoretical investigation has shown how the ratio of the mean square displacement along the c-axis to that perpendicular to this axis may be obtained from the scattering values measured at different temperatures and different values of ψ for a given angle ϕ. The formula for this ratio does not contain the spectral distribution and is the same for the general radiation we used as for monochromatic radiation. Our results indicate this ratio to have a value between 2.7 and 3.1. This is greater than Zener's theoretical value of 1.80.

9. Variation of the Atomic Structure Factor of Nickel with Wave-Length in the Region of the Nickel *K* Absorption Limit. WILLIAM P. JESSE, *University of Chicago.*—With a vacuum ionization spectrometer comparison measurements have been made between the diffracted intensities from a briquet of powdered nickel and those from standard planes in briquets of powdered NaCl or LiF. Wave-lengths on both sides of the nickel K absorption limit (1.4839A) have been used with a range from 0.56A (Ag K_α) to 2.74A (Ti K_α). The values of the atomic structure factor for nickel for such wave-lengths were computed from known values of the structure factors for the standard substances. Corrections were made for very small variations in the standards with wave-length. If the theoretical dispersion curve of Hönl is fitted to the experimental curve at one point on the short wave-length side of the absorption edge, fairly good agreement between theory and experiment is obtained for points on the long wave-length side far removed from the absorption edge. A marked discrepancy is found closer to the absorption limit where the experimental curve rises more sharply and higher than the theory predicts. The experimental curve is in agreement with that determined for nickel by another method by Lameris and Prins.

10. Widths of *L*-Series Lines and of Energy Levels of Ag(47). LYMAN G. PARRATT, *Cornell University.*—The width of an x-ray line depends on the life-times of the initial and final states of the emitting atom. With the concept of unsharp energy levels, the line width may be taken as the sum of the widths of the two energy levels involved. This simple sum relation may be checked experimentally if we assume (1) infinite spectrometric resolving power, (2) adequate resolution of a complex overlapping spectral contour into component lines, and (3) the perturbing effects of neighboring atoms to be negligible. Then the life-time of each of the two transition states is due to (1) what amounts to classical radiation damping and (2) radiationless transitions. Each of these two life-time contributions results in an absorption limit shape given by an arctangent curve (with certain assumptions)[1] and emission line shapes of the form $y=a/(1+(x/b)^2)$. These relations between line and level widths and line and level shapes have been experimentally studied for the L-series spectra, some 27 emission lines and the absorption limits, of Ag(47). The spectral (ionization) curves were recorded with a newly constructed two-crystal vacuum spectrometer.

[1] Richtmyer, Barnes and Ramberg, Phys. Rev. **46**, 843 (1934).

11. Geiger-Müller Counter Measurements of Reflected Mo $K\alpha$ X-Rays from Powdered Zinc. R. D. MILLER, *Washington University, St. Louis, Mo.*—Volz[1] has used the formula $n=n_0\exp(-n_0/2.718n_m)$, where n is the observed counting rate of the system, n_0 is the rate of production of pulses in the counter and n_m is the maximum possible counting rate. It was found that n_0, calculated from n and corrected for background count, varied as the inverse square of the distance from a gamma-ray source. Further, the absorption coefficient of Mo $K\alpha$ rays in aluminum was found to have the correct value when measured by means of this formula. Thus the formula was satisfactory. The absolute F values were obtained by comparison of the (11$\bar{2}$2) reflection from zinc with the (420)

reflection from KCl and the (220) reflection from MgO. An average of these gives $F(11\bar{2}2)=13.6$. Brindley, using Cu $K\alpha$ rays, obtains $F(11\bar{2}2)=12.0$. The difference is due to dispersion. The F values for other reflections very closely agree with those found by Brindley for Cu $K\alpha$ rays, when his values are corrected for dispersion. The very weak (0004) reflection, which was not obtained by Brindley, was found to have an F value of about 9.

[1] Volz, Zeits. f. Physik **93**, 540 (1935).

12. X-Ray and Optical Measurements of Multi-Molecular Films. CLIFFORD HOLLEY, *University of Chicago.*—Bragg diffraction and Michelson interference measurements of films of counted layers of barium stearate have been made. The films, kindly prepared by Dr. Blodgett, were of from 301 to 3000 molecular layers, counted as they were deposited upon the optically flat glass. The x-ray measurements showed equal thickness of the molecular layers in the various films within 0.08 percent, which is perhaps within experimental error. Two of the eight films used failed to show any diffraction. The interference measurements of the film thickness gave somewhat less consistent results, and indicated some expansion of the films with aging. Using the optically measured grating space of 48.40A, corresponding to a layer two molecules thick, the wave-length of the tungsten $M\alpha$ line is calculated to be 7.007A. This is to be compared with 6.969A from crystal measurements, or 6.984A as based on the ruled grating standard. Probable sources of error lie in the uncertainty of the refractive index of the stearate film for the x-rays, and possible phase changes when the light is reflected from the film and glass surfaces of the Michelson interferometer. The consistency of the results indicates that the method should become a valuable one for the determination of the absolute wave-length of x-rays.

13. Posnjak and Barth's Principle of "Variate Atom Equipoints," Superlattices and "Mixed Crystals." F. C. BLAKE, *Ohio State University.*—Seeking to understand, and if possible to legitimatize the idea of variate atom equipoints the writer has checked the results of the authors of the principle in the case of lithium ferrite and zinc stannate with material kindly supplied by them. In the case of the lithium ferrite, by quadrupling their lattice it is possible to obtain a perfect solution which is face-centered cubic in the fourth order. Since the first three orders for each of the components iron, lithium and oxygen go to zero the process of lattice enlargement can be generalized to any compound of the type ABX_2. The quadruple lattice with $a=16.564$ angstroms contains 64 molecules of $Li_2Fe_2O_4$. Due to destructive interference superlattices are entirely absent. For the double lattice, $a=8.282$ angstroms, superlattice lines should be present and it is evidently due to the interference process that they are removed in the larger lattice. Since the quadruple lattice contains more atoms than the present space-group theory allows its relation to this theory is discussed, as well as its relation to the theory of "mixed crystals." This paper is an attempt to elucidate the following sentence from Posnjak and Barth's[1] original paper on ithium ferrite, *viz.*, "Taking into consideration *not too small a portion of the crystal*, an equal number of points is occupied by iron and by lithium." Search should be made for other generalized simple cubic and body-centered cubic lattices as has been done for this generalized face-centered cubic lattice.

[1] Posnjak and Barth, Phys. Rev. **38**, 2237 (1931).

14. The Interpretation of the Red Shift of Extra-Galactic Nebulae. ARTHUR HAAS, *University of Notre Dame.*—The work required for an expansion of the system of nebulae is $q=\frac{1}{3}\pi fR^2\rho\alpha$ in erg/g/sec. (R, radius of system; f, gravitational constant; ρ, mean mass density; $\alpha=1.8\times10^{-17}$ sec.$^{-1}$ or reciprocal of 1700 million years). Hence $q=7\times10^{23}\rho y^2$, where $y=R/R^*$ and R^* ($=5\times10^{28}$ cm) is the largest observed nebular distance. Inserting Hubble's recent value ($\rho=10^{-26}$), we find $q\approx7000y^2$. Since 1 gram cannot produce more energy than 9×10^{20} erg, and the production must last for 1.7×10^9 years, we find that $7000y^2<9\times10^{20}\times\alpha$, or that $y<2$; even for $\rho=10^{-28}$, we find $y<20$. The expansion idea is therefore compatible with the empirical gravitational law only if we assume both that the system of nebulae does not extend much farther than 500 million light years, and that matter is subject to a process of dissolution not much slower than the expansion itself. To avoid the hypothesis of a dissolution, we must either modify Newton's gravitational law or interpret the red shift as a continual energy loss of the photons. In any case we find, irrespective of the value of ρ, agreement between the energy production by the nebulae and the continual diminution of radiant energy traveling in space, since both quantities amount to about 7×10^{-23} erg/cc/sec.

15. Dynamical Effects of Radiation in the Solar System. H. P. ROBERTSON, *Princeton University.*—At the instance of H. N. Russell, the author has reexamined from the standpoint of the theory of relativity the problem, treated by J. H. Poynting and by J. Larmor, of the motion of a small particle in the gravitational field of the sun, on the assumption that the radiation it receives from the sun is reemitted isotropically and at the same rate R. It is found that, in the classical approximation, such a particle suffers a retarding force Rv/c^2 (three times that found by Poynting and one-half of that found by Larmor), where v is its velocity relative to an inertial frame in which the sun is at rest, and c is the velocity of light. The resulting loss of angular momentum causes a secular decrease in the mean distance of the particle from the sun, which for particles of radius up to a few centimeters has the effect of drawing the particles into the sun in astronomically significant times, as predicted by Poynting.

16. Interatomic Distances of the Alkali Halides. L. R. MAXWELL, S. B. HENDRICKS AND V. M. MOSLEY, *Bureau of Chemistry and Soils.*—A determination of the interatomic distances of the alkali halide gas molecules has been made by the electron diffraction method. Heating the salts to a temperature of approximately 1200°C provided a molecular beam of sufficient density to give electron diffraction photographs. Since the molecules were diatomic the nuclear distances were easily obtained from visual measure-

ments of the interference maxima. Data obtained from I_2 and Cl_2 served as a method for calibration of the visual measurements since the internuclear distances for these molecules are well known from band spectra. The interatomic distances for the sodium, potassium and rubidium halides were found to be consistently smaller than the corresponding known distances in the crystal lattice. For the case of the caesium halides the distances obtained were still smaller than the separations found in the crystals. The following table gives the distances measured.

	Interatomic Distance (A)		Interatomic Distance (A)
NaCl	2.51±0.03*	RbCl	2.89±0.02
NaBr	2.64±0.02	RbBr	3.06±0.02
NaI	2.90±0.02	RbI	3.26±0.02
KCl	2.79±0.02	CsCl	3.06±0.03
KBr	2.94±0.03	CsBr	3.14±0.03
KI	3.23±0.04	CsI	3.41±0.03

* Variation given represents the average deviation obtained.

17. Λ-Type Doubling in the $^3\Pi$ State of OH^+. C. N. Challacombe, *University of Illinois.*—A method has been recently developed by Hebb for the calculation of the Λ-type doubling in the $^3\Pi$ states of diatomic molecules intermediate between Hund's cases *a* and *b*. Hebb has applied the method to the $^3\Pi$ state ($v'=6$) of the first positive bands of nitrogen in which the ratio of the molecular constants $A/B=27.9$, and Gilbert has applied the method to the $^3\Pi$ state of PH in which $A/B=-14.4$. It appeared worthwhile to apply Hebb's method to a state with a smaller value of A/B, which would therefore lie more definitely in the transition region, and for which the adequacy of the theory to represent the $^3\Pi$ transition levels could be more rigorously tested. The $^3\Pi$ state of OH^+ ($v'=0$) for which $A/B=-6.19$ is quite suitable for such a calculation. The Λ-type doubling in this state is considerably larger than it is in the two states previously investigated and the experimental data available for comparison with the calculated values are quite complete. The final equation from which the Λ-type doubling is computed contains three adjustable constants. With the values $C_0=-7.85$ cm^{-1}, $C_1=-0.190$ cm^{-1}, $C_2=0.0218$ cm^{-1}, a rather good agreement with the experimental data of Loomis and Brandt was obtained.

18. The Energy Levels of the Asymmetrical Rotator and the Correspondence Principle. Enos E. Witmer, *University of Pennsylvania.*—If *a*, *b*, and *c* are the reciprocals of the principal moments of inertia of an asymmetrical rotator, then the energy according to quantum mechanics[1] may be written

$$E=(h^2/8\pi^2)J(J+1)\{a+(c-a)\tau(s;\,n,\,J)\}, \qquad (1)$$

where $s=(b-c)/(a-c)$.

If $a\geqq b\geqq c$, then $0\leqq s\leqq 1$ and $0\leqq\tau(s;\,n,\,J)\leqq 1$. J and n are the quantum numbers used by Kramers and Ittmann. According to the old quantum theory

$$E=\frac{h^2}{8\pi^2}J^2\left\{a+(c-a)\tau_c\left(s;\frac{n_2}{J}\right)\right\}, \qquad (2)$$

where n_2 is the second quantum number. In the case when the energy levels form close doublets as measured by the difference in $\tau(s;\,n,\,J)$, it is now found that

$$\tau(s;\,n,\,J)\cong\tau_c\left(s;\frac{J+n+(1)}{2[J(J+1)]^{\frac{1}{2}}}\right) \qquad (3)$$

for motions of one class. The (1) in $J+n+(1)$ is used only when $(J+n)$ is odd. Formula (3) holds to a very high degree of approximation even when J is as small as 3. This means that *in the case of close doublets the classical quantum formula gives very accurate results, if J is replaced by $[J(J+1)]^{\frac{1}{2}}$ and n_2 by $\frac{1}{2}[J+n+(1)]$ for motions of one class.* For those of the other class a similar formula holds.

[1] E. E. Witmer, Phys. Rev. **47**, 340 (1935).

19. A Theoretical Test of the Franck-Condon Approximation. Hubert M. James and Albert Sprague Coolidge, *Purdue University and Harvard University.*—It has been shown[1] that there is a marked disagreement between observed intensity distributions in the continuous spectrum of H_2 and the results of a theoretical treatment involving the Franck-Condon principle as the only essential assumption. To check the conclusion that this is due to the failure of the Franck-Condon approximation we have computed the electric dipole moment between the electronic states involved ($1s\sigma 2s\sigma\ ^3\Sigma_g$ and $1s\sigma 2p\sigma\ ^3\Sigma_u$). This required the determination, by variational methods, of potential curves and electronic wave functions of these states for a considerable range of nuclear separation. It was found that the $^3\Sigma_u$ repulsive curve is given to only a poor approximation by the Heitler-London method, even for a nuclear separation of $2.9a_H$. The square of the dipole moment between the states, variation of which measures the error of the Franck-Condon approximation, was found to change by a factor of 10 within the relevant range of nuclear separation in the most favorable case; for ordinary types of excitation a still greater variation comes into account. The correction to the previous computations is of the right sign and order of magnitude. A complete theoretical treatment of this spectrum is under way.

[1] A. S. Coolidge, H. M. James and R. D. Present, J. Chem. Phys. **4**, 193 (1936).

20. On Electron Excitation in Crystals. Gregory H. Wannier, *Princeton University.* (*Introduced by J. C. Slater.*)—If we assume the wave function corresponding to the excitation of an electron in a crystal to be a linear combination of excitation waves

$$\psi=\sum_\beta U_\alpha(\boldsymbol{\beta})\cdot E(\mathbf{K}_\alpha,\,\mathbf{R}_\beta),$$

then $U_\alpha(\boldsymbol{\beta})$ has not the values which correspond to the Bloch picture. Its true value may be found from a study of the energy matrix, because the matrix equation can be approximated by a simple type of differential equation. Most forces which act on the electron or its "hole" have the periodicity of the lattice. Hence their Hamiltonian is a purely differential operator P acting on $U_\alpha(\boldsymbol{\beta})$. One finds

$$P\cdot U(\boldsymbol{\beta})=[e^{-\frac{1}{2}i\mathbf{K}_\alpha\cdot\boldsymbol{\beta}}W_{\text{exc}}(-i\partial/\partial\boldsymbol{\beta})e^{+\frac{1}{2}i\mathbf{K}_\alpha\cdot\boldsymbol{\beta}} - e^{+\frac{1}{2}i\mathbf{K}_\alpha\cdot\boldsymbol{\beta}}W_{\text{ground}}(-i\partial/\partial\boldsymbol{\beta})e^{-\frac{1}{2}i\mathbf{K}_\alpha\cdot\boldsymbol{\beta}}]U(\boldsymbol{\beta}),$$

where the $W_\nu(\mathbf{k})$ are the relations between the energy W and the wave vector $\mathbf{k}$ in the two Bloch bands. The largest

nonperiodic terms in the Hamiltonian arise from the Coulomb attraction between the electron and its hole. The nondiagonal terms are rather small and the diagonal ones are simply $-e^2/|\mathbf{R}_\beta|$. The operators W are symbolic power series, whose first significant term is const $\cdot\nabla^2$. The corresponding differential equation can be solved explicitly. In particular for the optically accessible levels, $\mathbf{K}_\alpha=\mathbf{O}$, it reduces to the Schrödinger equation for the hydrogen atom. We find therefore below the excited energy band a set of discrete states which carry no current. Their energies are approximately

$$E_n=-E_1/n^2,$$

where E_1 is a constant generally smaller than for hydrogen. These states must form the basis for the electrically inactive absorption of many crystals in the near ultraviolet.

21. The Application of the Virial Theorem to Approximate Eigenfunctions. JOSEPH O. HIRSCHFELDER AND JOHN F. KINCAID, *Princeton University.*—The virial theorem, $\bar{V}=-2\bar{T}$, is automatically satisfied if into any approximate molecular eigenfunction a scale factor, s, is introduced and varied to give the lowest energy, as Fock has shown for the atomic case. Here $\bar{V}$ and $\bar{T}$ are the averaged potential and kinetic energies of the system neglecting the motions of the nuclei from their mean positions. Since the scale factor multiplies every distance in the eigenfunctions by s, it follows from dimensional considerations that: $\bar{V}_s=s\bar{V}_{s=1}$ and $\bar{T}_s=s^2\bar{T}_{s=1}$. The total energy, $E=\bar{V}_s+\bar{T}_s$, is least when $s=-\frac{1}{2}\bar{V}_{s=1}/\bar{T}_{s=1}$ and $E_{(\min)}=\frac{1}{2}\bar{V}_s=-\bar{T}_s=-\frac{1}{4}\times\bar{V}^2_{s=1}/\bar{T}_{s=1}$. The Heitler-London eigenfunction for H_2 gives $\frac{1}{2}\bar{V}=-26.49$ ev, $-\bar{T}=-22.79$ ev, and $E=-30.20$ ev. The introduction of the scale factor, $s=1.166$, converts this to the Wang function and gives: $\frac{1}{2}\bar{V}_s=-\bar{T}_s=E_s=-30.83$ ev. The improvement in the total energy is only 0.63 ev while the potential energy changes 8.67 ev and the kinetic energy 8.04 ev. The Coolidge and James function for H_2 nearly satisfies the virial theorem since $\frac{1}{2}\bar{V}=-31.680$ ev, $-\bar{T}=-31.588$ ev, $E=-31.772$ ev. Introducing the scale factor $s=1.0029$ we obtain: $+\frac{1}{2}\bar{V}_s=-\bar{T}_s=E_s=-31.772$ ev. Physical properties proportional to the nth power of some distance are improved by the factor $s^{-n}=(\bar{V}/2\bar{T})^{-n}$ by introducing the scale factor and satisfying the virial theorem.

22. Van der Waals Forces between Helium Atoms. CHESTER H. PAGE, *Yale University.*—The Slater-Kirkwood variation method of calculating van der Waals energy has been extended to include the dipole-quadrupole interaction. The variation function used is $\psi=\psi_0(1+\lambda v e^{\beta R})$, where ψ_0 is the wave function of a normal helium atom, R the sum of the distances of the electrons from their proper nuclei, λ and β variation parameters, and v the interaction perturbation, taking only the dipole-dipole and dipole-quadrupole terms in the Taylor expansion of the classical mutual potential of the two atoms. Using $\psi_0=(r_1r_2)^{n-1}e^{-(s'/n)(r_1+r_2)}$, we find at a separation of 2.9A, that for $n=1$, $s'=1.6875$, the dipole-quadrupole energy is 13 percent of the dipole-dipole energy, as against the 26 percent found by Margenau, by an approximate second order perturbation method. For $n=0.75$, $s'=1$, we obtain correspondingly 26 percent against Margenau's estimated 32 percent. The method is being further extended, by using the complete perturbation function in closed form, instead of the first terms of the series expansion.

23. The Distortion of a Closed Shell due to Crystallic Fields. VIVIAN A. JOHNSON AND L. W. NORDHEIM, *Purdue University.*—The intensities of the electron diffraction pattern in zinc oxide show systematic anomalies as compared with the corresponding intensities of the x-ray diffraction pattern.[1] For explanation of these anomalies selective absorption, anisotropic heat motion or dynamical reflection has been suggested. The observed intensities have been formally accounted for by assuming a polarization of the M shell of the Zn atoms.[1] Such a distortion might be due to the electrostatic fields arising from a partly ionic character of the lattice and its deviation from perfect tetrahedral symmetry. To test this hypothesis we have worked out the changes in charge distribution of the M shell in zinc due to fields of linear or tetrahedral symmetry. Following a suggestion of Bethe the distorted wave functions have been obtained by numerical integration. The Thomas-Fermi potential was used to obtain the unperturbed wave functions. The possible magnitude of the internal electrostatic field has been estimated by computing the corresponding terms of lattice potentials for an ionic lattice. The distortion calculated under these assumptions is too small by a factor of about 1/30 to account alone for the observed anomalies, and some of the other effects, mentioned above, will have to be considered.

[1] K. Lark-Horovitz, H. J. Yearian, Phys. Rev. **42**, 905 (1932); H. J. Yearian, Phys. Rev. **48**, 631 (1935).

24. On the Electronic Constitution of Diamond. DOUGLAS H. EWING, *The University of Rochester.*—A self-consistent field for diamond is being constructed, following the method of Wigner and Seitz, and some preliminary results are described. This problem has already been attacked by Kimball,[1] but no anisotropy of charge density was displayed in his approximation. The approximation used in the present case employs more terms in the expansion of wave functions in terms of surface harmonics and leads to anisotropy. Plots of the charge distribution in different crystallographic directions are shown and the degree of concentration of charge in the classical bond direction discussed.

[1] Kimball, J. Chem. Phys. **3**, 560 (1935).

25. The Lattice Energy of Solid CO_2. H. SPONER AND M. BRUCH-WILLSTÄTTER, *Duke University.*—Carbon dioxide crystallizes at very low temperatures in a cubic face-centered lattice. For the calculation of its energy a two-center model has been used for the single linear and long shaped CO_2 molecules by assuming that the O atoms contribute mostly to the polarizability; furthermore that the polarizability of the two centers should not be located in the nucleus of the O atoms but should be somewhat shifted toward the C atom. The simple London theory of van der Waals forces is applied to this model. Different assumptions about the location of the polarizabilities have

been discussed and values of 5–6.6 kcal./mole, respectively, are obtained for the sublimation heat of solid CO_2. The experimental value is 6.44 kcal./mole. For a more accurate calculation the second approximation of van der Waals forces (Margenau's formula), electrostatic forces due to compensated dipoles in the CO_2 molecules and the repulsive forces have been considered. The charge distribution seems to be better represented with a model of point charges with definite distances than with the ordinary picture of short dipoles. The repulsive forces could be treated only in a rough way. Discussion shows, however, that one can account theoretically for the observed value.

26. Analytic Wave Functions for Nuclear and Atomic Collision Problems. PHILIP M. MORSE, *Massachusetts Institute of Technology.*—The wave function $\sin(kr+\delta) - \exp(-\alpha r)\sin(\delta)\cos(kr)$ is a good approximation to the $l=0$ continuous wave function for a centrally symmetric field, as long as the phase angle δ is less than 180 degrees. The parameters α and δ can be determined by a variational method, minimizing the average value of $(H-k^2)^2$. However, it is found that the ratio between α and the scale factor for any chosen potential field can be fixed, and the phase angle δ can be obtained for different values of k by setting the average value of $(H-k^2)$ equal to zero, a much simpler process. Such a procedure, used with the two fields $D\exp(-2\beta r) - 2D\exp(-\beta r)$ and $(Z/r)\exp(-\beta r)$, gave values of δ within a few degrees of the exact values, over the range of k from zero to two. The above wave function is useful in calculations of inelastic and exchange collision cross sections, giving much more accurate results than the Born approximation, which assumes δ to be zero. The function can also be modified to include approximately the polarization of the target atom.

27. Low Energy Collision of Neutron and Deuteron. L. I. SCHIFF, *Massachusetts Institute of Technology.*—The elastic scattering of neutrons by deuterons is considered theoretically for energies so small that only the $l=0$ part of the incident neutron beam is different from the corresponding part of a plane wave. An iteration method is employed using the same mixed Majorana-Heisenberg interaction between all pairs of particles. For the zero approximation wave-function which goes into the iteration integral, a form is used which has one variable parameter, the phase shift at infinity, which is fitted to an average deuteron field. This form takes into account the distortion of the $l=0$ part of the neutron wave near the deuteron, and gives the correct order of magnitude for the low energy elastic scattering cross section. The same form also gives very close to the correct $l=0$ phase shift for the neutron-proton collision over a wide range of energies. The iteration process serves to improve on this by taking account of the exchange nature of the forces and of ejection of the originally bound neutron with capture of the incident neutron. The same approximate wave-function can be used to compute the magnetic dipole capture cross section at low energies.

28. Variational Calculations on the Nuclear Three and Four Body Problem. HENRY MARGENAU AND DANA T. WARREN, *Yale University.*—The present method has the following advantages: (1) It can be used with potentials of the form Ae^{-r^2/a^2}, for which the constants are best known, (2) It is applicable to the four body problem, (3) The functions used form a complete set, and the results must converge to the true value. The method consists in expressing the relative coordinates of the particles in terms of the minimum number of independent coordinates. Simple harmonic oscillator functions in these coordinates are added systematically, the lowest one giving the exponential function of Feenberg and Bethe and Bacher. Thus completeness is assured, and the orthogonality of the functions limits the energy in the secular determinant to the diagonal elements, permitting very simple solution by successive approximations. This method has been thoroughly studied in the case of the deuteron. The constants $A=35.60$ MV, $a=2.25\times10^{-13}$ cm, $g=0.20$ are adopted. The use of ten functions for H^3 gives 7.21 MV for the binding energy (experimental value 8.3 MV).

29. Perturbation Theory of Light Nuclei: O^{16}. W. J. KROEGER AND D. R. INGLIS, *University of Pittsburgh.*—The limitations of the perturbation method of calculating nuclear properties, starting with independent particles in a central field,[1] come into evidence in a calculation of the binding energy of O^{16}. It is found that the third-order contributions of the doubly excited states are about as great as their second-order contributions. The convergence is thus not rapid enough to make a reasonably complete calculation practicable, contrary to the case[1] in Li^6. This difference appears in the calculation most prominently in factors of the type $H_{22}'-H_{00}'$, which occur in the third-order energy and increase in magnitude with increasing atomic number.

[1] Inglis, Phys. Rev., April 1, 1937; and first-order calculations by Heisenberg, Zeits. f. Physik **96**, 473 (1935); Bethe and Bacher, Rev. Mod. Phys. **8**, 82 (1936); Feenberg and Wigner, Phys. Rev. **51**, 95 (1937); Rose and Bethe, Phys. Rev. **51**, 205 (1937).

30. Depolarization by Neutron Proton Scattering. JULIAN SCHWINGER AND I. I. RABI, *Columbia University.*—The production of neutrons which are preferentially polarized in some given direction has been demonstrated by recent experiments. We wish to point out that these neutrons may be used to study spin dependent nuclear forces. If a stream of neutrons of average polarization σ_n is scattered by hydrogen it can be shown that the resultant polarization of the scattered neutrons after a single collision is given by

$$\sigma_n' = \left(1 - \frac{(a_1-a_0)^2}{3a_1^2+a_0^2}\right)\sigma_n.$$

The quantities a_1 and a_0 are connected with the phase shifts of the triplet and singlet scattered waves, respectively, by

$$a_{1,0} = \sin\delta_{1,0}/k.$$

The ratio a_0/a_1 depends upon the range of the nuclear forces. The sign of this ratio is positive if the singlet state

is real, negative if virtual. It is apparent that a measure of the depolarization gives important information about the nuclear forces. For example, an assumed range of $2\cdot10^{-13}$ cm gives $a_0/a_1=\pm3.41$ for slow neutrons. The upper sign gives $\sigma_n'=0.60\sigma_n$ whereas the lower sign yields $\sigma_n'=-0.33\sigma_n$.

31. Fluctuations in Radiative Energy Loss and Range of Fast Particles. W. H. FURRY, *Harvard University.*—If, as is indicated by recent experiments of Anderson and Neddermeyer, the Bethe-Heitler formula gives a correct description of the radiative losses of high energy electrons, then the fluctuations in these losses should be very great. For the case of absorption in lead, the ionization loss can reasonably be treated as simply proportional to the thickness, and applied as a correction at the end of the calculation. When this is done, the partial differentio-integral equation for the distribution in energy as a function of the thickness traversed can be solved without serious modification. The distribution curves are given with remarkably high accuracy by the saddle-point method. Results so far obtained are insufficient for the determination of mean ranges; it is already evident that the *median* ranges for various energies are markedly less than the "ranges" calculated from a simple differential equation, $dE/dx=-kE-\beta$, in which the mean radiative loss is used, but that the fluctuations are extremely large. Complete sets of curves for both energy loss and range will be shown.

32. Disintegrations of Very Heavy Nuclei by Deuterons. H. A. BETHE, *Cornell University.*—When deuterons interact with very heavy nuclei ($A\approx200$), the most probable primary processes are the emission of a neutron and a proton. The latter process follows the Oppenheimer-Phillips mechanism, the former the ordinary Bohr mechanism. The emission of protons or α-particles in the ordinary mechanism is very improbable because the number of possible states of the final nucleus is smaller than for neutron emission by a factor of about 100,000. Neutron emission and Oppenheimer-Phillips process should be about equally probable. The emitted neutron will have a kinetic energy of about 1 MV (nuclear temperature), the proton about half that of the incident deuteron. The residual nucleus is therefore left with an excitation energy of about 7 and 5 MV, respectively. Since even the ground state of heavy nuclei is energetically unstable against α-emission with about 4 MV, the residual nucleus will be able to emit α-particles. This process should be somewhat more probable than γ-emission for 7 MV excitation, somewhat less for 5 MV. Therefore the nuclei formed in the dn process will ordinarily, those formed in the dp process occasionally, disintegrate further with α-emission. The most probable processes with heavy nuclei are thus (approximately in order of their probability)

$$Z^A+H^2=Z^{A+1}+H^1, \qquad \text{I}$$
$$Z^A+H^2=(Z-1)^{A-3}+He^4+n^1, \qquad \text{II}$$
$$Z^A+H^2=(Z-2)^{A-3}+He^4+H^2, \qquad \text{III}$$
$$Z^A+H^2=(Z+1)^{A+1}+n^1. \qquad \text{IV}$$

Experimental evidence for process III was obtained by Cork and Thornton, for II by Cork and Lawrence; IV has not yet been observed.

33. The Evaporation Model of Nuclear Disintegrations. E. J. KONOPINSKI* AND H. A. BETHE, *Cornell University.*—The evaporation picture of nuclear disintegrations makes it possible to express the disintegration probability or "level width" of a compound nucleus in terms of its formation probability. This contains, besides certain known factors, a quantity ξ which expresses the "sticking probability" of a particle to a nucleus it strikes. ξ is expected to be unity for high excitations; for low excitations, its magnitude can be estimated from neutron experiments which gives the ratio of level width to spacing, Γ_n/D. The values of ξ thus obtained range from 0.01 to 0.7. A more detailed theoretical discussion of the evaporation will be made in terms of the interference of elastic waves in the nuclear liquid. When the expression for the average Γ_n/D in terms of ξ is introduced into the dispersion formula, for the probability of nuclear disintegrations, the result is gratifyingly simple: $\sigma=\pi R^2\xi(\Gamma_{BQ}/\Gamma)$. Thus the cross section for the disintegration of a compound nucleus into parts B and Q is given by the product of its formation cross section $\pi R^2\xi$ and of the probability of the disintegration mode BQ, in competition with the total possibilities, Γ.

* National Research Fellow.

34. The Magnetic Moment of the Proton. I. ESTERMANN, O. C. SIMPSON, AND O. STERN, *Carnegie Institute of Technology.*—The magnetic deflections of H_2 and HD molecules have been measured at room temperature and at 90°K. The deflection $S_\alpha^p(90°K)$, i.e., the deflection of a molecule having the most probable velocity α corresponding to 90°K and the magnetic moment of one proton, is calculated from these measurements. The results are given in the table.

	T	$S_\alpha^p(90°K)$
H_2	90°	7.52 mm/100
HD	90°	7.50 mm/100
H_2	291°	7.52$_5$ mm/100
HD	291°	7.82 mm/100

Each value of S_α^p represents the average of a large series of measurements agreeing within a few percent, except for the value for HD at 291°K which we did not attempt to measure with the same accuracy on account of the small deflection and the large number of rotational quantum states. The error in the mean value $\overline{S_\alpha^p}(90°K)=7.52$ mm/100 should be appreciably less than one percent. With the dimensions of our apparatus and a preliminary value of the inhomogeneity of the magnetic field, the above value of S_α^p gives a proton moment of about 2.6 nuclear magnetons. Our first measurements** gave 2.5±10 percent.

* R. Frisch and O. Stern, Zeits. f. Physik **85**, 4 (1933).
** I. Estermann and O. Stern, Zeits. f. Physik **85**, 17 (1933).

35. A New Method for the Measurement of the Bohr Magneton. O. STERN, *Carnegie Institute of Technology.*—The free fall of molecules could be measured by producing a long horizontal beam. In the case of magnetic atoms the force of gravity can be compensated for a part of the atoms by an inhomogeneous magnetic field. This field may be produced by the current I in a wire parallel to the beam and situated below it in the distance r. Exact cancellation of the two forces takes place if $mg=\mu_0(dH/dr)_0=\mu_0(2I_0/r^2)$.

If $I<I_0$ all atoms are deflected downward, if $I>I_0$ a part of the atoms is deflected upward. Thus I_0 can be determined by placing the detector above the "straight" beam and increasing I until we receive atoms. In this way we can measure μ_0, that is, $N\mu_0=(Mg/2I_0)r^2$. The magnetic splitting in many beams due to the nuclear moment does not matter because the most strongly deflected atoms have always one Bohr magneton.

36. The Reflection of Radio Waves in the Troposphere. R. C. COLWELL AND A. W. FRIEND, *West Virginia University.*—For the last year, daily measurements have been made of the *C* region in the troposphere. The height of the region and the polarization of radio waves reflected from it were recorded. At the same time observations were made upon the signal strength of nearby broadcasting stations, and the skip distance on short wave stations. These were correlated with the barometric pressure and other weather conditions. As a general rule, when the barometer is high, the *C* region is low and *vice versa*. The change in height affects the skip distance.

37. Variations of Cosmic Rays with Latitude on the Pacific Ocean. A. H. COMPTON, *University of Chicago* AND R. N. TURNER, *Canadian-Australasian Steamship Co.*—A series of 12 continuous measurements of the cosmic-ray ionization have been completed between Vancouver, Canada and Sydney, Australia, via Honolulu, Suva, and Auckland, with a Carnegie Model C meter. The repeated measurements give a higher precision than heretofore attainable in such work, and afford a basis for estimating the probable errors involved. The shape of the latitude effect curve is unsymmetrical with respect to the equator, and the latitudes at which the breaks in the curve occur differ in the two hemispheres.

38. The Influence of the Earth's Magnetic Field on Cosmic-Ray Intensities up to the Top of the Atmosphere. I. S. BOWEN, R. A. MILLIKAN AND H. V. NEHER, *California Institute of Technology.*—Measurement on cosmic-ray intensities like those made in July 1936 at San Antonio, Texas, and already published,[1] have now been made with equal accuracy in Madras, India. A comparison of the two resulting curves and that earlier obtained in the Fordney-Settle flight makes it possible for the first time to determine experimentally the complete law of absorption of electrons going through the atmosphere in two different ranges of energy, namely, from 2.5×10^9 Mev to 6×10^8 Mev, and from 6×10^8 Mev to 17×10^8 Mev. A law not greatly different from the Bethe-Heitler law as extended by Carlson and Oppenheimer[2] is found to reproduce reasonably well the observed findings.

[1] Phys. Rev. **50**, 992–998 (1936).
[2] Phys. Rev. **51**, 220 (1937).

39. On Diurnal Variation in Cosmic-Ray Intensity. S. E. FORBUSH, *Department of Terrestrial Magnetism, Carnegie Institution of Washington.*—Continuous cosmic-ray intensity data for some 360 complete days as recorded at the Cheltenham Magnetic Observatory of the United States Coast and Geodetic Survey are subjected to statistical analysis. Cheltenham is one of the world net of cosmic-ray recording stations established by the Carnegie Institution of Washington. The precision cosmic-ray meter used is after the design for the Institution by Compton, Wollan, and Bennett. The results indicate that the real barometric coefficient does not change from hour to hour or from month to month. The barometric coefficient obtained at this station is in good agreement with that indicated by certain altitude-intensity curves. The effect of external air-temperature upon the intensity, reported by some observers, has been examined by two independent statistical methods, both of which indicate that no such effect exists at Cheltenham. Finally, the data have been subjected to modern statistical methods which provide an objective measure for the probability that the observed diurnal-variation is real. The results indicate, for the period covered by this analysis, a physically significant 24-hour wave in apparent cosmic-ray intensity, with an amplitude of 0.17 percent of the total intensity, having its maximum at about 11^h, 75° west meridian mean time.

40. Penetrating Corpuscular Component of the Cosmic Radiation. J. C. STREET AND E. C. STEVENSON, *Harvard University.*—The confirmation of the validity of the Heitler theory of radiation and pair formation both by energy loss measurements[1] and by the nature of shower formation[2, 3] leaves no explanation for the penetrating corpuscular rays except to assume that they are protons. However, the evidence against protons is strong.[4] To investigate the penetrating rays a vertical column was set up as follows: a counter, 10 cm Pb, a second counter, a cloud chamber in a magnetic field, a third and fourth counter, 3 cm Pb, and finally a cloud chamber containing 3 separated lead plates 1 cm thick. The counter telescope selected particles directed toward the visible region of the lower chamber where their absorption and shower production was observed. The distribution of the particles with respect to range and $H\rho$ values was as follows:

$H\rho\times10^{-4}$	% OF TOTAL TRACKS	FRACTION WITH RANGE >3 cm Pb	FRACTION WITH RANGE >6 cm Pb
> 5	49	1	1
2.5 to 5	19	.9	.7
1.5 to 2.5	23	.9	.7
0.7 to 1.5	9	.7	.3

Only a single shower has been observed in 500 traversals of 1 cm of lead. The ionization density of protons with $H\rho<2.5\times10^6$ distinguishes them, and two were observed. From the data in the table it is evident that the penetrating particles cannot be described as electrons obeying the Heitler theory nor can an appreciable fraction be protons.

[1] Anderson and Neddermeyer, Phys. Rev. **50**, 263 (1936).
[2] Carlson and Oppenheimer, Phys. Rev. **51**, 220 (1937).
[3] L. Fussell, Jr., Abstract—Present meeting.
[4] C. G. and D. D. Montgomery, Phys. Rev. **50**, 975 (1936).

41. Production and Absorption of Cosmic-Ray Showers. L. FUSSELL, JR., *Massachusetts Institute of Technology and Harvard University.* (*Introduced by J. C. Street.*)—Cosmic-ray shower photographs taken with a large counter-controlled Wilson chamber[1] in which were mounted three horizontal lead scattering plates (0.63, 0.63 and 0.07 cm

thick, from top to bottom, respectively, at a spacing of 6 cm) show that most showers develop and multiply in several successive steps. In the very thin plate pairs are frequently created, but the formation of larger groups has never been observed. Thus the recognized divergence of showers from a point in the bottom millimeter of a thick plate (0.5 cm or more) is misleading. The observations give strong support to the radiation, pair-formation theory of showers[2, 3] and show that complex showers are not developed at a single point except in rare cases. Three photographs out of nine hundred show showers of this type, different in that dense tracks and numerous thin ones are involved, and the appearance is such that the assumption of divergence from a single point well inside the lead can hardly be avoided. With no selecting counter above the chamber, 0.36 of the ordinary showers produced in the top plate seem to be due to electrons, the rest to nonionizing radiation. The average number of particles increases by a factor 1.7 in passing through the second plate.

[1] J. C. Street and E. C. Stevenson, Rev. Sci. Inst. **7**, 347 (1936).
[2] Heitler and Bhabha, Nature **137**, 401 (1936).
[3] J. F. Carlson and J. R. Oppenheimer, Phys. Rev. **51**, 220 (1937).

42. The Absorption of Cosmic Rays in the Atmosphere. L. W. NORDHEIM, *Purdue University.*—The recently developed laws of energy degradation of electrons and photons[1] are applied to the problem of the absorption of the cosmic rays in the atmosphere. Making allowance for a "hard component" of a nature different from electrons (necessary to account for the geomagnetic effect at sea level and the penetration into thick layers of heavy material) all other effects can be explained satisfactorily by identifying the "soft component" with electrons and photons which behave according to theory. A primary distribution of electrons can be found which gives the Regener absorption curve in the atmosphere, the geomagnetic effect at higher altitudes, the dependence of showers on latitude and altitude. The distribution of electron energies comes out to be nearly independent of altitude between sea level and ~5000 m. This explains why the Rossi transition curves and the relative occurrence of showers of different size are nearly independent of altitude in this range. On the other hand it seems to be impossible to fit the facts with the assumption of a break down of the theory at very high energies and to identify the "hard component" with electrons which are too energetic to radiate because of such a break down.

[1] Carlson and Oppenheimer, Phys. Rev. **51**, 220 (1937); Bhabha and Heitler, Proc. Roy. Soc. **A159**, 432 (1937).

43. Cosmic-Ray Showers from Lead Plates. ROBERT B. BRODE AND MERLE A. STARR, *University of California.*—Eight thousand counter tripped photographs have been taken of showers produced in lead plates of thickness 1.5, 4, 6.5, 9 and 16.5 mm placed in a Wilson cloud chamber. The sea-level cosmic-radiation passed through an equivalent of 10 mm of lead before reaching the lead plates. The number of pairs of electrons below the plate in the chamber produced by a charged particle entering from above rose rapidly with the thickness of the plate to a maximum at 5 mm and then fell to a nearly constant value for thickness greater than 9 mm. The number of pairo elects frons produced by photons was about equal to the number produced by charged particles and the thickness for the maximum number was about 5 mm. The optimum thickness for the production of 3 particles was about 6 mm. The probability of producing 5 or more particles from either a charged particle or a photon increases with the thickness without a maximum in the range of plates used in these experiments. The observed thickness for the maximum pair production in lead is in good agreement with the theoretical estimate made by Carlson and Oppenheimer.[1] A number of interesting showers have been observed and several cases of disintegration in which high energy heavy particles were ejected.

[1] Phys. Rev. **51**, 220 (1937).

44. Effect of Galactic Rotation upon the Intensity of Cosmic Radiation. W. F. G. SWANN, *Bartol Research Foundation of The Franklin Institute.*—The paper presents a mathematical theory of dependence of cosmic-ray intensity upon galactic rotation, discussed by A. H. Compton and I. A. Getting. The formulae obtained by Compton and Getting for neutral particles are deduced by processes closely analogous to the processes used by those authors. It is shown, however, that the extension to charged particles may be formulated in a manner which makes use of the modified form of Liouville's dynamical theorem, which has been found successful in other cosmic-ray problems, and the result is that the intensity at any point on the earth's surface is expressed in simple manner in terms of the direction of the orbit of the charged particle when traced back to infinity. Attention is called to the modification demanded by the theory of relativity in the intuitive picture of the phenomenon. The simple naive picture of what happens visions a stream of charged particles with the earth moving, for example, towards them. In this picture there is the alteration of relative velocity produced by the earth's motion, which is responsible for the change of intensity. The theory of relativity demands, however, a picture in which there is no alteration of relative velocity by the earth's motion, but where there is a change of particle density which conspires to produce a result the equivalent of that produced by change of relative velocity in the simple picture.

45. The Shadow Effect of Cosmic Radiation and Some Associated General Dynamical Theorems. E. J. SCHREMP, *Massachusetts Institute of Technology.*—Lemaitre and Vallarta have shown[1] that the cosmic-ray allowed cone is generated in part by orbits tangent to the earth's surface prior to their arrival at a given point of observation. A study of this class of orbits with Bush's differential analyzer has led to the formulation of certain general theorems concerning this nonintegrable dynamical problem: When $0.78856 < \gamma_1 < 1$,[2] there exist two principal periodic orbits, between which all re-entrant orbits cross the equator within a definite pencil of directions. Since these orbits are either periodic or come indirectly from infinity, all orbits arriving at a given point come from infinity, except those blocked by the earth and the totality of periodic

orbits, which form a set of zero measure. The determination of the penumbral regions thus reduces to the shadow effect of re-entrant orbits. Since the principal periodic orbits vanish together when $\gamma_1=0.78856$, all re-entrant orbits, and in particular all periodic orbits, vanish with them. Thus when $\gamma_1<0.78856$, all orbits come directly from infinity, and there is no penumbra. By a similar theorem, for all points of observation and a given energy, there is a maximum $\gamma_1\leqq 1$ beyond which no penumbral allowed directions exist.

[1] G. Lemaitre and M. S. Vallarta, Phys. Rev. **50**, 493 (1936).
[2] For the definition of the parameter γ_1, cf. reference 1.

46. The Electric Spectrum of Liquid Water from Five to Twenty Centimeters. HENRY W. KNERR, *Pennsylvania State College*.—Continuous electromagnetic radiation with wave-lengths ranging from five to twenty centimeters was produced by a magnetron generator. Nineteen different wave-lengths in this region were used in the measurement of refractive index and absorption index of liquid water. A free wave method and a wire wave method suggested by the experiments of Seeberger* were set up and studied. The wire wave method gave surprisingly consistent results for this difficult region of the spectrum. A good agreement was secured between results obtained by the two methods. The details of these methods will appear in an early publication. No evidence of dispersion was found in this region, the refractive index at 22°C being 8.79 with no observation deviating more than 0.8 percent from the mean. This value is about 1.5 percent smaller than the value for long radio waves but shows no tendency to decrease toward infrared values. The absorption index increased steadily from 0.048 at 20.44 cm to 0.153 at 4.80 cm. The relaxation time was calculated from the Debye theory and found to be of the order of 7×10^{-12} sec.

* M. Seeberger, Ann. der Physik (5) **16**, 77 (1933).

47. The Isotopic Constitution of Mercury and Lead. ALFRED O. NIER,* *Harvard University*.—A new magnetic mass-spectrograph has been constructed for the purpose of making accurate determinations of the relative abundance of isotopes. The high intensity and high resolving power of the apparatus allow the search for rare isotopes to be extended beyond previously attainable limits. An investigation showed mercury to consist of the isotopes 204, 202, 201, 200, 199, 198, and 196 present in abundances proportional to the numbers 22.7, 100, 44.6, 78.7, 57.6, 34.2, and 0.50, respectively. The following upper limits can be set for other isotopes: Hg^{206} and Hg^{205}, 1/4000 of Hg^{204}; Hg^{203}, 1/5000 of Hg^{202}; Hg^{197}, 1/40 of Hg^{196}; Hg^{195} and Hg^{194}, 1/100 of Hg^{196}. A sample of ordinary lead kindly provided by Dr. v. Grosse was found to consist of the isotopes 208, 207, 206 and 204. Exact values of the isotope abundances will be published after additional data have been taken on ordinary lead from different sources and geographical locations. A search for Pb^{210}, Pb^{209}, Pb^{205} and Pb^{203} showed that if these isotopes exist at all it must be in amounts less than 1/100, 1/1000, 1/3, and 1/20, respectively, of the abundances given for them by Aston.

* National Research Fellow.

48. Separation of Isotopes by Diffusion. RUBBY SHERR, *Princeton University*.—Further investigations have been carried out on the system of diffusion pumps reported last year. A modification of Hertz' design was made in the construction of additional pumps in an attempt to obtain a mercury vapor jet more conducive to separation. Tests on eight new pumps gave a separation factor as high as 40 for a mixture of CO_2-A, for an initial ratio CO_2/A of 1/10. Calibration tests on the composite system of 29 pumps indicate a factor of 144 for the neon isotopes, the yield from 100 cc being 1.5 cc containing about 80 percent Ne^{22}, the system coming to equilibrium within 10 hours. Preliminary runs on methane indicate a factor of 13, the yield being 1.5 cc containing between 5 and 5.5 percent $C^{13}H_4$. By using a larger reservoir at the "light" end or by renewing the gas in order to keep the concentration up to its initial value, one can expect an enriched concentration of 12 percent.

49. The Products of Dissociation of Benzene Vapor by Electron Impact. P. KUSCH, J. T. TATE, AND A. HUSTRULID, *University of Minnesota*.—The dissociation of benzene vapor by electron impact has been investigated on a mass-spectrograph. At an electron energy of 75 volts the ions which have been identified and their intensities relative to the ion $C_6H_6^+$ as 100 are as follows: $C_6H_6^+$, 100; $C_6H_5^+$, 17; $C_6H_4^+$, 5; $C_6H_3^+$, 2; $C_6H_2^+$, 4; C_6H^+, 1.3; C_6^+, 0.25; $C_5H_3^+$, 2.5; $C_5H_2^+$, 0.6; C_5H^+, 0.5; C_5^+, 0.02; $C_4H_4^+$, 13; $C_4H_3^+$, 15; $C_4H_2^+$, 12; C_4H^+, 2; C_4^+, 0.3; $C_3H_3^+$, 6.7; $C_3H_2^+$, 3; C_3H^+, 2.5; C_3^+, 0.3; $C_2H_2^+$, 1.4; $C_2H_2^+$, 1.2; C_2H^+, 0.15; C_2^+, 0.03; CH_3^+, 0.2; CH_2^+, 0.02; CH^+, 0.03; C^+, 0.05; H_2^+; H^+; $C_6H_6^{++}$, 3.3; $C_6H_6^{++}$, 0.4; $C_6H_4^{++}$; $C_6H_3^{++}$, 0.9; $C_6H_2^{++}$; C_6H^{++}, 0.01. Some of these ions appear as doublets whose components have a constant energy separation independent of magnetic field. The components of these doublets have different appearance potentials. This would seem to indicate that these ions may be formed by either of two processes, one of which imparts considerable kinetic energy to the ions. Appearance potentials of some of the ions have been obtained.

50. Stark Effect in Argon and Krypton. J. S. FOSTER AND C. A. HORTON, *McGill University*. (*Introduced by Professor G. B. Pegram.*)—In a field of 100 kv/cm Stark effects have been observed for 86 normal levels in argon and for 75 in krypton. It has been found that the number of Stark levels is never greater than the number of $\pm m$ values allowed by the j-value of the term. The reversal of the direction of displacement of several terms in both gases with increasing field is discussed. Typical sections of the energy level diagrams for Ne, A, Kr, and Xe are drawn to represent the normal levels and their Stark effects. These diagrams serve as a basis for the qualitative explanation of the main features observed. Several lines in the arc spectra of argon and krypton are identified by their Stark effects. Certain corrections to the earlier work of Ryde are suggested. The full paper will appear shortly.

51. Shot Effect of Secondary Electron Currents from Nickel and Beryllium. BERNHARD KURRELMEYER, *Brooklyn College* AND LUCY J. HAYNER, *Columbia University*.—The

study of secondary emission shot effects of oxide-coated surfaces* has been extended to clean nickel and beryllium. The nickel was commercial sheet, the beryllium a thick layer evaporated in high vacuum. The tubes were cylindrical triodes having axial tungsten filaments. The ratio of plate (emitter) to grid (collector) voltage was kept constant. The shot effects were measured at 110 kilocycles, using temperature-limited shot effects as standards. The maximum primary energy was 1600 volts, well beyond the maximum of the secondary emission curves for both metals. The maximum secondary-primary ratios observed were 1.3 (nickel) and 4.4 (beryllium). For both metals the secondary shot effects increase continuously with the primary energy. In terms of the shot effect of equal temperature-limited currents, the secondary shot-effect values were about 3.2 (nickel) and 7.2 (beryllium) at their respective maximum secondary emissions, or 3.9 and 9.3 at 1600 volts primary energy. These results will be interpreted in terms of absorption and scattering of primary and secondary electrons within the metal. This work was done during the summers of 1935 and 1936 at the University of Michigan.

* L. J. Hayner, Physics **6**, 323 (1935).

52. Secondary Emission from Clean Tungsten. EDWARD COOMES, *Massachusetts Institute of Technology*. (*Introduced by W. B. Nottingham.*)—The secondary electron emission from clean tungsten has been investigated over an energy range for primary electrons of 50 to 2000 volts. Measurements were taken on a sealed-off tube. The primary beam was supplied by an electron gun of the cathode ray tube type; the beam was passed through slits and brought to focus on the target by means of an electrostatic lens. A slight deflection by a magnetic field allowed the visual observation of the position of the primary beam on a fluorescent screen placed immediately behind the target; during actual measurements the beam could be so well focused that the screen current was generally less than 0.1 percent of the primary current. The metal parts were constructed of tantalum, which allowed thorough outgassing. The target consisted of a tungsten ribbon, which was cleaned by long period heating at 1800°K and flashing at 2600°K. The ratio of secondary to primary current as a function of primary voltage mounts from 0.53 at 50 volts to a flat maximum of 1.28 at 475 volts; it slowly falls to unity at 1325 volts and reaches a value of 0.93 at 2000 volts. All measurements were taken with a cold target, and tests for reproducibility were carried out over a 48-hour period after flashing. No changes in the secondary emission characteristic were observed. An increase in secondary emission has been observed when thorium is evaporated onto the clean tungsten.

53. Electrical and Luminescence Properties of Willemite Screen Material. W. B. NOTTINGHAM, *Massachusetts Institute of Technology*.—A willemite screen was deposited on a glass surface containing two embedded fernico wires. With the fluorescence excited by an electron beam focused to cover the plate, the surface potential, resistivity and luminous output were determined. The surface potential of the screen differed very little from that of the anode for potentials below about 6000 volts depending on the particular sample. With anode voltages higher than this, the screen potential relative to the cathode tended to hold at a fixed value determined by the highest primary electron voltage for which one secondary electron was produced for each primary arriving at the screen. Up to this voltage, using a constant current to the screen, the light output was represented by $L=Q(V-V_0)^2$, where L is the phototube current, Q a constant nearly proportional to the beam current and V_0 the dead voltage which depends on the particular sample. The range of V_0 observed was from nearly zero to about 400 volts. The surface resistivity of the phosphor determined for one sample was approximately 300 megohms assuming the resistance of the sample studied was proportional to the distance between the fernico wires and inversely proportional to the lengths of the wires in contact with the phosphor.

54. Propagation of Potential in Discharge Tubes. L. B. SNODDY, J. R. DIETRICH AND J. W. BEAMS, *University of Virginia*.—The determination of the speed of propagation of potential waves in long discharge tubes has been continued using essentially the same type of apparatus as that previously described.[1, 2] Average speeds over an 8.5 meter section of a 16 meter tube have been determined for three tubes (internal diameter 1.7, 5 and 18 mm. Pressure range 0.02 mm to 5 mm. 125 kv impulse). With each tube the speed increases rapidly in the pressure range from 0.02 mm to about 0.2 mm. At higher pressures the rate of increase is much slower. The speed increases with increasing tube diameter at constant voltage and pressure. At 0.8 mm pressure the values are 24×10^3, 32×10^3 and 46×10^3 cm/sec. for diameters of 1.7, 5, and 18 mm respectively. The speed for negative impulses is approximately twice that for positive (measured only for 18 mm tube). The speed as a function of voltage at constant pressure (0.4 mm) is approximately linear in the voltage range from 70 kv to 190 kv. Dry air was used for all determinations.

[1] Phys. Rev. **50**, 469 (1936).
[2] Phys. Rev. **50**, 1094A (1936).

55. Recombination in the Afterglow of a Discharge. FRED L. MOHLER, *National Bureau of Standards*.—A discharge of 6 amperes or less through a 500 cm³ bulb with electrodes in side tubes was extinguished by short-circuiting with a motor-driven commutator, and electrical measurements were made of the number of ions per cm³ near the center of the bulb and the flow of current to the walls at time intervals ranging from 5×10^{-4} to 6×10^{-3} seconds after the cut-off. The change in the number of ions in the bulb in a given time interval is equal to the number flowing to the walls plus the number recombining in the space. Hence one derives the recombination coefficient, α, defined by the relation dn/dt (recombination) $=-\alpha n^2$ where n is the number of ions of either sign per cm³. Measurements made with a thermionic discharge in cesium vapor in the pressure range 8μ to 100μ give a value of $\alpha=3\pm1\times10^{-10}$ with an electron temperature about 1200°K. Measurements with a mercury arc at pressures of 50 and 290μ give $\alpha=2\pm0.5\times10^{-10}$ with an electron temperature of about

2000°K. With an ion concentration of 10^{12} the recombination loss and wall effect are of the same magnitude for the volume and pressure range used and the relative change in concentration of ions is approximately 50 percent in 10^{-3} seconds.

56. Potentials in the Intermittent Glow Discharge. LESTER BOCKSTAHLER AND HERMAN RITOW, *Northwestern University.*—A steady current supplied to an electrical condenser in parallel with a pair of electrodes in a partial vacuum of a few mm pressure gives rise to an intermittent glow. Potentials between the electrodes have been measured when (a) the initial glow appears, (b) the discharges strike during the intermittent glow, (c) the discharge is extinguished, and (d) the glow breaks into an arc. The potential for the initial discharge is constant for a given set of electrode and pressure conditions. The striking potential of the intermittent glow decreases with increasing charging current. The extinction potential is a constant. One cm aluminum electrodes (plane circular anode, conical cathode with vertical angle 60 deg.) separated 2 cm in hydrogen were used. An attempt is being made to explain the "effective" tube capacity of such a glow in terms of the residual ions between individual discharges which influence the striking potentials.

57. Magnetic Hysteresis in 35 Permalloy Sheet at Low Flux Densities. W. B. ELLWOOD, *Bell Telephone Laboratories, Inc.*—The energy loss per cycle in a ferromagnetic material subjected to small alternating fields is sometimes separated into three parts. The first is due to eddy-current loss; the second to hysteresis presumed to follow Rayleigh's law. The third is a residual of doubtful origin and has been variously termed "magnetic viscosity," "after effect," and "square law hysteresis." The search for an explanation of this residual loss has led to a more accurate review of the methods of measurement. To compare the a.c. losses with the ballistic hysteresis loop at the same flux densities, a new ballistic method has been developed with a relative precision in B_m of 0.01 percent. The method originally applied to a compressed iron dust ring of low permeability has been improved and used to study the properties of a well-annealed spirally wound roll of permalloy (35 percent Ni) sheet which has a very large residual loss. The hysteresis loops studied range from $B_m = 1.3$ to $B_m = 5.3$ gauss. They are lenticular and very slender, B_m being about 900 times the remanence for the smallest loop. The energy loss per cycle is proportional to B_m^2 and the proportionality factor agrees with the value inferred from the a.c. measurements assuming Rayleigh's law. No residual loss was found by the ballistic method.

58. Low Flux Density a.c. Losses in 35 Permalloy Sheet. V. E. LEGG, *Bell Telephone Laboratories, Inc.*—In making precise a.c. bridge measurements on a coil wound on a laminated 35 permalloy core, both the resistance and inductance are found to vary with frequency in a manner not predicted by classical theory. From the resistance measurements, the losses are separated in the usual way into hysteresis, eddy current and residual components. The hysteresis loss per cycle is found to be independent of frequency, and to agree with that obtained by ballistic galvanometer measurements (see above abstract). The eddy current loss coefficient observed in the range 500~ to 10,000~ is approximately 20 percent larger than computed from classical theory, and it appears to increase as the frequency decreases. The residual loss coefficient is found to be approximately constant at higher frequencies, but to decrease toward zero as the frequency approaches zero. Since excess eddy current and residual losses are both proportional to B_m^2, they are examined together as of possible common origin, and in relation to the anomalous inductance-frequency characteristic. This characteristic consists of a more rapid decline of inductance with frequency than predictable from the theory of eddy current shielding.

59. Magnetic Properties of Single Crystals of Silicon Iron. H. J. WILLIAMS, *Bell Telephone Laboratories, New York, N. Y.*—Single crystals of iron containing 3.9 percent silicon have been prepared and the magnetic anisotropy constants determined in three ways: (1) by determining the magnetization curves in the [100], [110] and [111] directions and measuring $\int HdI$ for each curve, (2) by fitting the theoretical magnetization curves to the data using the values of the constants that give the best fit, (3) measuring the torque upon a single crystal disk cut parallel to a (110) plane, in a magnetic field, as dependent upon the orientation of the disk in the field. The values of the constants so determined agree rather well and are $K_1 = 305{,}000$, $K_2 = -200{,}000$, in ergs/cm³. Measured in the [100] direction, the maximum permeability was 620,000, the coercive force 0.03 oersted.

60. Single Crystals with Exceptionally High Magnetic Permeabilities. P. P. CIOFFI, H. J. WILLIAMS, AND R. M. BOZORTH, *Bell Telephone Laboratories, New York, N. Y.*—Single crystals of purified iron and of an iron-nickel alloy containing 66 percent nickel have been prepared and some of their magnetic properties measured. For iron the maximum permeability was 680,000 measured at $B = 17{,}800$. The highest permeability reached for the alloy was 1,040,000, and was attained by combining several factors, each one of which is known to favor high permeability. These factors are: (1) Absence of strains associated with hard-working, dissolved impurities and grain boundaries; (2) choice of a proper crystallographic direction for magnetization; (3) presence of a magnetic field (in the direction chosen for test) during annealing; these are of unequal importance in different ferromagnetic metals and alloys so we may add: (4) appropriate composition. The materials were heat-treated in pure hydrogen just below the melting point. The specimens were cut in the form of hollow rectangles so oriented that each edge was parallel to a tetragonal axis and so to a direction of easy magnetization. Thus a closed magnetic circuit, necessary for accurate high permeability measurements, was obtained.

61. Magnetic Anisotropy in Silicon Steel. W. E. INGERSON AND F. J. BECK, JR., *Yale University.*—A new method,

which provides a convenient and rapid means of studying ferromagnetic anisotropy, has been developed. A specimen in the form of a circular disk placed in a uniform field with H in the plane of the specimen is rotated at uniform speed within a stationary search coil. The search coil, which can be turned so that its axis is in any radial direction, is connected through an integrating circuit and a linear amplifier to a D'Arsonval oscillograph. Oscillograms taken with the search coil axis parallel and perpendicular to the field represent the cyclic variation of the intensity of magnetization in these directions, (ΔI_{11}) and ($\Delta I_{\perp}$). The constant component of the intensity of magnetization (I_c) is determined ballistically with the disk rotating. Vectorial addition of ΔI_{11}, $\Delta I_{\perp}$, and I_c determines I for all magnitudes and directions of applied field. A sample of the silicon steel developed by Goss[1] has been investigated by this method. The $\Delta I_{\perp}$ curves are shown to correspond to torque-angle curves obtained by previous investigators, and to agree with the percentage orientation as determined by crystal count. The addition of ΔI_{11} and I_c gives magnetization curves in the directions of symmetry, which are found to be 0, 55, and 90 degrees from the rolling direction.

[1] N. P. Goss, Trans. A. S. M. E. **23**, 511 (1935).

62. The Relation of Ferromagnetic Anisotropy to Atomic Structure. L. W. McKeehan, *Yale University*.—The mutual potential energy of an unstrained crystal with equal magnetic elements at lattice points depends upon the distribution of magnetic moment in each element, upon the crystal structure, and upon the direction of the magnetic axes, supposed to be parallel. The dependence upon direction accounts for ferromagnetic anisotropy. Ferromagnetic atoms of iron, cobalt and nickel are now assigned simple distributions of magnetic moment, consistent with what is known about 3*d* electrons in these atoms, and the resultant anisotropy calculated to and including sextupole terms for the cubic and hexagonal arrangements observed to occur. The results are qualitatively in agreement with reported experimental results concerning these three metals and their solid solutions. The probable effect of heat motions in modifying the anisotropy improves the quantitative agreements.

63. An X-Ray Study of the A_{r_3} and A_{c_3} Points for Pure Fe and Fe-Ni Alloys. Sidney D. Smith and Wheeler P. Davey, *Pennsylvania State College*.—Roberts and Davey[1] reported a reversible A_3 point (between 907 and 910±3°C) for pure iron and gave data for irreversible A_{c_3} points for pure iron nickel alloys. The present work sets closer limits (between 907 and 908±2°C) on the A_3 point for pure iron, and gives both A_{c_3} and A_{r_3} points for pure iron-nickel alloys up to 5½ percent nickel. The A_{c_3} points found differed slightly from those of Roberts and Davey, probably because of the well-known difficulties of analysis of iron-nickel alloys, but the discrepancies are not at all serious. The graphs of the present data indicate an almost uniform difference of about 15 percent between the A_{r_3} and the A_{c_3} points for nickel contents of from 1 to 5½ percent nickel. This work was materially aided by a grant from the National Research Council Committee on Grants-in-Aid for making possible the purchase of certain necessary equipment.

[1] Metals and Alloys **1**, 1 (1930).

64. Magnetic Experiments at Very Low Temperatures. F. Simon, *Oxford University*. (Invited paper.) 20 minutes.

65. A Photoelectric Method for Tracing Current Wave Forms. W. S. Huxford, *Northwestern University*.—A photoelectric timing arrangement is used to obtain point by point plots of periodically varying currents. The circuit contains a three-electrode vacuum photo-cell in which electron emission occurs only when a short flash of light enters the cell through a narrow slit in a disk driven by a synchronous motor. The interval of the light flash is 50 micro-seconds. The potential set up by a current flowing in a non-inductive resistance is applied to the control grid of the photo-triode. The average value of this potential taken over the interval of the light flash is measured by means of a potentiometer. The "phase" of the light flash can be changed by rotating the motor in its geared housing. Potential differences of 0.001 of a volt are easily detected, the limit of error in the measured values of points on the wave plot being of the order of ±0.005 of a volt. The method is of particular value for the delineation of small current and potential changes, the amplification of which may result in serious distortion when a cathode ray oscillograph is used. Wave forms are shown for a.c. metal arcs, copper oxide rectifiers, and for the lag of current with time in gas-filled photo-cells.

66. Deuteron Bombardment of Barium, Lanthanum and Cerium. M. L. Pool* and J. M. Cork, *University of Michigan*.—These three elements of atomic numbers 56, 57 and 58 respectively have been bombarded in the cyclotron by 6.5 million volt deuterons. Barium becomes strongly radioactive with a half-life period of 85.6 min. The β-particles have the negative sign. Chemical analysis shows that the activity is most probably due to Ba^{139}. The single stable lanthanum isotope, 139, gives a radioactivity with a half-life period of 31 hours. The β-particles also have the negative sign. In the chemical analysis of the disintegration products lanthanum was separated from cerium by the bromate method. The activity is attributed to La^{140}. A Konopinski-Uhlenbeck plot, based upon a thousand Wilson cloud chamber tracks, has been made of the β-emission. When cerium is bombarded, a 2.4 hour period is obtained. Traces of various easily activated light element impurities have been quite troublesome in this work. The two rare earth elements were kindly prepared and purified for us by Professor L. L. Quill of the Ohio State University.

* Elizabeth Clay Howald Scholar.

67. Radioactivity in Iron by Deuteron Bombardment. B. T. Darling, B. R. Curtis and J. M. Cork, *University of Michigan*.—Chemically pure electrolytic iron has been bombarded in the cyclotron with a beam of deuterons of

6.3 Mev energy. After bombardment chemical separations were made to identify the active isotopes formed. The cobalt precipitate shows a very strong positive activity of half-life 18.2 hrs. This corresponds to the capture of a proton with the probable ejection of a neutron. The manganese precipitate shows an activity whose half-life is 21 min. This indicates the capture of the deuteron with the ejection of an alpha-particle. (This precipitate also shows the ordinary manganese period 2.5 hrs. when commercial impure iron is used.) No activity of half-life long enough to be observed after the chemical separation could be found in the iron itself due to neutron capture. The energies of the beta and gamma radiations have been determined.

68. The Disintegration of Lithium by Deuterons. J. H. WILLIAMS, W. G. SHEPHERD AND R. O. HAXBY, *University of Minnesota*.—The following disintegrations have been investigated from 100 kv to 250 kv deuteron energy.

$$Li^6+H^2 \rightarrow He^4+He^4, \quad (1)$$
$$Li^6+H^2 \rightarrow Li^7+H^1, \quad (2A)$$
$$Li^6+H^2 \rightarrow Li^{7*}+H^1, \quad (2B)$$
$$Li^7+H^2 \rightarrow He^4+He^4+n^1. \quad (3)$$

Efficiency curves for these reactions show that increasing deuteron energy causes a less rapid increase in yield for (1) than for (2A) contrary to the simple interpretation of the theory of Oppenheimer and Phillips.[1] The yield of alpha-particles of 2.8 cm range differentially selected from the continuous energy distribution of (3) rises even more rapidly with deuteron energy. Qualitative results on the disintegrations per deuteron of 212 kv energy from a thick Li target assuming isotropic angular distribution are: (1) 2.7×10^{-9}; (2A) 1.1×10^{-9}; (2B) 3.5×10^{-9}; (3) 6×10^{-7}. The relative yield of protons from (2B) to (2A) decreases in a linear manner by approximately 25 percent from 250 kv to 100 kv. A search for the gamma-ray of 400 kv energy corresponding to the return of Li^{7*} in (2B) to its normal state indicates a positive result.

[1] Oppenheimer and Phillips, Phys. Rev. **48**, 500 (1935); Rasetti, "Elements of Nuclear Physics," page 251.

69. The Radioactivities of Bromine. ARTHUR H. SNELL, *University of California*.—Although bromine possesses only two isotopes, Br^{79} and Br^{81}, it is known to give rise to three neutron-induced radioactivities, with decay periods 18 minutes, 4.2 hours, and 35 hours. The same three activities are now found to be induced when bromine is activated with deuterons. The 18 minute and the 35 hour activities are accompanied by γ-rays, but the 4.2 hour period has none. When arsenic is bombarded with artificially accelerated α-particles, another active bromine results. It emits positrons with a decay period of 6.3 minutes, and is described presumably by the reactions $_{33}As^{75}+{}_2He^4={}_{35}Br^{78}+{}_0n^1$ and $_{35}Br^{78}={}_{34}Se^{78}+e^+$. The identification has been checked chemically. Still another bromine appears in a chemical separation from selenium activated with deuterons. It has a period of 2.5 hours and is attributed to Br^{82}, the reactions being:

$$(1)\quad {}_{34}Se^{82}+{}_1H^2={}_{35}Br^{83}+{}_0n^1,$$
$$(2)\quad {}_{34}Se^{82}+{}_1H^2={}_{34}Se^{83}+{}_1H^1,$$
$$ {}_{34}Se^{83}={}_{35}Br^{83}+e^-,$$
and $$ {}_{35}Br^{83}={}_{36}Kr^{83}+e^-.$$

(Se^{83} has a period of 10–20 minutes.) There is good evidence for the double β-decay indicated in (2). The 35 hour activity also appears in this separation. These results seem at present to indicate that the 18 minute, 4.2 hour, and 35 hour activities must all belong to Br^{80} and Br^{82}, i.e., one of these isotopes appears to exist in two isomeric forms, from which it decays with different periods.

70. The Induced Radioactivity of Titanium. HAROLD WALKE,* *University of California, Berkeley*.—Under bombardment with 5.5 Mev deuterons titanium metal has been rendered strongly radioactive. Analyses of the gamma-ray decay curve indicate the formation of radioactive bodies with half lives of 2.8 ± 0.1 minutes, 33 ± 2 minutes, 15.7 ± 0.7 hours and 16.2 ± 0.4 days. The short lived isotope is probably Ti^{51}, for the radioactivity induced in titanium with slow neutrons decays with a half life of 2.9 ± 0.1 minutes. The 33 minute period may be due to V^{49} or V^{50} as a period of 35 ± 2 minutes was also observed when titanium was bombarded with 11 Mev alpha-particles. Thus we have:

$$Ti^{48,\,49}+H^2 \rightarrow V^{49,\,50}+n^1,$$
$$Ti^{46,\,47}+He^4 \rightarrow V^{49,\,50}+H^1.$$

The isotope with the half life of 15.7 hours emits high energy electrons and strong gamma-radiation and may be due to sodium contamination. The isotope with half life 16 days, however, emits positrons of energy 1.2 Mev. This radioactive body is probably an isotope of vanadium formed thus: $Ti^N+H^2 \rightarrow V^{N+1}+n^1$. Under bombardment with 11 Mev alpha-particles, periods were observed with values 35 ± 2 minutes, 2.7 ± 0.2 hours, 5.5 ± 0.3 hours and 85 ± 10 days. With fast neutrons two new periods of 2.3 ± 0.2 hours[1] and 18 ± 2 hours were detected.

* Commonwealth Fellow.
[1] Walke, Phys. Rev. **51**, 439 (1937).

71. A Discharge Tube Ion Source for the Cyclotron. C. P. BAKER AND M. STANLEY LIVINGSTON, *Cornell University*.—A capillary discharge tube has been developed to serve as a cyclotron ion source. The metal capillary (3/16″ I. D., 1/4″ O. D.) is mounted vertically in the center of the cyclotron between parallel tubes for anode and filament. A small hole (1 mm) drilled through the capillary wall provides an exit for the ions and gives a pressure differential between the arc (H_2 at $\sim10^{-2}$ mm) and the cyclotron chamber ($\sim10^{-6}$ mm). An arc of 2–5 amperes can be maintained between anode and cathode with an arc drop of about 100 volts, in the magnetic field of the cyclotron. Ions are pulled out of the hole by the high frequency field of the cyclotron or swept out by the gas flow. Calculations show that the initial spiral path of the ions allows them to clear the 1/4″ tube. With an emergent ion current of 20 microamperes a high voltage beam of 1 microampere is obtained. Possibilities of improving the emergent ion current (in one design 500 micro-

amperes) suggest that much higher intensities are available. The chief advantages are in the point source of ions and consequent improvement of the energy distribution of high voltage ions, and elimination of heating effects from filament sources.

72. Stopping of the Recoil Electrons Produced by the F+H^1 Gamma Rays. J. J. TURIN AND H. R. CRANE, *University of Michigan.*—The recoil electrons produced by the 6 Mev gamma radiation from fluorine bombarded with protons were allowed to pass through 5 mm carbon and $\frac{1}{4}$ mm lead absorbers placed across the center of a cloud chamber. The curvatures of the incident and emergent tracks in the magnetic field were measured, the difference giving the loss in passing through the absorber. Results on a total of 448 tracks are given in the table below.

ABSORBER	INCIDENT ENERGY	AVERAGE LOSS
5 mm carbon	2 to 4 Mev	1.70 Mev
5 mm carbon	4 to 6 Mev	1.73 Mev
$\frac{1}{4}$ mm lead	2 to 4 Mev	1.41 Mev
$\frac{1}{4}$ mm lead	4 to 6 Mev	1.73 Mev

The losses in carbon are in good agreement with the theoretical losses due to electron collisions, and this is satisfactory, since no radiative losses are expected in a substance of such low atomic number. In the case of lead, the data show clearly that radiative losses play a large part, and increase with increasing energy of incident particle. The losses found in lead are somewhat greater than those predicted by theory, but it may be possible to account for this by errors in the experiment.

73. Experiments on Li^8 and B^{12}. D. S. BAYLEY AND H. R. CRANE, *University of Michigan.*—We have attempted to make precise measurements of the upper limits of the Li^8 and B^{12} beta-ray spectra by the cloud chamber method. The path of the particles in the magnetic field was such that only those above 9 Mev were able to enter the chamber, which allowed us to work with a large intensity near the upper limit. The cut-off appears to be 12 Mev for both spectra. Excitation curves for the two reactions

$$(1)\quad Li^7+H^2\rightarrow Li^8+H^1,$$
$$(2)\quad B^{11}+H^2\rightarrow B^{12}+H^1$$

were compared. Reaction (1) seemed definitely to have a threshold between 400 and 450 kv deuteron energy, while reaction (2) extended at least as low as 300 kv. This probably indicates that the proton emitted in reaction (1) has very little energy, perhaps 0.1 or 0.2 Mev at 400 kv bombarding energy. On this assumption we can fill in the missing link in the energy equation and write it

$$Li^7+H^2+0.4\text{ Mev}\rightarrow Li^8+H^1+0.2\text{ Mev};$$
$$Li^8\rightarrow(Be^8)+e^-\rightarrow 2He^4+e^-+15\text{ Mev}.$$

Assigning 12 Mev to the beta-particle, 3 Mev is left for the two alpha-particles, which agrees with the most probable energy found by Delsasso, Fowler and Lauritsen.[1] As an explanation of the continuous nature of the alpha-particle distribution found by Lewis, Burcham and Chang,[2] we suggest that the lifetime of the daughter nucleus Be^8 for disintegration into two alpha-particles is so extremely short that the level is practically a continuum and the beta transition may sometimes occur so as to leave the alpha-particles with nearly all of the energy.

[1] Phys. Rev. **51**, 399 (1937).
[2] Nature **139**, 24 (1937).

74. The Capture of Protons by Oxygen. L. A. DUBRIDGE, S. W. BARNES, AND J. H. BUCK, *University of Rochester.*—The capture of protons of various energies by oxygen leading to the production of radiofluorine has been investigated with the cyclotron. The reaction sets in at a proton energy of about 1.4 Mev rising sharply as far as 2.5 Mev. Measurements are under way at higher energies. The preliminary measurements on the period of the radiofluorine give a value of 1 minute 21 seconds. This is slightly higher than previously reported values for radiofluorine produced in other reactions, a discrepancy which is being investigated. There is some suggestion of the presence of a considerably longer period produced by a reaction not yet definitely identified. The measurements have been made using a solid target of quartz and also by collecting recoil atoms on a platinum foil in oxygen.

75. Resonance Transmutation of Se(34) by Protons. J. H. BUCK, C. V. STRAIN, AND G. VALLEY, *University of Rochester.*—The excitation function for induced radioactivity of Se has been examined experimentally over the range from 1.7 to 3.6 Mev. Measurable activity is found to begin at 2.3 Mev and to increase very sharply at about 3.1 Mev. This excitation curve is compared with others taken for neighboring elements.

76. Proton-Induced Radioactivity of Elements of Atomic Number Greater than Eleven. S. W. BARNES, L. A. DUBRIDGE, E. O. WIIG, J. H. BUCK, AND C. V. STRAIN, *University of Rochester.*—Si, Ca, Ti, Cr, Mn, Co, Ni, Zn, As, Se, Cd, In, Sn, and Sb have been found to become radioactive under a bombardment of 3.6 Mev protons. Mg, Al, S, Cl, Fe, Cu, and Ag show no signs of induced activity under the same conditions. The relative activity of the members of the first group is 6, 21, 30, 5, 27, 6, 21, 40, 13, 2000, 10, 20, 3, 2, and 1. Preliminary measurements of the periods have been made and it is found that only Mn(11.3 min.) and Co(14.3 min.) yield products having a single period. Identification of the products of the reactions cannot be made from the periods, since practically none of the active substances have been reported previously. A program of identification by chemical separations is under way.

77. The Production of High Energy Alpha-Particles by the Princeton Cyclotron. M. G. WHITE, M. C. HENDERSON, W. J. HENDERSON, AND L. N. RIDENOUR, *Princeton University.*—Doubly charged helium ions have been accelerated in a cyclotron to 9 MV at a current of 0.05 microampere. The optimum helium pressure is about 10^{-4} mm Hg with a radiofrequency power input of 5 kw to the oscillatory circuit. Oscillographic studies of the wave shape of the ion beam indicate that a current of at least 0.3 microampere should be available when d.c. power for the

oscillators is substituted for the present unrectified a.c. The difference between the m/e for helium ions and for hydrogen mass two ions is sufficient to permit an almost complete separation of the helium beam from possible deuteron contamination. To make more certain of freedom from this contamination deuterium has never been used in the Princeton cyclotron. By electrostatic deflection the high velocity ion beam has been brought outside the vacuum chamber. A set of graded stopping foils for altering the energy of the ions has been arranged to operate in vacuum.

78. Radioactivity Induced by Alpha-Particles. L. N. RIDENOUR, W. J. HENDERSON, M. C. HENDERSON, AND M. G. WHITE, *Princeton University.*—The artificial radioactivity produced by the bombardment of light elements with 0.05 microampere of 9 Mev alpha-particles produced by the Princeton cyclotron has been studied. This alpha-particle beam is equivalent to that from 4 curies of ThC′. Preliminary results indicate that the accepted value of the half-life of P^{30} (3.3 minutes) is in error; measurements with the strong sources available to us give a half-life of 2.52 ± 0.05 minutes. Half-life measurements on other artificial radioelements produced by alpha-particle bombardment are summarized below.

TARGET	ACTIVE ISOTOPE	HALF-LIFE
B	N^{13}	10.5 min.
N	F^{17}	69 sec.
Al	P^{30}	2.52 min.

Measurement of the energy-yield curves of the reactions producing these radioelements is in progress.

79. Long-Period Radioactivity in Cobalt Induced by Slow Neutrons. J. R. RISSER, *Princeton University.*—Sampson, Ridenour and Bleakney[1] found an activity in cobalt after exposure to slow neutrons with a period of over a year. This activity is quite strong, considering the long mean life, and is perhaps to be attributed to the more abundant isotope, Co^{59}. The only other known activity induced in Co by slow neutrons, a 20-minute period observed by Rotblat, can be attributed to the less abundant isotope Co^{57}. The long-period activity has been investigated further. It is found that the response of even a thin-walled beta-ray counter is due to gamma-rays alone. By the use of a wire screen counter, with the cobalt and thin aluminium absorbers in the same envelope with the counter, particles emitted with low energies have been found. The aluminium screens were manipulated by a magnetic device from the outside and the absorption indicated that the upper limit of these soft beta-rays cannot be much greater than 175 kv. Preliminary absorption measurements in both lead and copper indicate that a gamma-ray of energy of the order of 2.0 ± 0.5 MV accompanies the reaction.

[1] Sampson, Ridenour and Bleakney, Phys. Rev. **50**, 382 (1936).

80. Transmutation-Processes of Li^6 and Li^7. L. H. RUMBAUGH, *Bartol Research Foundation of the Franklin Institute,* R. B. ROBERTS AND L. R. HAFSTAD, *Department of Terrestrial Magnetism, Carnegie Institution of Washington.*—Thin targets of the separated isotopes of Li^6 and Li^7 have been used for the investigation of alpha-particle, proton, neutron, and beta-particle excitation-functions under deuteron bombardment for voltages between 200 and 1000 kv. Observations have been made on the voltage-dependence of the separation and relative intensity of the components of the proton doublet from Li^6. The excitation-curves show markedly different characteristics, dependent both upon the disintegration product and the parent nucleus.

81. The Transmutation of Aluminum by Polonium Alpha-Particles. W. R. KANNE, *The Johns Hopkins University.*—In order to resolve the conflicting results of Pose[1] and of Chadwick and Constable[2] the absorption curve of the protons emitted from a thick aluminum target has been repeated. The recording apparatus was an FP-54 vacuum tube electrometer. Alpha-particles from polonium deposited on silver were entirely absorbed in an aluminum foil. The protons emitted in this foil passed through calibrated mica foils into an ionization chamber. The angles subtended by the target and chamber were similar to those used in previous experiments. More than 50 points, of probable error between 3 percent and 10 percent, were obtained. The eight groups described by Chadwick and Constable have been observed, and substantial agreement regarding ranges and yields confirms their results and interpretation. The energy of the gamma-ray from the final $_{14}Si^{30}$ nucleus is 2.5 Mev, and the ratio of the intensities of the short and long range groups is 3.5.

[1] Zeits. f. Physik **95**, 84 (1935) and Zeits. f. Physik **75**, 753 (1932).
[2] Proc. Roy. Soc. **135**, 48 (1932).

82. Maximum Energy of the Protons Emitted by Boron under Alpha-Particle Bombardment. GORDON BRUBAKER AND ERNEST POLLARD, *Yale University.*—Accurate values for the masses of the light elements up to O^{16} are now known. These masses are in good accord with energies determined in transmutation with the exception of the reaction

$$B^{10} + He^4 \rightarrow C^{13} + H^1 + 3.3 \text{ Mev},$$

in which 4.5 Mev should be released. This reaction has been studied carefully by several workers and the yield of any longer range group than hitherto found must certainly be very small. It is of interest to determine whether any longer range group exists, since if it does not this would be an example of a transmutation in which radiation is associated with the most energetic group of emitted particles. We have therefore studied the absorption curve using an automatic recording arrangement. This registers the numbers of protons entering a counter and producing large and small ionization on two separate traces simultaneously. Our results indicate the presence of a very weak group of Q value 4.7 Mev ($\pm .5$) having a yield of about one thirtieth that of the group of Q value 3.3 Mev. Since this represents one thousandth of the total number of protons emitted it is clear that this transition is extremely improbable.

83. Accelerating Tube for the Round Hill Electrostatic Generator. C. M. VAN ATTA, R. J. VAN DE GRAAFF AND L. C. VAN ATTA, *Massachusetts Institute of Technology.*—A cascade[1] accelerating tube for use with the Round Hill electrostatic generator[2] has been built and tested. The tube

rests on a 24-foot I-beam of Bakelite-impregnated plywood extending horizontally between the generator terminals and consists of four rigid 65-inch sections joined by flexible metal bellows. Each section has twelve porcelain cylinders and eleven steel electrodes, all clamped between heavy steel end plates by means of six plywood tension rods. The porcelain cylinders have external corrugations and are twelve inches in diameter. The electrodes consist of focusing cylinders three inches in diameter spaced with ½-inch gaps and held coaxially in the tube by diaphragms, the edges of which protrude slightly between the porcelain cylinders. Vacuum joints are made reliably tight by lead gaskets painted with Glyptal. The tube and I-beam are shielded against radial fields by seven rings consisting of tractor inner tubes coated with Aquadag and electrically connected to the tube at every sixth diaphragm. Voltage distribution is controlled by corona points attached to the edges of all diaphragms. The present tube, designed for half the generator voltage, reliably sustains its rated voltage of slightly over 2.5 megavolts and will be used for nuclear research while the parts are under construction for its extension to withstand the full voltage.

[1] W. D. Coolidge, J. Frank. Inst. **202**, 693 (1926); M. A. Tuve, G. Breit and L. R. Hafstad, Phys. Rev. **35**, 66 (1930).
[2] L. C. Van Atta, D. L. Northrup, C. M. Van Atta and R. J. Van de Graaff, Phys. Rev. **49**, 761 (1936).

84. Generating Voltmeter Measurements at Round Hill. D. L. NORTHRUP AND L. C. VAN ATTA, *Massachusetts Institute of Technology.*—There are certain requirements imposed upon an electrostatic generator and its housing by the necessity of making accurate generating voltmeter measurements. In particular, the capacity between the voltmeter and charged insulating surfaces should be made as small as possible by reducing these areas to a minimum and by properly locating the voltmeter. These requirements are satisfactorily met at Round Hill when a voltmeter is located in the top of each terminal. A generating voltmeter has been designed for this application with attention to all-over stability of calibration and convenience in use. A linear response on a short period d.c. output meter for a wide range of gradients (5 volts/cm to 10,000 volts/cm) is made possible by a 10-point range selector and a thermionic rectifier. Thus a calibrating voltage of 20 kilovolts is ample when measuring voltages up to 3 megavolts on one terminal. A discussion of technique will be given with special reference to the small corrections for the effect of insulator charge and interaction between terminals, necessary to obtain an accurate determination of total voltage.

85. Transmutation of Argon and Chlorine by Alpha-Particles. ERNEST POLLARD, H. L. SCHULTZ AND GORDON BRUBAKER, *Yale University.*—We have found the two elements argon and chlorine to emit neutrons when bombarded by alpha-particles from either RaC or ThC′. The yield from argon is larger than that from aluminum; that from chlorine is roughly one quarter as great. We suggest the following reactions take place:

$$A^{40}+He^{4}=Ca^{43}+n^{1},$$
$$Cl^{37}+He^{4}=K^{40}+n^{1}.$$

In the second reaction the radioactive isotope of potassium is formed. Particular attention has been paid to the excitation curves. The first reaction gives a curve which follows the Gamow penetration formula for zero orbital angular momentum very closely if a nuclear radius of $7.6\pm.3\times10^{-13}$ cm is supposed for A^{40}. This fits with a radius of 13.6×10^{-13} cm for the radioactive nuclei and agrees with Bethe's recent value of 13.0×10^{-13} cm. Applying the conservation of angular momentum the spin of Ca^{43} should differ from that of A^{40} by ½. The chlorine reaction is more uncertain because of the smaller yield but there are indications that the expected nuclear radius cannot explain the results unless the incident alpha-particle has an orbital angular momentum $l=1$ or $l=2$. This implies that K^{40} has a spin of 3 or greater. This would account for the abnormally great lifetime of K^{40}, for a transition to Ca^{40} would require a considerable change in angular momentum.

86. The Photodisintegration of the Deuteron. J. REGINALD RICHARDSON AND LORENZO EMO, *University of California.*—The photodisintegration of the deuteron by the gamma-radiation from radioactive sodium, Na^{24}, has been observed in a cloud chamber. The cloud chamber contained deuterium at a pressure slightly above one atmosphere. A sample of NaF was activated by deuteron bombardment in the cyclotron to a γ-ray strength equivalent to about 12 mg of radium, and was then brought close to the cloud chamber. Pictures were taken with a stereoscopic camera. Preliminary results on about 4000 pictures show a total of 42 measurable tracks. The range distribution of these tracks indicates a mean air equivalent range of about 4.5 mm. This corresponds to a mean energy of 300 kv for the photo protons, or, assuming the binding energy of the deuteron at 2.2 MV, it indicates that the energy of the most energetic Na^{24} gamma-ray is 2.8 MV. The angular distribution of the tracks indicates that the disintegration is predominantly photoelectric, although a small contribution from the photomagnetic effect is not ruled out. A rough calculation from the yield of tracks, knowing the sensitive time of the cloud chamber, indicates a cross section of about 1×10^{-27} cm². It is our opinion that this method is capable of considerable accuracy in the determination of the energy of gamma-radiation from strong sources when the energy is above 2.2 MV.

87. The Damping of Torsional Oscillations in Quartz Fibers. G. A. DOWNSBROUGH,* *Rutgers University, New Brunswick, N. J.*—The results obtained by previous workers have been qualitatively confirmed, but it was demonstrated that many of the perplexing features were characteristic of the material used to mount the quartz fibers, and not of the fibers themselves. When fused quartz joints were substituted, these features were eliminated, and in addition the damping became very much smaller than in any previous work. As a result, it was also necessary to investigate energy losses hitherto unimportant; several were found capable of affecting the results, but in the final arrangement they were all insignificant. On the assumption that the damping is a purely viscous phenomenon, it is shown that

the product of the period of oscillation and the logarithmic decrement should be a constant of the material. This was experimentally verified over a small range of periods; the value obtained was 1.3×10^{-5}. The coefficient of viscosity for quartz, derived from this, is 2.2×10^{5} g/cm sec.

* Now with the Research Laboratories of Johns-Manville Corporation, Manville, N. J.

88. The Mechanism of Internal Friction. CLARENCE ZENER, *Washington University.*—The concept of internal friction has been introduced many years ago to explain the gradual damping of vibrations in solids. The mechanism of internal friction has nevertheless remained obscure. In this paper such a mechanism is discussed from a theoretical viewpoint, and experiments are suggested whereby this mechanism can be tested. The theory of internal friction here discussed is obtained by considering solely the thermodynamical aspects of vibrations. If the vibrations were adiabatic, strain would be a linear function of stress. Similarly, if the vibrations were isothermal, strain would also be a linear function of stress. When, however, the vibrations are neither adiabatic nor isothermal, the relation between stress and strain is represented by a closed hysteresis curve. This hybrid type of vibration is obtained in the transverse vibrations of thin reeds. The area of the hysteresis loops has been exactly calculated for such reeds. The value of the logarithmic decrement thus obtained is of the same order of magnitude as the experimental values (which disagree from each other by several hundred percent), its precise value depending upon the frequency of vibration, the thickness of the reed, and its temperature.

89. The Elastic Constants of Crystalline Sodium at 80°K. SIDNEY SIEGEL, *Columbia University.*—The elastic constants of crystalline sodium at 80°K have been measured by the composite piezoelectric oscillator method of Balamuth and Rose.[1] The sodium is made by heating C.P. NaCl with metallic Ca. Single crystal cylinders 4.8 mm in diameter and 7 cm or less long are grown in vacuum in oiled glass crucibles by Bridgman's method. The experimental method yields the value of Young's modulus and the torsion modulus for the direction of the cylinder axis. The direction cosines of this axis with respect to the principal axes of the crystal are obtained from a series of Laue photographs, taken with the x-ray beam normal to the cylinder axis. The principal elastic constants are calculated with the formulae which relate these quantities to the observed Young's and torsion moduli. Observations are reported on three crystals whose axes lie approximately in the 100, 110 and 111 directions in the lattice. The values of the constants are, $s_{11}=5.02\pm.05$, $s_{12}=-1.78\pm.04$, $s_{44}=0.81\pm.04$, all times 10^{-11} cm²/dynes. These may be compared with the theoretical values calculated by Fuchs,[2] namely, $s_{11}=4.86$, $s_{12}=-2.24$, $s_{44}=1.72$, all times 10^{-11}. It is intended to extend these measurements to potassium and lithium, and to investigate the variation of the constants with temperature at low temperatures.

[1] Balamuth, Phys. Rev. **45**, 715 (1934); Rose, Phys. Rev. **49**, 50 (1936).
[2] Fuchs, Proc. Roy. Soc. **157**, 444 (1937).

90. The Estimation of Intergranular Surfaces and Volumes in Metals. HERMAN F. KAISER, *Naval Research Laboratory, Washington, D. C.*—In many instances the intergranular surfaces of separation in metals suggest an almost regular geometrical structure. For such cases it is possible to carry out an approximate treatment by visualizing the metal as built up of regular space-filling parallelohedra. In this paper expressions are derived, using the four parallelohedra of Fedorov, for the internal surface, the intergranular volume and the density of the model metal as functions of the grain size and composition of the metal. Results are applied to the computation of amounts of totally insoluble impurities required to produce grain envelopes of given thickness. The bearing on Tamman's theory of recrystallization is discussed.

91. The Formation of Metallic Bridges in Separated Contacts. G. L. PEARSON, *Bell Telephone Laboratories, Inc.*—Low resistance bridges were formed between gold, steel and carbon electrodes having separations of $2\text{–}70\times10^{-8}$ cm by applying voltages less than the minimum sparking potential. For a given pair of electrodes the field required to form the bridges is a constant and is $5\text{–}16\times10^{6}$ volts per centimeter. Measurements of the temperature coefficient of resistance of the bridges identify them as consisting of the material of the electrodes. A study of their resistance as a function of the displacement of one of the electrodes shows that they may be pulled out as well as crushed. At voltages less than those required to form the bridges, field currents exist. These increase rapidly as the field is raised and attain a value around 10^{-10} ampere before the bridges are formed. Calculation of the maximum electrostatic stress on the electrodes at the time of breakdown gives a value 0.05 to 0.0005 times the tensile strength of the electrode material at room temperature. The field is locally higher than that calculated because of surface roughness and the tensile strength is probably lowered by the local heating known to accompany field currents. The data therefore indicate that electrostatic force pulls material from the electrodes to bridge the gap.

92. Diffusion of Hydrogen through Iron at Temperatures between 780° and 90°C. W. L. RAST AND W. R. HAM, *Pennsylvania State College.*—Measurements in the temperature range 780° to 90°C of the rates of diffusion of hydrogen through different samples of highly decarburized carbonyl iron indicate abrupt changes in slope of log (Rate) *vs.* $1/T$°K graphs at the following temperatures: 767, 729, and in the region of 200°C. As previously observed by Ham,* the log (Rate) *vs.* $1/T$°K graph is found to be nonlinear in the Curie region extending from 767° to 729°C. Between 729° and approximately 200°C the graph is nearly linear, and the value of the constant b in the empirical equation $R=Ae-b/T$ (where R represents rate of diffusion, T the absolute temperature, A and b constants) is 4200, about the value found by most other observers. However, around 200°C an abrupt decrease in the rate of diffusion occurs, the rate falling to one-hundredth of its value in an interval of about 30 degrees. Below this discontinuity the decrease of the rate with decrease in temperature to 90°C is very small,

the value of "b" being approximately 1000. For each sample investigated a considerable hysteresis is noted in the vicinity of the 200°C discontinuity.

* "The Diffusion of Hydrogen through Nickel and Iron," by W. R. Ham, in process of publication in the Trans. Am. Soc. Metals.

93. The Diffusion of Hydrogen through Carbonyl Iron at Temperatures from 900° to 1125° Centigrade. C. B. POST AND W. R. HAM, *Pennsylvania State College.*—The diffusion of hydrogen through hydrogen-purified Mehl-Iron shows breaks in the log (Rate) *vs.* $1/T$ curves at 909°C (Body-Centered→Face-Centered phase change), 952, 1012, 1057, 1082, 1103 degrees centigrade. The experimental procedure at these high temperatures is difficult and the experimental technique is being improved, so that the above values from 1050° upwards are subject to revision. The curves of log R *vs.* $1/T$ are found to be straight segments of curves satisfying a relation, $\log R = A - b/T$, the segments being clearly differentiated from one another at the above temperatures.

94. The Change from γ-FeOOH and γ-Fe_2O_3 to α-Fe_2O_3 at Lower Temperatures and the Irreversible Transition: γ-FeOOH to α-FeOOH. LARS A. WELO, *Tottenville, Staten Island, New York* AND OSKAR BAUDISCH, *Saratoga Springs Authority, Saratoga Springs, New York.*[1]—In open containers γ-FeOOH dehydrates in an hour at 250°C, yielding ferromagnetic γ-Fe_2O_3. At 400°C this oxide, in turn, changes irreversibly to paramagnetic α-Fe_2O_3 in an hour. In sealed tubes, along with sufficient water for saturation, the overall change occurs in an hour at 136°C but intermediate γ-Fe_2O_3 does not appear. γ-Fe_2O_3 also changes in this "wet" way to α-Fe_2O_3 at the same temperature and rate as its parent hydrate. We infer the occurrence of the irreversible transition γ-FeOOH to α-FeOOH and that α-Fe_2O_3 is shed to satisfy the equilibrium requirements of the system α-FeOOH, α-Fe_2O_3 and water. If we start with γ-Fe_2O_3, transition is preceded by hydration of γ-Fe_2O_3 to γ-FeOOH. But this hydrate disappears by transition so that the reaction goes forward until all γ-Fe_2O_3 is consumed. Similar depression of the transformation temperature occurs in γ-Fe_2O_3 made by oxidation of precipitated magnetite and our observations support the generalization that when γ-Fe_2O_3 is stabilized against the irreversible transition to α-Fe_2O_3, this stabilization persists with respect to the transition between the corresponding hydrates.

[1] For the most part, this work was done in the Research Laboratory of the Consolidated Gas, Electric Light and Power Company of Baltimore.

95. Reciprocals to Ampere's Law. PRESTON B. CARWILE, *Lehigh University.*—Consider Ampere's law as expressed (in the *em* system) by the familiar vector equation (1) $d\mathbf{H} = id\mathbf{s}\times\mathbf{r}/r^3$. If we generalize this equation to include displacement current, then apply the well known principle of reciprocity between corresponding electric and magnetic entities and finally drop the term for magnetic convection current (since, as yet, we have no experimental evidence for the existence of free magnetic poles), we obtain (2) $d\mathbf{E} = -\dot{\Phi}d\mathbf{s}\times\mathbf{r}/4\pi r^3$, where $\dot{\Phi}$ is the time rate of change of total flux in a magnetic circuit. Eq. (2) is the effective reciprocal to Eq. (1). Or Eq. (2) may be regarded as a variant form of Faraday's law of electromagnetic induction. Again, starting with Ampere's law of the equivalence of an electric current i to a simple magnetic shell of strength ρ given by (3) $\rho = \mu i$, we obtain, by a similar application of reciprocity, the law of equivalence of a magnetic circuit in which flux is changing at the rate $\dot{\Phi}$ to a simple electric shell having the magnetic circuit as its boundary and having the strength (electric moment per unit area) given by (4) $\sigma = k\dot{\Phi}/4\pi$, where k is the dielectric constant. Eqs. (2) and (4) involve no new principle. Their explicit forms are believed to be new. They find ready use in an elementary treatment of magnetoelectric fields.

96. A New Recording Microphotometer.* H. V. KNORR AND V. M. ALBERS, *Antioch College.*—A new microphotometer has been constructed, using an emission type photocell as the light sensitive device and a Leeds and Northrup Speedomax Recorder. The photographic plate and the recording paper are moved by synchronous motors operated from the same a.c. source. An inked curve is traced by a pen, whose motion can be observed during the recording. An amplifier, using type 40 tubes in a balanced tube circuit, is employed to amplify the photoelectric current. The speed of the recording paper is fixed at 5 cm per minute. The relative speeds of the plate and recorder can be varied by means of a system of reducing gears mounted on the plate carriage. The plate holder is mounted to the plate carriage in the same manner as the plate holder in an ordinary camera. A drum is rotated through a gear system by a synchronous motor and pulls the plate carriage along a track by means of a steel ribbon. The sensitivity of the recorder can be varied from 2.5 to 8 millivolts for a full scale deflection of 25 cm. This microphotometer is very stable and is not affected by mechanical vibrations. The zero of the instrument is very constant.

* The present paper will appear in full in R .S. I.

97. The Effects of Elastic Stretch on the Infrared Spectrum of Rubber. DUDLEY WILLIAMS AND RICHARD TASCHEK, *University of Florida.*—The absorption spectrum of stretched rubber has been studied in the region between 2μ and 8μ. In the case of unilateral stretch transmission measurements indicate that the absorption bands near 3.25μ and 7μ become broader with increasing stretch while the background absorption becomes more pronounced. Radial stretch was found to produce similar effects in the 3.25μ and 7μ regions. The bands appearing near 6μ become less intense in the case of radial stretch. In the spectra of a number of samples which had been stretched radially a new band appeared near 4.8μ. Since both absorption and reflection are involved in transmission measurements, it was found necessary to determine both reflection and extinction coefficients. The results indicate that the reflection coefficient diminishes and the extinction coefficient increases with increasing stretch. The observed variations in the extinction coefficients are considerably larger than those arising from the known density changes which accompany stretching.

98. The Infrared Absorption of Aqueous Solutions of the Halogen Salts. E. K. PLYLER AND E. S. BARR, *University of North Carolina and Tulane University.*—The infrared absorption spectra of the aqueous solutions of NaCl, NH_4Br, KF, NH_4F and KI have been measured in the region from 3μ to 6.5μ. The concentrations of the solutions were varied from 1 N to 6 N. Some modification of the 3μ and 6.2μ water bands was noticed. The water band at 4.7μ, however, showed a shift in position which was always of the same amount when the negative ion in the solution was the same. All solutions containing fluorine had the maximum intensity at about 4.65μ. The chlorine shifted the band to 4.78μ, bromine to 4.8μ, and iodine to 4.9μ. The actual position of the band varied somewhat with the concentration. This effect was thought to be due to the varying amount of water present, and the overlapping of the 4.7μ absorption band in this region. It is difficult to state whether these bands are produced by the association of the negative ions, or if a shift is just produced in the water band itself. A number of other substances did not produce the corresponding effect on the 4.7μ water band.

99. The Infrared Absorption Spectrum of Formic Acid Vapor. LYMAN G. BONNER* AND ROBERT HOFSTADTER, *Princeton University.*—The spectrum of formic acid vapor has been measured in the region 1–15.5μ and at several temperatures between 25° and 140°C, using a rocksalt prism spectrometer. Since formic acid exists principally as double molecules at 25° and is largely dissociated at 140° this procedure has made it possible to separate the spectra of the dimer and monomer. The dimer shows strong absorption bands at 3080, 2530, 2380, 1905, 1740, 1350, 1205, 1090, 917 and 667 cm^{-1} while the monomer absorbs only at 3550, 2940, 2325, 1740, 1090 and 658 cm^{-1}. Using the method of rigid groups, force constants for the C—O and C=O bonds of the monomer have been calculated, the values being 5.4 and 11.8×10^5 dynes/cm respectively. Since the normal value for C—O is nearer 4.5×10^5 the above figure would indicate the existence of a certain amount of single-double bond resonance in this molecule, as postulated by Pauling and Sherman.[1]

* National Research Fellow. [1] J. Chem. Phys. **1**, 606 (1933).

100. Photographic Penetration of Haze. NORA M. MOHLER, *Smith College.*—Photographs have been taken from Mt. Nonotuck in the Connecticut valley, with plates and filters registering from 0.4 to 1.0μ, in steps of about 0.1μ. Visibilities varied from less than 3 miles to more than 50, weather conditions from thick haze and fine rain to very clear. The photographic "visibility" has been plotted against wave-length, and the curves compared with the theoretical curve given by Stratton and Houghton[1] and Hulburt.[2] The position of maxima and the change in slope of the curves make possible an estimate of the size of some drops by this comparison; typical results are: thick haze, visibility 3 miles, drops of radius 1.3μ and much larger; fine rain, visibility 6.5 miles, r is 1.1 with others less than 0.8 as well as some much larger; thin haze, visibility 12 miles, r is 1.1 and less than 0.7; extremely clear, r is less than 0.22μ.

[1] Phys. Rev. **38**, 159 (1931). [2] J. O. S. A. **25**, 125 (1935).

101. Optical Properties of Evaporated Films. D. H. ANDREWS, J. A. SANDERSON AND E. O. HULBURT, *Naval Research Laboratory.*—In the spectrum region from 0.185 to 10μ the reflectivity and transmission have been measured of films of Al, Sb, Be, B, Cr, Mg, Mn, Si and Te prepared by evaporation in vacuum. The reflectivities agreed in the main with previous measurements in as far as these exist. Minima of reflection in the infrared were noted for Sb, B, Si and Te which appeared to be due to interference, as evidenced by the spacing of the minima and their shift with film thickness.

102. The Scattering of Light by Water. L. H. DAWSON AND E. O. HULBURT, *Naval Research Laboratory.*—By means of a quartz spectrograph and a densitometer the relative intensity of light scattered by pure water was measured throughout the spectral region from 5461 to 2536A. The scattering coefficient was found to increase with decreasing wave-length in fair agreement with the $\lambda^{-4}f(\mu)$ expression derived from the density fluctuation theory of Einstein and Smoluchowski.

103. The Visible Absorption Spectra of Porphin and Its Isomer. V. M. ALBERS AND H. V. KNORR, *Antioch College.*—All porphyrins are characterized by a ring system composed of four pyrrole rings joined by carbon atoms between them. The simplest possible porphyrin is porphin, synthesized by Rothemund[1] in 1935. Rothemund obtained two substances with porphin properties which differ in hydrochloric acid number and which have been demonstrated to be isomers. This is the first case of isomerism observed for porphyrins. The substance having the larger hydrochloric acid number (3.3) has been named porphin and the one with the smaller hydrochloric acid number (0.5) has been named *iso* porphin. The absorption spectra of porphin and some of the *ms* substituted porphins have been reported by Albers and Knorr.[2] The absorption spectrum of *iso* porphin has been measured in the visible region. The general pattern is similar to that of porphin except for a shift in wave-length of the bands about 100A toward the red. The most pronounced difference in the spectra, however, is in the values of the absorption coefficients. The absorption coefficients in the bands are about three times as large for porphin as they are for *iso* porphin.

[1] Paul Rothemund, J. Am. Chem. Soc. **57**, 2010 (1935).
[2] V. M. Albers and H. V. Knorr, J. Chem. Phys. **4**, 422–425 (1936).

104. Energy Levels in Neon and Argon. J. B. SAMPSON, *Allegheny College.* (*Introduced by C. W. Ufford.*)—The energy levels in intermediate coupling for the neon $2p^53d$ and argon $3p^55d$ configurations were calculated. Shortley has already done so for several configurations of neon by neglecting the electrostatic interaction between groups having $^2P_{\frac{1}{2}}$ and $^2P_{3/2}$ as parents. The configurations treated here are the only two for which experimental results are completely available, and to which Shortley's approximation does not satisfactorily apply. The 6 radial integral parameters were found approximately from the available linear equations and were then adjusted by the process of least squares to fit all the observed values as well as possible. For neon the agreement with all the observed levels was to within 1 wave number in a spread of 900.

105. The First Spark Spectrum of Platinum. A. G. SHENSTONE, *Princeton University.*—The low multiplets of Pt II are mainly in the Schumann region. To obtain the lines in a source producing low excitation, arcs and sparks were run in pure nitrogen, the source being placed so as to be focussed on the slit of a vacuum spectrograph by a fluorite lens which formed the vacuum seal of the spectrograph. The nearly stigmatic images made the separation of stages of ionization very simple. The analysis has so far yielded the even levels given below. About 40 odd levels have been found. The wave number difference is approximately 155800 from $5d^9\ ^2D_{2\frac{1}{2}}$ to $5d^8\ ^3F_4$.

Even Levels of Pt II

Level	J	Probable Origin	Level	J	Probable Origin
−4786.4	$2\frac{1}{2}$	$d^9\ ^2D_{2\frac{1}{2}}$	16931.0	$\frac{1}{2}$	d^8s
0.0	$4\frac{1}{2}$	$d^8s\ ^4F$	18675.1	$2\frac{1}{2}$	$d^8s\ ^2F$
3633.4	$1\frac{1}{2}$	$d^9\ ^2D_{1\frac{1}{2}}$	19089.4	$1\frac{1}{2}$	d^8s
4569.6	$3\frac{1}{2}$	$d^8s\ ^4F$	20093.3	$4\frac{1}{2}$	$d^7s^2\ ^4F$
8542.7	$2\frac{1}{2}$	$d^8s\ ^4F$	22469.5	$\frac{1}{2}$	d^8s
11004.9	$1\frac{1}{2}$	$d^8s\ ^4F$	29861.1	$3\frac{1}{2}$	$d^7s^2\ ^4F$
12034.4	$2\frac{1}{2}$	$d^8s\ ^2D$	33091.5	$\frac{1}{2}$	$d^8s\ ^2S$
13311.3	$3\frac{1}{2}$	$d^8s\ ^2F$	91014.4	$4\frac{1}{2}$	d^97s
16382.4	$1\frac{1}{2}$	d^8s	91825.5	$3\frac{1}{2}$	d^97s

106. The First Spark Spectrum of Manganese. C. W. CURTIS, *Western Reserve University.*—The analysis of the Mn II spectrum has been extended to include a classification of over five hundred lines. From four members of the $3d^5(^6S)nf\ ^7F$ series an ionization potential of 126,147 wave numbers has been calculated by means of a Ritz formula. Pictures have been taken and measurements made covering the range from approximately 800A to 6000A. A hollow cathode discharge was used as a source, with each of the three gases, helium, argon and neon, as conducting media.

107. Interference Measurements in the Spectra of the Noble Gases in the Ultraviolet. C. J. HUMPHREYS, *National Bureau of Standards.*—Wave-length measurements in the first spectra of the noble gases, in the ultraviolet to 3369A, have been made, using F–P interferometers with aluminized quartz plates and étalons of 3, 7.5, 15, 20 and 25 mm length. The wave-lengths have been determined relative to the adopted International Standards in Kr I and Ne I. All but three of the thirty possible $1s$–$3p$ lines of Ne I are intense enough to permit interference measurements. Measurements in Kr I comprise 28 lines of shorter wave-length than λ4274, the limit of previous work. It is now possible to fix the various p-series of Kr I to four members by interference methods. Some extensions have also been made in A I and Xe I. The short wave-length limit to these measurements is set by the intensity decrement of lines approaching the series limits, the $1s$-levels (^1P, ^3P) of the noble gas spectra. It is expected that the more intense lines will prove useful as wave-length standards. The neon group is the most promising in this respect. The possibility of a pressure effect in higher series lines is being investigated by comparing wave-lengths obtained with Geissler tubes filled with "low" and "high" gas pressures. A series of measurements of A II comprising about 150 lines has also been carried out.

108. The Coupling of the Normal p-Electron Configurations. H. A. ROBINSON AND G. H. SHORTLEY, *Ohio State University.*—The application of the intermediate coupling theory has been considered in detail for the configurations p^2, p^3 and p^4 in the long isoelectronic sequences which have been recently analyzed. Curves have been plotted giving the ratios of various intervals in these configurations as a function of the single parameter which specifies the type of coupling. If the parameter be determined from an experimental value of one of these ratios, the other ratios may be predicted. In half the cases the agreement of the predicted values with experiment is very good; for the others the departure is sufficiently regular to permit accurate prediction of unknown terms. This, in at least one case, has led to definite classification of a new level. Of particular interest is the very rapid departure of the Landé interval ratio from its Russell-Saunders value, which explains most of the anomalous observed Landé ratios in these configurations. These considerations permit evaluation of the energy parameters occurring in the theoretical formulas. The electrostatic interaction parameter F_2 is a linear function of Z to a good approximation; the spin orbit parameter ζ varies as $(Z-S)^4$; their ratio, the coupling parameter, varies as $(Z-S)^2$. These are in accordance with the theoretical expectations.

109. A Pyrheliometer Having a Spherical Absorber is Used to Follow Sunspot Activities. L. F. MILLER, *University of Minnesota.*—A pyrheliometer employing a very thin blackened spherical absorber[1] enclosed in a highly evacuated quartz bulb was used to measure the solar radiations emitted during the passing of a group of sunspots during the first months of 1936 and the group now in progress since about August of this same year. This instrument has a geometrical, optical and thermal symmetry which gives it the same sensitivity for all positions of the sun. It may be known as the total intensity method for measuring sunspot activities. Other methods of following these sunspot activities are by the magnetic effect, the ultraviolet light, the variation of the solar constant, radio fading and by photographing the sunspots directly. From the latter are determined Wolf numbers which at present are accepted as the best index of these activities. Curves may be plotted for each of these different methods with the day as the abscissae unit and the ordinate as the measure of the effect observed. Ten day smoothed curves were made in each case. Using these smoothed curves, scatter diagrams and correlation coefficients were determined between the Wolf number curve and each of the other curves. A correlation coefficient of 0.5 has been obtained for the total intensity method and 0.435 for the magnetic effect as the next best value. Observations with two carefully coordinated instruments and a sun shield are being conducted over a period of six months to a year to obtain certain corrections for the total intensity values which should not alter the general synchronism between its curve and that of the Wolf numbers and should improve the correlation.

[1] Miller, Rev. Sci. Inst. **5**, 405 (1934).

110. The Spectrum of Caesium Hydride. M. P. RASSWEILER AND G. M. ALMY, *University of Illinois.*—A band system of CsH has been photographed in absorption with a 3-meter glass prism spectrograph having a dispersion of some 5A per mm. The absorption column was obtained by heating metallic caesium in a steel tube under hydrogen at atmospheric pressure. The center of the tube was heated to about 600°C, the ends being cooled to protect the windows. The spectrum is of the many line type and extends from 4500A to 6250A. About 90 percent of the observed lines have been assigned to 30 two-branch bands, falling in 3 v' progressions. The vibrational and rotational analysis and the calculation of constants have been completed, except that there remains an additive uncertainty in the v' numbering, due to the covering of the red end of the system by a Cs_2 system. The upper state shows the same anomalous behavior of B and ΔG as has been previously reported in the corresponding $^1\Sigma - {}^1\Sigma$ systems of LiH, NaH and KH.

111. Band Spectra of NiCl and CoCl. KENNETH R. MORE,* *Yale University.*—Band spectra attributed to the NiCl and CoCl molecules have been excited by a h.f. discharge in a quartz tube containing $NiCl_2$ and $CoCl_2$, respectively, in the two cases. The tube was heated externally in order to maintain the discharge. The bands were photographed with a grating having a dispersion of 2.5A per mm. The NiCl bands, which extend from 3900 to 4700A, show several prominent heads degrading to longer wave-lengths. A vibrational analysis shows that the bands can be arranged into four systems with the following constants, in cm^{-1}:

	$\sqrt{\nu_0}$	ω_e'	$x_e'\omega_e'$	ω_e''	$x_e''\omega_e''$
A_1	24623.8	402.9	1.6	420.4	1.1
A_2	24138.0	402.9	1.6	419.1	1.1
A_3	23233.2	399.6	1.7	420.4	1.1
A_4	22748.4	399.6	1.7	419.1	1.1

The vibrational constants indicate that A_1 and A_2 have a common upper state, as have A_3 and A_4. In addition A_1 and A_3 have a common lower state, as have A_2 and A_4. The electronic interval of 485 cm^{-1} between A_1 and A_2 and between A_3 and A_4 is attributed to the ground state. This is a reasonable electronic doublet splitting considering the A factors of the ground states of Ni I and Cl I. The CoCl bands fall in the region 4300 to 4900A and degrade to the red. The FeCl spectrum also is being investigated.

* Sterling Fellow.

112. Ultraviolet Bands of Magnesium Hydride. LOUIS A. TURNER AND W. T. HARRIS, *Princeton University.*—Plates were obtained with a Hilger E-1 quartz spectrograph. They show all of the structure of the bands of the 2430 system which have been measured by Pearse and by Guntsch. In addition they show the structure of a Q branch of the 1–0 band. The expected P and R branches of the 0–1 band hitherto unobserved, are well developed. They break off sharply as in the 0–0 band. In order to satisfy the combination relations of the type $Q_{1,\,1}(K) - Q_{1,\,0}(K) = Q_{0,\,1}(K) - Q_{0,\,0}(K)$ it is necessary to raise by one unit the values of K for the 1–1 band given by Guntsch. Other evidence for the necessity of making this change is obtained from the lines of the band itself. A few lines near the head of the Q branch of the 2–2 band appear.

113. The Spectra of Scandium IV and Scandium V and Their Relation to the Spectra of the Isoelectronic Sequences Starting with Argon and Chlorine. L. W. PHILLIPS AND P. GERALD KRUGER, *University of Illinois.*—The successful excitation of the spectra of scandium in a hot spark has made it possible to identify multiplets arising from electron transitions to the ground states of Sc IV and Sc V. With the help of displaced frequency diagrams, it has been possible to identify corresponding multiplets in Ca IV. The terms identified and corresponding transitions are given in Tables I and II.

Graphs showing the relation of these spectra to the spectra of other ions in the sequence will be shown.

TABLE I. *Scandium IV. Argon sequence.*

	$3p^64s$		$3p^65s$	
	$^2P_1$	$^1P_1$	$^3P_1$	$^1P_1$
Sc IV $3p^6\,{}^1S_0$	(3) 335,540	(4) 340,994	(1.5) 460,432	(1) 464,432

TABLE II. *Ca IV and Sc V. Chlorine sequence.*

	Calcium IV		Scandium V	
	$3s^23p^5$		$3s^23p^5$	
	$^2P^o_{3/2}$	$^2P^o_{1/2}$	$^2P^o_{3/2}$	$^2P^o_{1/2}$
$3s3p^6\,{}^2S_{1/2}$	(12) 152,440	(10) 149,316	(8) 174,419	(7) 170,084
$3s^23p^44s(^2P)\,{}^2P_{3/2}$	(25) 298,175	(5) 295,047	(15) 395,496	(3) 391,166
$3s^23p^44s(^2P)\,{}^2P_{1/2}$	(1) 300,249	(15) 297,128	(7) 398,437	(10) 394,107
$3s^23p^44s(^1D)\,{}^2D_{3/2}$	(15) 314,373		(12) 410,043	
$3s^23p^44s(^1D)\,{}^2D_{5/2}$	(4) 314,078	(10) 310,952	(1) 410,114	(11) 405,786
$3s^23p^44s(^1S)\,{}^2S_{1/2}$	(5) 337,207	(4) 334,096	(2) 437,503	(2) 433,178

* Identified by Bowen. Phys. Rev. **31**, 498 (1928).

114. The Spectra of Scandium VI and Scandium VII and Their Relation to the Isoelectronic Sequences Starting with Sulphur and Phosphorus. H. S. PATTIN AND P. GERALD KRUGER, *University of Illinois.*—The spectra of scandium have been photographed in the wave-length region $\lambda = 80$A to $\lambda = 700$A. Multiplets involving radiation from electron transitions to deep terms have been identified in Sc VI and Sc VII. These are given in Table I and Table II, respectively.

TABLE I.

$3s^23p^4$	$^3P_2$	$^3P_1$	$^3P_0$	$^1D_2$	$^1S_0$
Term Values	0	3350	4476	21,397	49,238
$3s^23p^34s$					
$(^4S)\,{}^5S^o_2$	(30) 452,073	(6) 448,722	(2) 447,590		
$(^2D)\,{}^3D^o_3$	(0) 472,375	(4) 469,056	(5) 467,930		
$\quad {}^3D^o_2$	(5) 472,553	(8) 469,210			
$\quad {}^3D^o_1$	(15) 472,985				
$(^2D)\,{}^1D^o_2$	(1) 478,354	(1) 474,991		(15) 456,955	
$(^2P)\,{}^3P^o_2$		(5) 488,460			
$\quad {}^3P^o_1$	(2) 492,092	(2) 488,750	(5) 487,646		
$\quad {}^3P^o_0$	(6) 492,800	(8) 489,452		(1) 471,405	
$(^2P)\,{}^1P^o_1$	(1) 497,983		(0) 493,491	(8) 476,585	(3) 448,744

TABLE II.

$3s^23p^24s$	$(^3P)\,{}^4P_{1/2}$	$^4P_{3/2}$	$^4P_{5/2}$	
$3s^23p^2$				
$^4S^o_{3/2}$	(7) 541,691	(543,650)	(12) 546,469	
	$(^3P)\,{}^2P_{1/2}$	$^2P_{3/2}$	$(^1D)\,{}^2D_{3/2}$	$^2D_{5/2}$
$^2D^o_{3/2}$	(8) 521,916	(525,192)	(1) 538,866	(7) 539,008
$^2D^o_{5/2}$		(8) 524,511	(10) 538,190	
$^2P^o_{1/2}$	(2) 502,101	(1) 505,380		(8) 519,192
$^2P^o_{3/2}$	(1) 501,193	(5) 504,467	(15) 518,135	(518,282)

115. An Extension of the Yt I and Yt II Spectra. I-DJEN HO AND R. A. SAWYER, *University of Michigan.*—The yttrium spectrum has been photographed from a hollow cathode discharge, with a concave grating vacuum spectrograph and with quartz and glass prism spectrographs. A total of 540 yttrium lines were identified in the region from λ5700 to λ780. Sixty-five new lines were found to be combinations of previously established Yt I and Yt II energy levels. The classification of 247 new lines fixed the position of 38 new Yt II levels which cover the range from 11,724.3 to 129,251.0 ν units. With the available data, the empirical analysis indicates that the Yt II energy scheme does not resemble that of the isoelectronic spectrum, Sr I, which has the series of $5s\ nX$ configurations well developed. The higher states of $4d\ nX$ and $5p\ nX$ of singly ionized yttrium atom are also excited. The closeness of the higher levels of same parity but of different configurations results in strong perturbations which destroy the appearance of multiplets and series among these levels and make their assignment difficult.

116. Term Values in Carbon. C. W. UFFORD, *Allegheny College.*—The energies of the terms of the normal state of CI, $1s^2 2s^2 2p^2$, and the excited state, $1s^2 2s 2p^3$, have been calculated using Torrance's values of the one-electron Hartree functions. This involved the numerical integration of 25 Slater integrals, from which the terms could then be found by his method. In this way the energy for the normal state is -37.6187 atomic units plus the contribution of $F^2(2p, 2p) = 0.2134$ giving the different terms. The lowest $^3P = -37.6614$. For the excited state $^1P = -37.1493$, and the separations of the other terms depend only on $F^2(2p, 2p) = 0.2197$ and $G^1(2s, 2p) = 0.3217$. Fried, working with Shortley, has found $F^2(2p, 2p) = 0.2137$ independently for the ground state by solving the differential equations. This agrees well with the value above, considering the different method used. The separations do not agree well with the observed values. This was to be expected, since the theoretical ratio of the singlet to the singlet-triplet separation is 1.5 in the normal state, whereas the experimental value is 1.13. The separations are somewhat closer to the calculated values of Bacher and Goudsmit.

117. Multiplet Intensities from Electric Furnace Absorption Spectra of Fe I and Ti I. ROBERT B. KING, *Massachusetts Institute of Technology* AND ARTHUR S. KING, *Mt. Wilson Observatory.*—The *total absorptions* of the lines of Fe I and Ti I in electric furnace absorption spectra have been measured and the relative intensities of the lines arising from different low levels derived from the *linear* portion of the *curve of growth* of an absorption line. The condition of thermal equilibrium at a known temperature in the furnace allows the observed intensities to be corrected for a Boltzmann distribution of the atoms among the different low energy levels from which they arise. The absorption spectra method is limited to lines arising from the lower energy levels in the atoms (low E.P. of 0.0 to 2.0 volts). The intensities of 145 lines in 22 multiplets of Fe I, in addition to those previously published,[1] and of 229 lines in 48 multiplets of Ti I. The lines lie between λλ2900–5500 for Fe and λλ3100–6700 for Ti. A comparison of the results with the solar intensities of many of these lines measured by Allen[2] permits a new determination of the temperature of the solar reversing layer.

[1] Astrophys. Jour. **82**, 377 (1935).
[2] Mem. Commonwealth Solar Observatory, Canberra, Australia, No. 5.

118. The Zeeman Effect in Neon. J. B. GREEN AND J. A. PEOPLES, JR., *Ohio State University.*—Back has studied the Zeeman effect in neon and has measured the g values of the $2p^5 3s$ and the $2p^5 3p$ configurations. Using a very powerful electrodeless discharge in pure neon gas in a small capillary between the poles of an electromagnet in a field of 28,000 gauss we have observed and measured the g values of the $2p^5 4p$ and $2p^5 3d$ and $2p^5 4d$ configurations. Our measurements are in excellent agreement with Back's measurements on the $2p^5 3s$ configuration. The $2p^5 4p$ g values are surprisingly different from those of the $2p^5 3p$ g values. Calculating the g values from the parameters determined by Bartberger for the $2p^5 4p$ configuration leads to excellent agreement with the theory and not to the difficulty experienced by Inglis and Ginsburg in the comparison between theory and experiment for the $2p^5 3p$ configuration. The g sums are very satisfactory. Practically all of the lines involving the $2p^5 4d$ and $2p^5 5d$ configurations show incipient Paschen-Back effect. The calculations for the study of these lines are very complicated but can be attacked by the methods of quantum mechanics. There is evidence for the appearance of forbidden transitions of the type $j = 2$ to $j = 0$ on several of the plates.

119. On the Measurement of Hyperfine Structure Separations. D. H. TOMBOULIAN AND R. F. BACHER, *Cornell University.*—In the determination of electric quadrupole moments from hyperfine structure data, it is very desirable to make accurate measurements of certain intervals. With a view to ascertain and possibly increase the precision of such measurements, an experimental study has been made using a Fabry-Pérot interferometer in conjunction with a Zeiss three prism spectrograph. With the three component line λ7852 $5s6p\ ^1P_1 \rightarrow 5s6s\ ^1S_0$ of In II as a test, spectrograms have been obtained with 3, 5, and 8 mm separators. The use of these different separators completely changes the grouping of the components. Measurements of 3 plates at 3 mm separation and 3 plates at 5 mm separation show for the larger interval a maximum deviation from the mean of 0.3×10^{-3} cm^{-1}; and for the smaller interval (which does not seem to be quite as favorable for accurate measurements) a maximum deviation of 0.6×10^{-3} cm^{-1}.

120. Diffuse Reflection of Neutrons from a Plane Surface. O. HALPERN, R. LUENEBURG AND O. CLARK, *New York University.*—The authors have solved rigorously the problem of multiple scattering of neutrons incident with an arbitrary velocity distribution upon the plane surface of an infinitely extended body which scatters the neutrons according to the following three assumptions: (1) The scattering is spherically symmetrical in the laboratory frame of reference. (2) There exists a finite probability for

capture. (3) The absolute value of the neutron velocity remains constant. These three assumptions are approximately verified in nature for nonhydrogenic bodies of not too small an atomic weight and all neutron velocities, and for hydrogenic bodies and slow neutrons. The problem is solved with the help of an exact integration of the modified Fokker integro-differential equation. The solution leads to explicit numerical expressions for the coefficient of reflection as function of the ratio of capture cross section to scattering cross section. Comparison with the experiments so far available leads to values for hydrogen which are 50 percent to 100 percent higher than those obtained by Fermi and collaborators. Work on other geometrical arrangements and generalizations as far as the scattering properties of the body are concerned is in progress.

121. Experimental Study of Neutron-Proton Interaction. CURTIS W. LAMPSON, *Princeton University;* DONALD W. MUELLER, *Cornell University;* AND HENRY A. BARTON, *American Institute of Physics.*—A neutron source was provided by bombarding a target of deuterium compound with a 1 mm diam. beam of deuterons. Neutrons passing into a photographic emulsion encounter protons which recoil and, on their passage through the emulsion, render developable the grains of silver bromide in their path. Microscopic examination of the developed plate reveals tracks containing as many as 45 grains and as great as 75μ in length. The length orientation and position with respect to neutron source of these tracks may be accurately measured. From these data the recoil angle of a track may be computed and thus a statistical distribution of the number of tracks with respect to recoil angle obtained. This distribution curve has a maximum between 20–30 degrees. If neutron-proton impacts could be regarded as occurring between elastic spheres the maximum should lie at 45 degrees. This discrepancy indicates the existence of comparatively long range forces between the neutron and proton. Assuming conservation of energy and momentum the energy of the impinging neutrons can be found and appear to form a fairly homogeneous group of 2.55 Mev.

122. Scattering of Neutrons of Homogeneous Energy by Protons. P. GERALD KRUGER, W. E. SHOUPP AND F. W. STALLMANN, *University of Illinois.*—An investigation of the angular scattering of neutrons, by protons, has been carried out. The neutrons were produced by bombarding D_2O ice with 1 Mev volt deuterons from a cyclotron. These neutrons have a homogeneous energy of 2.55 Mev.[1] The distance between the neutron source and the cloud chamber, in which the scattering was observed, was 52 cm. Photographs taken with the chamber filled with methane showed 1000 measurable tracks. Of these 400 had the proper length to satisfy the momentum condition and our results are based on these selected tracks. In measuring the tracks the azimuthal angle as well as the scattering angle was measured. The azimuthal distribution specifies the necessary correction which must be made for the solid angle cut off by the top and bottom of the chamber. When these data are plotted on a curve whose ordinate is the percent scattered at angle ϕ per unit solid angle and whose abscissa is the scattering angle ϕ, the curve is a cosine curve within the limit of experimental error. This indicates that the scattering is essentially elastic.

[1] Bonner and Brubaker, Phys. Rev. **49**, 19 (1936).

123. Scattering of Neutrons Absorbed by Iodine. ALLAN C. G. MITCHELL AND R. N. VARNEY, *New York University, University Heights.*—A quantitative study of the scattering of neutrons absorbed by iodine (I group) was undertaken to see if there was any marked dependence of scattering cross section on neutron energy. The method used was that previously described.[1] Neutrons, slowed down by paraffin, were filtered through 0.218 g/cm^2 of Cd to absorb the thermal neutrons. CHI_3 deposited in a thin layer of paraffin served as a detector of I neutrons. Complete scattering curves were run for the elements Fe, Ni, Pb and Ag, and relative cross sections for scattering determined on the same basis as that previously used.[1] The results showed that, for the first three elements, there was no marked difference between the scattering cross section for I neutrons and that for the groups *A*, *B*, *C*, and *D*. The scattering curve for Ag was similar to that obtained using a silver detector and neutrons filtered through Cd; 2 cm of Ag scatters back 25 percent of the incident neutrons.

[1] A. C. G. Mitchell, E. J. Murphy and M. D. Whitaker, Phys. Rev. **50**, 133 (1936).

124. Neutron Absorption Limit in Cadmium. M. STANLEY LIVINGSTON AND J. G. HOFFMAN, *Cornell University.*—In order to find the high energy limit of neutrons absorbed in Cd the absorption of the transmitted neutrons in boron was measured. Neutrons from a Rn-Be source in a paraffin sphere (10.75 cm radius) were detected in a boron fluoride ionization chamber with a linear amplifier and counter. The chamber was shielded with 0.5 mm Cd and 0.5 g/cm^2 of B_4C except for an aperture facing the sphere. Boron absorption curves were taken with and without 0.5 mm Cd using B_4C and Pyrex glass, respectively, in front of the aperture. After applying a 10 percent obliquity correction (calculated) the slow neutron absorption coefficient is found to be 36 cm^2/g B, in agreement with Amaldi and Fermi. The Cd penetrating neutrons are inhomogeneous in energy and therefore are not absorbed exponentially but according to the law: $(1-e^{-x})/x$, where $x=K\delta$ and K is the absorption coefficient for neutrons just penetrating Cd. K is found to be 9.5 cm^2/g B. The number of counts produced by neutrons penetrating 0.5 mm Cd is 8.4 percent of the total; 5.7 percent are absorbable in thick boron. The remaining 2.7 percent are probably due to fast neutrons disintegrating B or F or stray neutrons entering the chamber through the shields.

125. Neutron Absorption Limit of Cadmium. J. G. HOFFMAN AND H. A. BETHE, *Cornell University.*—The ratio of the absorption coefficients of Cd penetrating and thermal neutrons is $9.5/36=0.264$ (see preceding abstract). Therefore the absorption limit of Cd is $kT/.264^2=0.37$ volt. Thus Cd absorbs not only thermal neutrons but also neutrons of considerably higher energy. This result may be compared with that of the wheel experiment of Rasetti and

others[1] which gives the dependence of the capture probability p on the energy at thermal energies $(d \log p/d \log E)_{kT} = 0.28$. Accepting the Breit-Wigner formula for the capture probability, $p \sim [(E-E_r)^2 + \frac{1}{4}\Gamma^2]^{-1}$, the resonance energy E_r and the width of the resonance level Γ may be determined. The result is $E_r = 0.16$ volt, $\Gamma = 0.16$ volt which agrees with that obtained from the absorption of D neutrons in Cd[2]. The width is of the same order as for other neutron resonance levels. With these data, the cross section is almost independent of the energy from thermal energies up to about 0.2 volt. From the absolute cross section, the "neutron width" may be determined; it is about $\Gamma_n = 1.7 \times 10^{-3}$ volt, i.e., about the same as for Rh, Ag, etc.

[1] Phys. Rev. **49**, 104 (1936).
[2] Amaldi and Fermi, Phys. Rev. **50**, 899 (1936).

126. Absorption of Resonance Neutrons. H. H. GOLDSMITH AND J. H. MANLEY, *Columbia University*.—For a substance in which a single resonance level is effective, the neutron absorption coefficient varies as v^{-5}, provided the neutron energy is much greater than both the resonance width and the resonance energy. This v^{-5} law affords a sensitive method for measuring neutron energies in a limited range; different energy regions may be explored by choosing appropriate absorbers. In previous work the absorption in Cd was measured in order to check the boron v^{-1} law in the neighborhood of 1 ev. The method has now been extended, using Hg absorption to study the same region, and using Ir absorption to investigate the region of the I, As and Br resonance levels. The relative positions of the Gd, Sm, Hg, and Cd levels have been determined by the boron method. The order of the average energies of these levels as indicated by these measurements is $E_{Hg} > E_{Cd} \sim E_{Sm} > E_{Gd}$. Experiments in which boron absorption was replaced by Ag absorption led to similar results. Absorption experiments in which a V detector was used without a Cd filter yielded cross sections which were approximately equal to the C neutron cross sections. Similar results with Dy detector show that these elements are essentially C neutron detectors.

127. Neutron Energy Levels. J. H. MANLEY, H. H. GOLDSMITH AND J. S. SCHWINGER, *Columbia University*.—Absorption measurements have been performed on Rh, In, and Ir with the same substance as both absorber and detector. The experimental absorption curves have been compared with theory, taking into account the angular distribution of the neutrons and the absorption in the detector of both neutrons and electrons. In the case of Rh (detector thick with respect to electronic absorption) the experimental curve may be fitted by assuming a single, narrow resonance level with a cross section at resonance of about 6000×10^{-24} cm^2. For thick detectors and large absorber thickness the calculated curve is independent of the angular distribution of the neutrons and is practically independent of the cross section at resonance, being essentially determined by the electronic absorption coefficient, μ_e. It may be shown that the transmission in this region is approximately $(\pi \mu_e x)^{-1}$ where x is the absorber thickness. For thin detectors, however, the corresponding expression is $(\pi \mu_{Res} x)^{-1}$ where μ_{Res} is the absorption coefficient for homogeneous neutrons with the resonance energy. The correlation of the experimental data on resonance widths, resonance energies, and resonance cross sections with the theory will be discussed.

128. Experiments on the Magnetic Moment of the Neutron. P. N. POWERS, H. CARROLL AND J. R. DUNNING, *Columbia University*.—The experiment described recently,[1] involving the transmission of neutrons through three iron plates magnetized to saturation and then demagnetized, has been repeated using neutrons which are emitted from an "howitzer" cooled to approximately the temperature of liquid air. The results of this experiment are shown in Table I.

TABLE I.

	Total No. Counts	No./Min.	Differences
Magnetized	70,578	157.66 ± .60	4.7 ± .8
Demagnetized	68,517	153.01 ± .58	
Background with Cd	10,972	65.8 ± .6	87.2 ± .8

These differences represent a 5.3 percent ± 1.0 percent increase in cold neutron transmission when the plates are magnetized to saturation as compared to a 3.6 percent ± 0.6 percent increase for room temperature neutrons.[1]

Similar runs were made using only two of the plates. The results obtained indicate a 1.9 percent ± 0.7 percent effect for the room temperature neutrons and a 2.9 percent ± 0.7 percent effect for the cold neutrons. The increase is proportionately the same with two plates and with three plates, although with two plates the effects are so small that the increase is not significant.

In these experiments the "howitzer" was cooled by circulating liquid air through copper tubing embedded in the paraffin. The temperature of the paraffin averaged 105°K. Although it has not been ascertained that the neutrons have a Maxwellian distribution of velocities at this low temperature, these results are in qualitative agreement with theory.[2-4]

[1] Powers, Beyer and Dunning, Phys. Rev. **51**, 371 (1937).
[2] Bloch, Phys. Rev. **50**, 259 (1936).
[3] Hoffman, Livingston and Bethe, Phys. Rev. **51**, 214 (1937).
[4] Schwinger. (In Process of Publication.)

129. The Yield of Protons and Neutrons from the Deuteron-Deuteron Reaction. RUDOLF LADENBURG AND MORTON H. KANNER, *Princeton University*.—We have measured the yield of protons and neutrons by bombarding targets of heavy ice with deuterons between 100 and 200 kv. The arrangement was essentially the same as before used by Ladenburg-Roberts (Phys. Rev. **50**, 1190 (1936)). The cross section for scattering of the neutrons which has to be known for calculating the absolute yield of neutrons in our method, was determined for the homogeneous neutrons used. The result is that at 1μA and 100 kv the proton yield is 2.3×10^5 per second, taking into account the anisotropy of the yield; the neutron yield turned out to be about as large. When slowed down by paraffin, the neutrons were equivalent to +38 mc, Ra mixed with fine Be powder, so that 1 mc produces 6000 neutrons per second (Amaldi-

Fermi find 27,000 per second per mc). The effective cross section for the yield is constant within 5 percent in the investigated energy range; its absolute value is 1.7×10^{-26} for the neutron yield, but is subject to some uncertainty on account of the reduction of the results to a pure deuteron target.

130. Disintegration of the Deuteron under Fast Alpha-Particle Bombardment. H. L. SCHULTZ, *Yale University.*—Several attempts to observe the disintegration of the deuteron under bombardment by alpha-particles according to:

$$_1H^2+{}_2He^4\rightarrow{}_1H^1+{}_0N^1+{}_2He^4$$

have been made. Rutherford and Kempton using Po alpha-particles found no detectable yield of neutrons, and subsequent experiments of Dunning with RaC′ particles indicated a very small effect if any. In either case, however, the method of detection applied to fast neutrons only; moreover, in the latter case any slight yield might be explained by the photo-disintegration of the deuteron. In view of the theoretical importance of this reaction, it was thought desirable to extend the above measurements to higher energies (ThC′ particles) using a more sensitive neutron detecting arrangement, especially for lower energies. Accordingly, with a neutron detector consisting of a BF_3 filled ionization chamber surrounded by paraffin and connected to a linear amplifier, a large number of counts were taken alternately with the source exposed to 1.2 cm air equivalent of D_2 gas and with the source covered by a thin Cu plate. The data obtained in this manner indicate a small yield. Comparison with the yield from N^{14} under identical conditions gives a cross section roughly in agreement with theoretical estimates of Massey and Mohr. Preliminary experiments with RaC′ sources give no indication of a yield.

131. The Beta-Ray Spectrum of Radium E. J. S. O'CONOR, S.J.,* *Massachusetts Institute of Technology.*—The distribution in energy of electrons from radium E was examined by means of a magnetic spectrometer using Geiger-Müller coincidence counters. Special precaution in the form of a baffle system was employed to reduce scattering effects. The radioactive material was examined under different conditions of source strength, mounting material and aperture of defining slits with a view to determining the effect of these variables on the experimental distribution curve. It is concluded that the position of the high energy *experimental* end point depends on the source strength used as well as the width of the defining slits. Below a definite source strength and with narrow defining slits the results from radium E mounted on nickel and on platinum were self-consistent. Using data from these latter distribution curves an analysis was made to test the validity of the Fermi and the Konopinski-Uhlenbeck theories of beta disintegration after the manner introduced by Kurie, Richardson and Paxton. It was found that the linear relation, used as a criterion, did not exist for the Fermi function but appeared in the "K-U" plot within the limits of error set by statistical fluctuations and finite slit widths. From extrapolation of the "K-U" plot the high energy end point was found to be 1.25 Mev±0.03 Mev.

* Now at Woodstock College, Woodstock, Maryland.

132. Shape of the Beta-Ray Distribution Curve of Radium E at High Energies. LAWRENCE M. LANGER AND MARTIN D. WHITAKER, *New York University, University Heights.*—The beta-ray spectrum of radium E was measured by means of a magnetic spectrometer and coincident counters. Because of the strong source available, and the low background of the detecting mechanism, it was possible to obtain significant data much closer to the end-point than has been done heretofore. The distribution was found to end, without a tail, at $H\rho=5330$ oersted-cm, or 1.17×10^6 electron volts. The Fermi and K-U plots of the experimental data do not give straight lines as predicted by the theory. Extrapolation of the straight part of the K-U plot gives an end-point 17 percent higher than that observed.

133. The Calculation of Phase Shifts in Scattering Problems. E. L. HILL, *University of Minnesota.*—The calculation of elastic scattering problems in quantum mechanics is reducible to that of finding the asymptotic forms of the solutions of a family of equations of the type

$$g_L''+\gamma_L g_L=0, \quad L=0,\ 1,\ 2,\ \cdots,$$
$$\gamma_L(x,\epsilon)=\epsilon+\varphi_L(x)+\frac{B_L(x)}{x}-\frac{L(L+1)}{x^2},$$

where $B_L(x)$ and $\varphi_L(x)$ are finite at $x=0$. This equation is transformed as follows:

$$\gamma>0, \qquad g=a(x)\sin\sigma(x); \quad g'=\gamma^{\frac14}a(x)\cos\sigma(x);$$
$$\sigma'=\gamma^{\frac12}+\tfrac14(\ln\gamma)'\sin2\sigma; \quad (\ln a)'=-\tfrac14(\ln\gamma)'(1+\cos2\sigma);$$
$$\gamma>0, \qquad g=(\chi_1+\chi_2); \quad g'=-(-\gamma)^{\frac12}(\chi_1-\chi_2);$$
$$\chi_1'=-(-\gamma)^{\frac12}\chi_1-\tfrac14[\ln(-\gamma)]'(\chi_1-\chi_2);$$
$$\chi_2'=-(-\gamma)^{\frac12}\chi_2+\tfrac14[\ln(-\gamma)]'(\chi_1-\chi_2).$$

These transformations are regular except at $x=0$ and at points for which $\gamma=0$, but investigation shows that $\sigma(x)$ and $\chi=\chi_1/\chi_2$ do nothing peculiar there, even though $a(x)$ does. For the study of the asymptotic form of g, the function $\sigma(x)$ is important because its equation can be integrated (numerically) without evaluating $a(x)$, and the phase shifts computed directly. If $\gamma<0$ for $x<x_1$ and $x>x_2$, and $\gamma>0$ for $x_1<x<x_2$, a discussion shows that an approximate "quantum condition" for a proper function with n nodes in (x_1, x_2) is

$$\sigma(x_2)-\sigma(x_1)=(n+\tfrac12)\pi+\pi.$$

When γ'/γ is small compared to $\gamma^{\frac12}$ the standard approximate form $\sigma(x)=\sigma(x_0)+\int_{x_0}^{x}\gamma^{\frac12}dx$ can be used. Boundary conditions are as follows (continuous spectrum):

$$L=0, \quad \sigma_0(0)=0,$$
$$L>0, \quad \chi_L(0)=\{[L(L+1)]^{\frac12}-(L+1)\}/\{[L(L+1)]^{\frac12}+(L+1)\},$$
$$\chi_L\rightarrow-1 \quad \text{as} \quad x\rightarrow x_1-0,$$
$$\sigma_L\rightarrow0 \quad \text{as} \quad x\rightarrow x_1+0.$$

134. The Scattering of Protons by Protons. L. R. HAFSTAD, N. P. HEYDENBURG AND M. A. TUVE, *Department of Terrestrial Magnetism, Carnegie Institution of Washington.*—Observations on the scattering of protons by protons have been extended to the energy-region below 600 kv by using a Geiger point-counter to detect the

scattered and recoil protons. The angular variation of these protons was investigated at the fixed voltages, 200, 300, and 400 kv. The data definitely indicate a large decrease in the ratio of the observed scattering to Mott's theoretical scattering at 45° in the region of 300 to 400 kv, as would be expected on the basis of the attractive forces demonstrated by our measurements a year ago. The absolute values of the scattering are not yet satisfactorily quantitative due to the presence of residual counts probably caused by ultraviolet light.

135. The Multiple Scattering and Stopping of Electrons. MORRIS E. ROSE,* *Cornell University.*—The scattering and stopping of electrons in a thick foil have been investigated; the foil is considered thick enough so that it is necessary to treat multiple scattering. Because at high energies (above 1 Mev in Al) the stopping predominates and at lower energies the scattering is more important, it is permissible to treat each effect separately in the two energy regions. The angular distribution and "Umwegfactor" of electrons of any primary energy transmitted by a foil have been found. At low energies the scattering may be treated as a diffusion process with energy dependent diffusion coefficient. Taking into account both stopping and scattering a formula has been derived for the transmitted intensity of an initially homogeneous beam. This formula is easily generalized to arbitrary energy distribution and thus absorption curves can be found for the electrons (positrons) from artificial radioactivity or for the secondaries generated by γ-rays. For measurements of γ-ray energy it is important to have the relation between the half-value thickness, $d_{\frac{1}{2}}$, and γ-ray energy.[1] This has been obtained for Al. The results show that the assumption of linearity[1] is unsatisfactory. The computed $d_{\frac{1}{2}}$ in Al for the ThC″ (2.62 Mev) γ-ray is 0.27 g/cm² in exact agreement with the measured value of Fleischmann.

* This work was supported by a grant-in-aid from the Penrose Fund of the American Philosophical Society.

[1] F. Rasetti, Zeits. f. Physik **97**, 74 (1935); R. Fleischmann, Zeits. f. Physik **103**, 113 (1936).

136. Small Angle Scattering of Fast Electrons. J. B. H. KUPER, *Princeton University.*—A large sized electron scattering apparatus with an electrostatic energy analyzer has been used to study the elastic scattering of electrons with energies between 50 and 90 kilovolts in argon, neon, helium and hydrogen. The construction of the apparatus permits measurements in the range of angles from 0° to about 6°, but in the lighter gases it was impossible to carry the measurements beyond 3°, owing to a background current (presumably electrons multiply scattered from the walls). In order to secure sufficient intensity gas pressures of the order of 5×10^{-2} mm Hg (with differential pumping maintaining a pressure roughly 1000 times lower in the analyzer) and bombarding currents of about 3 microamperes were used. The work is being extended by a study of the inelastic scattering which necessitates the use of a counter in place of the Western Electric electrometer tube used for elastic scattering. The experimental curves seem to be in good agreement with the quantum mechanical predictions based on Born's approximation and the Hartree fields.

137. Electron Scattering and the Action of a Collector Electrode in an Electron Swarm. ERNEST G. LINDER, *RCA Manufacturing Co. Inc., Camden, N. J.*—It is shown that in cases where electrons execute cyclic orbits such that they return periodically to the neighborhood of the cathode, as in magnetrons and positive grid tubes, considerable electron scattering may occur. Due to this a fraction of the orbital velocity is converted to random velocity, and electrons, on the average, are therefore unable to return to the cathode surface, or to the surface of any collector at the same potential. If the scattering is such as to lead to a Maxwellian distribution, a virtual cathode forms about the real cathode or collector, its temperature being given by $\bar{V}e=(3/2)kT$, where $\bar{V}e$ is the part of the orbital energy converted to random energy. The potential difference between the real cathode, or collector, and the virtual cathode is also $\bar{V}$. For a collector not at zero potential the potential difference is $V_g-\bar{V}$. The Langmuir-H. M. Mott-Smith expression for current to an internal collector with a retarding field is applicable, and yields

$$I_g=\frac{(1-f)r_0I_c}{r_1+r_2}\exp\frac{e(V_g-\bar{V})}{k(T+T_0)},$$

where I_g is the collector current, f the electron reflection coefficient, r_0 the collector radius, r_1 and r_2 the virtual cathode radii about the cathode and collector, respectively, I_c the circulating current, and T_0 the filament temperature. Experimental data are in agreement with this expression.

138. The Compton Effect with Gamma-Rays. ROBERT S. SHANKLAND, *Case School of Applied Science.*—The studies using Geiger-Müller counters[1] of directional and coincidence effects in the Compton scattering of the gamma-rays from RaC have been continued. The scatterer used is an aluminum foil of thickness 0.00165 cm. Two complete series of observations have been made. In one series the electron counter was placed in the azimuth $+\theta$ demanded by the photon theory where 195 discharges were recorded coincident with those in the gamma-ray counter set in the azimuth ϕ. A comparison experiment showed that 94 of these coincidences were probably due to chance. In the second series of observations the electron counter was set in the azimuth $-\theta$, symmetrical with respect to the first position, but on the opposite side of the incident beam of radiation. In this position 141 coincidences were observed of which 105 were probably due to chance. Thus the ratio of the number of true coincidences to the total number observed is 0.52 in the predicted position of the electron counter, and 0.26 in the other position. The observation of true coincidences in the $-\theta$ position of the electron counter is due to the deflection which the recoil electrons may suffer in leaving the foil. This experiment checks the predictions of the theory in two respects. First, it shows a time-coincidence between the scattering of the gamma-ray and the appearance of the recoil electron. Second, the results are consistent with the angular relationship predicted by the Compton theory. The results may be interpreted as confirming this relationship to within ±21°.

[1] R. S. Shankland, Phys. Rev. **49**, 8–13 (1936); **50**, 571 (1936).

139. A Stable Source of Focused Ions. LLOYD P. SMITH AND GEORGE W. SCOTT, JR., *Cornell University.*—A considerable modification of the ion source already described (L. P. Smith and H. A. Carlock, Phys. Rev. **49**, 646 (1936)) has been made so as to produce a focused beam of positive ions when a gas is bombarded by a focused beam of electrons. Gas is admitted to a cylindrical chamber where the pressure is somewhat higher than in the remainder of the system. Electrons are produced by a cylindrical nickel cathode which is oxide coated on the interior and indirectly heated by a suitable tungsten heating coil. When proper potentials are applied to the ionization chamber and the cathode, which is placed close to the former and coaxial with it, the combination acts as a convergent electrostatic lens which focuses the electrons at the interior of the chamber. This, together with a somewhat larger cylinder located at the opposite end of the cathode and coaxial with it, served to focus the positive ions since such a lens system possesses focal properties which is independent of e/m. The ion current, as measured by a Faraday cylinder which was shielded and biased to remove all unfocused ions and possible secondary electrons from the measuring electrode, was found to be very steady when hydrogen was used, the pressure of which was about 2×10^{-4} mm Hg in the main part of the system.

140. Drift of Ions and Electrons under the Action of Concentration Gradient, Electric and Magnetic Fields. LEWI TONKS, *Research Laboratory, General Electric Company.*—The Boltzmann equation must be satisfied by any mobility equations when the drift velocities are put equal to zero, irrespective of the presence of a magnetic field. As a consequence, concentration gradient and field strength components must always appear in the combination $(neX/kT-\partial n/\partial x)$ which, set equal to zero, is a form of the Boltzmann equation. Neither Townsend's original equations[1] nor Huxley's later attempt at refinement[2] conforms to this requirement. Satisfactory equations from this point of view are: $nu/K_H=(neX/kT-\partial n/\partial x)+\omega\tau(neY/kT-\partial n/\partial y)$ and $nv/K_H=(neY/kT-\partial n/\partial y)-\omega\tau(neX/kT-\partial n/\partial x)$ where the magnetic field H is parallel to z, u and v are the drift components, $\omega=eH/mc$, τ is the mean free time of an ion, and $K_H=(1+\omega^2\tau^2)^{-1}K$ is the magnetic diffusion coefficient, K being the nonmagnetic one. A deducible conclusion which is important for high current arcs is that in the direction of drift, the motion is the same as that arising from the electric field and concentration gradient components in that direction alone in the absence of all other components and of the magnetic field itself.

[1] Proc. Roy. Soc. **86**, 571 (1912).
[2] Phil. Mag. **23**, 210 (1937).

141. Coefficient of Combination between Small Ions and Large Ions. G. R. WAIT, *Department of Terrestrial Magnetism, Carnegie Institution of Washington.*—The value of the coefficient of combination between small ions (mobility about 1.5 cm/sec./volt/cm) and the large ions (mobility about 5×10^{-4} cm/sec./volt/cm) has been determined from data simultaneously obtained on small ion and large ion concentrations in the atmosphere and on the rate of small ion formation. The average value found for the coefficient was about 9.0×10^{-6} with a considerable range in the values, the largest being more than two times the smallest. The combination coefficient was found to vary with temperature and absolute humidity of the air, the correlation with both being between $+0.5$ and $+0.7$. One interpretation of the results is that the combination coefficient varies because the size of the particle of which the large ion is composed varies with the absolute humidity. Evidence substantiating this interpretation is presented.

142. Convection Currents in Mercury Arcs. CARL KENTY, *General Electric Vapor Lamp Company.*—Convection currents in high intensity lamps (2.9 amp. arcs in 33 mm tubes in Hg vapor at 1 atmosphere) are studied by observing under a red glass the motions of incandescent particles of MgO. In the arc stream the smaller particles vaporize and enough light is produced for their motions to be photographed on a moving film (red filter). In the vertical position a strong upward current exists in the core and a much slower current of cold gas downward near the walls. On half wave operation a dark space of 2 cm develops at the bottom during the 0.01 sec. zero current period. This gives an upward core speed of 200 cm per sec. on the view that rising hot gas is being replaced by cold gas from below. Viscosity calculations following Elenbaas using his temperature distribution (5400°K at axis for this case) give a speed of around 90 cm per sec. Horizontal operation requires a magnetic field to keep the arc from bowing up. Force measured: 1.5 dynes per cm. Force roughly calculated using Archimedes principle and Elenbaas' temperature (density) distribution: 1.2 dynes per cm. Magnetic reaction forces the gas rapidly downward through the core, particles show.

143. The Frequencies and Nodal Lines on Circular Metallic Plates.* R. C. COLWELL, A. W. FRIEND AND H. C. HARDY.—The mathematical solution for circular plates was developed by Kirchhoff in 1850. His equation takes the form $J_n(kr)+\lambda J_n(ikr)=0$. When the plate is clamped at the center two more terms appear in the solution and the equation is $\alpha J_n(kr)+\beta G_n(kr)+\gamma I_n(kr)+\delta K_n(kr)=0$ (Southwell). It is possible to test these equations by means of an oscillating valve working into a magnetostrictive oscillator. Experiment shows that there is complete agreement between theory and experiment in so far as the nodal lines are concerned provided they are circles or diameters or combinations of these. The frequencies are in agreement for low values but above 5000 r.p.s. the necessary approximations in the theory cause a considerable error in the calculated frequencies.

* To be read by title.

144. Electrophoresis and Electroosmosis of Drugs Through the Skin.* HAROLD A. ABRAMSON, *Medical Service of Dr. George Baehr, The Mount Sinai Hospital, New York City.*—It has been customary to apply the classical equations for ion and water transport across the human skin when considering the conditions favorable to electroosmosis of certain chemical substances, especially

drugs. These classical equations for ion transport probably never apply across the skin but only to the movement of ions up to the skin. In the pores of the skin itself, a new set of conditions exist which may lead to the complete reversal of the effect anticipated from the classical equations. The classical equations may not be valid because of correction terms which include (1) decreases (increases) in the transfer number of effective ions in the pores of the skin; (2) the addition of an electroosmotic term; (3) reversal of the sign of the electrokinetic potential of the skin; (4) surface conductance in the pores of the skin. Application of these principles has as yet been only qualitative for a system so complicated as the human skin. They have, however, been made successfully with low current densities to the anesthetization of the skin with procaine as a preparatory measure for intradermal skin tests in hay-fever and allied conditions. These principles are also of service in elucidating the mechanisms of the electrical transfer of histamine through the skin irrespective of the charge of histamine ion.

* To be read by title.

145. A Physical Analysis of the Dead Beat Mechanism of the Auditory Ossicles. OTTO STUHLMAN, JR., *University of North Carolina.*—Bekesy (Akust. Zeits. **1**, 13 (1936)) shows by optical means the dead beat character of the plucked vibrations of the tympani and malleus. How does the ossicle chain transmit this motion to the stapes? A 24X scale model of the ossicles was constructed, with accurate scale reproductions of the articulating surfaces. Model mounted on horizontal turntable. Malleus, anterior process down on axis. Incus short crus up 80 degrees with axis of rotation. Lever arms 5–4–3. Rotation of malleus produced displacements of lenticular process of incus, measured with a 1/100 mm displacement gauge. One degree rotation of malleus produced via the articulation a superior, inferior, anterior and posterior displacement of 0.33, 0.75, 0.42 and 0.61 mm. Resultant motion makes 57 degree angle with axis of long crus. Helmholz' "Sperrzahne" here viewed as corrugations with no real locking properties. Stapes, possesses a Gothic superior arch and a parabolic inferior arch, bent 23 degrees downward. Gothic arch tension, parabolic arch compression. Thrust of incus up, articulation on inferior side of head. If motion of malleus is in, incus moves in, up and forward (anterior). If out, incus moves out, down and back (posterior). Resulting stapes motion, superior-anterior margin in, inferior-posterior margin out. First motion checked by stapedius tensor, second by tensor tympani making both in and outward motions of tympani dead beat.

146. The Time Lag in Gas-Filled Photoelectric Cells. A. M. SKELLETT, *Bell Telephone Laboratories, Inc.*—The origin of the time lag in gas-filled photoelectric cells has never been satisfactorily explained. Measurements were made of the time lag in such a cell having a small anode concentric with a spherical cathode, using variable light and constant potential. The light intensity was varied in accordance with the expression $A+B \sin \omega t$ and the alternating component of the output current of the cell was measured at frequencies of illumination varying from 60 to 20,000 c.p.s. The resulting response *vs.* frequency characteristic exhibited maxima and minima, a maximum falling at twice the frequency of the first minimum. This indicates a time lag in the output current equal to half the period of the light variation at the first minimum. The value thus determined is in excellent agreement with the value calculated from the positive ion mobility on the basis that the lag is due simply to the transit time of these ions. In other designs of cells the effect is obscured by secondary emission at the cathode though the mechanism which causes the lag is undoubtedly the same.

147. A Continuously Sensitive Cloud Chamber. ALEXANDER LANGSDORF, JR., *Massachusetts Institute of Technology.*—The thermally activated diffusion cloud chamber previously described[1] has been further developed. As before, a vapor is diffused vertically downward through a permanent gas from the heated top to the refrigerated bottom of a chamber, where it condenses. In an intermediate region supersaturation is sufficient to show tracks caused by ionizing particles. With proper regulation, the present chamber should show tracks in a volume about four inches deep and thirty inches in diameter. The chamber is built to allow operation with a partial vacuum; an air-lock arrangement permits introduction of radioactive samples during operation. A general rain of spontaneously formed droplets[1, 2] probably cannot be eliminated, but by careful regulation of all variable quantities it should be maintained at a low enough density to permit photography of the ion tracks. In addition to uses in nuclear and cosmic-ray research, this cloud chamber offers several possibilities in the study of the physical phenomena attending supersaturation and condensation.[3]

[1] A. Langsdorf, Jr., Phys. Rev. **49**, 422 (1936).
[2] R. E. Vollrath, Rev. Sci. Inst. **7**, 408 (1936).
[3] L. Farkas, Zeits. f. physik. Chemie **125A**, 236 (1927); M. Volmer and H. Flood, Zeits. f. physik. Chemie **170A**, 273, 286 (1934).

148. Grain Spacing of Alpha-Ray, Proton and Deuteron Tracks in a Photographic Emulsion. T. R. WILKINS AND H. J. ST. HELENS, *University of Rochester.*—The difference in the average separation of the grains in a photographic emulsion traversed by alpha-rays, protons and deuterons promises to provide an extremely valuable tool in nuclear research. The special Ilford R2 emulsion made for us has been exposed to ThC′ alpha-rays and to protons and deuterons from cyclotrons. An extended sensitometric study has indicated 3 min. development in D11 at the usual temperature (62°F). The tracks were viewed under a magnification of 900 (4 mm 45X objective and 20X hyperplane eyepiece) and dark field illumination. The average separation for all three types of particles increases with the length of the track. Graphs showing the scatter and the average grain spacing will be presented. The average grain separations for the last five grains of the tracks for this batch of the R2 emulsion were alpha 1.63μ deuterons 1.89μ protons 2.7μ. The technique has already been used by us in the study of cosmic-ray tracks.* Some further examples of its application to cosmic-ray proton group disintegrations obtained in plates exposed on Mt. Evans, Colorado, will be shown.

* National Geographic Society, Stratosphere Series No. 2.

149. Vacuum Tube Circuits for Scaling Down Counting Rates. E. C. STEVENSON AND I. A. GETTING, *Harvard University.*—The introduction of some regularity resulting from scaling down of randomly distributed pulses increases the efficiency of relatively slow mechanical counters by a ratio greater than to be expected from the scaling factor alone. The ultimate efficiency that can be reached is fixed by the resolving power of the scaling down circuit. If vacuum tubes are used instead of thyratrons, as in the Wynn-Williams scale of two, shorter resolving time as well as greater stability and durability is realized. Two very efficient circuits, operating at a great economy of plate power, have been devised and tested. The first circuit employs two tubes or one duplex tube in each halving section with a rectifying amplifier between each section. Its resolving time, found experimentally, is 1/2000 second. The second circuit employs four tubes or two duplex tubes in each halving section and an amplifier between each section. Its resolving time, found experimentally, is at least 1/20,000 second. At speeds greater than 1000 pulses per second, the circuit has successfully halved the input frequency of both sine waves as well as sharp pulses. These circuits should find application in recording rapid Geiger-Müller counter pulses and as adjuncts to frequency meters of limited range.

150. Discharge Mechanism and Characteristics of Geiger-Müller Counter Tubes. O. S. DUFFENDACK, M. M. SLAWSKY AND HAROLD LIFSCHUTZ, *University of Michigan.*—Experiments were made on counter tubes with 3 mil tungsten wire anodes and cathodes, 1 cm in diameter, of Al, Cu, Ni, and W. A, air, O_2, and H_2 at various pressures were used. The volt ampere characteristic curves were correlated with the voltage count characteristics using a Neher-Harper coupling circuit and a single thyratron operating a high impedance Cenco counter. Reliable counting characteristics and long plateaus were obtainable only with counters whose cathode surfaces were completely cleaned by a glow discharge in H_2 previous to filling. Al cathodes gave no plateaus in any gas. H_2 gave the longest plateaus, A the shortest. The results are in general accord with the conclusions of Werner and indicate that the operation of the tubes involves the initiation of a corona discharge in which the amplification depends upon both the ionization of the gas by electron collisions and the extraction of electrons from the cathode surfaces. All counters were observed to increase in photoelectric sensitivity with increasing applied voltage. Metastable atoms and the work function of the cathodes seem to play important roles in limiting the range of the plateau.

151. Determination of the Counting Losses in Thyratron Recording Circuits. HAROLD LIFSCHUTZ, O. S. DUFFENDACK AND M. M. SLAWSKY, *University of Michigan.*—To determine the counting losses in single and scale of eight thyratron recording circuits operating a Cenco counter, a known source of random pulses was obtained by two methods. The first consisted in recording the pulses from a Geiger-Müller tube counter on the sound track of a movie film. The recording apparatus had a resolving power of 1/10,000 sec. Playing the film back at various speeds gave a known and variable source of random pulses. The second method involved the successive addition of a number of weak radioactive sources in an apparatus designed to insure the same scattering from each source whether used alone or with others operating a G-M tube counter. The single thyratron circuit was found to lose 1 percent of the counts at an input rate of only 50 per minute, the losses increasing linearly with the input rate. This introduces a large error in much early work done with single thyratron circuits. The losses depend on the width and the amplitude of the pulses, being least for narrow pulses and minimum amplitude. This dependence prevents application of a purely statistical theory to calculate the losses. Similarly, the recording losses are less with the Neher-Harper circuit than with conventional coupling.

152. An Improved Electrical Telegauge. WAYNE C. HALL AND ROSS GUNN, *U. S. Naval Research Laboratory, Washington, D. C.*—A useful remote reading device to measure displacements of the order of 10 wave-lengths of red light and greater has been developed. A carefully designed vacuum tube with element spacing capable of variation and controlled by an externally applied displacement, is incorporated in balanced electrical circuits in such a way that first order variations of emission, or filament and plate potential, are not indicated. A portable direct current meter indicates deflections which are accurately proportional to the imposed displacement. Stable displacement amplifications of 5000 are readily obtained in a single tube used with portable equipment. The device has a high natural period and follows cyclical or impulsive displacements quite accurately if the period of the applied displacement is greater than 1/10th second. At 17 cycles per second extraneous harmonics of 4 percent are found but these may be readily reduced by proper damping. Hysteresis and aging effects are small with proper design. The investigation is continuing.

153. A Quantitative Study of Mountain Building on an Unsymmetrical Earth. ROSS GUNN, *U. S. Naval Research Laboratory, Washington, D. C.*—The principle of isostatic equilibrium is discussed and restated in a useful form which takes account of superposed vertical stresses in the crust. A quantitative study of the deformations produced in the earth's elastic crust by tangential compressional forces is made. The calculated physical properties of a suboceanic compressional downfold agree well with those observed in certain long and narrow ocean deeps. The properties of a downfault in continental regions are similarly deduced and it is shown that such a deformation evolves ultimately into a great sedimentary prism or geosyncline. The processes which fold and ultimately uplift the prism to form a mountain chain are quantitatively considered. A quantitative theory of mountain building leads to a law of mountain heights in good agreement with observation. The considered mechanisms are consistent with the principle of isostasy and with the author's earlier estimates concerning the concentration of stresses at the boundaries of the great continents. It is concluded that the circum-Pacific mountain chains could

only have been generated on an unsymmetrical earth resulting probably from a fission process much like that suggested in the author's binary star theory of the origin of the solar system. (Phys. Rev. **39**, 130, 311 (1932).)

154. A Combined Still and Diffusion Pump. WHEELER P. DAVEY AND R. J. PFISTER, *The Pennsylvania State College.*—K. C. D. Hickman[1] has traced the loss in efficacy of oil diffusion pumps to an accumulation of volatile matter which diffuses back past the jet. He proposes a combination still and pump "simple to construct, surprisingly difficult to render vacuum-tight." By using a nest of vertical concentric boilers we have overcome the difficulty. If the space between the top of the boiling oil and the condensate collector ring is filled with an appropriate still-packing, we have, in addition to the effect of the multiple boiler, the added advantage of the "packed column" type of still. A two-jet water-cooled jet still of the above design was built with glass exterior, brass jets, and brass inner boiler, using cotton string to fill the space between the glass and the brass. This was connected to a large McLeod gauge by means of a large rubber stopper made substantially vacuum tight by means of yellow vaseline. When charged with a mixture of water and *n*-butyl phthalate it rejected the water and within an hour gave an apparent vacuum, as measured on the McLeod gauge, of 2×10^{-6} cm Hg. This was in spite of evident charring of the cotton string. When charged with two volumes of *n*-butyl phthalate, one volume of acetone, and one volume of cyclohexane, it rejected the acetone and cyclohexane and in an hour gave again a measured pressure of 2×10^{-6} cm Hg. This is considered to be the vapor pressure of *n*-butyl phthalate at the temperature of our condenser.[1]

[1] K. C. D. Hickman, Jr. Frank. Inst. **221**, 215 (1936).

155. Production of Liquid Hydrogen Without the Use of a Compressor. J. E. AHLBERG AND W. O. LUNDBERG, *Johns Hopkins University* AND I. ESTERMANN, *Carnegie Institute of Technology.*—By using a "twisted tube" heat interchanger instead of the Linde or Hampson type interchanger, and by other simplifications in construction, it has been possible to build a hydrogen liquefier of great efficiency and small size. The heat capacity of the unit is low enough to make it possible to operate the liquefier from ordinary hydrogen cylinders without the use of a compressor. Using liquid nitrogen at a pressure of about 20 cm of Hg for precooling, about 16 percent of the hydrogen was liquefied at a flow of 1.6 cu. ft. per minute producing about 0.9 liter of liquid hydrogen per hour. It is possible to watch the progress of the liquefaction through an unsilvered strip in the Dewar vessel containing the heat interchanger and the expansion valve. The liquid nitrogen consumption amounts to about 7 liters per liter of liquid hydrogen.

156. A Type of High Potential Battery Which Combines Extreme Lightness with Long Shelf Life. WILLIS E. RAMSEY, *Bartol Research Foundation of The Franklin Institute.* (*Introduced by W. F. G. Swann.*)—In the conventional type of dry cell we may substitute for the usual zinc jacket a single turn of zinc wire, and allow the blotting paper which carries the electrolyte to provide a wall for the cell. Pencil graphite makes a very good substitute for the usual carbon rod. Cell units of this type may weigh as little as 0.60 gram per volt and be very satisfactory. A sheet of cardboard covered with a thin layer of Superla wax provides an excellent mounting for the units. A light but tight cardboard box will prevent evaporation. These cells are mounted dry and allowed to remain so until needed. Rejuvenation may be obtained by adding a drop or two of ammonium chloride to each unit with a medicine dropper. Repeated dehydration and rejuvenation fails to disturb the constancy of the potential (0.1 percent per week) and such a battery is activated only during periods of time when it is being used. Cell units have an internal resistance varying from 5 to 1000 ohms depending on moisture-temperature coefficient 0.04 percent per degree centigrade.

157. A Molecular Ray Method for the Separation of Isotopes.* O. STERN, *Carnegie Institute of Technology.*—The method of balancing the force of gravity by a magnetic field should allow effective separation of isotopes, because the compensating inhomogeneity $dH/dr = Mg/M$ depends on M. With Li, for example, choosing dH/dr between the limits $6g/M$ and $7g/M$, only the isotope 6 is deflected upwards and by collecting the Li above the straight beam we get pure Li_6. The intensity, however, would be very poor because, for practical reasons, the beam would have to be several meters long. But we can make the beam much shorter, replacing gravity by centrifugal force. Then it is easy to make the acceleration at least 10^4 times larger than g. For this case the beam needs to be only a few centimeters long giving a much larger intensity. Of course dH/dr has to be correspondingly larger, about 10^4 gauss/cm for Li_6 and a centrifugal acceleration of 10^4 g. Since the needed accuracy is small and the field has to be rotated, it would be convenient to use a permanent magnet. This method will give a pure isotope like the mass-spectrograph.

* To be called for after paper No. 35.

158. Quantitative Spectrographic Analysis of Biological Material. II.* J. S. FOSTER AND C. A. HORTON, *McGill University.* (*Introduced by Professor G. B. Pegram.*)—An internal standard method of general applicability has been developed for quantitative spectrographic analysis of fresh plant tissue without ashing or chemical treatment. The results obtained for boron, using 200 mg of fresh material, are reproducible with variations rarely in excess of ten percent. A photometer for wedge spectrograms is described. It is designed to avoid the problem of finding the ends of the spectral lines and to give directly the relative intensities.

* To be called for after paper No. 50.

159. The Stark Effect in Iron, and the Contrast with the Pole Effect.* F. PANTER AND J. S. FOSTER, *McGill University.* (*Introduced by Professor G. B. Pegram.*)—Through the use of a quartz tube which operates on very small current the Stark effects for a few hundred iron lines have been examined in fields from 100 to 200 kv/cm. The results lend no support to the view commonly expressed that the pole effect is a pure Stark effect. The Stark displacement of

a few lines is opposite to the pole shift, and generally speaking there is no quantitative correlation between the two effects. Since all iron terms known to be displaced by the electric fields are even, it is suggested that odd terms may yet be found with values which are rather well defined by the observed perturbations.

* To be called for after paper No. 158.

160. Effect of Crossed Electric and Magnetic Fields on the Helium Spectrum.* J. S. FOSTER AND E. R. POUNDER, *McGill University.* (*Introduced by Professor G. B. Pegram.*)—The visible spectrum of helium has been examined from a source in which the constant electric field (values range from 10,000 to 120,000 v/cm) is at right angles to the magnetic field of 26,000 gauss, and the direction of observation is perpendicular to each. The tips of the hollow poles of the magnet are the cathodes of a double canal-ray tube which sends beams in both directions along the lines of magnetic force. Light intensity is good, and the quality of the analysis is equal to the best secured in pure Stark effect. In accord with theory, the usual selection rule for Δm does not apply, and the magnetic splitting of Stark components shows marked asymmetry in the intensities.

* To be called for after paper No. 159.

161. Stark Effect in the HD and D_2 Spectra.* J. S. FOSTER, D. C. JONES, S. M. NEAMTAN, *McGill University.* (*Introduced by Professor G. B. Pegram.*)—The Stark effect in HD and D_2 has been investigated in the region from Hβ to Hα. Light from a Lo Surdo source was analyzed by a stigmatic concave grating spectrograph having a dispersion of 3.8A/mm. Plates have been obtained with electric fields from 80 to 100 kv/cm and with deuterium concentrations from 50 percent to 95 percent. Practically all the lines classified by Dieke[1] in this region of intensity over 1 have been photographed. Many unclassified lines have been observed and their behavior in an electric field noted as of possible assistance in the further analysis of the normal spectra. In addition to extending the range of the work of Hasunuma,[2] the use of greater dispersion and of plates with a practically pure deuterium spectrum has made possible the clarifying of several points left doubtful in the above investigation. In particular, the number of components observed is not in excess of the number predicted by theory. In the HD spectrum a number of interesting departures from the usual quadratic Stark effect have been observed.

* To be called for after paper No. 160.
[1] Phys. Rev. **47**, 261 (1935).
[2] Proc. Phys.-Math. Soc. Jap. **18**, 469 (1936).

AUTHOR INDEX TO ABSTRACTS OF WASHINGTON MEETING

Abramson, Harold A.—No. 144
Ahlberg, J. E., W. O. Lundberg and I. Estermann—No. 155
Albers, V. M.—see Knorr, H. V.
—— **and H. V. Knorr**—No. 103
Almy, G. M.—see Rassweiler, M. P.
Andrews, D. H., J. A. Sanderson and D. O. Hulburt—No. 101

Bacher, R. F.—see Tomboulian, D. H.
Baker, C. P. and M. Stanley Livingston—No. 71
Barnes, S. W.—see DuBridge, L. A.
——, **L. A. DuBridge, E. O. Wiig, J. G. Buck and C. V. Strain**—No. 76
Barr, E. S.—see Plyler, E. K.
Barton, Henry A.—see Lampson, Curtis W.
Baudisch, Oskar—see Welo, Lars A.
Bayley, D. S. and H. R. Crane—No. 73
Beams, J. W.—see Snoddy, L. B.
Beck, F. J., Jr.—see Ingerson, W. E.
Beese, N. C.—No. 2
Bethe, H. A.—see Hoffman, J. G.
—— see Konopinski, E. J.
—— No. 32
Blake, F. C.—No. 13
Bockstahler, Lester and Herman Ritow—No. 56
Bonner, Lyman G. and Robert Hofstadter—No. 99
Bowen, I. S., R. A. Millikan and H. V. Neher—No. 38
Bozorth, R. M.—see Cioffi, P. P.
Brode, Robert B. and Merle A. Starr—No. 43
Brubaker, Gordon—see Pollard, Ernest
—— **and Ernest Pollard**—No. 82
Bruce, W. A.—see Jauncey, G. E. M.
Buck, J. H.—see Barnes, S. W.
—— see DuBridge, L. A.
——, **C. V. Strain and G. Valley**—No. 75
Bruch-Willstätter, M.—see Sponer, H.

Caldwell, W. I. and K. Lark-Horovitz—No. 6
Carroll, H.—see Powers, P. N.
Carwile, Preston B.—No. 95
Challacombe, C. N.—No. 17
Cioffi, P. P., H. J. Williams and R. M. Bozorth—No. 60
Clark, O.—see Halpern, O.
Colwell, R. C. and A. W. Friend—No. 36
——, **A. W. Friend and H. C. Hardy**—No. 143
Compton, A. H. and R. N. Turner—No. 37
Coolidge, Albert Sprague—see James, Hubert M.
Coomes, Edward—No. 52
Cork, J. M.—see Darling, B. T.
—— see Pool, M. L.
Crane, H. R.—see Bayley, D. S.
—— see Turin, J. J.
Curtis, B. R.—see Darling, B. T.
Curtis, C. W.—No. 106

Darling, B. T., B. R. Curtis and J. M. Cork—No. 67
Davey, Wheeler P.—see Smith, Sidney D.
—— **and R. J. Pfister**—No. 154
Dawson, L. H. and E. O. Hulburt—No. 102
Dietrich, J. R.—see Snoddy, L. B.
Downsbrough, G. A.—No. 87
DuBridge, L. A.—see Barnes, S. W.
——, **S. W. Barnes and J. H. Buck**—No. 74
Duffendack, O. S.—see Lifschutz, Harold
——, **M. S. Slawsky and Harold Lifschutz**—No. 150
Dunning, J. R.—see Powers, P. N.

Ellwood, W. B.—No. 57
Emo, Lorenzo—see Richardson, J. Reginald
Estermann, I.—see Ahlberg, J. E.
——, **O. C. Simpson and O. Stern**—No. 34
Ewing, Douglas H.—No. 24

Forbush, S. E.—No. 39
Foster, J. S.—see Panter, F.
—— **and C. A. Horton**—No. 50
—— **and C. A. Horton**—No. 158
——, **D. C. Jones and S. M. Neamtan**—No. 161
—— **and E. R. Pounder**—No. 160
Frevel, Ludo K.—No. 1
Friend, A. W.—see Colwell, R. C.
Furry, W. H.—No. 31
Fussell, L., Jr.—No. 41

Getting, I. A.—see Stevenson, E. C.
Goldsmith, H. H.—see Manley, J. H.
—— **and J. H. Manley**—No. 126
Green, J. B. and J. A. Peoples, Jr.—No. 118
Gunn, Ross—see Hall, Wayne C.
—— No. 153

Haas, Arthur—No. 14
Hafstad, L. R.—see Rumbaugh, L. H.
——, **N. P. Heydenburg and M. A. Tuve**—No. 134
Hall, Wayne C. and Ross Gunn—No. 152
Halpern, O., R. Lueneburg and O. Clark—No. 120
Ham, W. R.—see Rast, W. L.
—— see Post, C. B.
Hardy, H. C.—see Colwell, R. C.
Harris, W. T.—see Turner, Louis A.
Harvey, G. G.—No. 4
Haxby, R. O.—see Williams, J. H.
Hayner, Lucy J.—see Kurrelmeyer, Bernhard
Henderson, M. C.—see Ridenour, L. N.
—— see White, M. G.
Henderson, W. J.—see Ridenour, L. N.
—— see White, M. G.
Hendricks, S. B.—see Maxwell, L. R.
Heydenburg, N. P.—see Hafstad, L. R.
Hill, E. L.—No. 133
Hirsh, F. R., Jr.—No. 3
Hirschfelder, Joseph O. and John F. Kincaid—No. 21
Ho, I-djen and R. A. Sawyer—No. 115
Hoffman, J. G.—see Livingston, M. Stanley
—— **and H. A. Bethe**—No. 125
Hofstadter, Robert—see Bonner, Lyman G.
Holley, Clifford—No. 12
Horton, C. A.—see Foster, J. S.
—— see Foster, J. S.
Hulburt, E. O.—see Dawson, L. H.
—— see Andrews, D. H.
Humphreys, C. J.—No. 107
Hustrulid, A.—see Kusch, P.
Huxford, W. S.—No. 65

Ingerson, W. E. and F. J. Beck, Jr.—No. 61
Inglis, D. R.—see Kroeger, W. J.

Jacobs, Robert B.—No. 7
James, Hubert M. and Albert Sprague Coolidge—No. 19
Jauncey, G. E. M. and W. A. Bruce—No. 8
Jesse, William P.—No. 9
Johnson, Vivian A. and L. W. Nordheim—No. 23
Jones, D. C.—see Foster, J. S.

Kaiser, Herman F.—No. 90
Kanne, W. R.—No. 81
Kanner, Morton H.—see Ladenburg, Rudolf
Kenty, Carl—No. 142
Kincaid, John F.—see Hirschfelder, Joseph O.
King, Arthur S.—see King, Robert B.
King, Robert B. and Arthur S. King—No. 117
Knerr, Henry W.—No. 46
Knorr, H. V.—see Albers, V. M.
—— **and V. M. Albers**—No. 96
Konopinski, E. J. and H. A. Bethe—No. 33
Kroeger, W. J. and D. R. Inglis—No. 29
Kruger, P. Gerald—see Pattin, H. S.
—— see Phillips, L. W.
——, **W. E. Shoupp and F. W. Stallmann**—No. 122
Kuper, J. B. H.—No. 136
Kurrelmeyer, Bernhard and Lucy J. Hayner—No. 51
Kusch, P., J. T. Tate and A. Hustrulid—No. 49

Ladenburg, Rudolf and Morton H. Kanner—No. 129
Lampson, Curtis W., Donald W. Mueller and Henry A. Barton—No. 121
Langer, Lawrence M. and Martin D. Whitaker—No. 132
Langsdorf, Alexander, Jr.—No. 147
Lark-Horovitz, K.—see Caldwell, W. I.
Legg, V. E.—No. 58
Lifschutz, Harold—see Duffendack, O. S.
——, **O. S. Duffendack and M. M. Slawsky**—No. 151
Linder, Ernest G.—No. 137
Livingston, M. Stanley—see Baker, C. P.
—— **and J. G. Hoffmann**—No. 124
Lundberg, W. O.—see Ahlberg, J. E.
Lueneburg, R.—see Halpern, O.

Manley, J. H.—see Goldsmith, H. H.
——, **H. H. Goldsmith and J. S. Schwinger**—No. 127
Margenau, Henry and Dana T. Warren—No. 28
Maxwell, L. R., S. B. Hendricks and V. M. Mosley—No. 16
McKeehan, L. W.—No. 62
Millikan, R. A.—see Bowen, I. S.
Miller, L. F.—No. 109
Miller, R. D.—No. 11
Mitchell, Allan C. G. and R. N. Varney—No. 123
Mohler, Fred L.—No. 55
Mohler, Nora M.—No. 100
Mooney, R. C. L.—No. 5
More, Kenneth R.—No. 111
Morse, Philip M.—No. 26
Mosley, V. M.—see Maxwell, L. R
Mueller, Donald W.—see Lampson, Curtis W.

Neamtan, S. M.—see Foster, J. S.
Nier, Alfred O.—No. 47

Neher, H. V.—see Bowen, I. S.
Nordheim, L. W.—see Johnson, Vivian A.
—— No. 42
Northrup, D. L. and L. C. Van Atta—No. 84
Nottingham, W. B.—No. 53

O'Conor, J. S., S.J.—No. 131

Page, Chester H.—No. 22
Panter, F. and J. S. Foster—No. 159
Parratt, Lyman G.—No. 10
Pattin, H. S. and P. Gerald Kruger—No. 114
Pearson, G. L.—No. 91
Peoples, J. A., Jr.—see Green, J. B.
Pfister, R. J.—see Davey, Wheeler P.
Phillips, L. W. and P. Gerald Kruger—No. 113
Plyler, E. K. and E. S. Barr—No. 98
Pollard, Ernest—see Brubaker, Gordon
——, **H. L. Schultz and Gordon Brubaker**—No. 85
Pool, M. L. and J. M. Cork—No. 66
Post, C. B. and W. R. Ham—No. 93
Pounder, E. R.—see Foster, J. S.
Powers, P. N., H. Carroll and J. R. Dunning—No. 128

Rabi, I. I.—see Schwinger, Julian
Ramsey, Willis E.—No. 156
Rassweiler, M. P. and G. M. Almy—No. 110
Rast, W. L. and W. R. Ham—No. 92
Richardson, J. Reginald and Lorenzo Emo—No. 86
Ridenour, L. N.—see White, M. G.
——, **W. J. Henderson, M. C. Henderson and M. G. White**—No. 78
Risser, J. R.—No. 79
Ritow, Herman—see Bockstahler, Lester
Roberts, R. B.—see Rumbaugh, L. H.
Robertson, H. P.—No. 15
Robinson, H. A. and G. H. Shortley—No. 108
Rose, Morris E.—No. 135
Rumbaugh, L. H., R. B. Roberts and L. R. Hafstad—No. 80

Sampson, J. B.—No. 104
Sanderson, J. A.—see Andrews, D. H.
Sawyer, R. A.—see Ho, I-djen
Schiff, L. I.—No. 27
Schremp, E. J.—No. 45
Schultz, H. L.—see Pollard, Ernest
—— No. 130
Schwinger, J. S.—see Manley, J. H.
Schwinger, Julian and I. I. Rabi—No. 30
Scott, George W., Jr.—see Smith, Lloyd P.
Shankland, Robert S.—No. 138
Shenstone, A. G.—No. 105
Shepherd, W. G.—see Williams, J. H.
Sherr, Rubby—No. 48
Shortley, G. H.—see Robinson, H. A.
Shoupp, W. E.—see Kruger, P. Gerald
Siegel, Sidney—No. 89
Simon, F.—No. 64
Simpson, O. C.—see Estermann, I.
Skellett, A. M.—No. 146
Slawsky, M.—see Duffendack, O. S.
—— see Lifschutz, Harold
Smith, Lloyd P. and George W. Scott, Jr.—No. 139
Smith, Sidney D. and Wheeler P. Davey—No. 63
Snell, Arthur H.—No. 69
Snoddy, L. B., J. R. Dietrich and J. W. Beams—No. 54
Sponer, H. and M. Bruch-Willstätter—No. 25
Stallmann, F. W.—see Kruger, P. Gerald
Starr, Merle A.—see Brode, Robert B.
Stern, O.—see Estermann, I.
—— No. 157
—— No. 35
Stevenson, E. C.—see Street, J. C.
—— **and I. A. Getting**—No. 149
St. Helens, H. J.—see Wilkins, T. R.
Strain, C. V.—see Barnes, S. W.
—— see Buck, J. H.
Street, J. C. and E. C. Stevenson—No. 40
Stuhlman, Otto, Jr.—No. 145
Swann, W. F. G.—No. 44

Taschek, Richard—see Williams, Dudley
Tate, J. T.—see Kusch, P.
Tomboulian, D. H. and R. F. Bacher—No. 119
Tonks, Lewi—No. 140
Turin, J. J. and H. R. Crane—No. 72
Turner, Louis A. and W. T. Harris—No. 112
Turner, R. N.—see Compton, A. H.
Tuve, M. A.—see Hafstad, L. R.

Ufford, C. W.—No. 116

Valley, G.—see Buck, J. H.
Van Atta, C. M., R. J. Van de Graaff and L. C. Van Atta—No. 83
Van Atta, L. C.—see Northrup, D. L.
—— see Van Atta, C. M.
Van de Graaff, R. J.—see Van Atta, C. M.
Varney, R. N.—see Mitchell, Allan C. G.

Wait, G. R.—No. 141
Walke, Harold—No. 70
Wannier, Gregory H.—No. 20
Warren, Dana T.—see Margenau, Henry
Welo, Lars A. and Oskar Baudisch—No. 94
Whitaker, Martin D.—see Langer, Lawrence M.
White, M. G.—see Ridenour, L. N.
——, **M. C. Henderson, W. J. Henderson and L. N. Ridenour**—No. 77
Wiig, E. O.—see Barnes, S. W.
Wilkins, T. R. and H. J. St. Helens—No. 148
Williams, Dudley and Richard Taschek—No. 97
Williams, H. J.—see Cioffi, P. P.
—— No. 59
——, **W. G. Shepherd and R. O. Haxby**—No. 68
Witmer, Enos E.—No. 18

Zener, Clarence—No. 88

1032